



National Library  
of Canada

Acquisitions and  
Bibliographic Services Branch

395 Wellington Street  
Ottawa, Ontario  
K1A 0N4

Bibliothèque nationale  
du Canada

Direction des acquisitions et  
des services bibliographiques

395, rue Wellington  
Ottawa (Ontario)  
K1A 0N4

*Vous lire - Votre référence*

*Vous lire - Votre référence*

## NOTICE

The quality of this microform is heavily dependent upon the quality of the original thesis submitted for microfilming. Every effort has been made to ensure the highest quality of reproduction possible.

If pages are missing, contact the university which granted the degree.

Some pages may have indistinct print especially if the original pages were typed with a poor typewriter ribbon or if the university sent us an inferior photocopy.

Reproduction in full or in part of this microform is governed by the Canadian Copyright Act, R.S.C. 1970, c. C-30, and subsequent amendments.

## AVIS

La qualité de cette microforme dépend grandement de la qualité de la thèse soumise au microfilmage. Nous avons tout fait pour assurer une qualité supérieure de reproduction.

S'il manque des pages, veuillez communiquer avec l'université qui a conféré le grade.

La qualité d'impression de certaines pages peut laisser à désirer, surtout si les pages originales ont été dactylographiées à l'aide d'un ruban usé ou si l'université nous a fait parvenir une photocopie de qualité inférieure.

La reproduction, même partielle, de cette microforme est soumise à la Loi canadienne sur le droit d'auteur, SRC 1970, c. C-30, et ses amendements subséquents.

Canada

Differentiation of Finite Element Approximations  
Based on Fundamental Solution of B.V.P.

*by*

Dževat Omeragić,  
Dipl.Ing., M.Sc.

A thesis submitted to the Faculty of Graduate Studies and  
Research in partial fulfillment of the requirements  
for the degree of Doctor of Philosophy



Computational Analysis and Design Laboratory

Department of Electrical Engineering

McGill University

Montréal, Québec, Canada

October, 1993

© Dževat Omeragić, 1993



National Library  
of Canada

Acquisitions and  
Bibliographic Services Branch

395 Wellington Street  
Ottawa, Ontario  
K1A 0N4

Bibliothèque nationale  
du Canada

Direction des acquisitions et  
des services bibliographiques

395, rue Wellington  
Ottawa (Ontario)  
K1A 0N4

*Your file*  *Votre référence*

*Our file*  *Notre référence*

The author has granted an irrevocable non-exclusive licence allowing the National Library of Canada to reproduce, loan, distribute or sell copies of his/her thesis by any means and in any form or format, making this thesis available to interested persons.

L'auteur a accordé une licence irrévocable et non exclusive permettant à la Bibliothèque nationale du Canada de reproduire, prêter, distribuer ou vendre des copies de sa thèse de quelque manière et sous quelque forme que ce soit pour mettre des exemplaires de cette thèse à la disposition des personnes intéressées.

The author retains ownership of the copyright in his/her thesis. Neither the thesis nor substantial extracts from it may be printed or otherwise reproduced without his/her permission.

L'auteur conserve la propriété du droit d'auteur qui protège sa thèse. Ni la thèse ni des extraits substantiels de celle-ci ne doivent être imprimés ou autrement reproduits sans son autorisation.

ISBN 0-315-94697-0

Canada

# Differentiation of Finite Element Approximations

*Dževat Omeragić*

## Abstract

In this thesis a method based on Green's second identity is developed for computing several orders of derivatives from finite element solutions with  $C^0$  continuity. The integration by parts implicit in Green's theorem permits numerical integration to replace numerical differentiation. This procedure is initially developed for harmonic functions, then extended to Poisson and Helmholtz equations for a circular region, as well as to harmonic potentials in axi-symmetric coordinates. For the 2-D Laplace operator three other base regions have been introduced: rectangle, sector of circle and sector of ring. The method is numerically stable, position independent and very accurate. Its accuracy is the same as of original finite element solution, or even better, when the point of interest is not close to the edge of the base region. Treatment of singular integrals is based on using the finite part integration concept. Integration formulas are given. The method is verified with analytical functions, using accurate values and finite element solutions. It is also applied in anisotropic nonlinear magnetic material modeling.

Accurate computation of derivatives from finite element solutions is an important step in CAD postprocessing. Direct differentiation of basis functions is inaccurate. Superconvergent methods give satisfactory results in gradient calculation, but their accuracy is position dependent and second or higher derivatives are unreliable. With the new technique it is possible to compute derivatives even where finite element solution itself has insufficient continuity, e.g. finding second order derivatives from  $C^0$  continuous solutions.

## Résumé

Dans cette thèse, une méthode basée sur la deuxième identité de Green est traitée. Cette approche permet de calculer les dérivées d'ordre supérieur à partir de solutions continues  $C^0$  obtenus par la méthode des éléments finis. L'intégration par parties, implicite dans le théorème de Green, permet de remplacer la différentiation numérique par une intégration numérique. Cette technique est d'abord développée pour les fonctions harmoniques. La méthode est, dans un deuxième temps, élargie aussi bien aux équations de Poissons et de Helmholtz pour une région circulaire qu'aux potentiels harmoniques dans un système de coordonnées axisymétriques. Pour le cas des opérateurs de Laplace en deux dimensions, trois autres formes élémentaires ont été examinées: le rectangle, le secteur d'un cercle et le secteur d'un anneau. La méthode est relativement stable, indépendante de la position et est très précise. La précision est la même que celle de la résolution par éléments finis et est même meilleure au cas où le point considéré n'est pas proche de la région élémentaire. L'approche, basée sur le concept de l'intégration par parties finies, a été appliquée aux intégrales singulières. Les formules d'intégration sont présentées. La méthode a été vérifiée à l'aide de fonctions analytiques en utilisant des valeurs précises et des solutions obtenus par la technique des éléments finis. La méthode est également utilisée pour la modélisation de matériaux magnétiques anisotropique non linéaires.

Un calcul précis de dérivées à partir des solutions obtenues par les éléments finis est un pas important pour l'étape d'exploitation des résultats en CAO. La différentiation directe des fonctions de base conduit à des résultats imprécis. La méthode de superconvergence pour le calcul du gradient donne une solution satisfaisante; néanmoins les précisions dépendent de la position et les dérivées d'ordre deux et supérieur ne sont pas fiables. Pour cette nouvelle méthode, il est possible de calculer des dérivées même dans le cas où la solution par les éléments finis présente une continuité insuffisante; par exemple, lorsqu'il s'agit de trouver les dérivées d'ordre deux à partir de solutions continues  $C^0$ .

### Contributions to Original Knowledge

- (a) A general procedure for computation of high order derivatives from approximate solutions of the Poisson and Helmholtz partial differential equations is described and applied. The method is based on Green's second identity;
- (b) Derivatives of Green's functions and generalized Poisson kernel functions of Laplacian differential operator are generated for new elementary shapes: rectangle, sector of circle and sector of ring. The library of kernels for a circle is extended with expressions for the point on the boundary and a new, simpler, formula for the  $m, n$ th order derivative of the Poisson kernel;
- (c) Generalized Poisson kernels for the Helmholtz differential operator in the case of circle as a base region are derived, expressing the Green's function as a sum of Bessel functions. Using this method it is possible to compute derivatives of any order;
- (d) A differentiation procedure for axisymmetric problems described by Laplace's equation is derived. The method uses fundamental solutions for a torus and a sphere on the axis of symmetry;
- (e) The one-dimensional smoothing method of Zhu and Zienkiewicz is generalized to two and three dimensions.

## Acknowledgement

I would like to express my deepest gratitude to Dr. Peter P. Silvester, my thesis advisor, for his guidance, encouragement, patience and provision of financial support which made the completion of this work possible. During the past period we had many useful and intellectually stimulating discussions. His calm and cheerful attitude inspired new ideas and renewed enthusiasm for this project.

I am indebted to Professor Salih Sadović of University of Sarajevo, Bosnia-Herzegovina, for introducing me to CAD and sharing with me his broad expertise in computer methods.

I also thank to my colleagues from CADLab for their friendship and cooperation and pleasant working environment.

Special thanks go to my parents, Sanija and Šefket for their love, care and encouragement from far away. Most of all, I would like to thank my wife, Nidžara, and my lovely daughters, Emina and Leyla, who stayed right by me when I needed it most.

Financial support from the Natural Science and Engineering Research Council (NSERC) of Canada, Canadian Center for International Studies (CCIS), Centre de Recherche Informatique de Montreal (CRIM) and McGill University is gratefully acknowledged.

## Table of Contents

Abstract	<i>i</i>
Résumé	<i>ii</i>
Acknowledgments	<i>iii</i>
Table of Contents	<i>iv</i>
CHAPTER 1 Introduction	1
1.1 Derivatives and postprocessing in CAD	2
1.2 Review of existing differentiation methods	5
1.2.1 Direct differentiation of finite element functions	5
1.2.1.1 Straight differentiation	6
1.2.1.2 Weighted averages	7
1.2.2 Superconvergent methods	9
1.2.2.1 Points of exceptional accuracy	9
1.2.2.2 Local smoothing of finite element results	10
1.2.2.3 The one-dimensional smoothing algorithm of Zhu and Zienkiewicz	12
1.2.3 Global smoothing	14
1.2.4 Superconvergent techniques for recovery in error estimation	15
1.2.4.1 Zhu-Zienkiewicz superconvergent patch recovery procedure	15
1.2.4.2 Application of self-equilibrium conditions	18
1.2.5 Function extraction methods	22
1.2.6 Method based on Green's second identity	23
1.3 The objective of thesis	25
1.3.1 Claims of originality	25
1.4 Outline of the thesis	26

CHAPTER 2	Formulation of the proposed methodology	28
2.1	Fundamental solution of boundary value problems	28
2.1.1	Application of Fourier series expansion for a circular disk	29
2.1.2	Fundamental solution for a circular ring	31
2.1.3	Harmonic functions in axisymmetric coordinates	34
2.1.3.1	Torus	34
2.1.3.2	Sphere with the center on $z$ axis	37
2.2	Mathematical background of the differentiation method based on Green's second identity	38
2.2.1	Green's second identity	38
2.2.2	Generalization to Helmholtz operator ( $\nabla^2 + \kappa^2$ )	41
2.2.3	Formulations for the Helmholtz equation	43
2.3	Problems in implementation of the modified Poisson integral method	45
2.4	Concluding remarks	45
CHAPTER 3	Generation of Green's function and Poisson kernels and their derivatives	47
3.1	Construction of Green's functions	47
3.1.1	Methods of generating Green's functions	47
3.1.1.1	Method of images	48
3.1.1.2	Conformal mapping	50
3.1.1.3	Eigenfunctions expansion method	51
3.1.1.4	Applicability of various forms of Green's function	54
3.1.2	Construction of Green's functions and Poisson kernels for elementary shapes	55
3.1.2.1	Circle	56
3.1.2.2	Rectangular region	58
3.1.2.3	Sector of circle of angle $\pi/m$	59
3.1.2.4	Sector of ring with angle $\pi/m$	61
3.1.3	Generation of Green's functions for Helmholtz operator ( $\nabla^2 + \kappa^2$ )	64

Table of Contents

3.2	Differentiation of fundamental solutions of boundary value problems	67
3.2.1	Method based on Fourier series expansion	67
3.2.2	Differentiation of harmonic functions in axisymmetric coordinates	68
3.2.2.1	Torus	68
3.2.2.2	Sphere with the center on $z$ axis	69
3.3	Derivatives of harmonic functions if point $P$ is close to or on the edge	70
3.3.1	Regularization of the Poisson kernels for the circle	70
3.3.2	Point $P$ on the edge - normal derivative on the boundary	73
3.4	Treatment of the surface integral	75
3.4.1	Differentiation of surface integral term for an interior point $P$	76
3.4.2	Differentiation of surface integral for point on the edge	79
CHAPTER 4	Validation of the method	81
4.1	Numerical experiments with Poisson equation solutions	81
4.1.1	Results using exact values of a test-function	81
4.1.1.1	Experiments with a circular disk	81
4.1.1.2	Experiments with a rectangular region	88
4.1.1.3	Experiments with a sector of circle	89
4.1.1.4	Experiments with a sector of ring	90
4.1.2	Error amplification analysis	93
4.2	Experimental results with solutions of the Helmholtz equation	98
4.2.1	Tests against the exact solution	99
4.2.2	Error sensitivity tests	101
4.3	Tests of procedure for axisymmetric problem derivatives	102
4.3.1	Numerical efficiency	102
4.3.2	Error sensitivity	104
CHAPTER 5	Evaluation of singular and near-singular integrals	107
5.1	Finite Part Integrals	108
5.1.1	Analytic continuation and definition	108

*Table of Contents*

5.1.2	Quadrature formulae for finite part integrals	109
5.1.3	Generation of quadrature formulae	122
5.2	Computation of near-singular integrals	122
5.2.1	Generation of specialized Gaussian quadrature formulae	113
5.3	Computational verification of the quadrature methods	115
5.3.1	Normal derivative computation using the Poisson integral method	115
5.3.2	Second derivative of the Poisson equation solution	119
5.4	Concluding remarks	123
CHAPTER 6 Gradient recovery by local smoothing of finite element solutions		124
6.1	The fundamental equations	124
6.2	Taylor series analysis of error	125
6.3	Derivation for the two-dimensional problem	127
6.4	Generalization of the local smoothing of gradients to three dimensions	132
6.4.1	Hinton-Campbell conventional local smoothing	132
6.4.2	Derivation of extended Zhu-Zienkiewicz method for 3-D problems	133
6.4.3	Brick elements and homogeneous linear materials	136
CHAPTER 7 Application to finite element method		139
7.1	Application to two-dimensional cases	139
7.2	Comparative study of differentiation methods	147
7.2.1	Second-order quadrilateral elements	149
7.2.2	Triangular elements	155
7.2.3	Non-uniform triangular mesh	162
7.3	Tests of procedures dealing with singular and nearly singular integrals	164
7.3.1	The normal derivative computation using the Poisson integral method	164
7.3.2	Second derivative of the Poisson equation solution	165

Table of Contents

7.4	Application to axisymmetric problems	169
7.5	Three dimensional local smoothing results	175
7.6	Differentiation of the Helmholtz equation solution	185
7.7	Concluding remarks	190
CHAPTER 8 Conclusions		192
8.1	Characteristics of the generalized Poisson integral method	192
8.2	Characteristics of the generalized Zhu-Zienkiewicz method	194
8.3	Results of comparative analysis	194
8.4	Further work	195
Appendix 1	Poisson kernels and surface integral kernels for a circular region	196
Appendix 2	Extended Poisson kernels and surface integral kernels for a rectangular region	202
Appendix 3	Extended Poisson kernels for a sector of circle of angle $\pi/m$	207
Appendix 4	Extended Poisson kernels and surface integral kernels for a sector of ring of angle $\pi/m$	211
Appendix 5	Extended Poisson kernels for the Helmholtz operator in a circular region	220
Appendix 6	Formulae for differentiation of harmonic function in axisymmetric coordinates	223
Appendix 7	Application to modeling of soft magnetic materials	228

*Table of Contents*

Appendix 8	Published work based in part or whole on this thesis	232
REFERENCES		233

## CHAPTER 1

### Introduction

The use of computational electromagnetics in the solution of problems arising in engineering design is common today. Modern design techniques offer powerful tools that blend electromagnetic field theory, numerical mathematics, and computer graphics.

The finite element method is almost universally used in its various forms in detailed computer aided analysis of electromagnetic problems. Analysis methods for electromagnetics problems are now considered to be sufficiently known (Chari and Silvester (1980), Lowther and Silvester (1986), Sabonnadière and Coulomb (1987), Hoole (1989), Silvester and Ferrari (1990)), with numerical software available. These methods provide the design engineer simulations and solutions to problems of very high complexity, even to those not expert in numerical methods.

The process of computer aided design (CAD) using numerical approximation methods such as finite element method (FEM) consists of three main stages:

- (a) description of the problem, geometry definition, input of material physical characteristics and definition of boundary conditions corresponding to the physical problem. It is followed by finite element mesh generation. The set of procedures doing all these operations is usually called a *pre-processor*;
- (b) assembling and solving the resulting system of equations; and
- (c) extraction of physical results from the solver output, visualization and graphical presentation of these results, as well as manipulation of the solution of a problem. These known as *post-processing* or *post-solution* operations.

Software designers of modern electromagnetic design and analysis systems have a wide choice of techniques and well established algorithms for the first two phases. The third segment is the major part of any design system. This stage may also be defined as the activity of converting mathematical solution into engineering results.

In post-processing, mathematical operations, such as differentiation, integration, and other, arithmetic, vector or functional operations, may be required. All of them are performed on finite element approximations, which are usually constructed so that the potential solution is continuous elsewhere. But since differentiation reduces the order of approximation and destroys continuity, potential derivatives are not continuous on the element edges. Arithmetic operations do not affect the finite element approximations, so long as the problem of round-off error accumulation may be neglected. It is well known from elementary numerical analysis that the formation of small differences should be avoided, so differentiation is an error-amplifying process (Lowther and Silvester (1986)). Integration is generally an error-attenuating process, which smoothes the result. Difficulties may occur in contour integration, if very sharp fluctuations of the integrand are present.

### 1.1 Derivatives and postprocessing in CAD

In post-processing of pure finite element results, the critical process is numerical differentiation. Finding partial derivatives of various orders is an error-prone process, having a tendency to amplify the error in the original data because of the oscillatory nature of finite element solutions. It is well known that in the finite element method a small error in an average may mean a huge pointwise error. The designer must keep in mind the recommendation (Lowther and Silvester (1986)) that differentiation operations on field quantities should be avoided if possible, especially the computation of high order derivatives. This is true for derivatives computed by direct differentiation of underlying basis

functions. Such an operation is considered dangerous, yielding unreliable results. There are occasions in magnetic torque computation, when even the sign of the computed value is not correct.

The continued popularity of the finite element method has led to increasingly large amounts of attention among both engineers and mathematicians being paid to the problem of assessing the quality of computed approximations. The techniques for finding derivatives of approximate potentials therefore play a key role in the design and construction of post-processing software for magnetics, as well as other fields in engineering.

In the process of electromagnetic design, rarely are designers of magnetic devices interested in potential values. Quantities of primary interest in design are usually related to derivatives of the potential. These quantities may have global character, as a total amount of flux, total force, etc. However, the distributions, and the local values of field, flux densities, stress intensity factors, displacements, temperatures, forces, torques, energy densities, field uniformities, may be the primary concern of a design engineer. These post-processing quantities are to be determined at points or along lines in two-dimensional problems, and over surfaces in three dimensions. Some examples where accurate derivatives are needed are: magnetic resonance imaging (MRI) system design, where field uniformity is the main design objective; high voltage insulation systems, where field values and their derivatives are required; computation of magnetic forces and modeling of anisotropic soft magnetic materials. Derivatives are also used in further computation procedures, as driving functions.

Another need for accurate differentiation arises in the error estimation process, where the criterion is energy norm, closely related to root-mean-square error in fields or stresses. Error control is fundamental in all computational mechanics. Its role is to predict the mesh refinement necessary to achieve the desired accuracy, and to achieve refinement in the most economical manner.

In Figure 1 the configuration of a typical MRI device is presented. It consist of coils carrying direct current to produce a field as uniform as possible

over the region of interest. The uniformity to be achieved should be of order  $10^{-6}$  (Infolytica (1992)). A naive approach to achieve the necessary degree of accuracy would be to use a dense mesh or a high degree of approximation.

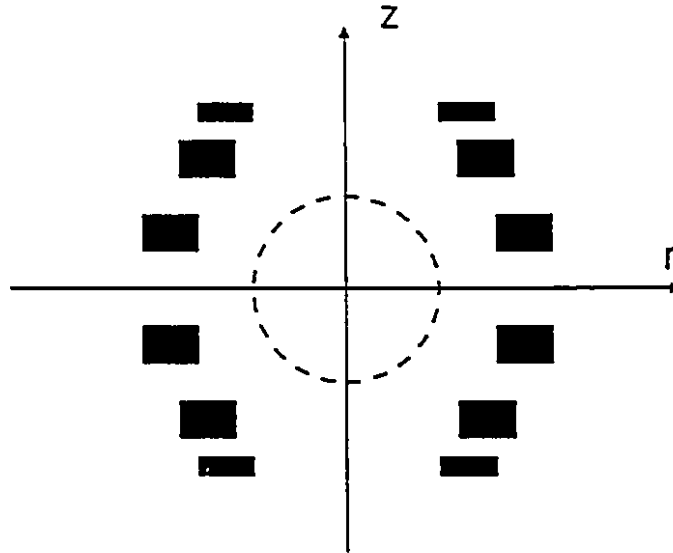


**Figure 1.1.** Geometry of Magnetic Resonance Imaging coil system. The aim is to achieve uniform field over a central region.

Modern electromagnetic engineers must be familiar with the many numerical methods available. Even after selecting differentiation methods carefully, a wide choice is still in hand. It is therefore of considerable interest to the finite element software engineer to have guidelines for the tradeoffs between accuracy and execution time that may be provided by the algorithms. Silvester and Omeragić (1993a) gave a review of five differentiation methods from an algorithmic point of view, to establish estimates for operation and evaluation counts. They described key results, and concluded with recommendations on the

circumstances in which the several methods may find use.

## 1.2 Review of existing differentiation methods

The techniques for evaluating derivatives from numerical approximate solutions in various problems of mathematical physics may be grouped into three distinct approaches: direct differentiation methods, smoothing methods based on superconvergence properties, and methods based on integral transformations.

This section will deal with methods of computing the first derivative, since most of the articles referred to deal with that case. The problem is always: *How to make use of the finite element approximation in a suitable approximation of gradients.* For finding higher order derivatives, no systematic analysis appears in the literature. A two-step method proposed by Sohn and Heinrich (1990) seeks the first derivative by global smoothing, then in a second step direct differentiation of these results is performed. Since the global smoothing method does not give particularly high accuracy of derivatives (Hinton and Campbell (1974)) despite its high cost, this method is less promising than might have been hoped. Another alternative is using global smoothing again for second order derivatives, as suggested by Zienkiewicz and Taylor (1989). This method is computationally expensive, not necessarily giving high accuracy. The nature of the approximation is such that it is not likely to behave better than the global smoothing used in gradient computations.

A brief survey of the more common derivative computation methods follows.

### 1.2.1 Direct differentiation of finite element functions

Direct differentiation methods are widely used in field visualization and in smoothing computed results. These methods differ mainly in their treatment of the derivative discontinuities that inevitably arise in piecewise-smooth

approximation. Among this group of methods, nodal averaging of derivatives on simplex elements is probably the most often used. Although the idea of averaging is as old as the finite element method itself, a complete error analysis on a uniform finite element mesh was only achieved in the nineteen-eighties (Křížek and Neittaanmäki (1984), Levine (1985), Goodsell and Whiteman (1989)). A natural extension of this method, the use of averages weighted by surface, angle or (rarely) centroidal distance, is common in practice and is applied in most of the existing finite element packages. Generally, smoothed gradients give pleasing graphical displays, but their numerical values may be no more accurate than those obtained by direct differentiation of the finite element solution. Occasionally special elements, for example high-order elements with derivative continuity (Wong and Cendes (1986), Tarnhuvud and Reichert (1988)) are also used, but not enough results have been reported to indicate the levels of accuracy obtainable. If, for example, the Morley triangle is used, where the derivative is continuous at some special points, and for elements with derivative continuity there is no evidence of improved results over classical quadratic elements.

#### 1.2.1.1 Straight differentiation

On each finite element, the approximate potential solution  $\phi$  is known in terms of the finite element interpolation functions (shape functions)  $\alpha_i(x,y,z)$  and their associated nodal potentials, as

$$\phi = \sum_i \phi(P_i) \alpha_i(x,y,z) \quad (1.1)$$

where  $\{P_i \mid i = 1, \dots, M\}$  is the set of nodes on a single finite element. Derivatives can be obtained by direct differentiation of the interpolation functions. To evaluate the  $x$ -directed derivative, for example,

$$\frac{\partial \phi}{\partial x} = \sum_i \phi(P_i) \frac{\partial \alpha_i(x,y,z)}{\partial x}. \quad (1.2)$$

On triangular and tetrahedral elements, this work reduces to straightforward matrix multiplication by the universal matrices of the triangle (Silvester (1978))

or tetrahedron (Silvester (1972)). For brevity, all the following will refer to triangular elements; but all statements made here generalize directly to tetrahedra. Using the chain rule, differentiation with respect to  $x$  is replaced by differentiations with respect to the local coordinates  $\zeta_1, \zeta_2, \zeta_3$ , on the triangle. Then

$$\frac{\partial \phi}{\partial x} = \sum_i \phi(P_i) \sum_{k=1}^{N+1} \frac{\partial \alpha_i(\zeta_1, \zeta_2, \zeta_3)}{\partial \zeta_k} \frac{\partial \zeta_k}{\partial x} \quad (1.3)$$

where  $N$  is the dimensionality of the geometric problem space (i.e.,  $N = 2$  for triangles). Now  $\partial \zeta_k / \partial x$  is merely a geometric constant (a scaling factor multiplied by a direction cosine) that describes the element; in the literature of simplex elements it is usually denoted by  $b_k$ . Similarly  $\partial \zeta_k / \partial y = c_k$ . The derivative of an interpolation polynomial  $\alpha_i$  is clearly a polynomial, of degree lower by one; thus it can always be expressed as a linear combination of the interpolation polynomials  $\alpha_j$  themselves. Consequently,

$$\frac{\partial \phi}{\partial x} = \sum_j \left( \sum_i \sum_{k=1}^{N+1} b_k D_{ij}^{(k)} \phi(P_i) \right) \alpha_j, \quad \text{where} \quad D_{ij}^{(k)} = \sum_j \frac{\partial \alpha_i}{\partial \zeta_k} \Big|_{P_j}. \quad (1.4)$$

There are  $N + 1$  matrices  $D^{(k)}$ , but they are row and column permutations of each other so only one need be stored in programs. These matrices have been tabulated and are available for all the commonly used orders of finite element.

It should be noted that in this method all the required information is strictly local to a single element. This fact, much more than any consideration of operation counts, may be of significance in parallel processing applications.

### 1.2.1.2 Weighted averages

This method apparently was first applied to simplicial finite element meshes on a purely intuitive basis. The field values computed by direct differentiation for first order elements are constant in each element and discontinuous at interelement boundaries. Weighted averaging of derivatives is used, so that the  $x$ -derivative at node  $k$  is calculated by

$$\frac{\partial \phi_k}{\partial x} = \frac{\sum_{i=1}^{N_s} w_i \left( \frac{\partial \phi}{\partial x} \right)_i}{\sum_{i=1}^{N_s} w_i} \quad (1.5)$$

where  $N_s$  is the number of surrounding elements. This procedure is applicable to elements with the same material characteristics. Otherwise, coefficients  $w_i$  must be modified to take into account material property (permittivity, permeability, etc.) values. Three different weighting criteria may be used: a) area of the element, b) angle subtended at the node  $k$ , c) distance between the node and the centroid of the element. The equivalent quantities in three dimensions are volume, solid angle and centroidal distance.

This method was proposed on purely intuitive grounds and justified heuristically on the basis of its performance in practical problems. It is rather crude, but it often results in surprisingly good approximations of the gradients, compared to direct differentiation. Levine (1985) first derived a complete error analysis and proved that averaged results are superconvergent for a uniform mesh. He expressed the view that averaging would also be beneficial on non-uniform meshes, but gave no further analysis. Křížek and Neittaanmäki (1984) as well as Goodsell and Whiteman (1989) generalized this procedure, with a treatment of points on the boundary of the solution region, and at corners.

To be applied effectively, this method requires all derivatives and areas of corresponding elements to be stored. The derivative at an arbitrary point can be found from nodal derivative values by

$$\frac{\partial \phi}{\partial x} = \sum_i \alpha_i(x,y,z) \left( \frac{\partial \phi}{\partial x} \right)_i \quad (1.6)$$

requiring  $O(N+1)$  arithmetic operations per point where derivatives is to be computed, in addition  $O((N+1)^2)$  operations to compute  $\alpha_i$ .

## 1.2.2 Superconvergent methods

The second group of techniques is based on superconvergence. Superconvergence is exhibition of exceptional rates of convergence of the approximate solution at certain points whose location is known *a priori*. These points, sometimes referred to as “stress points” (Barlow (1976)), are the Gaussian quadrature nodes for quadrilateral isoparametric elements and Gaussian points on the edges of a triangle. As the mesh is refined, the error at these points diminishes much faster than the global error. One can then recover derivatives of the solution through extrapolation of the derivatives themselves. There are many possible ways to carry out this process. Křížek and Neittaanmäki (1987) have given a comprehensive review, classification and a bibliography of 200 items of existing superconvergent methods for differential and integral equations. Global smoothing (over the whole solution domain), which is in essence a reformulation of finite elements, and local smoothing (on each finite element) (Hinton and Campbell (1974), Zienkiewicz and Taylor (1989)) followed by averaging of derivatives are the two standard methods for accurate derivative computation. Hinton and Campbell (1974) have shown that global superconvergence does not lead to better accuracy of the computed derivatives, so global smoothing has not been followed up extensively in this study. On the other hand, gradient recovery by the approximation method of Zhu and Zienkiewicz (1990), a further improvement of this method, gives very good accuracy for one-dimensional problems. A two and three-dimensional extension of this method is included in this thesis.

### 1.2.2.1 Points of exceptional accuracy

The phenomenon of superconvergence may best be viewed (MacKinnon and Carey (1989), Strang and Fix(1973)) in terms of classical error analysis based on Taylor series expansions. The potential  $\phi(x)$  on a finite element of order  $p$ , taken to be one-dimensional for simplicity in discussion, is known to an accuracy of order  $O(h^p)$ . A Taylor series expansion of the potential error  $\epsilon_\phi$  must then begin with a term of order  $p + 1$ :

$$\varepsilon_\phi(x) = k_{p+1}(x-x_0)^{p+1} + k_{p+2}(x-x_0)^{p+2} + \dots \quad (1.7)$$

Correspondingly, the error  $\varepsilon_E(x)$  in field value  $E(x)$  is given by

$$\varepsilon_E(x) = -(p+1)k_{p+1}(x-x_0)^p - (p+2)k_{p+2}(x-x_0)^{p+1} + \dots \quad (1.8)$$

Like any polynomial of order  $p$ , this expression can always be rewritten so that the leading term is the Legendre polynomial of order  $p$ , and the following terms are of order  $p+1$  or higher:

$$\varepsilon_E(x) = K_p P_p(x-x_0) + O(h^{p+1}). \quad (1.9)$$

The Legendre polynomial of order  $p$  has  $p$  zeros within the element. At its zeros, the first term in (1.9) vanishes so the error in derivative cannot exceed  $O(h^{p+1})$ .

#### 1.2.2.2 Local smoothing of finite element results -

On second order, numerically integrated quadrilateral elements, local smoothing as proposed by Hinton and Campbell (1974) is so commonly used as to amount to standard practice (Zienkiewicz and Taylor (1989)). This method is based on the known fact that on a  $p$ th order element, the first derivative of the potential function has exceptional accuracy at the  $p$  Gauss-Legendre points, i.e., at the zeros of the Legendre polynomial of order  $p$ . In essence, the Hinton-Campbell procedure is simply a bilinear extrapolation of the  $2 \times 2$  Gaussian point values. The smoothed function is obtained by a least squares fit, defined by the computed derivatives at the Gaussian points. If the smoothing shape function is linear, the smoothed corner nodal gradient components  $\bar{e}_1, \bar{e}_2, \bar{e}_3, \bar{e}_4$  may be obtained from the expression

$$\begin{bmatrix} \bar{e}_1 \\ \bar{e}_2 \\ \bar{e}_3 \\ \bar{e}_4 \end{bmatrix} = \begin{bmatrix} 1 + \frac{\sqrt{3}}{2} & -\frac{1}{2} & 1 - \frac{\sqrt{3}}{2} & -\frac{1}{2} \\ -\frac{1}{2} & 1 + \frac{\sqrt{3}}{2} & -\frac{1}{2} & 1 - \frac{\sqrt{3}}{2} \\ 1 - \frac{\sqrt{3}}{2} & -\frac{1}{2} & 1 + \frac{\sqrt{3}}{2} & -\frac{1}{2} \\ -\frac{1}{2} & 1 - \frac{\sqrt{3}}{2} & -\frac{1}{2} & 1 + \frac{\sqrt{3}}{2} \end{bmatrix} \begin{bmatrix} e_I \\ e_{II} \\ e_{III} \\ e_{IV} \end{bmatrix} \quad (1.10)$$

where  $e_I, e_{II}, e_{III}, e_{IV}$  are the gradients at Gaussian points. Generally, for a  $p$ th order function  $e(\xi)$  sampled at the  $p$  Gaussian points (where  $-1 \leq \xi \leq 1$ ), these values uniquely define a smoothed function  $\bar{e}(\xi)$  of order  $p-1$  that is a least squares fit to  $e(\xi)$ ,

$$\bar{e} = \sum_i \alpha_i(\xi, \eta) \bar{e}_i. \quad (1.11)$$

Hinton and Campbell noted that the results at the centroid of an element are of exceptional accuracy, for this value is the arithmetic mean of Gaussian point values which are themselves of exceptional accuracy. However, gradients computed using local smoothing are not unique at nodal points at element edges. Nodal averaging may be used at element edges to secure uniqueness.

For higher order triangular elements (Andreev and Lazarov (1988)), tangential derivatives are superconvergent at the Gaussian points of an element edge. Gradients can be recovered by averaging extrapolated results at the nodal points, and applying a similar procedure. Hawken, Townsend and Webster (1991) averaged values of the gradients in adjoining elements at each mid-side node, and calculated vertex node gradients as the averages of the nodal gradient contributions evaluated at elements which share that node. Superconvergence on triangular elements is also discussed by Moan (1974), who has shown that the best derivative values are obtained where the function values of the orthogonal polynomials of a given order are minimal. For second order elements, there are

three points with local triangle coordinates:

$$\frac{8 - \sqrt{10}}{27}, \frac{8 + \sqrt{10}}{27}, \frac{11 + 2\sqrt{10}}{27} \quad (1.12)$$

and the two corresponding symmetrically placed points. Derivative values may be extrapolated from these values. Also, Lin Qun and Xi Jinchao (1985) proved that there exist local averaging operators which allow recovering the derivatives under strong assumptions on the mesh regularity. They showed how any domain can be triangulated into uniform meshes, and how averaging techniques apply in that case (Lin and Zhu (1984), Ciarlet and Lions (1990)).

Gallagher and Nagtegaal (1989) stated that the process of smoothing adds another level of approximation. The smoothed iso-surfaces give a good graphical impression of the nature of solution, but no general statement can be made that smoothing of discretized results gives a better or worse quantitative representation of the exact solution.

### 1.2.2.3 The one-dimensional smoothing algorithm of Zhu and Zienkiewicz

This method is a least-squares fitting technique for derivative recovery. It is proposed by Zhu and Zienkiewicz (1990) for one-dimensional problems. They observed that  $O(p-1)$  derivative estimates could be improved by adding a term proportional to the Legendre polynomial  $P_p(x)$ . Accuracy at the points of exceptional accuracy is unaffected, since the points of exceptional accuracy are the zeros of  $P_p(x)$ ; but enlargement of the approximating function space will inevitably lead to improved accuracy elsewhere.

Zhu and Zienkiewicz constructed an improved approximation  $E_i^*$  to the field in element  $i$  by taking

$$E_i^* = E_i + \alpha_i P_p(x) \quad (13)$$

where  $E = -d\phi(x)/dx$  and the equation to be solved by finite element methods is the one-dimensional Helmholtz equation which often arises in the two-point

boundary value problem,

$$\frac{d}{dx}(a(x)E(x)) + b(x)\phi(x) = f(x). \quad (14)$$

The unknown coefficient  $\alpha_i$  in the  $i$ th element is determined by minimizing the squared residual of this equation,

$$\frac{\partial}{\partial \alpha_i} \int_{I_i} (r^-)^2 dx = \frac{\partial}{\partial \alpha_i} \int_{I_i} \left( \frac{d}{dx}(aE^-) + b\phi - f \right)^2 dx = 0 \quad (15)$$

where the integrations are taken over element  $i$ . This procedure readily yields

$$\alpha_i = \frac{\int_{I_i} \left( \frac{d}{dx}(aP_p) \right) \left( \frac{d}{dx}(aE) + b\phi - f \right) dx}{\int_{I_i} \left( \frac{d}{dx}(aP_p) \right)^2 dx}. \quad (16)$$

Nodal averaging may again be applied at element nodes. Particularly if numerical solution is required, the computational costs are higher than for conventional local smoothing; how much higher, depends on the order of numerical quadrature. The second derivatives have to be computed, increasing the costs further. On the other hand, higher accuracy results than with simple smoothing.

This procedure uses only information local to a single element, so it appears well suited to implementation on parallel computers.

Zhu and Zienkiewicz expressed the view that this technique for field improvement could probably be generalized to two and three dimensions, but did not suggest how this might be done. The method will be generalized to two and three dimensions later on in this thesis.

To find higher order derivatives Feuillebios (1990) derived an equi-distant formula for numerical differentiation based on the classical Lagrange and Hermite interpolation. This idea may be used and eventually extended to two and three dimensional problems.

## 1.2.3 Global smoothing

This procedure applies the least-squares technique directly to gradients. Instead of approximating gradients by

$$E = \sum_i \frac{\partial \alpha_i(x,y,z)}{\partial g} \phi_i \quad (1.17)$$

the gradient components are interpolated by

$$E^* = \sum_i \alpha_i(x,y,z) E_i \quad (1.18)$$

where  $E$  is the derivative in some specified direction  $g$ . Least squares approximation, by minimization of the squared difference

$$\mathfrak{F}(E^*) = \int_{\Omega} (E^* - E)^2 d\Omega \quad (1.19)$$

with respect to the  $\alpha_i$  leads to the system of equations (Zienkiewicz and Taylor (1989), Hinton and Campbell (1974)).

$$\mathbf{M}\mathbf{e} = \mathbf{f} \quad (1.20)$$

where

$$M_{ij} = \int_{\Omega} \alpha_i \alpha_j d\Omega \quad (1.21)$$

$$f_i = \int_{\Omega} \left( \alpha_i \sum_j \frac{\partial \alpha_j}{\partial g} \phi_j \right) d\Omega. \quad (1.22)$$

The metric  $\mathbf{M}$  is often 'lumped' by structural analysts, i.e., replaced by a diagonal matrix  $\mathbf{M}_L$  constructed on heuristic grounds (Zienkiewicz, Villotte,

Toyoshima and Nakazawa (1985), Zienkiewicz and Taylor (1989)). After such diagonalization the solution is trivial.

$$\mathbf{e} = \mathbf{M}_L^{-1} \mathbf{f}. \quad (1.23)$$

Lumping may naturally lead to a loss of accuracy. The solution can be improved by the iterative cleanup procedure

$$\mathbf{e}^n = \mathbf{e}^{n-1} - \mathbf{M}_L^{-1} (\mathbf{M} \mathbf{e}^{n-1} - \mathbf{f}). \quad (1.24)$$

This technique unfortunately yields a large system of equations, so it is an expensive way of computing derivatives. Given that it is not consistently better than simple local smoothing (Hinton and Campbell (1974)), it is rarely used, even though it may have advantages in two-dimensional interpolation.

#### 1.2.4 Superconvergent techniques for recovery in error estimation

Recently two new methods were developed for accurate derivative recovery from finite element solutions. The first one is a relatively simple superconvergent patch recovery procedure by Zienkiewicz and Zhu (1992a, 1992b). It is recommended by Zienkiewicz and Zhu as a post-processing technique in the finite element method. The idea of the method is to use the derivatives computed at points of exceptional accuracy on the patch of finite elements. Another approach was presented by Ohtsubo and Kitamura (1990, 1992a, 1992b), who implemented the idea of Kelly (1984) in two and three dimensional problems. They extended the existing idea of adding the estimated error to the original solution, by applying certain additional conditions.

##### 1.2.4.1 Zhu-Zienkiewicz superconvergent patch recovery procedure

This procedure uses a single and continuous polynomial expansion of the function describing the derivatives. It is applied on a patch of elements surrounding the

nodes at which recovery is desired, using the superconvergent points.

If  $E_i$  are nodal derivatives and  $\alpha_i$  are basis functions, then the smoothed continuous gradient field may be defined as

$$E^* = \sum_i \alpha_i(x, y, z) E_i. \quad (1.25)$$

The polynomial expansion is assumed

$$E_p^* = P^T \mathbf{a}, \quad (1.26)$$

where  $P$  contains the polynomial terms, and  $\mathbf{a}$  is the set of unknown parameters. For example, for two-dimensional quadratic expansion,

$$P = [1, x, y, x^2, xy, y^2]^T. \quad (1.27)$$

To determine the parameters  $\mathbf{a}$  in previous expansion, a fit to the set of highly accurate sampling points in an element patch is performed by minimizing the expression

$$\begin{aligned} F(\mathbf{a}) &= \sum_{i=1}^n (E(x_i, y_i) - E_p^*(x_i, y_i))^2 \\ &= \sum_{i=1}^n (E(x_i, y_i) - P^T(x_i, y_i) \mathbf{a})^2. \end{aligned} \quad (1.28)$$

Here  $(x_i, y_i)$  are coordinates of the group of sampling points, and  $n$  is the total number of sampling points. After minimization of  $F(\mathbf{a})$ , the matrix equation

$$A \mathbf{a} = \mathbf{b}, \quad (1.29)$$

is obtained, where

$$A = \sum_{i=1}^n P(x_i, y_i) P^T(x_i, y_i) \quad \text{and} \quad \mathbf{b} = \sum_{i=1}^n P(x_i, y_i) E(x_i, y_i). \quad (1.30)$$

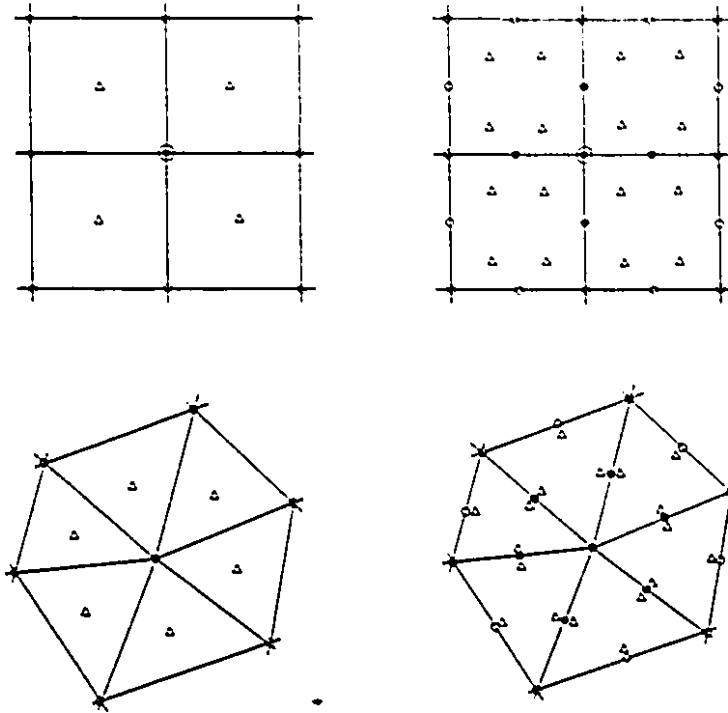


**Figure 1.2.** Computation of superconvergent nodal values for linear and quadratic triangular and rectangular elements. (•) – nodes where derivatives are determined by recovery procedure; (o) – finite element nodes; (Δ) – superconvergent nodes.

It should be noted that  $A$  is the same for all components of  $E_p^*$ , so only one evaluation is necessary. After computing  $a$ , the recovered nodal values of  $E_i$  are calculated simply. Only nodes inside the patch are considered here. If a node is contained in several patches, it is recommended to use the average value. The critical cases occur when the point of interest belongs to a corner element, so the patch contains one or two elements only.

The alternative to this procedure is application of a least squares procedure, and minimization of the functional

$$\begin{aligned}
F(\mathbf{a}) &= \int_{\Omega_S} (E(x,y) - E_p^*(x,y))^2 d\Omega \\
&= \int_{\Omega_S} (E(x,y) - \mathbf{P}^T(x,y)\mathbf{a})^2 d\Omega,
\end{aligned} \tag{1.31}$$

where  $\Omega_S$  is the domain of the element patch. In that case, the matrix  $A$  and source  $\mathbf{b}$  take the following forms:

$$A = \int_{\Omega_S} \mathbf{P}(x,y)\mathbf{P}^T(x,y)d\Omega \quad \text{and} \quad \mathbf{b} = \int_{\Omega_S} \mathbf{P}(x,y)E(x,y)d\Omega. \tag{1.32}$$

Zhu and Zienkiewicz discovered that the application of this procedure does not yield superconvergence of nodal values for quadratic elements though considerable improvement of these results was noted. This phenomenon is still being investigated. For quadratic elements, both quadrilateral and triangular, they found that convergence is two orders higher than normal. The term *ultraconvergence* is suggested for such a convergence.

#### 1.2.4.2 Application of self-equilibrium conditions

This procedure is based on estimating the error and adding it to the original finite element solution. Kelly (1984) first applied the idea of estimating the error from the gradient jump along the element boundaries. This is the error induced by finite element discretization. Application of the self-equilibrium condition which has to be satisfied for each element yields the induced 'equivalent sources'.

The error distribution in an element is expressed using interpolation functions one order higher than that of the finite element solution. That is how a complete representation of the dominant error term is accomplished.

Consider the elasticity problem described by the following equation with corresponding boundary condition:

$$\nabla \cdot (\bar{\epsilon} \nabla \phi) + f = 0, \quad \text{in } \Omega,$$

$$\begin{aligned}\phi &= \bar{\phi} && \text{on } \partial\Omega_D, \\ (\bar{\epsilon} \nabla \phi) \cdot \mathbf{n} &= \bar{q} && \text{on } \partial\Omega_F.\end{aligned}$$

where  $\phi$  is the vector of displacements,  $\bar{\epsilon}$  is the elasticity tensor,  $\sigma = (\bar{\epsilon} \nabla \phi)$  is the stress tensor,  $(\bar{\epsilon} \nabla \phi) \cdot \mathbf{n}$  defines surface tractions and  $f$  is the body force. Let  $\hat{\phi}$  be a finite element approximation of the displacement. Then the residual  $r_i$  for the  $i$ th element is given by

$$r_i = \nabla \cdot (\bar{\epsilon} \nabla \hat{\phi}) + f \quad \text{in } \Omega_i, \quad (1.33)$$

Multiplication by the virtual displacement  $\varphi$  and summing over the all elements yields

$$\begin{aligned}\sum_i \int_{\Omega_i} \nabla \varphi \cdot \bar{\epsilon} \nabla \hat{\phi} d\Omega &= \\ \sum_i \left\{ \int_{\Omega_i} \varphi \cdot f d\Omega - \int_{\Omega_i} \varphi \cdot r_i d\Omega + \int_{\partial\Omega_i} \varphi \cdot (\bar{\epsilon} \nabla \hat{\phi}) \cdot d\Gamma \right\}, & (1.34)\end{aligned}$$

where  $\Omega_i$  and  $\partial\Omega_i$  are the  $i$ th domain and the element boundary, respectively. Since the stresses are not continuous along the element boundaries, the last term in the right-hand side corresponds to traction discontinuities. Let these tractions be viewed as equivalent boundary sources  $\rho_{ij}$ ; then

$$\begin{aligned}\int_{\Omega} \nabla \varphi \cdot \bar{\epsilon} \nabla \hat{\phi} d\Omega &= \int_{\Omega} \varphi \cdot f d\Omega - \int_{\Omega} \varphi \cdot r d\Omega \\ &+ \int_{\partial\Omega} \varphi \cdot \bar{q} d\Gamma + \sum_{ij} \int_{\partial\Omega_{ij}} \varphi \cdot \rho_{ij} \cdot d\Gamma, & (1.35)\end{aligned}$$

where

$$\rho_{ij} = (\hat{\sigma}_i - \hat{\sigma}_j) \cdot \mathbf{n}_i \quad \text{on } \partial\Omega_{ij}, \quad (1.36)$$

$$\rho_{ij} = \hat{\sigma}_i \cdot \mathbf{n}_i - \bar{q} \quad \text{on } \partial\Omega_F. \quad (1.37)$$

The stress obtained by the finite element method is denoted by  $\hat{\sigma}$ .  $\partial\Omega_F$  corresponds to that part of the boundary with prescribed traction  $\bar{q}$ . If the error

of the approximate solution is written as

$$e = \phi - \hat{\phi}, \quad (1.38)$$

then from equations (1.48) and (1.51),

$$\int_{\Omega} \nabla \phi \cdot \bar{\epsilon} \nabla e d\Omega = \int_{\Omega} \phi \cdot r d\Omega - \sum_{ij} \int_{\partial\Omega_{ij}} \phi \cdot \rho_{ij} d\Gamma. \quad (1.39)$$

This equation says that the error  $e$  is the response to the residual  $r_i$  in the element and to the unbalanced tractions  $-\rho_{ij}$  on the element boundary. Now, the finite element method may be applied to solve equation (1.39), and obtain the error  $e$ . The dominant interpolation polynomial used is one degree higher than that for  $\phi$ . Equation (1.39) corresponds to a partial differential equation

$$\nabla \cdot (\bar{\epsilon} \nabla e) + r_i = 0 \quad \text{in } \Omega_i; \quad (1.40)$$

$$(\bar{\epsilon} \nabla e) \cdot \mathbf{n} = -\bar{\rho}_i \quad \text{on } \partial\Omega_i; \quad (1.41)$$

where  $\bar{\rho}_i$  is a portion of  $\rho_{ij}$  corresponding to the  $i$ th element. The resulting finite element equation for the element  $i$  is

$$\mathbf{M}e = f \quad (1.42)$$

with standard finite element coefficient matrices. To find  $e$ , values  $\bar{\rho}_i$  and  $r_i$  are determined so as to satisfy the self-equilibrium conditions. The normal stress jump  $\rho_{ij}$  must satisfy three conditions:

$$\rho_{ij} = \bar{\rho}_i + \bar{\rho}_j \quad (1.43)$$

$$\int_{\Omega_i} r_i d\Omega - \int_{\partial\Omega_i} \bar{\rho}_i d\Gamma = 0, \quad (1.44)$$

$$\int_{\Omega_i} r_i \times (x - x_0) d\Omega - \int_{\partial\Omega_i} \bar{\rho}_i \times (x - x_0) d\Gamma = 0, \quad (1.45)$$

where  $x_0$  is the position of an arbitrary point.

The process of allocating of the traction jump  $\rho$  consists of three stages. In the first stage, initial allocation, the unbalanced traction is divided according to the ratio of distances  $l_i$  and  $l_j$  from the element boundary to the centroid of each element,

$$\bar{\rho}_i = \frac{l_j}{l_i + l_j} \rho_{ij} \quad \bar{\rho}_j = \frac{l_i}{l_i + l_j} \rho_{ij}. \quad (1.46)$$

The second stage is undertaken, so the tractions satisfy the balance of forces. Nodal forces for each node  $F_m = (F_x, F_y)_m$  are first computed according to

$$F = \int_{\Omega_i} \alpha r_i d\Omega - \int_{\partial\Omega_i} \alpha \bar{\rho}_i d\Gamma. \quad (1.47)$$

After that, the corrective nodal forces  $(\Delta F_x, \Delta F_y)_m$  are obtained from the following conditions:

$$\sum_{m=1}^8 (F_x + \Delta F_x)_m = 0 \quad \sum_{m=1}^8 (F_y + \Delta F_y)_m = 0. \quad (1.48)$$

The final step is to correct  $\bar{\rho}$  so as to satisfy the moment equilibrium condition. Since the moment of nodal forces around the centroid does not vanish, corrective forces  $\Delta G_m$  are applied to satisfy the moment equation:

$$\sum_{m=1}^8 (F + \Delta F)_m \times (x_m - x_c) + \sum_{m=1}^8 \Delta G_m \times (x_m - x_c) = 0. \quad (1.49)$$

The source side for the finite element expression is now known, so it is possible to calculate the error on a finite element. From the error, the stress solution can be updated,

$$\sigma = \hat{\sigma} + \Delta\sigma = \hat{\sigma} - \bar{\epsilon} \nabla e. \quad (1.50)$$

Ohtsubo's and Kitamura's experience is that this method improves the solution if the stress does not change too severely with respect to mesh size. A procedure for implementation of the above algorithm is based on a objective function and a particular optimization technique defined in their paper.

### 1.2.5 Function extraction methods

Babuška and Miller (1984b, 1984c, 1984d) presented a generalized theory of postprocessing finite element solutions. They described a general approach to averaging using an integral method with various extraction functions, as well as novel methods for a general region, with reentrant corners treated through an asymptotic expansion of known form. These extractions can be performed on boundary locations as well as in the interior of the domain of interest. The important fact is that extractions do not require a uniform mesh, i.e. there is no mesh regularity pre-condition. They proved that the maximal rate of convergence is the square of the rate of the error in energy norm. Babuška, Izadpanah and Szabo (1984a) and others, as well as Niu and Sheppard (1993) applied the Babuška-Miller ideas to extract stresses for interior of a domain (Babuška, Izadpanah and Szabo (1984a)) and at locations on the boundary (Niu and Sheppard (1993)).

To this group of methods belongs also a procedure based on the convolution method with Bramble-Schatz kernel (Bramble and Schatz (1974)). These kernels, or extraction functions, are recursively defined two-dimensional B-splines. This method is applicable to regions which can be decomposed into a union of rectangles, where the basic integral formula can be decomposed into a sum of analytically solvable integrals. It was extended by Louis (1979) to non-uniform finite element meshes, but the resulting integrals are not analytically solvable and their numerical evaluation increases the computational costs of an already quite expensive method. Some authors (Zienkiewicz and Zhu (1992a)) refer to extraction methods as of limited practical use owing to high cost and

complexity of implementation.

### 1.2.6 Method based on Green's second identity

A new technique (Silvester (1991a)) has recently been added: differentiation based on Green's second identity. It is useful for high precision derivative calculation. If the base region for Green's identity is chosen to be a circle, then for Laplace's equation this method reduces to the Poisson integral method. In essence, this method applies integration by parts to substitute numerical integration, which is a stable process, for numerical differentiation. This new technique is more powerful than the older ones — it can determine derivatives of high order — but it is relatively costly. The method may be classified as belonging to the group of function extraction methods. In the special case of a circle, the exact Green's functions and Poisson kernel functions and their derivatives are used in computation of higher order derivatives.

Start from the classical Poisson integral:

$$\phi_P = \oint_{\partial\Omega} K_{00}(P;Q) \phi_Q dS_Q \quad (1.51)$$

where the Poisson kernel  $K_{00}(P;Q)$  represents the interior normal derivative of the Green's function,

$$K_{00}(P;Q) = \nabla_Q G(P;Q) \cdot \mathbf{l}_{nQ}. \quad (1.52)$$

Here and in the following,  $\mathbf{l}_{nQ}$  is the unit normal vector to  $\partial\Omega$  at the point  $Q \in \partial\Omega$ ;  $G(P;Q)$  is the Green's function appropriate to the region  $\Omega$ . As fully detailed by Kellogg (1967), this formula permits finding the potential  $\phi_P$  at any interior point  $P \in \Omega$ , provided its values are known along the region boundary  $\partial\Omega$ . Application of this method to arbitrarily shaped problem regions  $\Omega_p$  hinges on noting that the integration region  $\Omega$  must be embedded in  $\Omega_p$ ,  $\Omega \subseteq \Omega_p$ , but it

may be of any convenient shape, e.g. a circular disk of radius  $R$  for which the Poisson kernel is known. Further direct differentiation (Mihklin (1970)) of the Poisson integral yields

$$\frac{\partial^{m+n} \phi_P}{\partial x^m \partial y^n} = \oint_{\partial\Omega} \phi_Q K_{mn}(P;Q) dS_Q, \quad (1.53)$$

where the  $m, n$ th extended Poisson kernel is given by

$$K_{mn}(P;Q) = \frac{\partial^{m+n}}{\partial x^m \partial y^n} \nabla_Q G(P;Q) \cdot \mathbf{1}_{nQ}. \quad (1.54)$$

Any desired derivative of the potential  $\phi$  is thus obtainable by integration along the contour  $\partial\Omega$ , even in finite element solutions where the approximate potential may not possess a derivative of degree  $m, n$ . The derivatives often have higher accuracy than the approximate potential values, the integration process having contributed to error averaging.

Computation of the  $m, n$ th derivative requires a contour integration, which typically involves a  $q$ -point quadrature. Achieving quadrature precision of degree  $k$  in  $D$ -dimensional problems requires approximately  $O(k^D)$  quadrature nodes. At each quadrature node the approximate potential  $\phi_P$  must be evaluated, along with the appropriate Poisson kernel. The potential evaluation requires approximately  $p^{D+1}$  multiplicative operations on a  $D$ -dimensional finite element. Evaluation of a Poisson kernel amounts to the evaluation of a few transcendents, mainly logarithms and trigonometric functions. The number  $t$  of operations, typically a few dozen multiplications, varies a little with the indices  $m, n$  but it is nearly independent of  $p$ . Thus the cost of finding a derivative value is  $O(k^D p^{D+1} t)$ . Typically,  $k = 10$ , so the cost of differentiation in this fashion is high but the accuracy is high also.

The main advantages of this method are stability and accuracy, and the ability to compute derivatives of high order. In contrast to other integral methods, kernels and their derivatives are known analytically.

### 1.3 The objective of this thesis

This research contributes to the field of post-processing of numerical approximate solutions such as finite element solutions. The thesis extends the methodology based on Green's second identity, to calculate derivatives from finite element solutions of Poisson and Helmholtz equations in two dimensions. For Laplace's equation, derivatives are also obtained by differentiation of the base solution in an axisymmetric coordinate system. The objective includes comparing the new method with existing methodologies for derivative computation, and giving recommendations on the circumstances in which the several methods may best find use.

The new method can be applied in all areas where precise derivatives are needed, e.g., in magnetic material modeling; in high-voltage engineering to find maximum field or its derivative; in force and torque calculation (first and second order derivative of potential); in electron ballistics and magnetic resonance imaging design (magnetic field uniformity criterion), etc.

#### 1.3.1 Claims of originality

This thesis generalizes the Silvester differentiation method, originally restricted to harmonic functions in the interior of a circular disk, to more general elliptic differential operators and a wider range of base regions. It makes the following original contributions:

- (a) A general procedure for computation of high order derivatives from approximate solutions of the Poisson and Helmholtz partial differential equations is described and applied. The method is based on Green's second identity;
- (b) Derivatives of Green's functions and generalized Poisson kernel functions of Laplacian differential operator are generated for new elementary shapes:

- rectangle, sector of circle and sector of ring. The library of kernels for a circle is extended with expressions for the point on the boundary and a new, simpler, formula for the  $m, n$ th order derivative of the Poisson kernel;
- (c) Generalized Poisson kernels for the Helmholtz differential operator in the case of circle as a base region are derived, expressing the Green's function as a sum of Bessel functions. Using this method it is possible to compute derivatives of any order;
  - (d) A differentiation procedure for axisymmetric problems described by Laplace's equation is derived. The method uses fundamental solutions for a torus and a sphere on the axis of symmetry;
  - (e) The one-dimensional smoothing method of Zhu and Zienkiewicz is generalized to two and three dimensions.

#### 1.4 Outline of the thesis

This thesis is organized in seven chapters as follows:

Chapter 2 gives a brief description of the proposed methodology. Fundamental solutions for the Laplace, Poisson and Helmholtz equations in two dimensions are presented, as well as the solution of Laplace's equation in the  $r$ - $z$  coordinate system. Green's second identity and the differentiation formula based on it are derived and discussed, together with the definition of Green's functions and corresponding Poisson kernels. This chapter closes with a discussion of implementation problems of the proposed methodology.

Generation of Green's functions and Poisson kernels and their derivatives are presented in Chapter 3. Various methods for construction of Green's functions for the Laplacian operator ( $\nabla^2$ ) for different region shapes and the Helmholtz operator ( $\nabla^2 + \kappa^2$ ) for a circle as the elementary region are given. Applicability of various forms of Green's functions, as well as methods of their construction, are discussed. This chapter also deals with differentiation of base solutions of boundary value problems, in cases where Green's second identity is

not used.

Validation of the method is given in Chapter 4. Experiments with analytically known functions for various kinds of base regions and problems are presented. Error sensitivity was analyzed with particular care. The differentiation formulae were tested using random error sensitivity analysis for all four base regions. From these results conclusions were drawn about behavior and numerical efficiency and characteristics of the new method.

Chapter 5 describes the treatment of singular and nearly singular integrals. Singular curvilinear and surface integrals are evaluated using the specialized quadrature, based on the finite part integration concept. The quadrature formulae were derived using Paget's approach. The evaluation of nearly singular curvilinear integrals using various methods is discussed.

Chapter 6 generalizes the gradient recovery procedure originally proposed by Zhu and Zienkiewicz to two and three dimensional problems. This is an element-wise method based on local smoothing which uses values of gradients at superconvergent points to extrapolate results.

The results of applications to finite element approximations are given in Chapter 7. Computed results were compared to analytical solutions. Results were also compared to some of the existing differentiation methods. Efficiency of the new methods is investigated.

Chapter 8 gives a summary of characteristics of the new methods presented in this dissertation. Computational performance and effectiveness (advantages and disadvantages) of the differentiation of finite element approximation based on fundamental solution of boundary value problems are discussed. Recommendations are made for the use of various differentiation methods, with a comparison of characteristics, generalization and possible extensions of the new method.

## CHAPTER 2

### Formulation of the proposed methodology

This chapter is intended to cover the mathematical fundamentals used in formulation of the methodologies proposed in this thesis. The topics covered include: definition of the problem, including fundamental solutions, Green's second identity for the Laplace and Helmholtz operators, the basic differentiation formula and the problems involved in application of the generalized Poisson integral method.

The chapter begins with definitions and derivation of the basic formulas used in this thesis. It continues with formulation of the proposed technique. Once having established the fundamentals, attention turns to difficulties in implementation of the method.

#### 2.1 Fundamental solution of boundary value problems

In the derivations and analyses developed in this thesis, only the first boundary value problem (the Dirichlet problem) is considered. The problem is to find the function  $\phi(x, y)$ , satisfying the partial differential equation

$$\mathfrak{D}\phi(x, y) = -g \quad \text{in } \Omega, \quad (2.1)$$

subject to the boundary conditions

$$\phi(x, y) = f(x, y) \quad \text{on } \partial\Omega, \quad (2.2)$$

where  $\mathfrak{D}$  is a differential operator, the Laplacian or Helmholtz's operator.

Generally, fundamental solutions are obtained by separation of variables. In this section, they are derived for harmonic functions inside a circular disc and a circular ring for two-dimensional problems, and torus and a sphere in axisymmetric coordinate system. The expressions for fundamental solutions are used to derive the influence function of a point source, i.e. to find the Green's function.

### 2.1.1 Application of Fourier series expansion for a circular disk

The potential inside a circle can be computed from known values on the boundary, using the formula

$$\phi(r_P, \theta_P) = \frac{a_0}{2} + \sum_{i=1}^{\infty} \left(\frac{r_P}{R}\right)^i [a_i \cos(i\theta) + b_i \sin(i\theta)] \quad (2.3)$$

where  $a_i$  and  $b_i$  are Fourier coefficients, which can be derived from known boundary values of the harmonic function  $f(\theta)$  using

$$a_i = \frac{1}{2\pi} \int_{\partial\Omega} f(\theta) \cos(i\theta) d\theta \quad (2.4)$$

$$b_i = \frac{1}{2\pi} \int_{\partial\Omega} f(\theta) \sin(i\theta) d\theta \quad (2.5)$$

The formula (2.3) may be derived using by separation of variables, by assuming a function of the form  $\phi(r, \theta)$ :

$$\phi(r, \theta) = R(r)\Theta(\theta). \quad (2.6)$$

Then the Laplace's equation in polar coordinates reduces to two simple differential equations with known solutions.

The formula (2.3) is valid for  $r \leq R$ , and in fact it is equivalent to the Poisson integral. The advantage of this method is that (2.3) is regular for

$$r_P = R.$$

A point source  $q$  is placed at  $Q(r_Q, \theta_Q)$ , a point inside the circle of radius  $R$  with the boundary potential fixed at zero, is considered. The potential at an arbitrary point  $P(r_P, \theta_P)$  has to be determined, the solution is assumed to have the same form as (2.3), which corresponds to the influence of the boundary, plus the influence of  $q$  if there is no boundary:

$$\phi(r_P, \theta_P) = -\frac{q}{2\pi} \log s_Q + \frac{A_0}{2} + \sum_{n=1}^{\infty} r_P^n (A_n \cos n\theta_P + B_n \sin n\theta_P), \quad (2.7)$$

where  $s_Q$  is the distance between  $P$  and  $Q$ , given by

$$s_Q^2 = r_P^2 + r_Q^2 - 2r_P r_Q \cos(\theta_P - \theta_Q). \quad (2.8)$$

The logarithmic term may be expanded in a series, as follows:

$$-\log s_Q = \begin{cases} \sum_{n=1}^{\infty} \left(\frac{r_P}{r_Q}\right)^n \frac{\cos n(\theta_P - \theta_Q)}{n} - \log r_Q & \text{for } r_Q > r_P \\ \sum_{n=1}^{\infty} \left(\frac{r_Q}{r_P}\right)^n \frac{\cos n(\theta_P - \theta_Q)}{n} - \log r_P & \text{for } r_Q < r_P. \end{cases} \quad (2.9)$$

Using the condition that  $\phi(R, \theta) = 0$ , and after equating the coefficients of  $\sin n\theta_P$  and  $\cos n\theta_P$ ,  $A_n$  and  $B_n$  can be found:

$$A_n = \frac{1}{2\pi n} \left(\frac{r_P}{R}\right)^n \cos n\theta_Q \quad (2.10)$$

$$B_n = \frac{1}{2\pi n} \left(\frac{r_P}{R}\right)^n \sin n\theta_Q. \quad (2.11)$$

Then the potential at the point  $P$  is

$$\phi(r_P, \theta_P) = -\frac{q}{2\pi} \log s_Q - \frac{q}{2\pi} \sum_{n=1}^{\infty} \left(\frac{r_P r_Q}{R}\right)^n \frac{\cos n(\theta_P - \theta_Q)}{n}. \quad (2.12)$$

After the application of expansion (2.9), the following is obtained:

$$\phi(r_P, \theta_P) = -\frac{q}{2\pi} \log \frac{R s_Q}{r_Q} + \frac{q}{2\pi} \log \sqrt{r_P^2 + \frac{R^4}{r_Q^2} - 2r_P \frac{R^2}{r_Q} \cos(\theta_P - \theta_Q)}. \quad (2.13)$$

Normal (radial) differentiation of the influence function of equation (2.13) with respect to  $r_Q$ , on the boundary, will give the Poisson kernel briefly described in Chapter 1.

### 2.1.2 Fundamental solution for a circular ring

The influence of a unit charge placed inside the circular ring with the boundary at zero potential will be derived in this subsection.

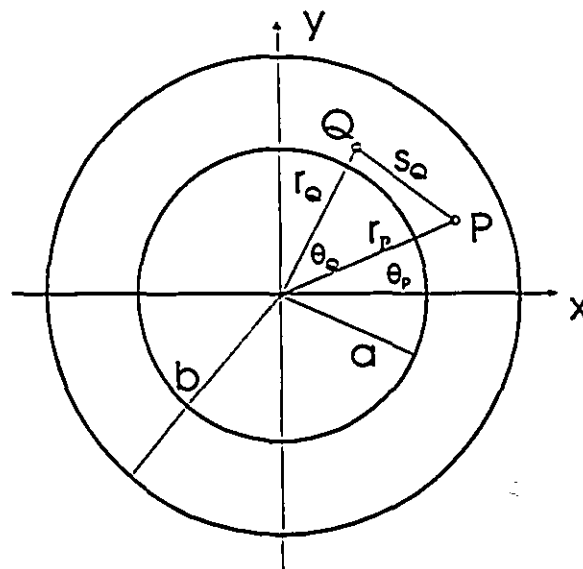


**Figure 2.1.** The geometry of a circular ring with inner and outer radii  $a$  and  $b$ , with the source placed at point  $Q$  and the observation point  $P$ .

The source  $q$  is located at point  $Q$  ( $r_Q, \theta_Q$ ). The potential at the observation point  $P$  is computed by assuming a solution of the form

$$\begin{aligned} \phi(r_P, \theta_P) = & -\frac{q}{2\pi} \log s_Q + \frac{A_0}{2} + \frac{B_0}{2} \log r_P \\ & + \sum_{n=1}^{\infty} \left\{ A_n r_P^n + \frac{B_n}{r_P^n} \right\} \cos n(\theta_P - \theta_Q), \end{aligned} \quad (2.14)$$

where the distance  $s_Q$  is given by

$$s_Q^2 = r_P^2 + r_Q^2 - 2r_P r_Q \cos(\theta_P - \theta_Q). \quad (2.15)$$

The first term in equation (2.14) represents a free space solution, while the influence of the boundaries is given by the remainder of the expression (2.14). Coefficients  $A_n$  and  $B_n$  are calculated using the condition that

$$\phi(a, \theta_P) = \phi(b, \theta_P) = 0 \quad \text{for } 0 \leq \theta_P \leq 2\pi. \quad (2.16)$$

Using the expansion (2.9), the conditions (2.16) may be written as

$$\begin{aligned} \phi(a, \theta_P) = 0 = & \frac{q}{2\pi} \sum_{n=1}^{\infty} \left( \frac{a}{r_Q} \right)^n \frac{\cos n(\theta_P - \theta_Q)}{n} - \frac{q}{2\pi} \log r_Q \\ & + \frac{A_0}{2} + \frac{B_0}{2} \log a + \sum_{n=1}^{\infty} \left\{ A_n a^n + \frac{B_n}{a^n} \right\} \cos n(\theta_P - \theta_Q) \end{aligned} \quad (2.17)$$

and

$$\begin{aligned} \phi(b, \theta_P) = 0 = & \frac{q}{2\pi} \sum_{n=1}^{\infty} \left( \frac{r_Q}{b} \right)^n \frac{\cos n(\theta_P - \theta_Q)}{n} - \frac{q}{2\pi} \log b \\ & + \frac{A_0}{2} + \frac{B_0}{2} \log b + \sum_{n=1}^{\infty} \left\{ A_n b^n + \frac{B_n}{b^n} \right\} \cos n(\theta_P - \theta_Q). \end{aligned} \quad (2.18)$$

By equating the common terms, the following is obtained:

$$A_n a^n + \frac{B_n}{a^n} = -\frac{q}{2\pi n} \frac{a^n}{r_Q^n} \quad (2.19)$$

$$A_n b^n + \frac{B_n}{b^n} = -\frac{q}{2\pi n} \frac{r_Q^n}{b^n}. \quad (2.20)$$

The coefficients for  $n > 0$  can be readily obtained:

$$A_n = -\frac{q}{2\pi n} \frac{1}{r_Q^n} \frac{r_Q^{2n} - a^{2n}}{b^{2n} - a^{2n}} \quad (2.21)$$

$$B_n = -\frac{q}{2\pi n} \frac{a^{2n}}{r_Q^n} \frac{b^{2n} - r_Q^{2n}}{b^{2n} - a^{2n}}. \quad (2.22)$$

It is easy to prove that the leading coefficients are

$$A_0 = -\frac{q}{\pi} \frac{\log \frac{b}{r_Q}}{\log \frac{b}{a}} \log a + \frac{q}{\pi} \log r_Q \quad (2.23)$$

$$B_0 = \frac{q}{\pi} \frac{\log \frac{b}{r_Q}}{\log \frac{b}{a}}. \quad (2.24)$$

Then, the final expression for potential is

$$\begin{aligned} \phi(r_P, \theta_P) = & -\frac{q}{2\pi} \log s_Q + \frac{q}{2\pi} \frac{\log \frac{b}{r_Q}}{\log \frac{b}{a}} \log \frac{r_P}{a} + \frac{q}{2\pi} \log r_Q \\ & - \frac{q}{2\pi} \sum_{n=1}^{\infty} \left\{ \frac{r_Q^{2n} - a^{2n}}{b^{2n} - a^{2n}} \frac{r_P^n}{r_Q^n} + \frac{b^{2n} - r_Q^{2n}}{b^{2n} - a^{2n}} \frac{a^{2n}}{r_P^n r_Q^n} \right\} \frac{\cos n(\theta_P - \theta_Q)}{n}. \end{aligned} \quad (2.25)$$

This expression will be used in Chapter 3 for derivation of the Green's function for sector of a circular ring. The solution of the boundary value problem for a ring may be found in textbooks (Tyn Myint (1973), Mikhlin (1967), Budak, Samarskii and Tikhonov (1964)).

### 2.1.3 Harmonic functions in axisymmetric coordinates

The solution of the Dirichlet problem for a torus and a sphere with the center on the  $z$ -axis is used in the differentiation procedure. In this sub-section the fundamental solution is derived.

#### 2.1.3.1 Torus

Consider the torus of cross-sectional radius  $a$ , and radius  $l$  in  $r$ - $z$  coordinate system. The geometry with all distances noted is given in Figure 2.2.

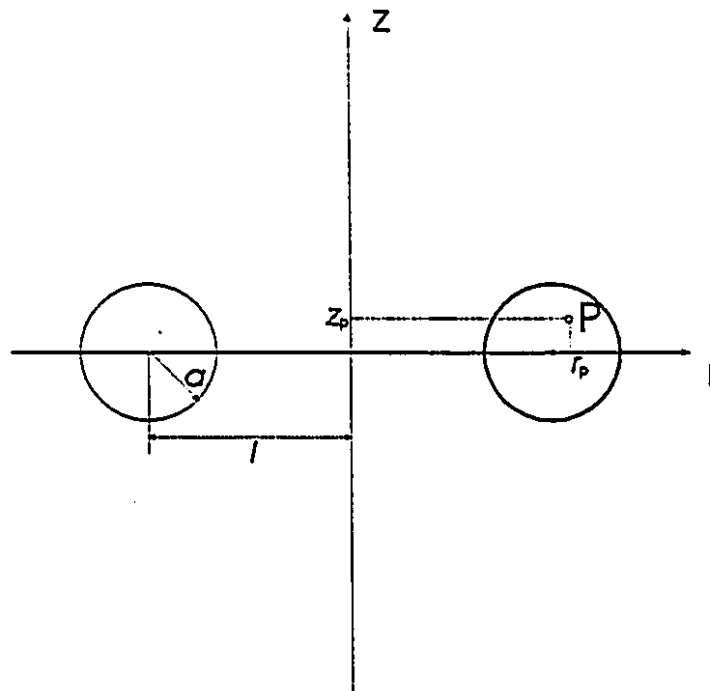


Figure 2.2. Geometry of the torus

To obtain the fundamental solution, toroidal coordinates may be used. Toroidal coordinates  $(\alpha, \beta)$ ,  $0 \leq \alpha < \infty$  and  $-\pi < \beta \leq \pi$ , are related to cylindrical

coordinates  $(r, z)$  by

$$r = \frac{c \sinh \alpha}{\cosh \alpha - \cos \beta} \quad z = \frac{c \sin \beta}{\cosh \alpha - \cos \beta}. \quad (2.26)$$

If the torus is defined by  $\alpha = \alpha_0$ , then

$$\begin{aligned} c \coth \alpha_0 &= l & \frac{c}{\sinh \alpha_0} &= a \\ c &= \sqrt{l^2 - a^2} & \cosh \alpha_0 &= \frac{l}{a}. \end{aligned} \quad (2.27)$$

Conversion from cylindrical to toroidal coordinates may be done using the following relationships:

$$\cos \beta = \frac{z^2 + r^2 - c^2}{\sqrt{((r-c)^2 + z^2)((r+c)^2 + z^2)}}, \quad (2.28)$$

$$\sin \beta = \frac{2cz}{\sqrt{((r-c)^2 + z^2)((r+c)^2 + z^2)}}, \quad (2.29)$$

$$\cosh \alpha = \frac{z^2 + r^2 + c^2}{\sqrt{((r-c)^2 + z^2)((r+c)^2 + z^2)}}, \quad (2.30)$$

$$\sinh \alpha = \frac{2cr}{\sqrt{((r-c)^2 + z^2)((r+c)^2 + z^2)}}, \quad (2.31)$$

$$\chi^2(\alpha, \beta) = \cosh \alpha - \cos \beta = \frac{2c^2}{\sqrt{((r-c)^2 + z^2)((r+c)^2 + z^2)}}. \quad (2.32)$$

It is supposed that the fundamental solution of the Laplace's equation has the following form (Lebedev (1965)):

$$\phi(\alpha, \beta) = \sqrt{2 \cosh \alpha - 2 \cos \beta} \sum_{n=0}^{\infty} \{M_n \cos(n\beta) + N_n \sin(n\beta)\} Q_{n-1/2}(\cosh \alpha) \quad (2.33)$$

where  $Q_{n-1/2}(\cosh \alpha)$  are Legendre functions of second kind of non-integral order.

If  $f(\beta) = \phi(\alpha_0, \beta)$  are given potential values on the boundary, then Equation (2.33) becomes

$$f(\beta) = \sqrt{2 \cosh \alpha_0 - 2 \cos \beta} \sum_{n=0}^{\infty} \{M_n \cos(n\beta) + N_n \sin(n\beta)\} Q_{n-1/2}(\cosh \alpha_0). \quad (2.34)$$

After multiplication, first by  $\cos(n\beta)$ , and after that by  $\sin(n\beta)$  and integrating, the following is obtained:

$$\frac{f(\beta)}{\sqrt{2 \cosh \alpha_0 - 2 \cos \beta}} = \sum_{n=0}^{\infty} \{M_n \cos(n\beta) + N_n \sin(n\beta)\} Q_{n-1/2}(\cosh \alpha_0) \quad (2.35)$$

Then, the coefficients  $M_n$  and  $N_n$  emerge as

$$M_0 = \frac{1}{2\sqrt{2\pi} Q_{-1/2}(\cosh \alpha_0)} \int_{-\pi}^{+\pi} \frac{f(\beta)}{\sqrt{2 \cosh \alpha_0 - 2 \cos \beta}} d\beta, \quad (2.36)$$

$$M_n = \frac{1}{\sqrt{2\pi} Q_{n-1/2}(\cosh \alpha_0)} \int_{-\pi}^{+\pi} \frac{f(\beta) \cos(n\beta)}{\sqrt{2 \cosh \alpha_0 - 2 \cos \beta}} d\beta, \quad (2.37)$$

$$N_n = \frac{1}{\sqrt{2\pi} Q_{n-1/2}(\cosh \alpha_0)} \int_{-\pi}^{+\pi} \frac{f(\beta) \sin(n\beta)}{\sqrt{2 \cosh \alpha_0 - 2 \cos \beta}} d\beta. \quad (2.38)$$

The final expression is:

$$\phi(\alpha, \beta) = \sqrt{2 \cosh \alpha - 2 \cos \beta} \sum_{n=0}^{\infty} \{M_n \cos(n\beta) + N_n \sin(n\beta)\} Q_{n-1/2}(\cosh \alpha) \quad (2.39)$$

By substituting

$$a_n = \frac{M_n}{\sqrt{2}} \quad \text{and} \quad b_n = \frac{N_n}{\sqrt{2}}, \quad (2.40)$$

Equation (2.39) may be transformed into

$$\phi(\alpha, \beta) = \chi(\alpha, \beta) \sum_{n=0}^{\infty} \{a_n \cos(n\beta) + b_n \sin(n\beta)\} Q_{n-1/2}(\cosh \alpha). \quad (2.41)$$

This is the base formula to be differentiated in order to obtain derivatives from an approximate solution.

### 2.1.3.2 Sphere with the center on $z$ axis

The geometry of a sphere in  $r-z$  coordinates, with the center on the  $z$ -axis is shown in Figure 2.3. The radius of the sphere is  $R$ . The problem is to find the potential inside the sphere if its values on the boundary are known.

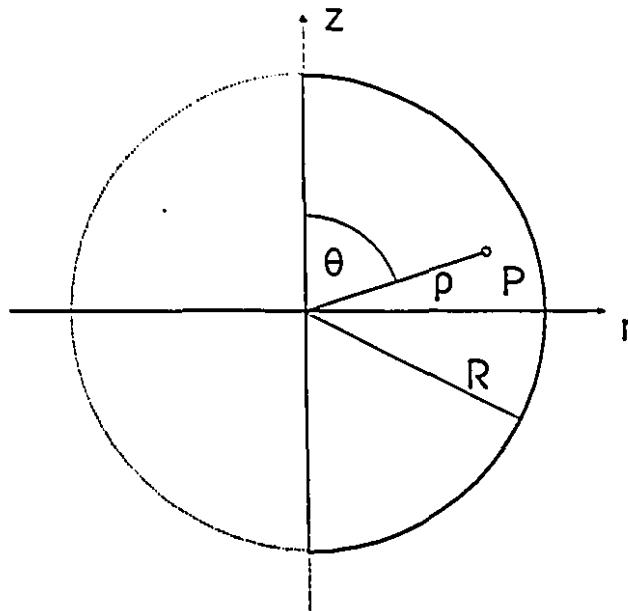


*Figure 2.3.* Geometry of the sphere with a center on the  $z$ -axis.

Suppose that the known potential on the boundary of a sphere of radius  $R$  has the form (Lebedev (1965))

$$f(\theta) = \sum_{n=0}^{\infty} f_n P_n(\cos \theta), \quad 0 \leq \theta \leq \pi \quad (2.42)$$

where  $P_n$  are Legendre functions of  $n^{\text{th}}$  order. Then the coefficients  $f_n$  are

$$f_n = (n+1) \int_0^\pi f(\theta) P_n(\cos \theta) \sin \theta d\theta. \quad (2.43)$$

The potential inside the sphere may be expressed as

$$\phi(\rho, \theta) = \sum_{n=0}^{\infty} f_n \left(\frac{\rho}{R}\right)^n P_n(\cos \theta). \quad (2.44)$$

Equation (2.44) is the expression to be differentiated and used in derivative computation.

## 2.2 Mathematical background of the differentiation method based on Green's second identity

Like its earlier counterpart restricted to harmonic potentials (Silvester (1991a)), the method developed in this thesis is based on Green's second identity. To find derivatives at some point  $P$  the potential problem is restated in integral form, for a region in the neighborhood of  $P$ . An integration by parts then transfers the differentiation operator from the approximate solution (which is prone to numerical instability) to the Green's function, which is analytically known and can therefore be differentiated without error. No numerical differentiation of the approximate solution  $\phi$  is ever required, only integration.

### 2.2.1 Green's second identity

For two sufficiently differentiable functions  $\phi$  and  $\psi$  in a simply connected space region  $\Omega$  with boundary  $\partial\Omega$ , Green's second identity reads

$$\int_{\Omega} (\phi \nabla^2 \psi - \psi \nabla^2 \phi) d\Omega = \oint_{\partial\Omega} (\phi \nabla \psi - \psi \nabla \phi) d\Gamma. \quad (2.45)$$

Let  $\phi$  be some function of interest, and let  $\psi = G(P;Q)$ , where  $G(P;Q)$  is the Green's function for the simply connected region  $\Omega$  with boundary  $\partial\Omega$ , defined for the Laplacian operator by:

$$\begin{aligned} \nabla^2 [G(P;Q)] &= -\delta(P;Q) && \text{in } \Omega \\ G(P;Q) &= 0 && \text{on } \partial\Omega. \end{aligned} \quad (2.46)$$

Then (2.45) becomes

$$\phi_P = - \int_{\Omega} G(P;Q) \nabla_Q^2 \phi d\Omega_Q - \oint_{\partial\Omega} \phi(Q) \nabla_Q G(P;Q) d\Gamma_Q. \quad (2.47)$$

This expression is well established in potential theory (Kellogg (1967), Sneddon (1957)). The subscript  $Q$  is used as a reminder that the integral and differential operators refer to coordinates of the source point  $Q$ .

If a function  $\phi$  is the solution of a boundary-value problem described by the Poisson equation

$$\nabla_Q^2 \phi = -g(Q), \quad Q \in \Omega, \quad (2.48)$$

subject to boundary conditions that render the solution unique, then Green's identity takes the form

$$\phi_P = \int_{\Omega} G(P;Q) g(Q) d\Omega_Q - \oint_{\partial\Omega} \phi_Q \nabla_Q G(P;Q) d\Gamma_Q \quad (2.49)$$

or

$$\phi_P = \int_{\Omega} G(P;Q) g(Q) d\Omega_Q - \oint_{\partial\Omega} K_{00}(P;Q) \phi_Q d\Gamma_Q \quad (2.50)$$

where

$$K_{00}(P;Q) = \mathbf{1}_{nQ} \cdot \nabla_Q G(P;Q). \quad (2.51)$$

Here  $\mathbf{1}_{nQ}$  denotes the outward normal derivative to the boundary  $\partial\Omega$  at  $Q \in \partial\Omega$ . Derivatives of  $\phi_P$  are then formally

$$\begin{aligned} \frac{\partial^{m+n}}{\partial x^m \partial y^n} \phi_P &= \frac{\partial^{m+n}}{\partial x^m \partial y^n} \int_{\Omega} G(P;Q) g(Q) d\Omega_Q \\ &\quad - \oint_{\partial\Omega} K_{mn}(P;Q) \phi_Q d\Gamma_Q. \end{aligned} \quad (2.52)$$

with

$$K_{mn}(P;Q) = \frac{\partial^{m+n}}{\partial x^m \partial y^n} \nabla_Q G(P;Q) \cdot \mathbf{1}_{nQ}. \quad (2.53)$$

The integration and differentiation operations have been interchanged in the boundary integral term. This is admissible because the integral is convergent at all interior points  $P$ . Derivatives of any order can be expressed this way. Differentiation of the surface integral term is treated separately in the following chapter. It needs special treatment, since the Green's function is singular at  $P = Q$ . The formulas for differentiation of some specific integrals will be derived analytically. For convenience, equation (2.52) is rewritten in the following form:

$$\frac{\partial^{m+n}}{\partial x^m \partial y^n} \phi_P = \int_{\Omega} J_{mn}(P;Q) g(Q) d\Omega_Q - \oint_{\partial\Omega} K_{mn}(P;Q) \phi_Q d\Gamma_Q. \quad (2.54)$$

It is convenient to work with a region  $\Omega$  of simple shape embedded within the problem region  $\Omega_0$ , rather than with the original problem region itself. The development in the following chapter will focus on two-dimensional problems, with  $\Omega$  being a circle, rectangle, sector of a circle and sector of a ring. If the simply-shaped region  $\Omega$  is a circular disc of radius  $R$ , and if  $P$  is some interior point of  $\Omega$ , the appropriate Green's function is (Morse and Feshbach (1953), Courant and Hilbert (1953))

$$G(P;Q) = -\frac{1}{2\pi} \log \frac{R s_Q}{r_Q s_I}, \quad (2.55)$$

and the Poisson kernel function  $K_{00}(P;Q)$  is

$$K_{00}(P;Q) = -\frac{1}{2\pi r_Q} \frac{r_Q^2 - r_P^2}{s_Q^2} \quad (r_Q = R). \quad (2.56)$$

Here  $s_Q$  is the distance between the observation point  $P(r_P, \theta_P)$  and the source point  $Q(r_Q, \theta_Q)$ , and  $s_I$  represents the distance from  $P$  to point  $I(R^2/r_Q, \theta_Q)$  image of  $Q$  with respect to a circle.

If  $\phi(x, y)$  is harmonic in  $\Omega$ , the first integral on the right of Equation (2.52) vanishes and the potential  $\phi_P$  is given by the remaining contour integral, the Poisson integral. This special case has already been treated in detail (Silvester (1991 a)). Because differentiation proceeds in the coordinates of  $P$ , it affects the Poisson kernel but not the potential  $\phi_Q$ . Thus

$$\frac{\partial^{m+n}}{\partial x^m \partial y^n} \phi_P = - \oint_{\partial\Omega} K_{mn}(P;Q) \phi_Q dS_Q. \quad (2.57)$$

An extensive catalog of the necessary kernel functions  $K_{mn}(P;Q)$  has been published by Silvester (1991 b).

### 2.2.2 Generalization to Helmholtz operator ( $\nabla^2 + \kappa^2$ )

Consider a Dirichlet problem described by the Helmholtz equation, subject to appropriate boundary conditions:

$$\mathfrak{D}\phi = (\nabla^2 + \kappa^2)\phi = -g \quad \text{in } \Omega \quad (2.58)$$

$$\phi = f \quad \text{on } \partial\Omega. \quad (2.59)$$

The Green's function  $G(P;Q)$  for the operator  $\mathfrak{D}$  is defined by

$$\begin{aligned} \mathfrak{D}[G(P;Q)] &= -\delta(P;Q) && \text{in } \Omega \\ G(P;Q) &= 0 && \text{on } \partial\Omega. \end{aligned} \quad (2.60)$$

Multiplication by  $G(P;Q)$  of both sides of the equation (2.58), followed by integration gives

$$\iint_{\Omega} G(P;Q) \mathfrak{D}[\phi_Q] d\Omega_Q = \iint_{\Omega} G(P;Q) g_Q d\Omega_Q \quad (2.61)$$

Let Green's second identity be applied to the left side,

$$\iint_{\Omega} \{ \mathfrak{D}[G(P;Q)] \phi_Q - G(P;Q) g_Q \} d\Omega_Q = \quad (2.62)$$

$$\oint_{\partial\Omega} \left\{ \frac{\partial G(P;Q)}{\partial n_Q} \phi_Q - G(P;Q) \frac{\partial \phi_Q}{\partial n} \right\} d\Gamma_Q,$$

then, since a property of the Green's function is

$$\iint_{\Omega} \mathfrak{D}[G(P;Q)] \phi_Q d\Omega_Q = -\phi_P, \quad (2.63)$$

the final expression is

$$\phi_P = \iint_{\Omega} G(P;Q) g_Q d\Omega_Q - \oint_{\partial\Omega} K(P;Q) f_Q d\Gamma_Q. \quad (2.64)$$

This expression is now used to effect high-accuracy derivative computation from a numerical approximation method. Differentiating (2.64) under the integral sign, if  $G(P,Q)$  does not have a strong singularity, an expression like (2.54) is obtained:

$$\frac{\partial^{m+n}}{\partial^m x \partial^n y} \phi_P = \iint_{\Omega} \frac{\partial^{m+n} G(P;Q)}{\partial^m x \partial^n y} g_Q d\Omega_Q - \oint_{\partial\Omega} \frac{\partial^{m+n} K(P;Q)}{\partial^m x \partial^n y} f_Q d\Gamma_Q. \quad (2.65)$$

The derivative of  $\phi$  is thus obtained by differentiating the Green's function — a stable process, since this function is known analytically — and by integrating the approximate solution numerically. Thus, again the notoriously error-prone process of numerical differentiation has been replaced by numerical integration, which is well known to be much more stable.

### 2.2.3 Formulations for the Helmholtz equation

In approximate derivative computation for the Helmholtz equation, two different procedures are available:

- (a) rewriting the Helmholtz equation to resemble the Poisson equation,
- (b) treating it analogously to Laplace's equation, but with an appropriate Green's function.

Case (a) will be treated first. The inhomogeneous Helmholtz equation can be rewritten by transposing the  $\kappa^2\phi$  term to the right:

$$\nabla^2 \phi = -(g + \kappa^2 \phi) \quad (2.66)$$

This reformulation does not, contrary to appearances, put an unknown quantity on the right. It is supposed from the outset that the Helmholtz equation has already been solved (approximately), so that  $\phi$  is already known as accurately as it ever will be. Specializing the above version of Green's second identity (2.45) to this case,

$$\phi_P = \iint_{\Omega} G_L(P;Q)(g_Q + \kappa^2 \phi_Q) d\Omega_Q - \oint_{\partial\Omega} K_L(P;Q)\phi_Q d\Gamma_Q. \quad (2.67)$$

Here  $G_L(P;Q)$  and  $K_L(P;Q)$  are the Green's function of the Laplacian operator and the Poisson kernel function, respectively. In general, for the general  $m, n^{\text{th}}$

derivative of  $\phi$ ,

$$\frac{\partial^{m+n}}{\partial^m x \partial^n y} \phi_P = \iint_{\Omega} G_{Lmn}(P;Q) (g_Q + \kappa^2 \phi_Q) d\Omega_Q - \oint_{\partial\Omega} K_{Lmn}(P;Q) \phi_Q d\Gamma_Q. \quad (2.68)$$

where

$$K_{Lmn}(P;Q) = \frac{\partial^{m+n}}{\partial^m x \partial^n y} K_L(P;Q) \quad (2.69)$$

and  $G_{Lmn}(P;Q)$  will be defined in the following chapter.

The second approach is to use the Green's function for the Helmholtz operator  $G_H$  (Tyn Myint (1973)). Analogously to the Laplace's equation problem, the  $m, n^{\text{th}}$  derivative is now given by

$$\frac{\partial^{m+n}}{\partial^m x \partial^n y} \phi_P = \iint_{\Omega} G_{Hmn}(P;Q) g_Q d\Omega_Q - \oint_{\partial\Omega} K_{Hmn}(P;Q) \phi_Q d\Gamma_Q. \quad (2.70)$$

where the generalized kernels are defined similarly, by

$$G_{Hmn}(P;Q) = \frac{\partial^{m+n}}{\partial^m x \partial^n y} G_H(P;Q), \quad (2.71)$$

$$K_{Hmn}(P;Q) = \frac{\partial^{m+n}}{\partial^m x \partial^n y} K_H(P;Q). \quad (2.72)$$

Expression (2.71) is valid only if  $G_{Hmn}(P;Q)$  has a non-singular form. In the homogeneous case ( $g = 0$ ), only the boundary integral needs to be evaluated,

$$\frac{\partial^{m+n}}{\partial^m x \partial^n y} \phi_P = - \oint_{\partial\Omega} K_{Hmn}(P;Q) \phi_Q d\Gamma_Q. \quad (2.73)$$

Using this formulation, derivatives of any order may be computed. This contrasts with the first formulation where, for good theoretical reasons, only the first two orders of derivative are available. Because the surface integral term has disappeared, far fewer integration points will be required for comparable accuracy, so computing times, accuracy, or both, can be expected to improve.

### 2.3 Problems in implementation of the modified Poisson integral method

Three principal groups of problems need to be solved, before applying these methods to approximate results of finite element analysis:

- Derivation of Green's functions, generalized Poisson kernels and their derivatives. Also, generation of expressions for differentiating the fundamental solution of the boundary value problems based on separation of variables. Doing this manually is a very difficult task, even to find the first and second order derivatives. With the help of symbolic packages like MATHEMATICA, Maple or Derive this job can be done successfully.
- Evaluation of singular surface integrals and singular and nearly singular curvilinear integrals. The singularity arising in these problems is 'hard', so it is necessary to make some additional assumptions in order to evaluate these integrals. Also, the solution of nearly singular integrals is not standard. The specialized quadrature formulas need to be adapted for the general case.
- Verification of the methods. This includes not only the analytical verification, but also checking the error amplification when methods are applied to data containing numerical error.

In the following chapters the problems mentioned above will be analyzed, and ways to overcome difficulties will be proposed and verified.

### 2.4 Concluding remarks

New methods of computing derivatives from approximate solutions of the Poisson and Helmholtz equations are presented. They are based on Green's second identity.

For the Helmholtz equation there are two methods of derivative computation. One uses the Green's functions for the Laplacian operator, essentially viewing solutions of the Helmholtz equation as equivalent to solutions of the Poisson equation; the other employs Green's functions appropriate to the Helmholtz operator. The second approach is particularly attractive for differentiating solutions of the homogeneous Helmholtz equation. It is capable of computing derivatives of any order, instead of only up to the second order using the Poisson equation approach, and it is computationally more economic than the first technique.

Derivatives of harmonic functions in axisymmetric coordinates can be obtained by differentiation of the fundamental solution of the boundary value problems for a torus and a sphere.

## CHAPTER 3

### Generation of Green's function and Poisson kernels and their derivatives

In this chapter attention turns from the general mathematical formulation to generation of kernels and their derivatives, differentiation of the fundamental solutions of boundary value problems, differentiation of the surface integrals and special cases when the observation point is close to the region edge or on its edge. The chapter is divided into four sections. The first one deals with the generation of Green's functions and Poisson kernels for Laplacian and Helmholtz operators, the second describes the differentiation of fundamental solutions of the boundary value problem, and the last two discuss the near boundary case and treatment of surface integrals.

#### 3.1 Construction of Green's functions

The existence of a Green's function is equivalent to the existence of a unique solution of the boundary value problem for the differential equation (2.46) with the corresponding boundary conditions.  $G(P;Q)$  denotes the influence of a point source, placed at  $Q$ , at the observation point  $P$ .

##### 3.1.1 Methods of generating Green's functions

The Green's function of the region  $\Omega$  bounded by  $\partial\Omega$  has the following properties:

(a) For each  $P, Q \in \Omega$ , it can be represented in the form

$$G(P;Q) = g(P;Q) + \gamma(P;Q). \quad (3.1)$$

where function  $g(P;Q)$  is the fundamental solution for a free space, and  $\gamma(P;Q)$  is a harmonic function, representing the influence of the boundary;

- (b) The function  $G(P;Q)$  is harmonic and continuous at all points  $P \in \Omega$  except at  $P = Q$ , where it tends to  $+\infty$ . It satisfies prescribed boundary conditions, i.e.  $G(P;Q) = 0$  for  $Q \in \partial\Omega$ .
- (c) It satisfies the symmetry condition

$$G(P;Q) = G(Q;P) \quad (3.2)$$

which is the another expression for physical reciprocity.

- (d) By definition, it satisfies the Poisson equation in a generalized sense for each  $Q \in \Omega$ , so it might be interpreted as a Coulomb potential generated inside the conducting surface  $\partial\Omega$  at the point  $Q$ .

In this section three methods of construction of Green's functions will be briefly described.

### 3.1.1.1 Method of images

Method of images, or method of reflection (Vladimirov (1971)) is the most effective way of constructing a Green's function for a region having a sufficiently wide symmetry group. It is based on two fundamental laws of reflection, known from elementary electrostatics theory (Atkin (1962), Weber (1950), Van Bladel (1985) Kellogg (1967)). The method describes the induced charge in electrostatics or a reflected wave in acoustics. This fact is used to determine the function  $\gamma(P;Q)$ . The solutions may be obtained by means of inversion from a plane and in a sphere, or in the case of two-dimensional problems, inversion in a circle.

If the point  $Q$  lies in  $(x_Q, y_Q, z_Q)$ , then its image from a plane  $x = 0$  is a

point  $I$  with coordinates  $(-x_Q, y_Q, z_Q)$ . The line source at  $Q(x_Q, y_Q)$  has an image at  $I(-x_Q, y_Q)$ . Then the Green's function, which represents the influence at the observation point  $P$  of a unit charge at  $Q$  for two-dimensional problems is

$$\begin{aligned} G(P; Q) &= \frac{1}{2\pi} \log \sqrt{\frac{(x_P + x_Q)^2 + (y_P - y_Q)^2}{(x_P - x_Q)^2 + (y_P - y_Q)^2}} \\ &= \frac{1}{2\pi} \log \frac{s_I}{s_Q}, \end{aligned} \quad (3.3)$$

where  $s_Q$  and  $s_I$  are distances from the observation point  $P$  to a source placed at  $Q$  and to its image  $I$ .

An inversion mapping about a circle of radius  $R$  carries the point  $I$ , the image of  $Q(r_Q, \theta_Q)$ , to the polar coordinates  $(R^2/r_Q, \theta_Q)$ . The point  $Q$  and  $I$  are said to be symmetric with respect to circular surface  $\partial\Omega$ . This is a one-to-one mapping of the exterior of a circle (or sphere, in 3D) into the interior of a circle  $\Omega$ . The Kelvin transformation (Kellogg (1967), Courant and Hilbert (1953)) of a function  $\phi(r, \theta)$  is defined as

$$\phi^*(r, \theta) = \frac{R}{r} \phi\left(\frac{R^2}{r}, \theta\right). \quad (3.4)$$

The Kelvin inversion theorem may be given a quasi-physical interpretation, that the potential at point  $r$  inside the region  $\Omega$  is given by the equation

$$\phi(r, \theta) = \phi_0(r, \theta) - \frac{R}{r} \phi_0\left(\frac{R^2}{r}, \theta\right), \quad (3.5)$$

where  $\phi_0(r)$  is the free space potential.

The Green's function is supposed to have the form

$$G(P; Q) = -\frac{1}{2\pi} \log s_Q + \frac{1}{2\pi} \log s_I + c, \quad (3.6)$$

where  $s_Q$  and  $s_I$  are again distances between the observation point  $P$  and the

source point  $Q$  and its image  $I$ . The constant  $c$  is determined from the condition that  $G(P; Q)$  becomes zero on the boundary  $\partial\Omega$ , i.e.

$$\begin{aligned} & -\frac{1}{4\pi} \log(R^2 + r_Q^2 - 2Rr_Q \cos(\theta_P - \theta_Q)) \\ & + \frac{1}{4\pi} \log\left(R^2 + \frac{R^4}{r_Q^2} - 2\frac{R^3}{r_Q} \cos(\theta_P - \theta_Q)\right) + c = 0, \end{aligned} \quad (3.7)$$

giving

$$c = \frac{1}{2\pi} \log \frac{r_Q}{R}. \quad (3.8)$$

Then the Green's function will become

$$G(P; Q) = \frac{1}{2\pi} \log \frac{r_Q s_I}{R s_Q}. \quad (3.9)$$

### 3.1.1.2 Conformal mapping

Let the function  $z = z(\zeta) = x(\xi, \eta) + jy(\xi, \eta)$  conformally map a domain  $A$  of the  $\zeta$ -plane into  $\Omega$  of the  $z$ -plane. The correspondence is one to one. If  $u(x, y)$  is a harmonic function, then function  $\tilde{u}(\xi, \eta) = u(x(\xi, \eta), y(\xi, \eta))$  is harmonic in  $A$ . Conformal mapping transforms the harmonic function into another harmonic function, and a Dirichlet or Neumann problem into another Dirichlet or Neumann problem (Kantorovich (1964), Spiegel (1981), Morse and Feshbach (1953)).

The solutions to the Dirichlet problems for the circle and circular annulus are presented in Chapter 2. Thus if the conformal mapping of a given domain into a circle or circular ring is known, then it is possible to find solutions to the Dirichlet problem for that domain.

Some standard transformations are:

- (a) A half-plane is transformed into a circle by a bilinear transformation;
- (b) The exterior of an ellipse is mapped into a circle by the transformation

$$z = a\zeta + \frac{b}{\zeta};$$

- (c) A polygon is mapped on to a circle using a Schwartz-Christoffel transformation;
- (d) The annular domain between two circumferences is mapped on to a circular annulus with the aid of a bilinear transformation;
- (e) The annular region between two confocal ellipses can be mapped on to a circular annulus with  $z = a\zeta + \frac{b}{\zeta}$ .

The Green's function is related to the conformal map of the domain  $\Omega$  into a unit circle. If the analytic function  $\zeta = f(x + jy)$  maps the domain  $\Omega$  conformally onto a unit circle in  $\zeta$ -plane, in such a way that point  $Q$  goes into the origin, then

$$G(P;Q) = -\frac{1}{2\pi} \log |f(x + jy)| \quad (3.10)$$

is the Green's function belonging to  $\Omega$ . Generally, any simply connected bounded domain with piecewise smooth boundaries, according to Riemann's fundamental theorem of geometric function theory (Courant and Hilbert (1953)) may be conformally mapped (Gibbs (1958)).

### 3.1.1.3 Eigenfunctions expansion method

In practice, the precise solutions using the eigenfunction method are available for separable coordinate systems only. They allow the separation of partial differential equation in terms of coordinates, resulting in a set of ordinary differential equations with some separation constants. Solutions of the ordinary differential equations satisfying the boundary conditions are called *eigenfunctions*, and values of separation constants allowing it are *eigenvalues*.

Suppose that a function  $\psi$  satisfies the equation

$$\nabla^2 \psi + \lambda \rho \psi = 0, \quad (3.11)$$

for a given differential operator  $\mathfrak{D}$ , where  $\rho$  is continuous over the domain of interest  $\Omega$ . Then, if  $\psi$  is not identically equal to zero, it is called an eigenfunction, and the number  $\lambda$  is called an eigenvalue. Two eigenfunctions corresponding to different eigenvalues are orthogonal. A sequence of eigenfunctions is able to represent an arbitrary function with an arbitrary boundary conditions.

The expansion of Green's function is limited by the ease with which eigenfunctions can be determined (Morse and Feshbach (1953)). If the eigenfunctions are  $\psi_{mn}$  and corresponding eigenvalues are  $\kappa_{mn}$ , they satisfy the following equation:

$$\nabla^2 \psi_{mn} + \kappa_{mn}^2 \psi_{mn} = 0. \quad (3.12)$$

For eigenfunctions  $\psi(P)$ , the Green's functions are assumed to be of the following form:

$$\phi_P = \sum_{m,n} A_{mn} \psi_{mn}(P). \quad (3.13)$$

After introducing this expansion into the equation (3.12), the form of Green's function expansion for the Helmholtz operator is obtained

$$G(P;Q) = \sum_{m,n} \frac{\psi_{mn}(P)\psi_{mn}(Q)}{\|\psi_{mn}\|(\kappa_{mn}^2 - \kappa^2)}. \quad (3.14)$$

Consider the rectangular region  $0 \leq x \leq a$ ,  $0 \leq y \leq b$ , where function  $\phi$  satisfies the Poisson equation

$$\nabla^2 \phi = -g. \quad (3.15)$$

The method of separation of variables is applied to obtain the eigenfunctions and Green's function. The form of eigenfunction is assumed

$$\psi(x, y) = X(x) Y(y). \quad (3.16)$$

Substitution of (3.16) into (3.15) yields

$$\begin{aligned} X'' + \alpha^2 X &= 0 \\ Y'' + (\kappa^2 - \alpha^2) Y &= 0. \end{aligned} \quad (3.17)$$

Since  $X$  and  $Y$  satisfy homogeneous boundary conditions, they are found to be

$$\begin{aligned} X_m(x) &= A_m \sin \frac{\pi m x}{a} \\ Y_n(y) &= B_n \sin \frac{\pi n y}{b}. \end{aligned} \quad (3.18)$$

Then

$$\kappa_{mn}^2 = \pi^2 \left( \frac{m^2}{a^2} + \frac{n^2}{b^2} \right) \quad \alpha = \frac{m\pi}{a}. \quad (3.19)$$

Thus the eigenfunctions are

$$\psi_{mn} = \sin \frac{\pi m x}{a} \sin \frac{\pi n y}{b}. \quad (3.20)$$

Then using (3.14) Green's function is found as

$$G(P; Q) = \frac{4}{ab\pi^2} \sum_{m,n} \frac{\sin \frac{\pi m x_P}{a} \sin \frac{\pi n y_P}{b} \sin \frac{\pi m x_Q}{a} \sin \frac{\pi n y_Q}{b}}{\left(\frac{m}{a}\right)^2 + \left(\frac{n}{b}\right)^2}. \quad (3.21)$$

The alternate, but equivalent method is based on expansion of solution as a double Fourier series

$$\phi_P = \sum_{m,n} A_{mn} \sin \frac{\pi m x_P}{a} \sin \frac{\pi n y_P}{b}. \quad (3.22)$$

Expansion of the source function  $g(x, y)$  in a Fourier series gives

$$g(x, y) = \sum_{m,n} P_{mn} \sin \frac{\pi m x}{a} \sin \frac{\pi n y}{b}, \quad (3.23)$$

where

$$P_{mn} = \frac{1}{ab\pi^2} \int_0^a dx_Q \int_0^b g(x_Q, y_Q) \sin \frac{\pi m x_Q}{a} \sin \frac{\pi n y_Q}{b} dy_Q. \quad (3.24)$$

Then, after inserting both expansions into the equation (3.15), the potential becomes

$$\phi_P = \sum_{m,n} \frac{P_{mn}}{\left(\frac{m}{a}\right)^2 + \left(\frac{n}{b}\right)^2} \sin \frac{\pi m x_P}{a} \sin \frac{\pi n y_P}{b} \quad (3.25)$$

$$= \int_0^a dx_Q \int_0^b G(P; Q) g_Q dy_Q, \quad (3.26)$$

where

$$G(P; Q) = \frac{4}{ab\pi^2} \sum_{m,n} \frac{\sin \frac{\pi m x_P}{a} \sin \frac{\pi n y_P}{b} \sin \frac{\pi m x_Q}{a} \sin \frac{\pi n y_Q}{b}}{\left(\frac{m}{a}\right)^2 + \left(\frac{n}{b}\right)^2} \quad (3.27)$$

is the Green's function.

#### 3.1.1.4 Applicability of various forms of Green's function

Theoretically, it is possible to generate a Green's function using conformal mapping for a wide variety of regions, but practical realization involves very difficult problems, such as evaluation and differentiation of the resulting expressions. There are some conventional methods (Kantorovich (1964)) as well as universal programs for evaluation of Schwarz-Christoffel transformations for a general  $n$ -sided polygon (Trefethen (1980)), but these are approximate. The

Green's functions generated are approximate and difficult to differentiate.

The typical example is a triangle. The Schwarz-Christoffel transformation involves incomplete Beta functions, or in the best case elliptic integrals of the third kind. In the case of a rectangle Jacobian elliptic integrals have to be evaluated. The resulting expressions are difficult to evaluate, and their differentiation is also relatively complex.

The method of eigenfunction expansion for a circle and rectangle seems attractive for both operators (Laplacian and Helmholtz operator), but the summation and differentiation operators are not always commutative. The resulting series are slowly convergent, even to recover potential function. Experience shows that the first order derivative for Helmholtz operator can be hardly recovered with satisfactory accuracy.

The imaging method to construct a Green's functions is recommended for use whenever possible, because of the simplicity of its application. By mirroring from a plane and a circle a system of images may be constructed. There are still open questions. For example, it would be desirable to find a way how to organize imaging for triangle, a very important and attractive region.

### 3.1.2 Construction of Green's functions and Poisson kernels for elementary shapes

It is convenient to work with a region  $\Omega$  of simple shape embedded within the problem region  $\Omega_0$ , rather than with the original problem region itself. The following development will focus on two-dimensional problems with  $\Omega \subseteq \Omega_0$ . The elementary regions for which Green's functions and extended Poisson kernels were generated are: circle, rectangle, sector of circle and sector of ring.

## 3.1.2.1 Circle

The simply-shaped region  $\Omega$  is taken as a circular disc of radius  $R$ . If  $P$  is some interior point of  $\Omega$ , as in Figure 3.1. the appropriate Green's function is (Courant and Hilbert (1953))

$$G(P;Q) = -\frac{1}{2\pi} \log \frac{R s_Q}{r_Q s_I} \quad (28)$$

where  $s_Q$  is the distance from the observation point  $P$  to the source point  $Q$ , and  $s_I$  represents the distance from  $P$  to the image of  $Q$  with respect to the circle, i.e., to the point  $I$  located at  $(R^2/r_Q, \theta_Q)$ . Here and in the following,  $r_P$  and  $r_Q$  are the radial positions of points  $P$  and  $Q$  respectively. From this Green's function, the conventional Poisson kernel  $K_{00}(P;Q)$  immediately follows as

$$K_{00}(P;Q) = -\frac{1}{2\pi r_Q} \frac{r_Q^2 - r_P^2}{s_Q^2} \quad (r_Q = R). \quad (29)$$

An extensive catalog of the necessary kernel functions  $K_{mn}(P;Q)$  has been published by Silvester (1991b). The list of kernels up to third order together with an example of a MATHEMATICA program is given in Appendix 1.

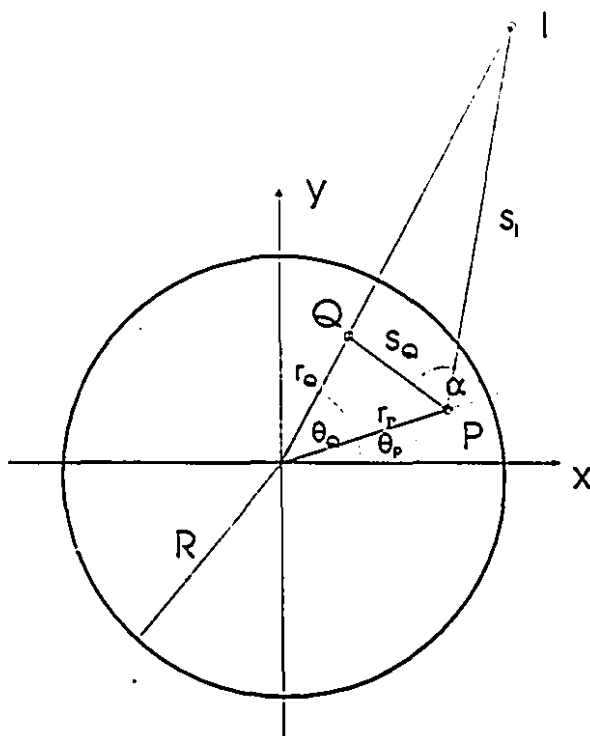


Figure 3.1. Images on the circle. Potential at point  $P$  depends on the location of source  $Q$  and its image  $I$  relative to the circular boundary.

In order to simplify the integration process, integration is performed in  $(s_Q, \alpha)$  instead of the  $(r_Q, \theta_Q)$  coordinate system

$$d\Omega_Q = s_Q ds_Q d\alpha. \quad (3.30)$$

Integration with respect to  $s_Q$  is performed from 0 to  $S_{\max}(\alpha)$ , while the angle  $\alpha$  takes values from 0 to  $2\pi$ . From Figure 3.1 it is easy to verify that

$$S_{\max}(\alpha) = \sqrt{R^2 - r_p^2 \sin^2 \alpha} - r_p \cos \alpha \quad (3.31)$$

$$r_Q^2 = r_p^2 + s_Q^2 + 2r_p s_Q \cos \alpha \quad (3.32)$$

$$r_Q s_I = \sqrt{(R^2 - r_P^2)(R^2 - r_P^2 - 2r_P s_Q \cos \alpha) + r_P^2 s_Q^2} \quad (3.33)$$

$$r_Q \cos(\theta_P - \theta_Q) = s_Q \cos \alpha + r_P \quad (3.34)$$

$$r_Q \sin(\theta_P - \theta_Q) = s_Q \sin \alpha. \quad (3.35)$$

Using these new integration variables, the order of singularity of the surface integrals is reduced by one.

### 3.1.2.2 Rectangular region

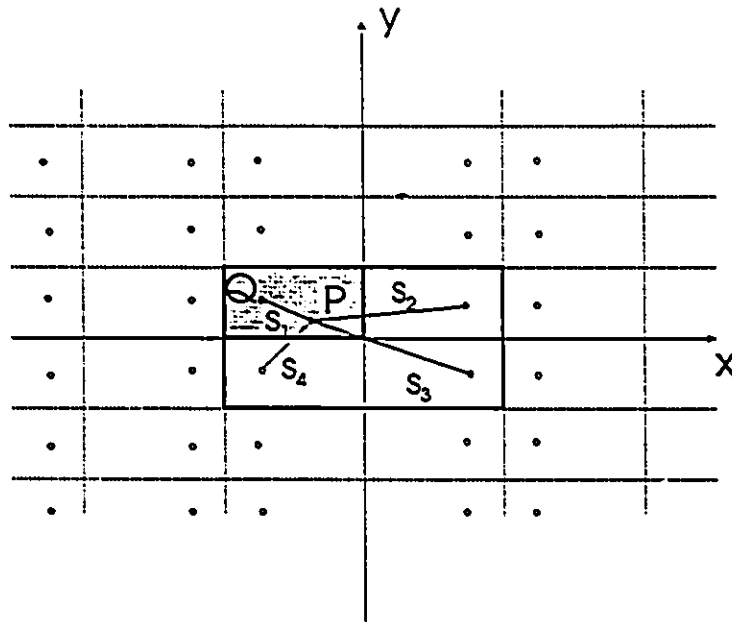


**Figure 3.2.** Method of images applied to solve Dirichlet problem on the rectangle

Using the method of images, as shown in Figure 3.2, the Green's function is

$$G(P;Q) = \sum_{m=1}^{\infty} \sum_{n=1}^{\infty} G_{mn}(P;Q), \quad (3.36)$$

where

$$G_{mn}(P;Q) = \frac{1}{2\pi} \log \frac{s_{2mn} s_{4mn}}{s_{1mn} s_{3mn}}. \quad (3.37)$$

The extended Poisson kernel function is the normal derivative of the Green's function on the boundary, taken with respect to the  $Q$  coordinates.

For  $x = 0$  and  $x = a$ , the normal derivative of the  $m,n$ th Green's function term is

$$\begin{aligned} \frac{\partial G_{mn}}{\partial n} = \frac{\partial G_{mn}}{\partial x_Q} &= (x_Q + 2ma + x_P) \left( \frac{1}{s_{2mn}} - \frac{1}{s_{3mn}} \right) \\ &+ (x_Q + 2ma - x_P) \left( \frac{1}{s_{4mn}} - \frac{1}{s_{1mn}} \right). \end{aligned} \quad (3.38)$$

For  $y = 0$  and  $y = b$ , the normal derivative of the  $m,n$ th Green's function term is

$$\begin{aligned} \frac{\partial G_{mn}}{\partial n} = \frac{\partial G_{mn}}{\partial y_Q} &= (y_Q + 2nb + y_P) \left( \frac{1}{s_{4mn}} - \frac{1}{s_{3mn}} \right) \\ &+ (y_Q + 2nb - y_P) \left( \frac{1}{s_{2mn}} - \frac{1}{s_{1mn}} \right). \end{aligned} \quad (3.39)$$

The symbolic analysis package MATHEMATICA was used to generate derivatives of these kernels. They are tabulated in Appendix 2.

### 3.1.2.3 Sector of circle of angle $\pi/m$

The sector of circle element is restricted to an angle  $\pi/m$ , where  $m$  is any integer since only these angles allow the application of method of images.

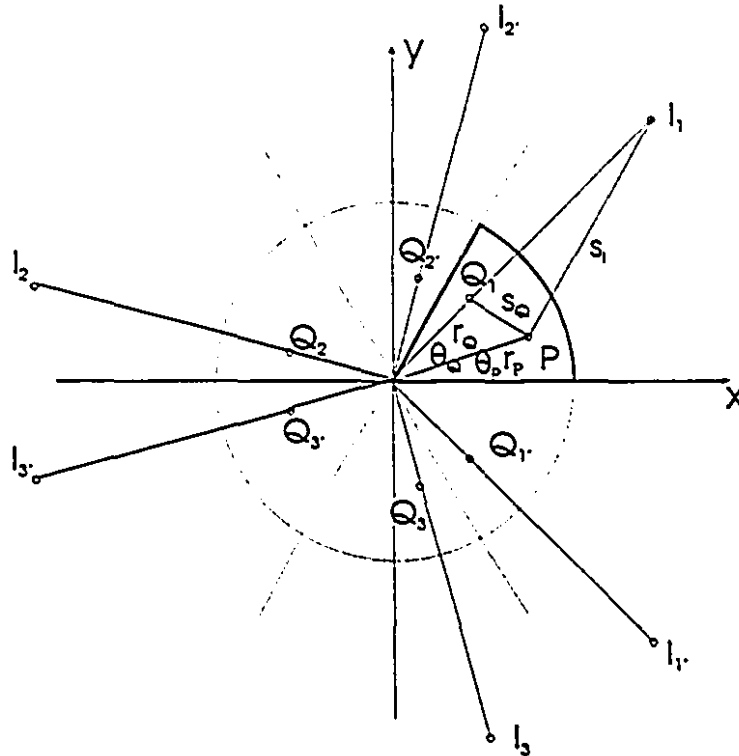


Figure 3.3. Method of images applied to solve Dirichlet problem on the sector of a circle of radius  $R$  and angle  $\pi/m$ .

The organization of imaging is illustrated in Figure 3.3, where two set of images are obtained. The first are  $(2m - 1)$  images from the sides, and the second set is their images mirrored on the circle, making the total number of images  $4m - 1$ . Then, the Green's function formula may be found by summing all their influences,

$$G(P;Q) = \frac{1}{2\pi} \sum_{i=1}^m \left( \log \frac{r_Q s_{Ii}}{R s_{Qi}} - \log \frac{r_Q s_{Ii'}}{R s_{Qi'}} \right) \tag{3.40}$$

$$= \frac{1}{2\pi} \sum_{i=1}^m \log \frac{s_{Qi'} s_{Ii}}{s_{Ii'} s_{Qi}} = \sum_{i=1}^m G_i(P;Q) \tag{3.41}$$

where distances  $s$  are given by

$$s_{Q_i}^2 = r_P^2 + r_Q^2 - 2r_P r_Q \cos\left(\theta_P - \theta_Q - (i-1)\frac{2\pi}{m}\right) \quad (3.42)$$

$$s_{i_i}^2 = r_P^2 + \frac{R^4}{r_Q^2} - 2r_P r_Q \cos\left(\theta_P - \theta_Q - (i-1)\frac{2\pi}{m}\right) \quad (3.43)$$

$$s_{Q_i'}^2 = r_P^2 + r_Q^2 - 2r_P r_Q \cos\left(\theta_P + \theta_Q - (i-1)\frac{2\pi}{m}\right) \quad (3.44)$$

$$s_{i_i'}^2 = r_P^2 + \frac{R^4}{r_Q^2} - 2r_P r_Q \cos\left(\theta_P + \theta_Q - (i-1)\frac{2\pi}{m}\right) \quad (3.45)$$

The normal derivative on the sides ( $\theta_Q = 0$  and  $\theta_Q = \frac{\pi}{m}$ ) is

$$\frac{\partial G_i}{\partial n} = \frac{1}{r_Q} \frac{\partial G_i}{\partial \theta_Q} = \frac{r_P}{\pi} \left( \frac{1}{s_{Q_i}^2} - \frac{R^2}{r_Q^2 s_{i_i}^2} \right) \sin\left(\theta_P - \theta_Q - (i-1)\frac{2\pi}{m}\right). \quad (3.46)$$

For the arc the Poisson kernel functions become

$$\frac{\partial G_i}{\partial n} = \frac{\partial G_i}{\partial r_Q} = \frac{r_Q^2 - r_P^2}{2\pi r_Q} \left( \frac{1}{s_{Q_i}^2} - \frac{1}{s_{Q_i'}^2} \right). \quad (3.47)$$

All kernels are generated using the MATHEMATICA symbolic package, and tabulated in Appendix 3.

#### 3.1.2.4 Sector of ring with angle $\pi/m$

The ring-shaped sector as element used in accurate derivative computation is also restricted to an angle  $\pi/m$ . Only these angles allow the application of method of images.

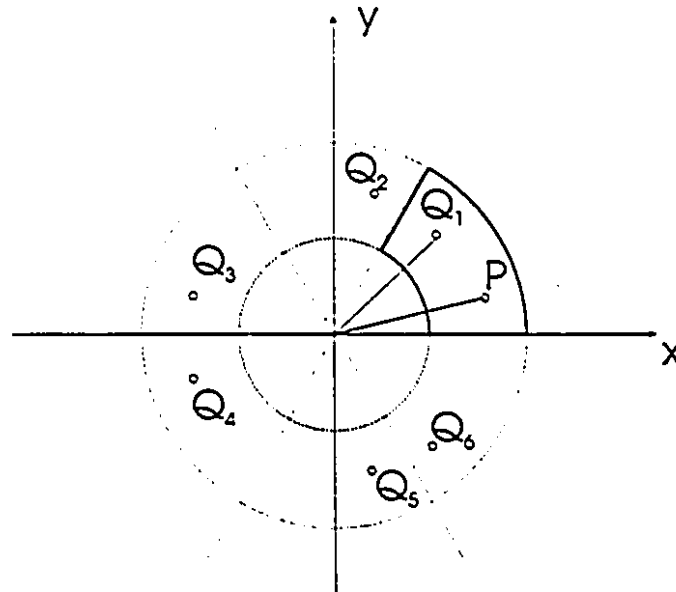


*Figure 3.4.* The geometry of the sector of a circular ring of inner and outer radii  $a$  and  $b$ , and angle  $\pi/m$ .

The base geometry is illustrated on Figure 3.4. Again, two sets of images are obtained. The first corresponds to images from the circular boundary, and the second are  $(2m - 1)$  images from the sides. The first set is infinite as can be seen from the fundamental solution for a circular ring, derived in Chapter 2. The Green's function may be found by summing all the influences. Since the number of positive and negative sources is in balance, the term

$$\frac{\log \frac{b}{r_Q}}{\log \frac{b}{a}} \log \frac{r_P}{a} + \log r_Q$$

will vanish. Then the Green's function is

$$G(P;Q) = \frac{1}{2\pi} \sum_{i=1}^m \left( \log \frac{s_{Qi'}}{s_{Qi}} - 2 \sum_{n=1}^{\infty} \left\{ \frac{r_Q^{2n} - a^{2n} r_P^n}{b^{2n} - a^{2n} r_Q^n} + \frac{b^{2n} - r_Q^{2n}}{b^{2n} - a^{2n} r_P^n} \frac{a^{2n}}{r_P^n r_Q^n} \right\} \right. \\ \left. \times \frac{\sin n(\theta_P - (i-1)\frac{2\pi}{m}) \sin n\theta_Q}{n} \right) \quad (3.48)$$

$$= \sum_{i=1}^m G_i(P;Q) \quad (3.49)$$

where distances  $s$  are given by

$$s_{Qi}^2 = r_P^2 + r_Q^2 - 2r_P r_Q \cos(\theta_P - \theta_Q - (i-1)\frac{2\pi}{m}) \quad (3.50)$$

$$s_{Qi'}^2 = r_P^2 + r_Q^2 - 2r_P r_Q \cos(\theta_P + \theta_Q - (i-1)\frac{2\pi}{m}). \quad (3.51)$$

The normal derivative on the sides  $\theta_Q = 0$  and  $\theta_Q = \frac{\pi}{m}$  is

$$\frac{\partial G_i}{\partial n_1} = -\frac{1}{r_Q} \frac{\partial G_i}{\partial \theta_Q} \Big|_{\theta_Q=0} \quad (3.52)$$

$$\frac{\partial G_i}{\partial n_2} = \frac{1}{r_Q} \frac{\partial G_i}{\partial \theta_Q} \Big|_{\theta_Q=\frac{\pi}{m}} \quad (3.53)$$

where

$$\frac{\partial G_i}{\partial \theta_Q} = -\frac{r_P r_Q}{2\pi} \left\{ \frac{\sin(\theta_P - \theta_Q - (i-1)\frac{2\pi}{m})}{s_{Qi}^2} + \frac{\sin(\theta_P + \theta_Q - (i-1)\frac{2\pi}{m})}{s_{Qi'}^2} \right\} \\ + \frac{1}{\pi} \sum_{n=1}^{\infty} \left\{ \frac{r_Q^{2n} - a^{2n} r_P^n}{b^{2n} - a^{2n} r_Q^n} + \frac{b^{2n} - r_Q^{2n}}{b^{2n} - a^{2n} r_P^n} \frac{a^{2n}}{r_P^n r_Q^n} \right\} \sin n(\theta_P - (i-1)\frac{2\pi}{m}) \cos n\theta_Q. \quad (3.54)$$

For the arcs the Poisson kernel functions become

$$\frac{\partial G_i}{\partial n_3} = - \frac{\partial G_i}{\partial r_Q} \Big|_{r_Q = a} \quad (3.55)$$

$$\frac{\partial G_i}{\partial n_4} = \frac{\partial G_i}{\partial r_Q} \Big|_{r_Q = b} \quad (3.56)$$

where

$$\begin{aligned} \frac{\partial G_i}{\partial r_Q} = & \frac{r_Q - r_P \cos(\theta_P - \theta_Q - (i-1)\frac{2\pi}{m})}{2\pi s_{Q_i}^2} - \frac{r_Q - r_P \cos(\theta_P + \theta_Q - (i-1)\frac{2\pi}{m})}{2\pi s_{Q_i}^2} \\ & + \frac{1}{\pi r_Q} \sum_{n=1}^{\infty} \left\{ \frac{r_P^{2n} - a^{2n} r_Q^n}{b^{2n} - a^{2n} r_P^n} - \frac{b^{2n} - r_P^{2n}}{b^{2n} - a^{2n} r_P^n} \frac{a^{2n}}{r_P^n r_Q^n} \right\} \sin n(\theta_P - (i-1)\frac{2\pi}{m}) \sin n\theta_Q. \end{aligned} \quad (3.57)$$

The convergence of the series in these expressions for the kernels is dependent on the position of the observation point  $P$ . All kernels are generated using the MATHEMATICA symbolic package, and tabulated in Appendix 4.

### 3.1.3 Generation of Green's functions for Helmholtz operator ( $\nabla^2 + \kappa^2$ )

A circle is taken to be the base region used in accurate derivative computation of solutions of the Helmholtz equation. In the classical literature of mathematical physics (Tyn Myint (1973), Mikhlin (1967)) there are three standard ways of deriving the Green's function for an arbitrary region. The first is expansion of the Green's function as a formal sum of eigenfunctions, analogous to the Laplacian operator case. Eigenfunction expansions yield slowly convergent series, which do not give a satisfactory accuracy unless a very large number of terms is included. After differentiation convergence is slow, even for the zeroth derivative, and worse for higher derivatives. In second approach, the form  $G(P;Q) = \gamma(P;Q) + h(P;Q)$  is assumed for the Green's function, where  $\gamma(P;Q)$  is

a fundamental solution and  $h(P;Q)$  takes care of the boundary conditions  $G(P;Q)$  has to satisfy. The resulting expressions are rather complicated, with coefficients expressed in terms of integrals of Bessel functions of the second kind,  $Y_i$ . The most suitable appears to be an approach based on solution of the homogeneous equation with appropriate boundary conditions. Then, the Green's function is expanded as a sum of Bessel functions of the first kind,  $J_i$ .

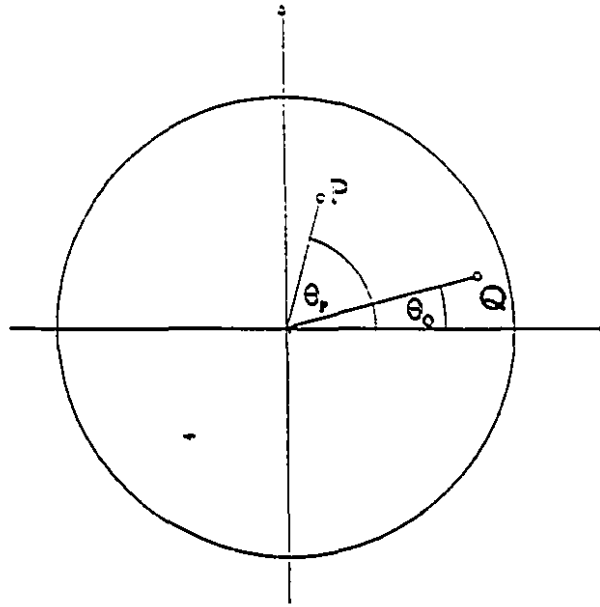


*Figure 3.5.* The base geometry.  $P$  is the observation point, and  $Q$  is the source point.

For the circular region shown in Figure 3.5, with  $Q$  as the source point and  $P$  the observation point, the influence of a unit source is (Tyn Myint (1973))

$$G_H(P;Q) = \sum_i b_i J_i(kr_P) \cos[i(\theta_P - \theta_Q)], \quad r_P < r_Q$$

$$= \sum_i c_i [J_i(kr_P) Y_i(kR) - Y_i(kr_P) J_i(kR)] \cos[i(\theta_P - \theta_Q)], \quad r_P > r_Q \quad (3.58)$$

where

$$b_i = \frac{1}{2\epsilon_i} \left\{ Y_i(kr_Q) - \frac{Y_i(kR)}{J_i(kR)} J_i(kr_Q) \right\}, \quad r_P < r_Q \quad (3.59)$$

$$c_i = \frac{J_i(kr_Q)}{2\epsilon_i J_i(kR)} \quad (3.60)$$

and

$$\begin{aligned} \epsilon_i &= 2, & i &= 0 \\ &= 1, & i &\neq 0. \end{aligned} \quad (3.60)$$

The Poisson kernel function is defined as the normal derivative of the Green's function,

$$K_H(P; Q) = \frac{\partial G_H(P; Q)}{\partial n_Q} = \frac{\partial G_H(P; Q)}{\partial r_Q} \Big|_{r_Q = R} \quad (3.62)$$

Since  $r_P < R$  in the present case (i.e., the observation point  $P$  is always inside the circle of integration), the kernel function takes the form

$$K_H(P; Q) = \sum_{i=0}^{\infty} a_i J_i(kr_P) \cos[i(\theta_P - \theta_Q)] \quad (3.63)$$

where

$$a_i = \frac{k}{2\epsilon_i} \left\{ Y_{i+1}(kR) - \frac{Y_i(kR)}{J_i(kR)} J_{i+1}(kR) \right\}. \quad (3.64)$$

This series converges comparatively fast, at any rate fast enough to be computationally practical. The kernels  $K_{Hmn}(P; Q)$  and  $G_{Hmn}(P; Q)$  are also derived using the MATHEMATICA package. They are tabulated in Appendix 5.

## 3.2 Differentiation of fundamental solutions of boundary value problems

### 3.2.1 Method based on Fourier series expansion

The potential inside the circle can be computed from known values on the boundary, using the formula

$$\phi(r_P, \theta_P) = \frac{a_0}{2} + \sum_{i=1}^{\infty} \left(\frac{r_P}{R}\right)^i [a_i \cos(i\theta) + b_i \sin(i\theta)] \quad (3.65)$$

where  $a_i$  and  $b_i$  are Fourier coefficients derived from known boundary values of the harmonic function  $f(\theta)$ , given in Chapter 2. Then the  $m$ th order derivatives of  $\phi$  may be calculated as

$$\frac{\partial^m}{\partial x^m} \phi(r, \theta) = \frac{1}{R^m} \sum_{i=0}^{\infty} \frac{(i+m)!}{i!} \left(\frac{r_P}{R}\right)^i [a_{i+m} \cos(i\theta_P) + b_{i+m} \sin(i\theta_P)], \quad (3.66)$$

$$\frac{\partial^m}{\partial x^{m-1} \partial y} \phi(r_P, \theta_P) = \frac{1}{R^m} \sum_{i=0}^{\infty} \frac{(i+m)!}{i!} \left(\frac{r_P}{R}\right)^i [a_{i+m} \sin(i\theta_P) - b_{i+m} \cos(i\theta_P)]. \quad (3.67)$$

Other derivatives may be obtained from these two,

$$\frac{\partial^m}{\partial x^{m-2k} \partial y^{2k}} \phi(r_P, \theta_P) = (-1)^k \frac{\partial^m}{\partial x^m} \phi(r, \theta) \quad \text{for } 2k \leq m, \quad (3.68)$$

$$\frac{\partial^m}{\partial x^{m-2k-1} \partial y^{2k+1}} \phi(r_P, \theta_P) = (-1)^k \frac{\partial^m}{\partial x^{m-1} \partial y} \phi(r_P, \theta_P) \quad \text{for } 2k < m. \quad (3.69)$$

This method is equivalent to the Poisson integral method (Tyn Myint (1973)). It gives exactly the same results for a number of samples equal to the number of integration points if point  $P$  is not close to the edge ( $r_P < 0.8$ ). Otherwise, the Poisson integral method becomes unstable, and convergence of Fourier series is slower, because the convergence factor ( $r_P/R$ ) comes close to 1. In practical applications this method yields better results, but it is more error sensitive. It is necessary to know the nature of the solution, and to take an

adequate number of samples, because the influence of higher harmonics, becomes large and affects the accuracy.

The Fourier series expansion may also be used to evaluate the boundary integral in (2.65) if the function analyzed is not harmonic. This fact will be used in differentiating the Poisson equation solution.

### 3.2.2 Differentiation of harmonic functions in axisymmetric coordinates

The solution of the Dirichlet problem for a torus and a sphere with the center on the  $z$ -axis is used in the procedure of differentiation.

#### 3.2.2.1 Torus

In Chapter 2, the expression for the potential inside the torus for known boundary values is derived as

$$\phi(\alpha, \beta) = \chi(\alpha, \beta) \sum_{n=0}^{\infty} \{ a_n \cos(n\beta) + b_n \sin(n\beta) \} Q_{n-1/2}(\cosh\alpha). \quad (3.70)$$

Coefficients  $a_n$  and  $b_n$ , toroidal coordinates  $(\alpha, \beta)$  and function  $\chi(\alpha, \beta)$  are explained and given in Chapter 2.

Knowing the derivative formula for the Legendre functions of nonintegral order,

$$\frac{\partial Q_{n-1/2}(\delta)}{\partial \delta} = \frac{n + \frac{1}{2}}{\delta^2 - 1} (Q_{n+1/2}(\delta) - \delta Q_{n-1/2}(\delta)), \quad (3.71)$$

and other derivatives used,

$$\begin{aligned} \frac{\partial \beta}{\partial r} &= -\frac{\sinh\alpha \sin\beta}{c} & \frac{\partial \beta}{\partial z} &= \frac{\cosh\alpha \cos\beta - 1}{c} \\ \frac{\partial \alpha}{\partial r} &= -\frac{\cosh\alpha \cos\beta - 1}{c} & \frac{\partial \alpha}{\partial z} &= -\frac{\sinh\alpha \sin\beta}{c} \end{aligned} \quad (3.72)$$

$$\frac{\partial \chi(\alpha, \beta)}{\partial r} = -\frac{\sinh \alpha \cos \beta}{2c} \chi(\alpha, \beta) \quad \frac{\partial \chi(\alpha, \beta)}{\partial z} = -\frac{\cosh \alpha \sin \beta}{2c} \chi(\alpha, \beta).$$

Derivatives in the  $r$  and  $z$  directions may be found.

$$\frac{\phi(\alpha, \beta)}{\partial r} = -\frac{\sinh \alpha \cos \beta}{2c} \phi(\alpha, \beta) + \frac{\chi(\alpha, \beta)}{c} x \quad (3.73)$$

$$\left\{ -\sinh \alpha \sin \beta \sum_{n=0}^{\infty} n \{ -a_n \sin(n\beta) + b_n \cos(n\beta) \} Q_{n-1/2}(\cosh \alpha) + \frac{1 - \cosh \alpha \cos \beta}{\sinh \alpha} \sum_{n=0}^{\infty} \left( n + \frac{1}{2} \right) \{ a_n \cos(n\beta) + b_n \sin(n\beta) \} Q_{n+1/2}(\cosh \alpha) + \frac{1 - \cosh \alpha \cos \beta}{\sinh \alpha} \cosh \alpha \sum_{n=0}^{\infty} \left( n + \frac{1}{2} \right) \{ a_n \cos(n\beta) + b_n \sin(n\beta) \} Q_{n-1/2}(\cosh \alpha) \right\},$$

$$\frac{\phi(\alpha, \beta)}{\partial z} = -\frac{\cosh \alpha \sin \beta}{2c} \phi(\alpha, \beta) + \frac{\chi(\alpha, \beta)}{c} x \quad (3.74)$$

$$\left\{ (-1 + \cosh \alpha \cos \beta) \sum_{n=0}^{\infty} n \{ -a_n \sin(n\beta) + b_n \cos(n\beta) \} Q_{n-1/2}(\cosh \alpha) - \sin \beta \sum_{n=0}^{\infty} \left( n + \frac{1}{2} \right) \{ a_n \cos(n\beta) + b_n \sin(n\beta) \} Q_{n+1/2}(\cosh \alpha) + \cosh \alpha \sin \beta \sum_{n=0}^{\infty} \left( n + \frac{1}{2} \right) \{ a_n \cos(n\beta) + b_n \sin(n\beta) \} Q_{n-1/2}(\cosh \alpha) \right\}.$$

The formulas for higher derivatives of harmonic functions in the axisymmetric coordinate system are derived and tabulated in Appendix 6.

### 3.2.2.2 Sphere with the center on $z$ axis

To obtain derivatives the fundamental solution of the Dirichlet problem for a sphere of radius  $R$ , given in the previous chapter, is differentiated. The potential inside the sphere may be expressed as

$$\phi(\rho, \theta) = \sum_{n=0}^{\infty} f_n \left( \frac{\rho}{R} \right)^n P_n(\cos \theta). \quad (3.75)$$

Knowing that:

$$\frac{\partial \phi(\rho, \theta)}{\partial \rho} = \frac{1}{R} \sum_{j=0}^{\infty} j f_j \left( \frac{\rho}{R} \right)^{j-1} P_j(\cos \theta), \quad (3.76)$$

$$\frac{\partial \phi(\rho, \theta)}{\partial \theta} = \frac{1}{\sin \theta} \sum_{j=0}^{\infty} j f_j \left( \frac{\rho}{R} \right)^j \left\{ \cos \theta P_j(\cos \theta) - P_{j-1}(\cos \theta) \right\}, \quad (3.77)$$

and that derivatives are

$$\frac{\partial \phi}{\partial r} = \frac{\partial \phi}{\partial \rho} \sin \theta + \frac{1}{\rho} \frac{\partial \phi}{\partial \theta} \cos \theta, \quad (3.78)$$

$$\frac{\partial \phi}{\partial z} = \frac{\partial \phi}{\partial \rho} \cos \theta - \frac{1}{\rho} \frac{\partial \phi}{\partial \theta} \sin \theta, \quad (3.79)$$

it can be proved that the general  $m, n$ th derivative of a harmonic function is

$$\frac{\partial^{m+n} \phi}{\partial^m \rho \partial^n z} = \frac{1}{R^{m+n} \sin^m \theta} \sum_{j=0}^{\infty} \frac{(j+m+n)!}{j!} f_{j+m+n} \left( \frac{\rho}{R} \right)^j \times \left\{ \sum_{k=0}^m (-1)^k \binom{m}{k} \cos^k \theta P_{j+m-k}(\cos \theta) \right\}. \quad (3.80)$$

### 3.3 Derivatives of harmonic functions if point $P$ is close to or on the edge

Formulas and forms of Poisson kernel functions to deal with specific cases when point  $P$  (where the derivative is to be computed) is close to the edge or it is right on the edge are derived in this section.

#### 3.3.1 Regularization of the Poisson kernels for the circle

In order to reduce the order of singularity of the surface integrals, the variables are changed. The same transformation may be performed on the boundary

integral. Instead of the polar coordinates  $(r, \theta)$  the coordinate system  $(s, \alpha)$  is used, where  $s = s_Q$ , and  $\alpha$  is the angle measured from the line  $PO$  to line  $PQ$ . The geometry is shown in Figure 3.1. This variable transformation yields a more natural and suitable form of kernels. Then, the general form of  $m$ th order modified Poisson kernels is

$$K_{m,0}(P;Q) = \frac{m!}{\pi R s^{m+1}} \left\{ \frac{r^2 - R^2}{s} \cos(m\alpha + m\theta_P) + r \cos((m-1)\alpha + m\theta_P) \right\} \quad (3.S1)$$

$$K_{m-1,1}(P;Q) = \frac{m!}{\pi R s^{m+1}} \left\{ \frac{r^2 - R^2}{s} \sin(m\alpha + m\theta_P) + r \sin((m-1)\alpha + m\theta_P) \right\} \quad (3.S2)$$

$$K_{m-2k,2k}(P;Q) = (-1)^k K_{m,0}(P;Q) \quad \text{for } 2k \leq m \quad (3.S3)$$

$$K_{m-2k-1,2k+1}(P;Q) = (-1)^k K_{m-1,1}(P;Q) \quad \text{for } 2k < m \quad (3.S4)$$

In that case  $d\Gamma = s d\alpha$ , so the degree of denominator for the  $m$ th derivative is reduced to  $m$ . For  $r_P = R$  it is the order of singularity, since

$$\lim_{\substack{r_P \rightarrow R \\ \theta_Q \rightarrow \theta_P}} \frac{R^2 - r_P^2}{s} = 2R. \quad (3.S5)$$

Using this modification, the nature of the quadrature is changed. If the edge is approached, the sampling points are concentrated closer to the observation point  $P$ . Equi- $\alpha$  quadrature yields a non-uniform distribution of integration points on the perimeter of the circle. Before, sampling points were equi-spaced, while now the quadrature points are concentrated closer to the observation point.

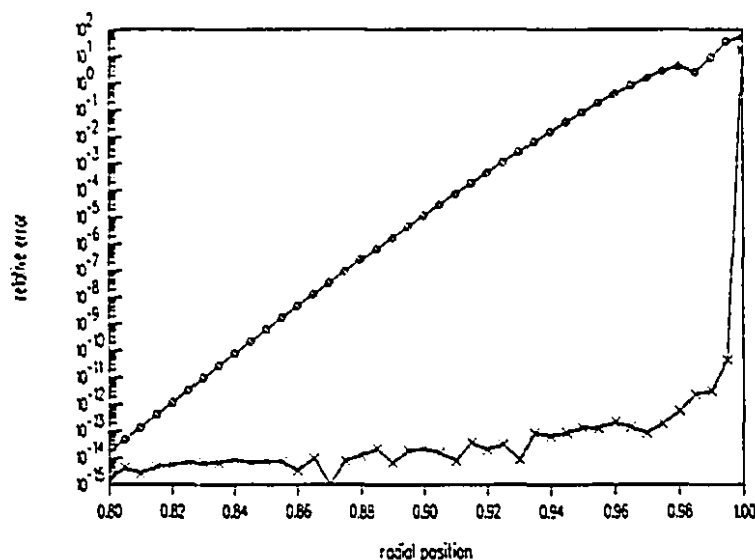


Figure 3.6. Accuracy of  $\partial^2 f / \partial x^2$  derivative, for different positions of the observation point. Results obtained using modified kernels ( $\times$ ) and using standard formula ( $\circ$ ). The test function is  $f(x, y) = x^3 y - x y^3$ ,  $\theta_P = 20^\circ$ . 300 point quadrature was used.

Kernels defined in this way are more natural and consistent with respect to the original definition of the Fourier transform<sup>1</sup> (Böcher (1906), Kellogg (1967)), since the Poisson integral is equivalent to Fourier series expansion solution of boundary value problems on the circular disk. Numerical experiments confirm this. Figure 3.6 presents the results obtained using the conventional approach and by modified integration. Exact values of an analytical function were used in all experiments.

<sup>1</sup>Böcher gave an elegant interpretation of the Poisson integral:

*If we imagine that at each point of the unit circle the value  $f(s)$  at that point has been marked, then the value  $F(r, \varphi)$  at any point  $P$  within the circle is equal to the average of these values as they would be read of by an observer at  $P$  who tours with uniform angular velocity and who is situated in a refracting medium which causes the rays of light reaching his eye to take the form of circular arcs orthogonal to the unit circle.*

The problem with the above approach is that the information used in computation of derivatives has an increasingly local character as the boundary is approached, so the beneficial effect of averaging is lost. Instead of data in the broader region being averaged, more local data are used. This implies that the numerical error in the region close to the point of interest is amplified. Error sensitivity of this formulation, if applied to finite element results is increased.

### 3.3.2 Point $P$ on the edge - normal derivative on the boundary

To derive directional derivatives of the kernels, one may start from the azimuthal and radial derivatives,

$$\frac{\partial}{\partial \theta_P} K_{00}(P; Q) = -\frac{R^2 - r_P^2}{\pi s_Q^4} r_P \sin(\theta_P - \theta_Q), \quad (3.86)$$

$$\frac{\partial}{\partial r_P} K_{00}(P; Q) = \frac{2Rr_P - (R^2 + r_P^2) \cos(\theta_P - \theta_Q)}{\pi s_Q^4}. \quad (3.87)$$

Then, first order kernels, corresponding to  $x$  and  $y$  directional derivatives, may be obtained from the azimuthal and radial derivatives,

$$K_{10}(P; Q) = \frac{\partial K_{00}}{\partial \theta_P} \frac{\partial \theta_P}{\partial x_P} + \frac{\partial K_{00}}{\partial r_P} \frac{\partial r_P}{\partial x_P}, \quad (3.88)$$

$$K_{01}(P; Q) = \frac{\partial K_{00}}{\partial \theta_P} \frac{\partial \theta_P}{\partial y_P} + \frac{\partial K_{00}}{\partial r_P} \frac{\partial r_P}{\partial y_P}. \quad (3.89)$$

If point  $P$  is on the edge,  $r_P = R$ ,

$$s_Q = R \sqrt{2(1 - \cos(\theta_P - \theta_Q))} = 2R \sin \frac{\theta_P - \theta_Q}{2}, \quad (3.90)$$

and since

$$\lim_{\substack{r \rightarrow R \\ \theta_Q \rightarrow \theta_P}} \frac{R^2 - r^2}{s_Q^4} = 2R, \quad (3.91)$$

azimuthal and radial derivatives of the Poisson kernels are

$$\frac{\partial}{\partial \theta_P} K_{00}(P; Q) = \begin{cases} 0 & \text{for } \theta_P \neq \theta_Q \\ \infty & \text{for } \theta_P = \theta_Q \end{cases} \quad (3.92)$$

$$\frac{\partial}{\partial r_P} K_{00}(P; Q) = -\frac{1}{4\pi R^2 \sin^2[(\theta_P - \theta_Q)/2]} \quad (3.93)$$

If  $\theta_P = \theta_Q$ , a derived radial kernel has a second order singularity. It is obvious that the azimuthal derivative kernel has an irregular form. It is not possible to find that derivative of a harmonic function from known potentials if the point of interest  $P$  is on the edge. This is consistent with the mathematical physics theory (Miranda (1970)).

In order to compute a first order derivative on the edge in an arbitrary direction the theory of distributions may be applied (Stakgold (1979)). The fundamental assumption of the theory of distributions is the following:

$$\oint_{\partial\Omega} \phi_Q \frac{\partial K_{00}}{\partial \theta_P} d\Gamma_Q = - \oint_{\partial\Omega} K_{00} \frac{\partial \phi_Q}{\partial \theta_P} d\Gamma_Q \quad (3.94)$$

Then, the directional derivative is

$$\begin{aligned} \frac{\partial \phi_P}{\partial x} &= - \oint_{\partial\Omega} \phi_Q K_{10}(P; Q) d\Gamma_Q \\ &= - \frac{\partial \theta_P}{\partial x_P} \oint_{\partial\Omega} \frac{\partial \phi_Q}{\partial \theta_P} K_{00} d\Gamma_Q - \frac{\partial r_P}{\partial x_P} \oint_{\partial\Omega} \phi_Q \frac{\partial K_{00}}{\partial r_P} d\Gamma_Q \end{aligned} \quad (3.95)$$

After substitutions

$$\frac{\partial \theta_P}{\partial x_P} = -\frac{\sin \theta_P}{r_P}, \quad \frac{\partial r_P}{\partial x_P} = \cos \theta_P, \quad (3.96)$$

and using the property of the Poisson integral for the point on the edge

$$\frac{\partial \phi_P}{\partial x} = -\frac{\sin \theta_P}{r_P} \frac{\partial \phi_P}{\partial \theta_P} - \cos \theta_P \oint_{\partial\Omega} \phi_Q \frac{\partial K_{00}}{\partial r_P} d\Gamma_Q \quad (3.97)$$

Here  $\partial\phi_P/\partial\theta_P$  is computed using some other method. Thus, from the potential known on the boundary of the region, using the modified Poisson integral method, only the radial derivative can be found

$$\frac{\partial\phi_P}{\partial r} = - \oint_{\partial\Omega} \phi_Q \frac{\partial K_{00}}{\partial r_P} d\Gamma_Q = \frac{1}{4\pi R^2} \oint_{\partial\Omega} \phi_Q \frac{1}{\sin^2[(\theta_P - \theta_Q)/2]} d\Gamma_Q. \quad (3.98)$$

Because  $d\Gamma_Q = R d\theta_Q$ , the last expression reduces to

$$\frac{\partial\phi_P}{\partial r} = \frac{1}{4\pi R} \int_{-\pi}^{+\pi} \phi_Q \frac{1}{\sin^2[(\theta_P - \theta_Q)/2]} d\theta_Q. \quad (3.99)$$

The last integral has a strong (second order) singularity. It cannot be solved using classical methods, and requires special treatment.

### 3.4 Treatment of the surface integral

In the general case where the source function  $g(Q)$  does not vanish, all terms in Equation (2.65) must be considered. In other words, the surface integral contribution must be computed as well as the Poisson integral over its boundary. Point  $P$  is located within the circle, so the integral kernel becomes singular at  $P = Q$ . Hence this calculation is computationally somewhat more difficult than the boundary integration required for harmonic functions. With the boundary integral term absent, finding any derivative requires evaluation of the integral

$$\frac{\partial^{m+n}}{\partial x^m \partial y^n} \phi_P = \frac{\partial^{m+n}}{\partial x^m \partial y^n} \int_{\Omega} G(P; Q) g(Q) d\Omega_Q. \quad (3.100)$$

It is tempting to assume that the differentiation and integration operators on the right commute; but this assumption cannot be made without investigation. The first few values of  $m$  and  $n$ , which are in any case the most important, will therefore be developed in detail.

Two specific cases are treated separately. The first arises when the

observation point  $P$ , where the derivative is to be computed, is an interior point of the circle. The case when point  $P$  is on the boundary needs a separate analysis, since kernels take a different form.

### 3.4.1 Differentiation of surface integral term for an interior point $P$

To begin, the apparently trivial case  $m = n = 0$  is important. The integral kernel  $G(P; Q)$  is singular, having a pole at  $P = Q$ . However, this singularity is weak,

$$\lim_{P \rightarrow Q} \int_{\Omega} G(P; Q) d\Omega_Q < \infty, \quad (3.101)$$

so the potential  $\phi$  is known to exist for any bounded and piecewise continuous source function  $g(P)$ . The first derivatives,  $m + n = 1$ , are dealt with next, by direct differentiation. Differentiating with respect to (say)  $x$ ,

$$\frac{\partial}{\partial x} G(P; Q) = \frac{\partial}{\partial x} \left( -\frac{1}{2\pi} \log \frac{R s_Q}{r_Q s_I} \right) = -\frac{1}{2\pi} \left( \frac{x_P - x_Q}{s_Q^2} - \frac{x_P - x_I}{s_I^2} \right). \quad (3.102)$$

The two terms in parentheses may be interpreted as projections of the distance vectors  $s_Q$  and  $s_I$  onto the  $x$ -axis. Thus

$$\frac{\partial}{\partial x} G(P; Q) = \frac{1}{2\pi} \left( \frac{\mathbf{1}_x \cdot \mathbf{s}_Q}{s_Q^2} - \frac{\mathbf{1}_x \cdot \mathbf{s}_I}{s_I^2} \right) = \frac{1}{2\pi} \left( \frac{\cos(\alpha_Q + \theta_P)}{s_Q} - \frac{\cos(\alpha_I + \theta_P)}{s_I} \right) \quad (3.103)$$

where  $\alpha_Q$  and  $\alpha_I$  represent the angles between  $x$ -axis and the distance vectors  $s_Q$  and  $s_I$  respectively. The second term in parentheses is obviously regular, because the image  $I$  is always outside the circle,  $|s_I| > 0$ . The first is singular at  $s_Q = 0$ . However, this singularity is integrable,

$$\lim_{P \rightarrow Q} \int_{\Omega} \frac{\cos \alpha_Q}{s_Q} d\Omega_Q < \infty. \quad (3.104)$$

To continue, let second derivatives be formed in the same manner.

Differentiating formally with respect to  $x$ ,

$$\frac{\partial^2}{\partial x^2} G(P; Q) = \frac{1}{2\pi} \left( -\frac{\cos 2(\alpha_I + \theta_P)}{s_I^2} + \frac{\cos 2(\alpha_Q + \theta_P)}{s_Q^2} \right). \quad (3.105)$$

This formal differentiation of the kernel alone leads directly to an expression for  $\partial^2 \phi_P / \partial x^2$  if, and only if, the differentiation and integration operators can be exchanged in (3.100). In this case they do not commute. Differentiation under the integral sign is not allowed in the singular integral. It is, however, permissible in the second term, so that

$$\begin{aligned} \frac{\partial^2 \phi}{\partial x^2} = & -\frac{1}{2\pi} \int_{\Omega} \frac{\partial}{\partial x} \frac{\cos(\alpha_I + \theta_P)}{s_I} g(Q) d\Omega_Q \\ & + \frac{1}{2\pi} \frac{\partial}{\partial x} \int_{\Omega} \frac{\cos(\alpha_Q + \theta_P)}{s_Q} g(Q) d\Omega_Q. \end{aligned} \quad (3.106)$$

Fortunately, all is not lost; a second derivative in weak form (Mikhlin (1965)) is still obtainable. The rightmost integral may be transformed, integrating by parts

$$\begin{aligned} \frac{\partial}{\partial x} \int_{\Omega} \frac{\cos(\alpha_Q + \theta_P)}{s_Q} g(Q) d\Omega_Q = & \int_{\Omega} g(Q) \frac{\partial}{\partial x} \frac{\cos(\alpha_Q + \theta_P)}{s_Q} d\Omega_Q \\ & + g(P) \oint_{\partial\Omega} \frac{\cos(\alpha_Q + \theta_P)}{s_Q} \frac{\partial s_Q}{\partial x} dS_Q. \end{aligned} \quad (3.107)$$

The rightmost integral is readily evaluated, for

$$\frac{\partial s_Q}{\partial x} = -\cos(\alpha_Q + \theta_P) \quad (3.108)$$

so that

$$\oint_{\partial\Omega} \frac{\cos(\alpha_Q + \theta_P)}{s_Q} \frac{\partial s_Q}{\partial x} dS_Q = -\oint_{\partial\Omega} \frac{\cos^2(\alpha_Q + \theta_P)}{s_Q} dS_Q = -\frac{1}{2}. \quad (3.109)$$

According to Mikhlin (1965), this operation is permissible wherever the source density  $g(Q)$  satisfies the Lipschitz condition

$$|g(P) - g(Q)| < K |s_Q|^p. \quad (3.110)$$

with  $p > 0$ . This condition is likely to be met in any practical case. After collecting terms the result is

$$\frac{\partial^2}{\partial x^2} \phi_P = \int_{\Omega} \frac{\partial^2 G(P; Q)}{\partial x^2} g(Q) d\Omega_Q - \frac{1}{2} g(P). \quad (3.111)$$

By an interchange of coordinates, there immediately results

$$\frac{\partial^2}{\partial y^2} \phi_P = \int_{\Omega} \frac{\partial^2 G(P; Q)}{\partial y^2} g(Q) d\Omega_Q - \frac{1}{2} g(P). \quad (3.112)$$

The cross derivative is simpler to deal with. Its general form is

$$\begin{aligned} \frac{\partial^2}{\partial x \partial y} \phi_P = \int_{\Omega} \frac{\partial^2 G(P; Q)}{\partial x \partial y} g(Q) d\Omega_Q \\ + g(P) \oint_{\partial\Omega} \frac{\cos(\alpha_Q + \theta_P) \sin(\alpha_Q + \theta_P)}{s_Q} d\Gamma_Q, \end{aligned} \quad (3.113)$$

where the final integral evaluates to zero. Hence

$$\frac{\partial^2}{\partial x \partial y} \phi_P = \int_{\Omega} \frac{\partial^2 G(P; Q)}{\partial x \partial y} g(Q) d\Omega_Q. \quad (3.114)$$

As a matter of notational convenience, let kernel functions  $J_{mn}(P; Q)$  be defined, analogously to  $K_{mn}(P; Q)$  for the boundary integration:

$$\frac{\partial^{m+n}}{\partial x^m \partial y^n} \phi_P = \int_{\Omega} J_{mn}(P; Q) g(Q) d\Omega_Q. \quad (3.115)$$

For  $m+n < 2$ , these kernels are simply the formal derivatives of the Green's function. For  $m+n = 2$  (but  $m \neq n$ ), they need to be augmented by the delta function  $\delta(P-Q)$ , so as to provide the added  $g(P)$  term. The values of such kernel functions appear in Appendix 1.

## 3.4.2 Differentiation of surface integral for point on the edge

If the observation point  $P$  is on the boundary, the first derivative of the Green's function with respect to  $x$  is

$$\frac{\partial}{\partial x} G(P; Q) = \frac{\cos \theta_P}{2\pi R} \left( 1 + \frac{2R \cos \alpha_Q}{s_Q} \right) \quad (3.116)$$

with clearly integrable singularity,

$$\lim_{P \rightarrow Q} \int_{\Omega} \frac{\cos \alpha_Q}{s_Q} d\Omega_Q < \infty. \quad (3.117)$$

To obtain a second derivative in weak form (Mikhlin (1965)), one has to proceed as follows:

$$\begin{aligned} \frac{\partial}{\partial x} \int_{\Omega} \frac{s_Q + 2R \cos \alpha_Q}{2\pi R s_Q} g(Q) d\Omega_Q &= \frac{1}{2\pi R} \int_{\Omega} g(Q) \frac{\partial}{\partial x} \frac{s_Q + 2R \cos \alpha_Q}{s_Q} d\Omega_Q \\ &+ g(P) \frac{\cos \theta_P}{2\pi} \oint_{\partial\Omega} \frac{s_Q + 2R \cos \alpha_Q}{s_Q} \frac{\partial s_Q}{\partial x} d\Gamma_Q. \end{aligned} \quad (3.118)$$

Knowing

$$\frac{\partial s_Q}{\partial x} = -\cos(\alpha_Q + \theta_P) \quad (3.119)$$

the rightmost integral becomes

$$\oint_{\partial\Omega} \frac{s_Q + 2R \cos \alpha_Q}{s_Q} \frac{\partial s_Q}{\partial x} d\Gamma_Q = - \oint_{\partial\Omega} \frac{s_Q + 2R \cos \alpha_Q}{s_Q} \cos(\alpha_Q + \theta_P) d\Gamma_Q.$$

This integral reduces to

$$- \oint_{\partial\Omega} 2 \cos^2 \alpha_Q \cos \theta_P d\alpha_Q = -2\pi \cos \theta_P$$

and the final expression is

$$\frac{\partial}{\partial x} \int_{\Omega} J_{10}(P; Q) g(Q) d\Omega_Q = \int_{\Omega} \frac{\partial^2 G(P; Q)}{\partial x^2} g(Q) d\Omega_Q - \cos^2 \theta_P g(P). \quad (3.120)$$

Similarly for the mixed derivative,

$$\begin{aligned} \frac{\partial}{\partial y} \int_{\Omega} \frac{s_Q + 2R \cos \alpha_Q}{2\pi R s_Q} g(Q) d\Omega_Q &= \frac{1}{2\pi R} \int_{\Omega} g(Q) \frac{\partial}{\partial y} \frac{s_Q + 2R \cos \alpha_Q}{s_Q} d\Omega_Q \\ &+ g(P) \frac{\cos \theta_P}{2\pi} \oint_{\partial\Omega} \frac{s_Q + 2R \cos \alpha_Q}{s_Q} \frac{\partial s_Q}{\partial y} d\Gamma_Q. \end{aligned} \quad (3.121)$$

Since

$$\frac{\partial s_Q}{\partial y} = -\sin(\alpha_Q + \theta_P), \quad (3.122)$$

the rightmost integral is readily evaluated,

$$\oint_{\partial\Omega} \frac{s_Q + 2R \cos \alpha_Q}{s_Q} \frac{\partial s_Q}{\partial y} d\Gamma_Q = - \oint_{\partial\Omega} \frac{s_Q + 2R \cos \alpha_Q}{s_Q} \sin(\alpha_Q + \theta_P) d\Gamma_Q.$$

This integral reduces to

$$- \oint_{\partial\Omega} 2 \cos^2 \alpha_Q \sin \theta_P d\alpha_Q = -2\pi \sin \theta_P, \quad (3.123)$$

and after substitution in (3.121), the final expression is

$$\frac{\partial}{\partial y} \int_{\Omega} J_{10}(P; Q) g(Q) d\Omega_Q = \int_{\Omega} \frac{\partial^2 G(P; Q)}{\partial x \partial y} g(Q) d\Omega_Q - \frac{\sin 2\theta_P}{2} g(P). \quad (3.124)$$

Using an analogous procedure for  $\partial^2/\partial y^2$ , the result is

$$\frac{\partial}{\partial y} \int_{\Omega} J_{01}(P; Q) g(Q) d\Omega_Q = \int_{\Omega} \frac{\partial^2 G(P; Q)}{\partial y^2} g(Q) d\Omega_Q - \sin^2 \theta_P g(P). \quad (3.125)$$

## CHAPTER 4

### Validation of the method

An extensive series of numerical experiments was performed to verify the theories and to explore the precision achievable with the methods proposed in the previous chapter.

#### 4.1 Numerical experiments with Poisson equation solutions

The objective of this section is to establish the validity of the method. The experiments were confined to two dimensions, with the region  $\Omega$  a circular disk of unit (normalized) radius, a rectangular region, a sector of a circle and a sector of ring.

##### 4.1.1 Results using exact values of a test-function

###### 4.1.1.1 Experiments with a circular disk

Except in the first set of experiments, the number of quadrature nodes was taken large enough to ensure negligible integration error. Computing times were thus at times quite long, but this approach ensures that the conclusions are unaffected by the choice of integration method.

The first run of experiments sought to establish a technique of numerical integration satisfactory for the remaining tests. To integrate, a local coordinate system was established, centered on point  $P$ . Product quadrature formulae were used, with Gaussian integration in the radial direction, circular quadrature in the azimuthal direction (Davis and Rabinowitz (1984), Krylov (1962)). In the radial

direction. quadrature nodes were placed at appropriately scaled points on radial lines from  $P$  to the perimeter of  $\Omega$ . The analytically known function

$$f_1(x, y) = x^3y + xy^3 \quad (\text{with } \nabla^2\phi = 12xy) \quad (4.1)$$

was differentiated using the method described in section 2.2.1, the contour integral of Equation (2.65) being in all cases evaluated with very high precision so as to suppress any error. Figures 4.1 and 4.2 show how accuracy of computed derivatives changes if quadrature formulae of various precision levels in the radial and azimuthal directions are used. In Figure 4.3 the relative error in computed derivative  $\partial f_1/\partial y$  is given for various radial positions of the observation points  $P$ , obtained using the four specific numbers of quadrature nodes in azimuthal direction. Accuracy improves in much the expected fashion as the number of quadrature nodes grows, until it is limited by machine precision. These tests establish beyond doubt that the method works, and that roughly 100 quadrature nodes in the azimuthal direction, about 9 or 10 radially, suffice to ensure that full floating-point precision (over 10 significant figures) is reached. All succeeding experiments employed significantly more nodes, so as to guarantee absence of quadrature error.

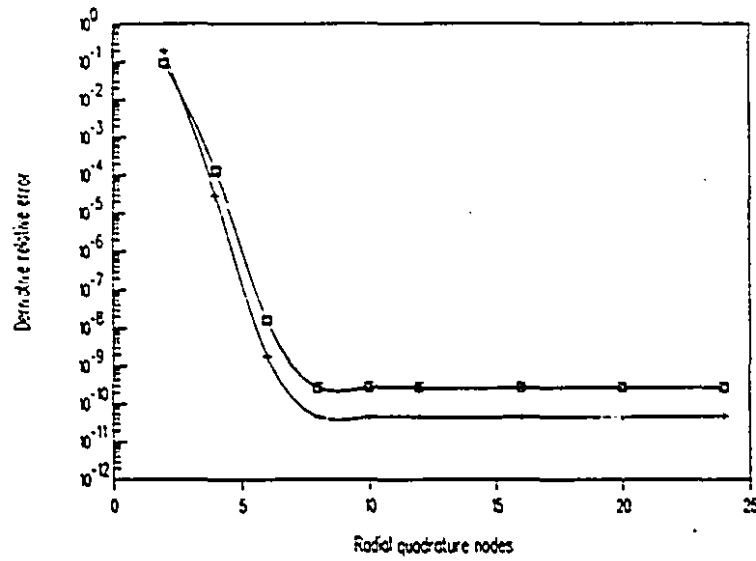


Figure 4.1. Derivatives  $\partial f_1 / \partial y$  (+),  $\partial^2 f_1 / \partial x \partial y$  (x) and  $\partial^2 f_1 / \partial x^2$  (□) of  $f_1(x, y) = x^3 y + x y^3$ , for quadrature formulae of varying precision in radial direction.

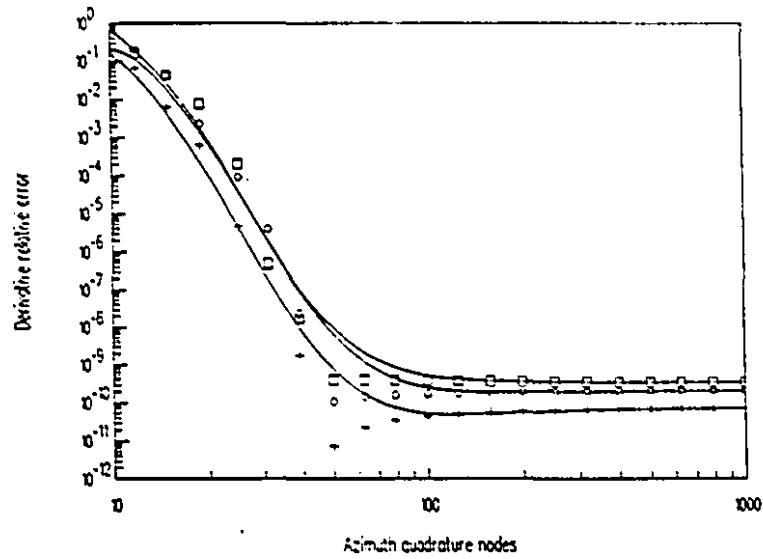


Figure 4.2. Derivatives  $\partial f_1/\partial y$  (+),  $\partial^2 f_1/\partial x \partial y$  (x) and  $\partial^2 f_1/\partial x^2$  (□) of  $f_1(x,y) = x^3y + xy^3$ , for quadrature formulae of varying precision in azimuthal direction.

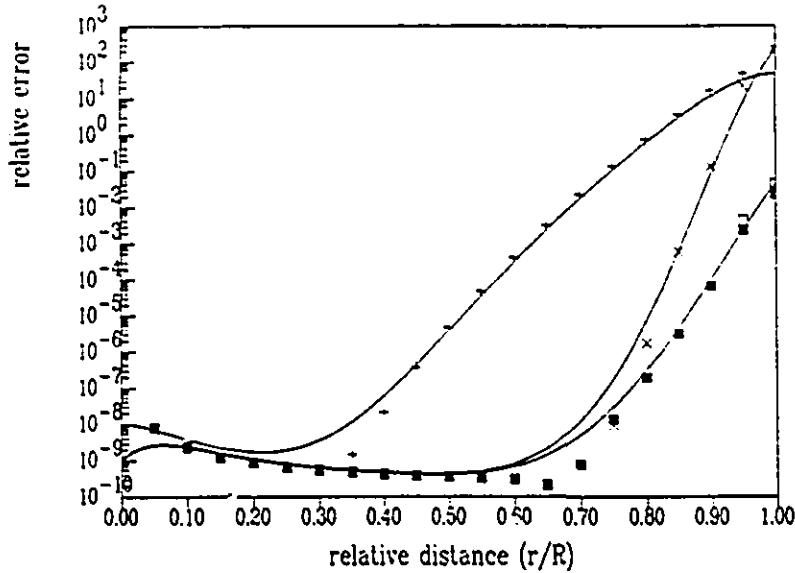


Figure 4.3. Relative error in derivative  $\partial/\partial y$  of  $f_1(x,y) = x^3y + xy^3$ , for 30 (+), 100 (x), 300 (□) and 1000 (■) integration points in  $\theta$  direction.

The behavior of accuracy in evaluation of the curvilinear term was analyzed in detail when harmonic functions were treated (Silvester (1991a)). In order to test the algorithm for evaluation of the surface integral alone, experiments were performed using a test function vanishing on the boundary of a circle:

$$f_2(x,y) = (x^2 + y^2) (R^2 - x^2 - y^2)/R^4. \quad (4.2)$$

Ten-point Gaussian quadrature was used in the radial direction in numerical evaluation of all surface integrals.

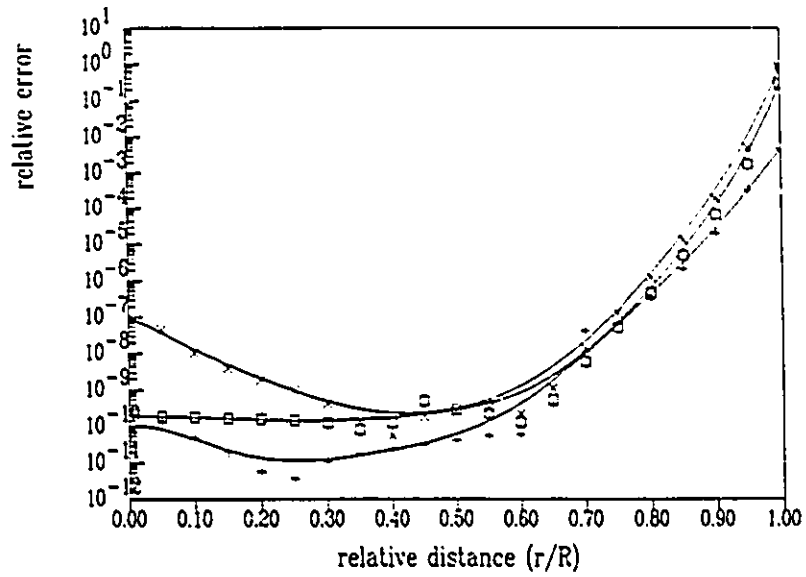
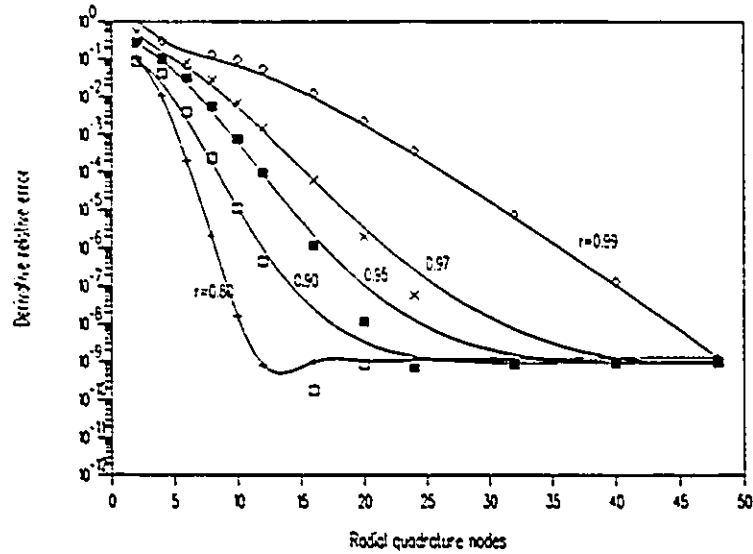


Figure 4.4. Relative error in derivatives  $\partial/\partial x$  (+),  $\partial^2/\partial x\partial y$  (x) and  $\partial^2/\partial x^2$  (□) of function  $f_2(x, y) = (x^2 + y^2)(R^2 - x^2 - y^2)/R^4$ .



**Figure 4.5.** Error in second derivative as a function of quadrature precision, for evaluations at  $r = 0.8R, \dots, 0.99R$ .

It should be noted that the method proposed here is stable in the interior of the circular region, but loses precision near the bounding circle. To illustrate, Figure 4.4 shows the relative error in the second derivatives  $\partial^2\phi/\partial x\partial y$  and  $\partial^2\phi/\partial x^2$  at various points  $P$ . Within the central portion of the circle, say  $r \leq 0.75R$ , the integrals are entirely stable and no difference in accuracy is observed when  $P$  is moved. For placements near the circular edge, the error rises. That this is not intrinsic in the mathematical method, but an artifact resulting from quadratures, is demonstrated by Figure 4.5: accuracy is recovered by increasing the precision of numerical integration.

## 4.1.1.2 Experiments with a rectangular region

The second set of numerical experiments was done using a rectangle as the region for which the derivatives were extracted. Results were obtained using the harmonic function

$$f_3(x, y) = x^3y - xy^3. \quad (4.3)$$

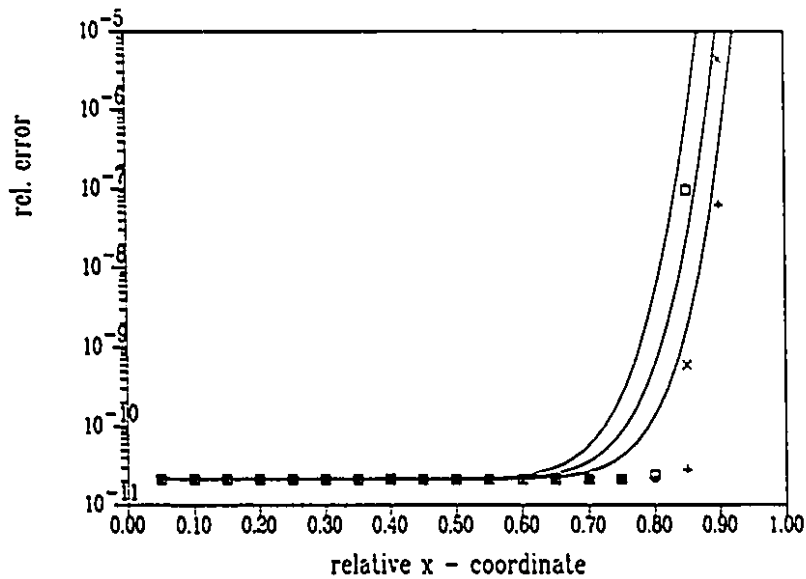


Figure 4.6. Derivatives  $\partial/\partial x$  (+),  $\partial^2/\partial x^2$  (x) and  $\partial^3/\partial x\partial y^2$  (□), of  $f_3(x, y) = x^3y - xy^3$ .

Derivatives up to third order were computed using the exact values of the function  $f_3(x, y)$  on the boundary. Ten-point Gaussian quadrature was used in

numerical computation of the boundary integral. Figure 4.6 demonstrates the accuracy of the algorithm. The precision is stable in the interior of the rectangle, while in the region near the boundary, 15% of dimension of the rectangle, the accuracy is poor. Experiments undertaken using the Poisson equation solution  $f_1(x, y)$  behave similarly to the case of a circular disk.

#### 4.1.1.3 Experiments with a sector of circle

Numerical results for the sector of a circle as the base region were obtained using the harmonic function  $f_3(x, y)$ . Since the quadrature becomes more complicated in this case, adaptive quadrature was used. Results shown in Figure 4.7 confirm the correctness of the derived formulas. Derivatives are obtained using the sector with angle  $\theta = 30^\circ$ , along the line with the angular coordinate  $\theta_p = 10^\circ$ , while the radial coordinate was varied.

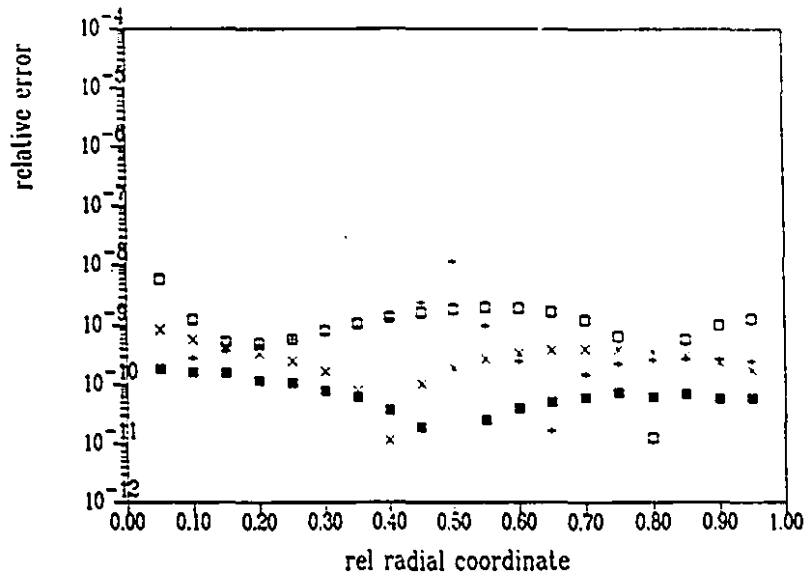


Figure 4.7. Relative error in derivatives for sector using adaptive quadrature;  $\partial f_3/\partial x$  (+),  $\partial f_3/\partial y$  (■),  $\partial^2 f_3/\partial x^2$  (x) and  $\partial^3 f_3/\partial x \partial y^2$  (□). Results are obtained using  $f_3(x, y) = x^3 y - xy^3$ .

#### 4.1.1.4 Experiments with a sector of ring

To test the characteristics of a sector of a ring as the base element from which derivatives are extracted, again the harmonic function  $f_3(x, y)$  was used. Results are obtained using adaptive Gauss-Kronrod quadrature on both linear and circular parts.

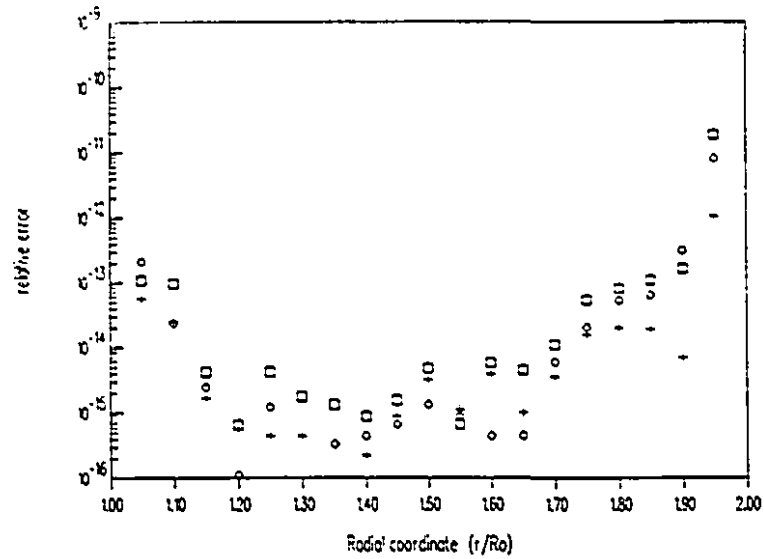
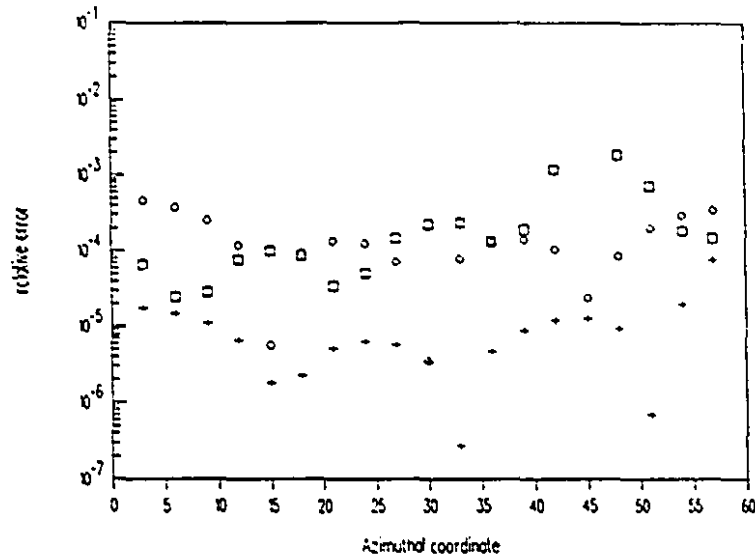


Figure 4.8. Relative error in derivatives for sector of ring using adaptive quadrature;  $\partial f_3/\partial x$  (+),  $\partial^2 f_3/\partial y^2$  (□) and  $\partial^2 f_3/\partial x\partial y$  (o). Results are obtained using  $f_3(x,y)=x^3y - xy^3$ , with  $\theta_P = 20^\circ$ .



**Figure 4.9.** Relative error in derivatives for sector of ring using adaptive quadrature;  $\partial f_3/\partial x$  (+),  $\partial^2 f_3/\partial y^2$  (□) and  $\partial^2 f_3/\partial x\partial y$  (o). The radial position was constant at  $r_p = 1.7$ .

The results shown in Figures 4.7 and 4.8 confirm that the derived formulas are correct, and that computed derivatives are stable inside the sector of ring, while the accuracy is reduced on approaching the boundary. Derivatives were computed using the sector of a ring with angle  $\theta = 45^\circ$  and inner and outer radii  $R_i = 1.0$  and  $R_o = 2.0$ , respectively. Derivatives from Figure 4.7 were obtained along the line with the angular coordinate  $\theta_p = 20^\circ$ , while the radial coordinate was varied. Results shown in Figure 4.8 were obtained along the arc with constant radial position  $r_p = 2.7$ .

## 4.1.2 Error amplification analysis

The main practical value of differentiation schemes such as described here is in computing derivatives of functions  $\phi$  whose values are known only approximately. Thus, having established that the scheme works, it is next of interest to determine how sensitive the results are to error in the function  $\phi$ .

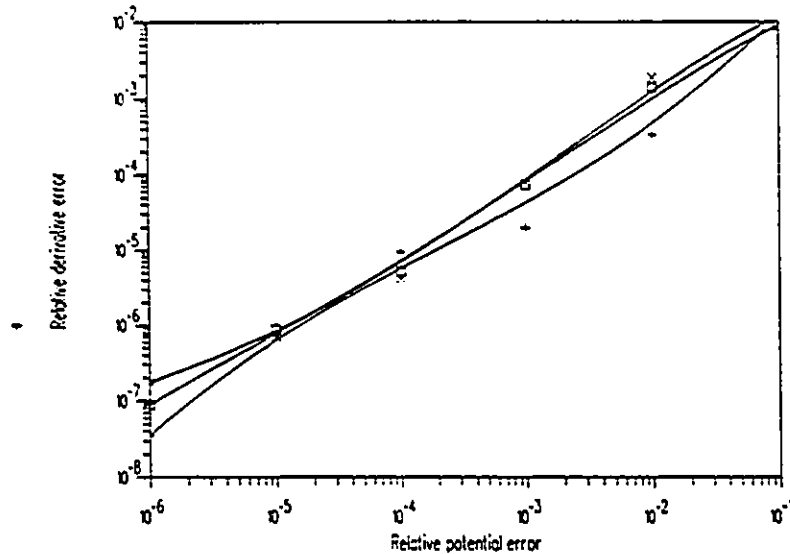


Figure 4.10. Relative error in derivatives  $\partial\phi/\partial y$  (+),  $\partial^2\phi/\partial y^2$  ( $\times$ ),  $\partial\phi/\partial x$  ( $\square$ );  $\phi = (x^2 + y^2)(R^2 - x^2 - y^2)/R^4$ . The potential  $\phi$  contains random error ("white noise").

For this purpose, a potential function  $\phi$  was differentiated after corruption by the introduction of random error. A random number generator with uniform error distribution was used, so that the average error in  $\phi$  remains zero. The measure of stability of the method is error amplification, defined as

$$\text{Error amplification} = \frac{(\text{Error in result}) - (\text{Average error in data})}{(\text{Average error in data})}. \quad (4.4)$$

Typical results appear in Figures 4.9–4.12, where potential was successively corrupted in the sixth significant figure, then the fifth, and so on until only one correct significant figure survived. For derivatives computed from a circle and shown on Figure 4.9, the error amplitude in the derivative is essentially linear with error in the function. It is noteworthy, however, that the error in derivative is not larger than the error introduced in the function; quite the contrary, the computed derivatives contain one more valid significant figure than the potential itself! In other words, this differentiation process *improves* results, contrary to most numerical differentiation processes which are well known to *degrade* them.

Results obtained for the other three elementary regions have similar characteristics, except that for the third order derivative the accuracy of results is lower than the accuracy of the original data.

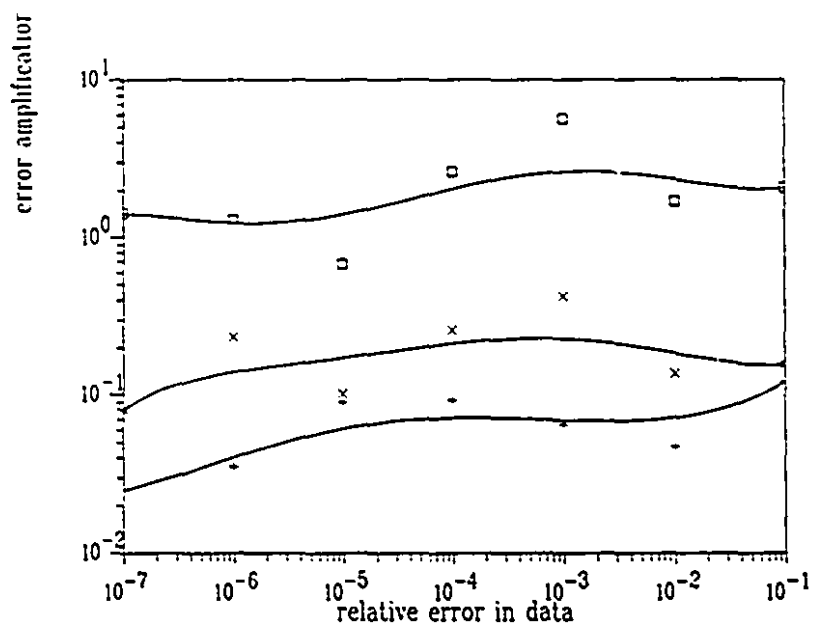


Figure 4.11. Error amplification in derivatives extracted from a rectangle,  $\partial f_3/\partial y$  (+),  $\partial^2 f_3/\partial x^2$  (x),  $\partial^3 f_3/\partial x^2 \partial y$  (□). Results obtained using function  $f_3(x, y) = x^3 y - xy^3$  and adaptive quadrature.

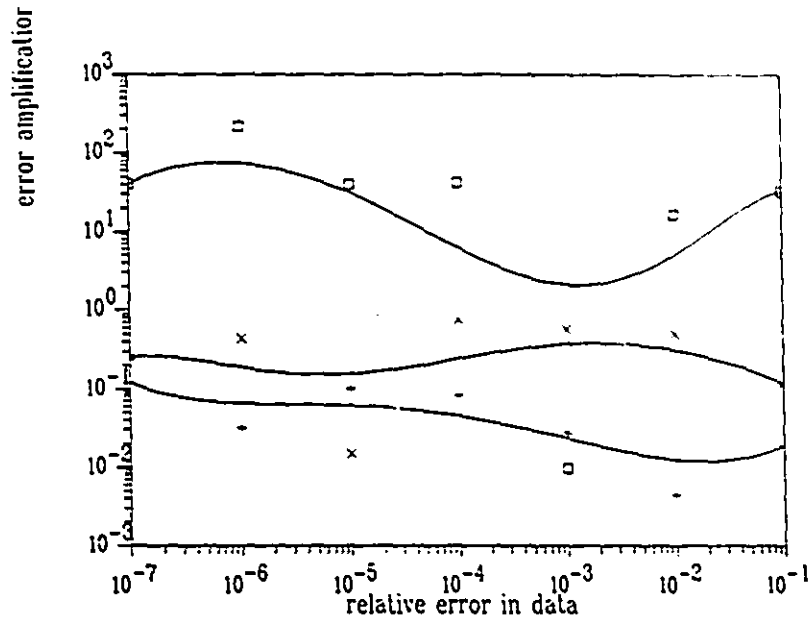


Figure 4.12. Error amplification in derivatives extracted from a sector of circle,  $\partial f_3/\partial x$  (+),  $\partial^2 f_3/\partial y^2$  (x),  $\partial^3 f_3/\partial x \partial y^2$  ( $\square$ ). Results obtained using function  $f_3(x,y)=x^3y - xy^3$  and adaptive quadrature.

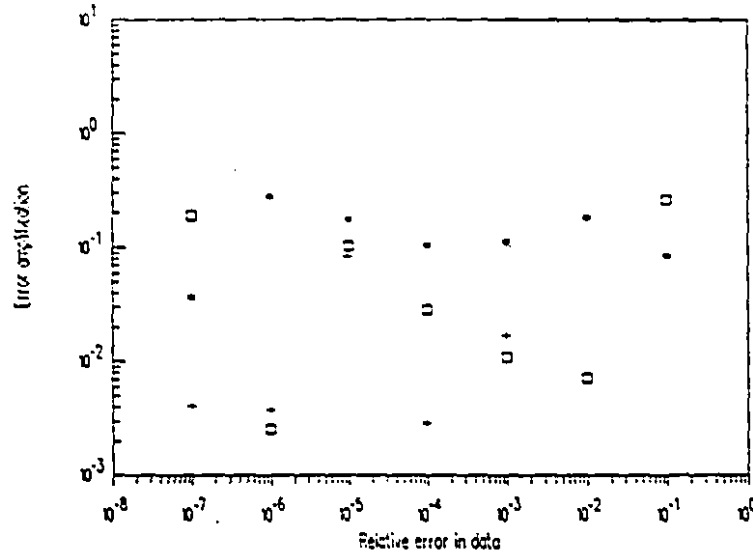


Figure 4.13. Error amplification in derivatives extracted from a sector of a ring,  $\partial f_3 / \partial x$  (+),  $\partial^2 f_3 / \partial x \partial y$  (□),  $\partial^2 f_3 / \partial y^2$  (o). Results obtained using function  $f_3(x, y) = x^3 y - xy^3$  and adaptive quadrature.

It is unclear whether a uniform error distribution is an adequate model for most numerical methods. For the finite element method, and some related least-squares methods, it may not be. Such techniques tend to be much more tolerant of small errors than large ones and therefore may well produce quasi-Gaussian rather than uniform error distributions in many problems. It is therefore fair to say that the figures given in this section demonstrate the error-attenuating property of the present method, but do not prove that this is necessarily a good way of post-processing finite element solutions. Tests with true finite element solutions are therefore warranted.

## 4.2 Experimental results with solutions of the Helmholtz equation

To test both methods described in section 2.2.3, the  $TM_{11}$  and  $TM_{31}$  modes of a rectangular waveguide were analyzed. The terms *method L* and *method H* are used to denote techniques of using the Green's function for the Laplacian operator and for the Helmholtz operator, respectively.

To evaluate the differentiation kernels of the Helmholtz operator 20 terms of the summation were used; this number appeared to give more than adequate convergence in all cases. Relative error results for the second derivative of the  $TM_{11}$  mode function are presented in Figure 4.13. Results were obtained along a line inclined at an angle of  $18^\circ$  to the  $x$ -axis, and by changing the number of terms in evaluation of kernel function. For the case analyzed, 7 terms in the summation is enough to obtain  $10^{-8}$  or better relative error.

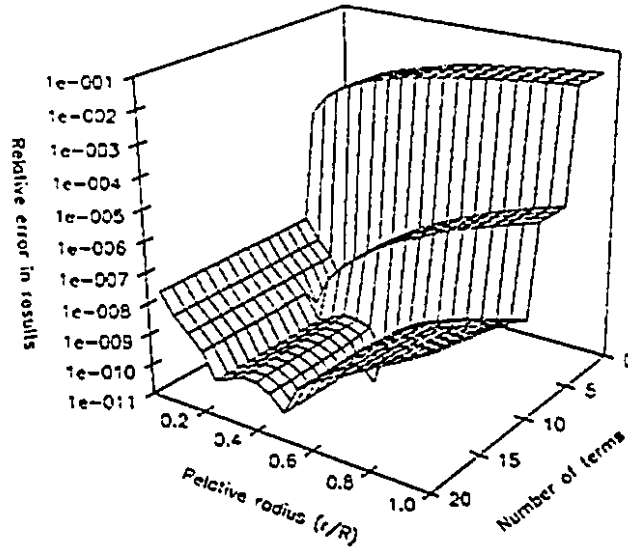


**Figure 4.14.** Relative error in second derivative as a function of position and number of terms in Green's function.

#### 4.2.1 Tests against the exact solution

Figure 4.14 shows results for the  $TM_{11}$  waveguide mode, with derivatives computed from point values of the exact solution. Results are shown for derivatives up to second order, which is the highest theoretically possible, using method L; and up to third order using method H. The solution was differentiated along a line inclined at an angle of  $25^\circ$  to the  $x$ -axis, using the circle of radius  $R = 1$  as the region of integration. From Figure 4.14 it is obvious that *method L* yields poor accuracy for  $r/R > 0.8$ . In the case of *method H*, the computed derivative values are not quite so position-dependent as for *method L*, and useful results are obtained even when the observation point  $P$  is fairly close to the edge

of the circle. At points near the middle of the integration region, derivatives of high accuracy are clearly obtainable.

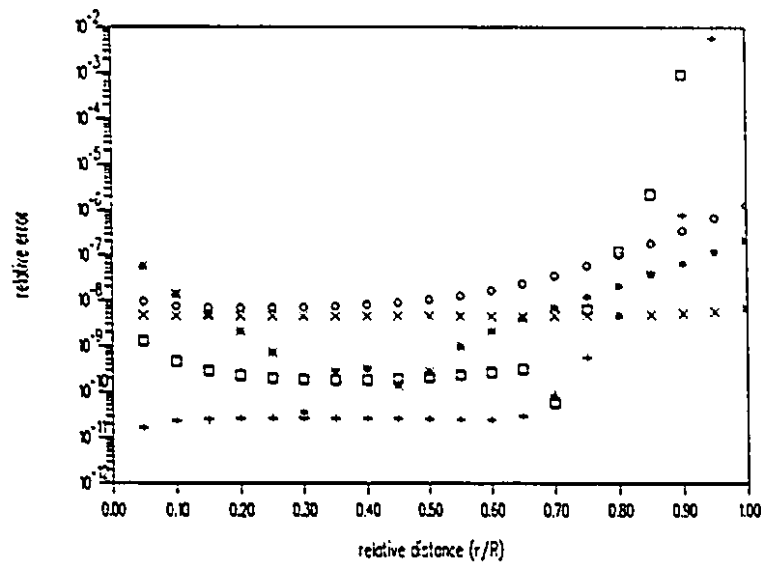


**Figure 4.15.** Comparison with analytic results: Relative error in derivatives. Using Green's functions for the Helmholtz operator:  $\partial/\partial y$  ( $\times$ ),  $\partial^2\phi/\partial x^2$  ( $*$ ),  $\partial^3\phi/\partial x\partial y^2$  ( $o$ ); using Green's functions for the Laplacian operator:  $\partial\phi/\partial y$  ( $+$ ),  $\partial^2\phi/\partial x^2$  ( $\square$ ).

All results were obtained using 180 quadrature nodes in azimuthal direction, and 8 radially. Experimentally it was confirmed that this order of quadrature is enough to ensure sufficient accuracy. In evaluation of the Bessel functions in *method H*, an algorithm with  $10^{-8}$  relative error was used. That is why *method H* results achieved a maximum of nine significant digits.

#### 4.2.2 Error sensitivity tests

To obtain the error amplification results the same function was used as previously, but this time containing a random error. The goal is to estimate how sensitive are differentiation methods when results are known approximately. A uniform error distribution was used in analysis to contaminate the function. Although this approach is not perfect, it gives an idea of error behavior of the results obtained from numerical approximation methods using the proposed algorithms.

In Figure 4.15 derivatives obtained using the function with error are presented. The maximum level of function error was  $10^{-3}$ . The radial position of the observation point was changed. The first derivatives obtained with both methods are of similar sensitivity. The second derivative obtained using *method H* is less position dependent than the one obtained using *method L*. For  $r/R < 0.4$  the computed third derivative contains an error of the same order as the error in original function.

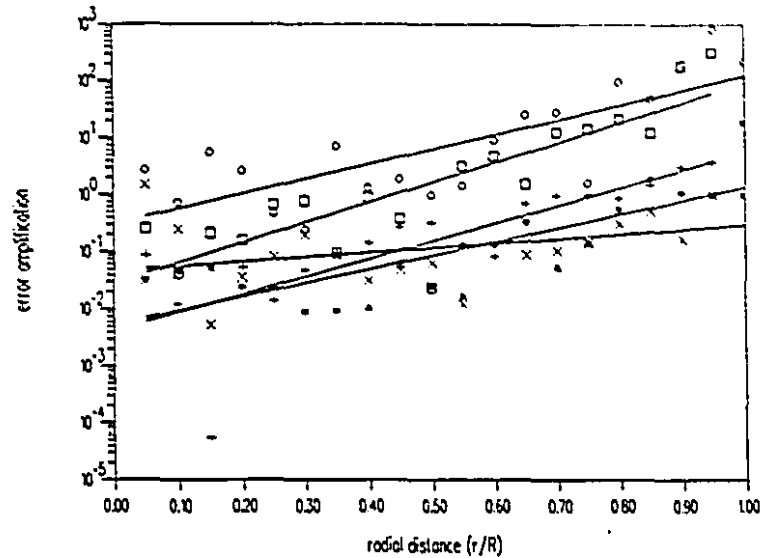


Figure 4.16. Error sensitivity results: Relative error in function was  $10^{-3}$ . Using Green's functions for the Helmholtz operator:  $\partial\phi/\partial x$  ( $\times$ ),  $\partial^2\phi/\partial x\partial y$  ( $*$ ),  $\partial^3\phi/\partial x\partial y^2$  ( $\circ$ ); using Green's functions for the Laplacian operator:  $\partial\phi/\partial x$  ( $+$ ),  $\partial^2\phi/\partial x\partial y$  ( $\square$ ).

### 4.3 Tests of procedure for axisymmetric problem derivatives

#### 4.3.1 Numerical efficiency

The two elementary shapes used for extraction of derivatives from a solution of Laplace's equation in axisymmetric coordinates are tested using the same procedures.

Figures 4.17 and 4.18 show the accuracy of derivatives extracted from a

torus and a sphere. The harmonic function  $\phi(r, z)$  used in both cases was

$$\phi(r, z) = r^3y - xy^3. \quad (4.5)$$

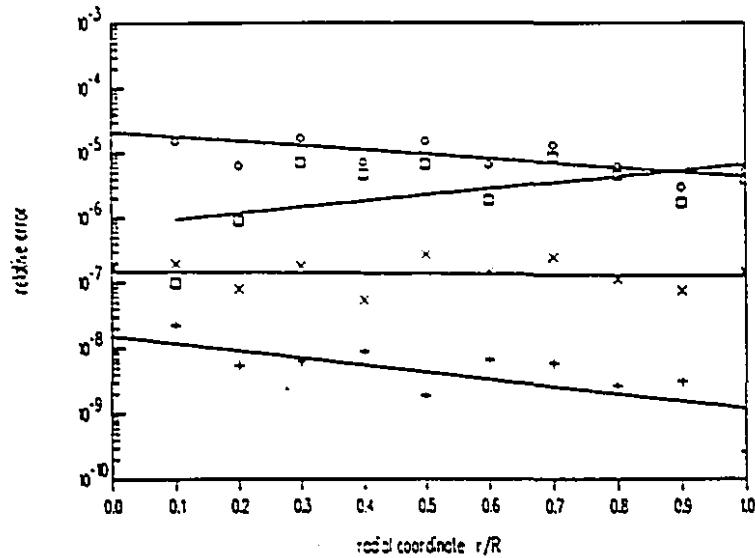


**Figure 4.17.** Comparison with analytic results: Relative error in derivatives extracted from a torus, potential  $\phi$  (+),  $\partial/\partial r$  (x),  $\partial\phi/\partial z$  ( $\square$ ),  $\partial^2\phi/\partial r^2$  (o).

The torus has radius  $l = 2.0$ , cross-sectional radius  $a = 1.0$  and it is positioned at  $z = 1.0$ . Derivatives were computed along the radius, at an angle  $\theta_P = 10^\circ$  to the  $r$ -axis. Although double precision was used, the accuracy does not exceed  $10^{-9}$ . The source of error is evaluation of Legendre's functions of nonintegral order, which is based on recursive computation from elliptic integrals of the first and second kinds. To compute elliptic integrals the AGM—arithmetic-geometric method was used (Spanier and Oldham (1987)). The accuracy of the algorithm is not position dependent.

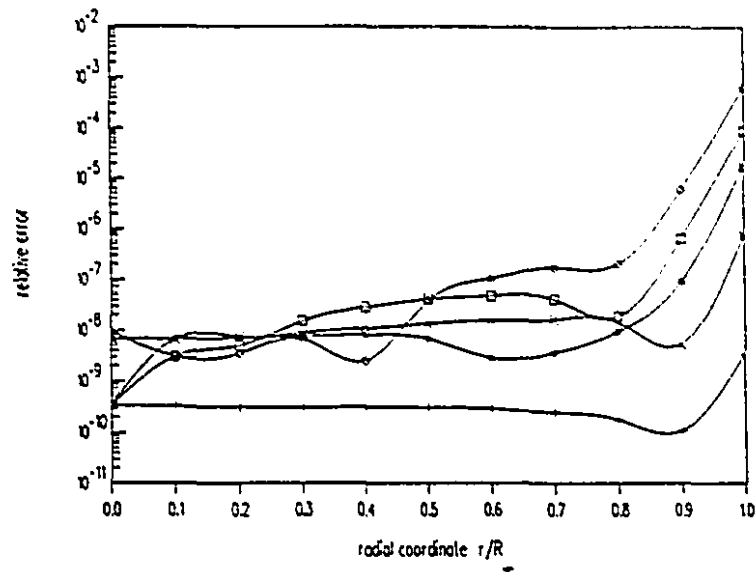


Figure 4.18. Comparison with analytic results: Relative error in derivatives extracted from a sphere, potential  $\phi$  (+),  $\partial/\partial r$  ( $\times$ ),  $\partial^2\phi/\partial r\partial z$  ( $\square$ ),  $\partial^2\phi/\partial z^2$  (\*),  $\partial^3\phi/\partial r^2\partial z$  ( $\circ$ ).

A second sequence of tests was performed using a sphere as the base region. It is located at  $z_c = 2.0$ , and has radius  $R = 1.0$ . Derivatives are computed along the radius at the angle  $\psi = 40^\circ$  with respect to  $z$ -axis. Accuracy of the computed derivatives is position dependent. As it can be seen from the Figure 4.18, derivatives computed for  $r_p/R \geq 0.8$  have poor accuracy.

#### 4.3.2 Error sensitivity

A procedure identical to that described in 4.1.2 and 4.2.2 is used to obtain the error amplification results for a torus and sphere. The same function  $\phi(r, z)$  was

used, but this time containing a uniform random error. These tests were performed with the aim to estimate the behaviour and robustness of the method when applied to an approximate solution.

Figure 4.19 shows the error amplification results obtained using the same torus as before. Derivatives are computed at point  $P$  with radial distance  $\rho = 0.2$ , and angular coordinate  $\theta_P = 10^\circ$ . The results show much the same accuracy as that of potentials when the first derivative is computed, and that 1-2 significant digits are lost in the case of second derivative computation.

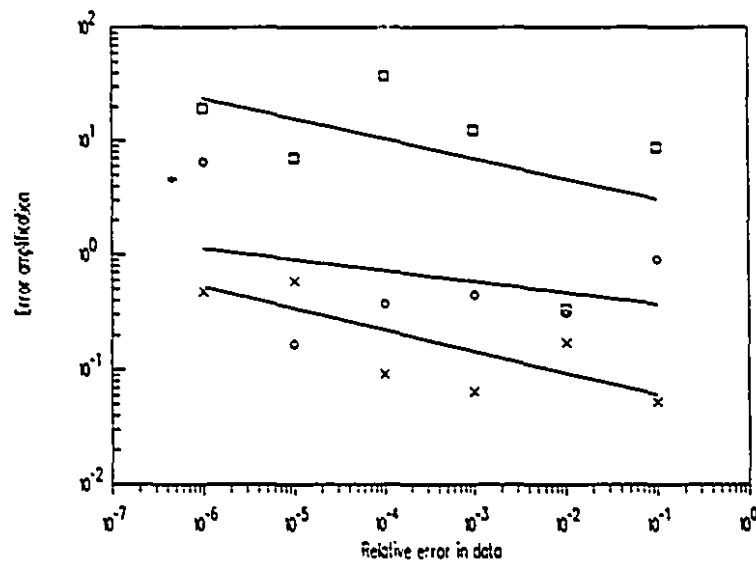


Figure 4.19. Error sensitivity results: derivatives extracted from a torus:  $\partial\phi/\partial r$  ( $\times$ ),  $\partial\phi/\partial z$  ( $\square$ ),  $\partial^2\phi/\partial r^2$  (o).

Results obtained using the sphere are presented in Figure 4.20. It shows the error amplification results of derivatives computed at point  $P$  with radial distance  $\rho = 0.2$ , and angular coordinate  $\psi_P = 40^\circ$ . The performances of sphere are better than those of torus. The error amplification is negative, meaning that the computed derivatives have better accuracy than the potential.

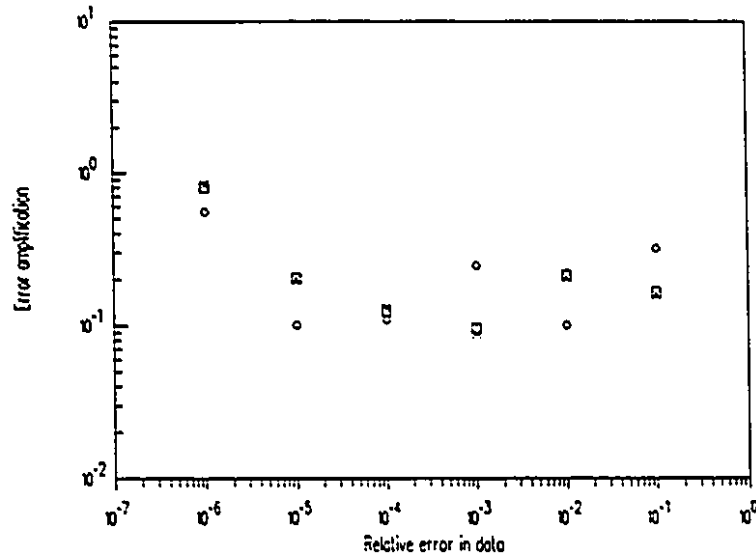


Figure 4.20. Error sensitivity results: derivatives extracted from a sphere: potentials  $\phi$  (+),  $\partial\phi/\partial r$  (x),  $\partial^2\phi/\partial z^2$  (□),  $\partial^3\phi/\partial r^2\partial z$  (o).

## CHAPTER 5

### Evaluation of singular and near-singular integrals

In Chapter 3 differentiation of singular integrals is treated in detail. It is shown that the surface integrals are always singular. Variable transformations may reduce the order of singularity by one. When the method is applied to first derivative calculation the singularity in the surface integral is eliminated. In the case of second derivatives, the singularity is 'strong', but it may be reduced to order  $1/s$ . One way to evaluate these integrals, described in Chapter 4, is ignoring singularity (Davis and Rabinowitz (1984)) with increased number of quadrature nodes. As the boundary of the region is approached, the number of quadrature nodes has to be increased, as shown in Chapter 4, otherwise the error is large.

The curvilinear term becomes singular when the observation point is right on the edge of a region. If the point of interest is close to the region edge, the results are also very sensitive to the number of quadrature nodes used (Silvester (1991 a)). Unfortunately, practical problems often requires the values of derivatives on some surface, or along a boundary. This corresponds to evaluating singular and near-singular integrals. So it is necessary to make the methodology of accurate derivative computation efficient by applying robust methods of evaluating these integrals.

In this Chapter the finite part integration concept is presented and used to compute singular integrals, both surface and curvilinear (Ioakimidis (1985), Ioakimidis and Pitta (1988), Kutt (1975), Paget (1981 a and 1981 b), Davis and Rabinowitz (1984)). The method is based on analytic continuation of the analytic function which is the solution of the convergent singular integral (Ninham (1966)), by taking only the finite part of the divergent integral.

Application of various methods for evaluation of near-singular curvilinear

integrals is discussed. Although it is possible to generate efficient quadrature formula, after application to approximate solution they become inefficient.

## 5.1 Finite Part Integrals

The way of manipulating divergent integrals to obtain correct results is sometimes not well understood (Ninham (1966)). Ninham (1966) presented a method of interpretation of a class of divergent integral, dealing with integrands continuous over the integration interval except at a finite number of algebraic singularities. This approach is the basis for the finite part integration theory (Kutt (1975), Paget (1981 a and 1981 b), Ioakimidis and Pitta (1988)).

### 5.1.1 Analytic continuation and definition

Consider the integral

$$I(f, m) = \int_a^b \frac{w(x)f(x)}{(x-s)^m} dx \quad (5.1)$$

where  $m$  is a positive constant,  $w(x)$  is a weight function integrable on  $[a, b]$ . If  $s$  does not belong to  $[a, b]$ , this type of integral behaves as a regular integral. In the case that  $s$  belongs to  $[a, b]$  and  $m \geq 1$ , the integral diverges and is not solvable analytically. Then this integral may be considered as the analytic continuation of the function  $I(f, m)$  to the region  $m < 1$ . It has a meaning in generalized function theory (Ninham (1966)),

$$\int_0^1 \frac{dx}{x^m} = \int_{-\infty}^{+\infty} \frac{H(x) - H(1-x)}{x^m} dx = \frac{1}{m+1}, \quad (5.2)$$

where  $H(x)$  is the step function.

These integrals are called finite part integrals, or Hadamard finite parts of

the divergent integral. Usually the symbol  $\int_a^b$  or  $\int_a^b$  is used to represent those integrals. The first symbol is used for the *generalized principal value integral*, if the integral exists in a Cauchy principal value sense, as a natural extension of the Cauchy principal value of the integral (Kutt (1975)). The second symbol is used to label general finite part integrals, and may also be defined as

$$\frac{d^m}{ds^m} \int_a^b \frac{w(x)f(x)}{x-s} dx = m! \int_a^b \frac{w(x)f(x)}{(x-s)^{m+1}} dx \quad (5.3)$$

where the integral on the left side denotes the Cauchy principal value of the integral. These integrals satisfy the usual rules of Riemann integration theory, as to integration by parts and transformation of variables.

The fundamental finite part integral  $I(1, m)$  is defined by

$$I(1, m) = \int_0^1 x^{-m} dx = \begin{cases} 0 & \text{if } m = 1 \\ (1-m)^{-1} & \text{if } m \neq 1 \end{cases} \quad (5.4)$$

If  $m < 1$ , the finite part integral coincides with the regular integral. If the function  $f(x)$  is  $m$  times differentiable and  $m \geq 1$ , then the general finite part integral may be defined as (Paget (1981a))

$$\int_0^1 \frac{f(x)}{x^m} dx = \frac{1}{(m-1)!} \left\{ \sum_{k=1}^{m-1} k^{-1} f^{(m-k)}(0) - \sum_{k=0}^{m-2} (m-2-k)! f^{(k)}(1) - \int_0^1 \ln(x) f^{(m)}(x) dx \right\} \quad (5.5)$$

The formula (5.5) is obtained using the  $m$ -term Taylor series expansion of  $f(x)$ .

### 5.1.2 Quadrature formulae for finite part integrals

Formulae for calculation of finite part integrals may be divided into three major groups: (i) equidistant quadrature formulae (Kutt (1975)), (ii) Gaussian-type quadrature formulae (Kutt (1975), Tsamasphyros and Dimou (1990)) and (iii)

computational procedures based on modification of the standard Gaussian quadrature (Paget (1981a and 1981b)).

Kutt (1975) first derived quadrature formulae for finite part integrals. He used two approaches. The first is the equidistant formula, and the second is a Gaussian-type specialized quadrature formula. The equidistant quadrature formula is of the following type:

$$(b-a)^{1-m} \sum_{i=1}^n f(x_i) \left\{ w_i^{(m)} + c_i^{(m)} \frac{\log |b-a|}{(m-1)!} \right\} \quad (5.6)$$

where  $w_i^{(m)}$  are the weights at  $n$  equispaced points  $x_i \in [a, b]$  and  $c_i^{(m)}$  are the coefficients for the  $(m-1)$ -th derivative of  $f$  at the origin. The accuracy depends on the nature of the integrand and the length of the integration interval. The weights vary in sign and their values increase with the number of integration points and the order of singularity. The consequence of this property is reduced accuracy.

The second method uses generated orthogonal polynomials. It is considered the conventional finite part integration. A quadrature formula for the first order singularity is published in the standard boundary element textbook (Brebbia (1984)). Quadrature nodes are found in usual way, as zeros of orthogonal polynomials, as well as the weights, using the standard formula. Ioakimidis and Pitta (1988) derived a universal procedure of generating orthogonal polynomials for finite path integrals. They are expressible as linear combinations of successive shifted Legendre polynomials. In the case of a first order singularity one root of the orthogonal polynomials is outside the integration domain, and for higher order some of zeros are complex. Tsamasphyros and Dimou (1990) proved these properties of zeros of orthogonal polynomials.

The method used in this thesis belongs to a third group. There are two approaches derived from conventional Gaussian quadrature methods (Paget (1981 a, 1981 b), Hunter (1972)). One may be characterized as an adaption of the quadrature rule for Cauchy principal value integrals (Hunter (1972), Paget (1981 a)). The general formula has the following form (Paget (1981 a)):

$$I(f, 2) = \sum_{i=1}^n \frac{\mu_{i,n} f(x_{i,n})}{(x_{i,n} - s)^2} + \frac{d}{ds} \left( \frac{q_n(s)}{p_n(s)} \right) f(s) + \frac{q_n(s)}{p_n(s)} f'(s) + R_n(f; s). \quad (5.7)$$

For problems of normal derivative computation, the term  $q_n(s)/p_n(s)$  is analytically known and equal to zero. Then, this method corresponds to *ignoring the singularity*. In practical application of this formula instead of  $f(x_{i,n})$ , most often  $f(x_{i,n}) - f(s)$  is used. The second method will be described in the following section. It gives a general procedure for derivation of quadrature rules of arbitrary order. Both methods are compared later in this chapter.

### 5.1.3 Generation of quadrature formulae

If  $p_k(x)$  are orthogonal polynomials with respect to the weight function  $w(x)$ , then an  $n$ -point Gaussian rule gives

$$\int_{-1}^{+1} w(x) f(x) dx = \sum_{i=1}^n \mu_{i,n} f(x_{i,n}). \quad (5.8)$$

A numerical solution of the finite part integral is supposed to have the form

$$I(f, \lambda) = \int_0^1 \frac{w(x) f(x)}{x^\lambda} dx = \sum_{i=1}^n w_{i,n} f(x_{i,n}), \quad (5.9)$$

where  $x_{i,n}$  are the abscissas of the  $n^{\text{th}}$  order Gaussian quadrature. The weights  $w_{i,n}$  of the quadrature formula (5.9) may be obtained from the original weights  $\mu_{i,n}$  corresponding to the non-singular case using the formula

$$w_{i,n}(\lambda) = \mu_{i,n} \sum_{k=0}^{n-1} h_k^{-1} p_k(x_{i,n}) b(\lambda), \quad (5.10)$$

where  $h_k$  is the leading term of the orthogonal polynomial  $p_k$ . The coefficients  $b(\lambda)$  are moments defined by

$$b_k(\lambda) = \int_0^1 x^{-\lambda} p_k(2x-1) dx, \quad k = 1, \dots, n-1. \quad (5.11)$$

The universal tool for deriving quadrature rules of finite part integrals from the corresponding regular integrals is defined by the last three expressions. Paget (1981b) also gave an upper bound for the remainder term of the quadrature rule.

The advantage of this method is that the abscissas are always in the domain of integration, although the weights change sign. When Gaussian quadrature is applied, negative or complex roots of orthogonal polynomials appear. In the case of an equidistant formula there is no closed form algorithm comparable to the one described above. Another advantage of Paget's method is its simplicity of application and the existence of general expressions for coefficients of the quadrature formulae. These features make the approach presented here attractive, especially in conjunction with symbolic algebra packages like MATHEMATICA (Silvester (1992)).

In the singular surface integral, the singularity is of first order if the second order derivative is to be computed. Thus the Gauss-Legendre quadrature formula is modified to obtain the quadrature formula for this finite part integral. The curvilinear integral for the normal derivative on the edge contains a second order singularity of type  $(\sin\theta)^{-2}$ , where integration is performed with respect to the polar coordinate  $\theta$ . In that case the weights of the Gauss-Chebyshev formula (Davis and Rabinowitz (1984)) are to be modified. In both cases evaluation of the modified weights is straightforward.

## 5.2 Computation of near-singular integrals

Accurate computation of near-singular integrals is the most difficult problem in the process of computing derivatives using the methodology based on Green's second identity. What makes this problem complicated is the fact that the finite element solution is approximate. The consequence is that error in potentials obtained using the finite element solver is amplified, so the local error determines the error in computed derivatives.

The classical methods for computing these integrals are based on the Taylor series expansion of a distribution function, or one part of it. The number of terms in the expansion depends of the nature of the integrand. It has to be done around  $P'$ , the point on the boundary closest to the observation point  $P$ . Because only the approximate potentials are known the only improvement is to use  $\phi_Q - \phi_{P'}$ , instead of  $\phi_Q$  in formula (2.65),

$$\begin{aligned} \frac{\partial^{m+n}\phi_P}{\partial^m x \partial^n y} = & - \oint_{\partial\Omega} (\phi_Q - \phi_{P'}) K_{mn}(P; Q) d\Gamma_Q - \phi_{P'} \oint_{\partial\Omega} K_{mn}(P; Q) d\Gamma_Q \\ & + \iint_{\Omega} g_Q J_{mn}(P; Q) d\Omega_Q. \end{aligned} \quad (12)$$

The second integral is equal to zero, except for  $m = n = 0$ , when it is 1. The conventional equidistant Gaussian quadrature formula for a circle Krylov (1962), which corresponds to a Gauss-Chebyshev quadrature formula, is usually applied to evaluate these integrals. This simple method does not yield a much better accuracy, compared to the standard formula. This technique can be applied together with regularization of the Poisson kernel, described in section 3.3.1 of this thesis. The alternative Fourier series expansion method is slowly convergent, and not efficient. Another conventional method often used is a kind of adaptive quadrature with repeated subdivision. In that case the information used is more local, so the averaging over a wide domain is lost.

### 5.2.1 Generation of specialized Gaussian quadrature formulae

The existing algorithm developed by Silvester (1990) was used to compute the Gaussian quadrature weights and nodes. This algorithm is suitable for integrands with a rapid variation of the weight function  $w(x)$ . The required number of operations is  $O(N^3)$  for an  $N^{\text{th}}$  order quadrature.

If the weight function  $w(x)$  is given, then it is possible to find weights  $w_j$  and nodes  $x_j$ , such that

$$\int_a^b w(x) f(x) dx = \sum_{j=1}^N w_j f(x_j) \quad (5.13)$$

is exact if  $f(x)$  is a polynomial of degree  $(2N - 1)$  or lower. Nodes  $x_j$  are the zeros of  $N$  orthogonal polynomials  $p_j$  generated with respect to weight  $w(x)$ . The weights  $w_j$  can be computed by

$$w_j = \frac{p_j^2(x_j)}{\sum_{i=0}^{N-1} \int_a^b w(x) p_i^2(x) dx}. \quad (5.14)$$

The complete procedure of generating orthogonal polynomials, their factoring, as well as computing the weights is given in Silvester's paper (Silvester (1990)).

This method may be extended by application of parametrized Gaussian quadrature (Lutz (1992)). The specialized Gaussian quadrature formulae can be derived for a finite number of normalized radial positions of the observation point  $P$ , since the corresponding integrals may be rewritten to a form independent of  $\theta_P$ , the angular coordinate of point  $P$ . The generated Gaussian points and weights are now considered as functions of relative radial position. After generation of the sets of abscissas and weights for various orders of quadrature and various positions of the observation point the interpolation has to be done. Cubic Lagrangian polynomials are usually used in the interpolation process (Lutz(1992)).

Specialized quadrature formulae were generated for first and second order Poisson kernels. Their accuracy is high when applied to exact values of potentials. But, application of the method to finite element solution does not yield a satisfactory results. Again, the information used is local, and the local error is amplified, since the ratio of generated weights is very high ( $\sim 10^3$ ) for  $r/R > 0.9$ .

### 5.3 Computational verification of the quadrature methods

For illustration of all the methods considered, a sequence of tests has been done. They cover both cases, curvilinear singular integrals in the normal derivative computation and singular surface integrals arising in second order derivative calculation.

#### 5.3.1 Normal derivative computation using the Poisson integral method

This group of results consists of two subsets. First, calculations were done using exact analytical harmonic function values. To test error sensitivity of the method, data were corrupted with random error. Tests were done using the harmonic function

$$f_3(x, y) = x^3y - xy^3. \quad (5.15)$$

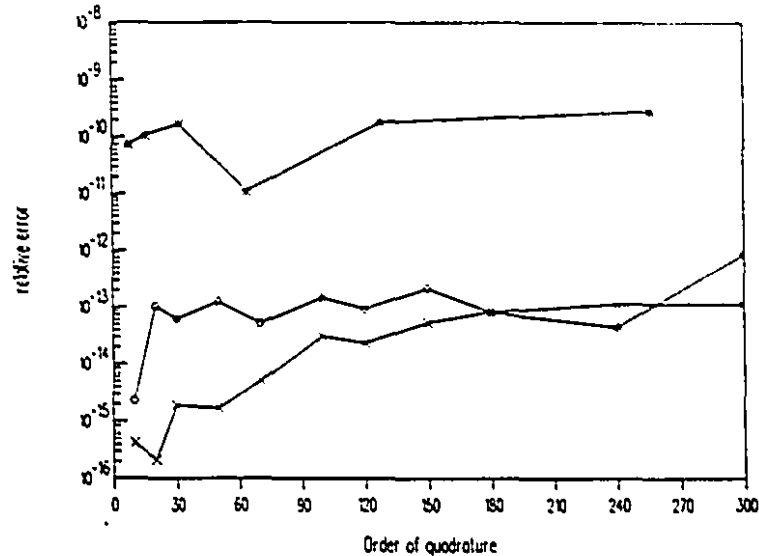


*Figure 5.1.* Accuracy of normal derivative for different number of quadrature nodes used. Results obtained using finite part integrals (o), Fourier series expansion (\*) and by ignoring the singularity (x).

A comparative analysis using all the available methods is presented in Figures 5.1 and 5.2. Figure 5.1 shows how accuracy of the calculated normal derivative depends on the number of quadrature nodes, or number of samples used. The case of using finite part integrals and results obtained by ignoring the singularity, which corresponds to the second concept of finite part integration used by Paget (1981b), and standard boundary element practice (Sladek and Sladek (1992)) is presented.

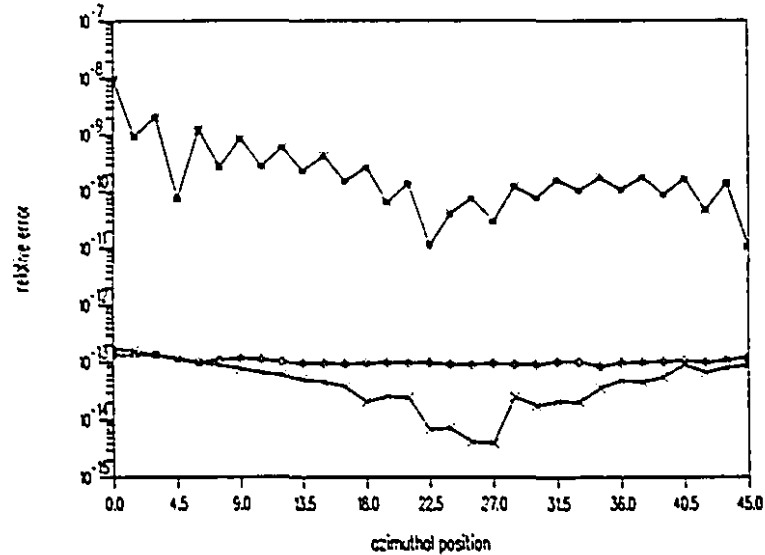


*Figure 5.2.* A comparative analysis. Normal derivative obtained using:

Figure 5.2 shows the accuracy of computed derivatives for different azimuthal positions of the observation point. It may be seen that both finite part integration approaches give good results. But this analysis does not lead directly to finite element applications. First, the error sensitivity of the method, since it is intended to be applied to approximate solutions must be investigated. A uniform random error generator was used to corrupt exact data. The measure of stability of the method is error amplification, defined by (4.4).

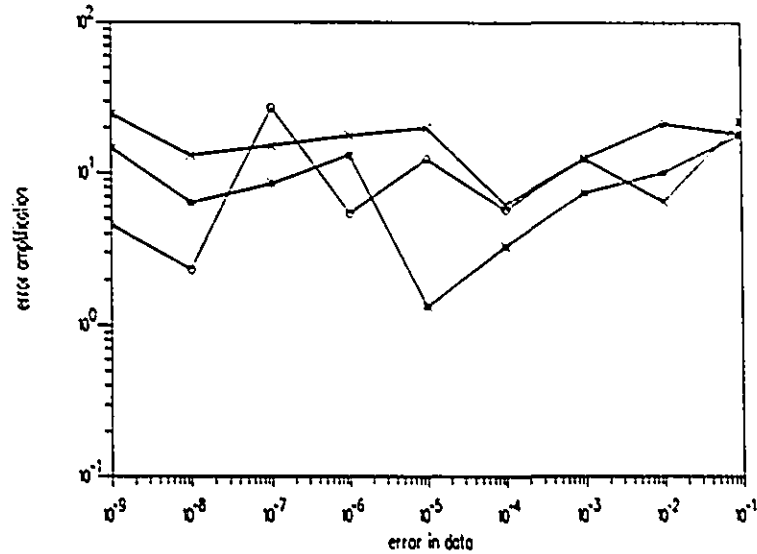


**Figure 5.3.** Error sensitivity results. Error amplification for different average error in potential data. Poisson integral method with Paget's finite part integration (o), Fourier series method (\*) and ignoring singularity (x).

Figure 5.3 gives error sensitivity as a function of average error in data. 300 point quadrature was used in these tests. This is the highest order for which quadrature formula is derived. Despite the fact that the number of samples is not too high, the results illustrate the stability of methods used in computation of normal derivatives. The finite part integration technique based on modification of Gaussian quadrature rule proposed by Paget had up to ten times better accuracy than the ignoring singularity method, except for two cases. Fourier series results were obtained using 1024 samples. Using the lower order expansion gave poor results.

### 5.3.2 Second derivative of the Poisson equation solution

To analyze the efficiency of Paget's formulae for finite part integration in this case tests were performed with exact function values. The functions used in numerical experiments are

$$f_1(x, y) = x^3y + xy^3, \quad (5.16)$$

$$f_2(x, y) = (x^2 + y^2)(1 - x^2 - y^2). \quad (5.17)$$

Function  $f_2(x, y)$  was chosen to eliminate the error in boundary integral computation. Since a circle of radius  $R = 1$  was used as a base region, this function vanishes on its edges. So all derivatives are computed using the domain integral only. Function  $f_1(x, y)$  represents the general case when both integrals must be computed.

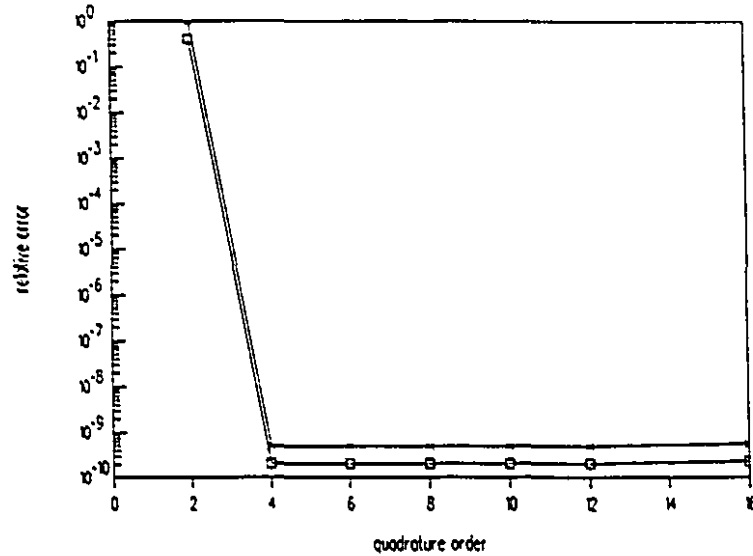


Figure 5.4. Derivative  $\partial^2 f_2 / \partial x \partial y$  ( $\times$ ) and  $\partial^2 f_2 / \partial y^2$  ( $\square$ ) for different number of quadrature nodes in  $s$  direction. Derivatives are computed at  $P$  ( $r_P = 0.4, \theta_P = 20^\circ$ ).

Two cases are typical, when point of observation  $P$  is on the edge and when it is an interior point of the circle.

The results in Figure 5.4 show the behavior of relative error in the computed derivative  $\partial^2 f_2 / \partial x \partial y$  for different numbers of quadrature nodes in the  $s$  direction. These results were obtained using the function  $f_2(x, y)$  on a circle of radius  $R = 1$ , centered at  $(0, 0)$ . Derivatives were computed for  $r_P = 0.4$ ,  $\theta_P = 20^\circ$ . From the results presented it is clear that a four-point quadrature formula gives satisfactory results, compared to the ten nodes used earlier. From now on, the four-node finite part integration is used. Figure 5.5 presents the behavior of those methods as the radial position is varied. The finite part

integration is seen to be stable even when the point  $P$  is close to the edge. The accuracy decreases for  $r/R > 0.92$ . Results presented in Chapter 4 of this thesis showed that accuracy is rapidly decreasing for  $r/R > 0.5$ . So the finite part integration reduced two to three times the order of quadrature, and has significantly increased the region where the accuracy of computed derivatives is satisfactory.

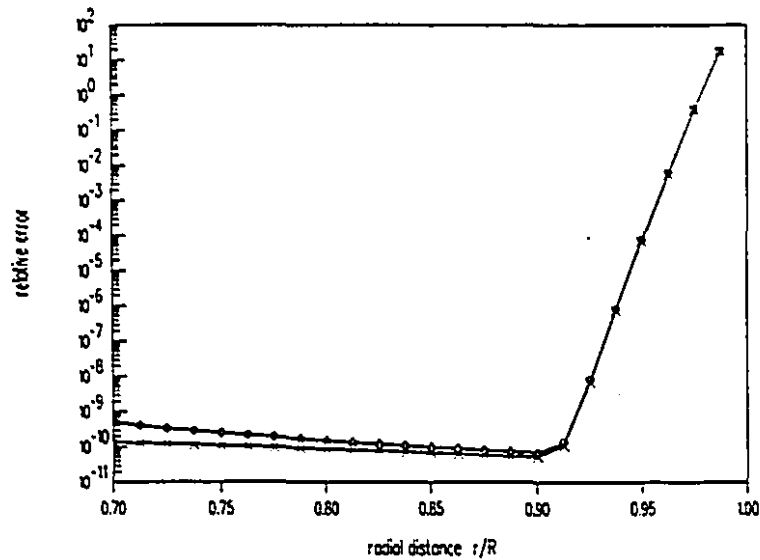


Figure 5.5. Accuracy of computed derivative  $\partial^2 f_2 / \partial x \partial y$  ( $\times$ ) and  $\partial^2 f_2 / \partial y^2$  ( $\circ$ ) when radial position is varied. Finite part integration with 4 nodes is used.

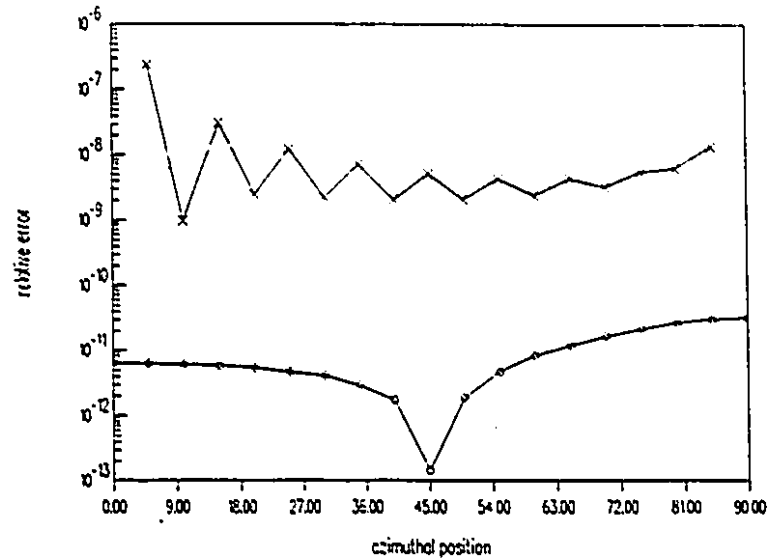


Figure 5.6. Results of computed  $\partial^2 f_1 / \partial x^2$  (x) and  $\partial^2 f_2 / \partial x^2$  (o) for point  $P$  on the edge, for various angular position. Curvilinear integral was computed using the Fourier series expansion.

Figure 5.6 shows results of computed  $\partial^2 f_2 / \partial x^2$  for point  $P$  on the edge, for various angular positions. Results are given for both functions  $f_2$  and  $f_3$ . Four point finite part integration was used in  $s$ -direction, with 90 points taken in  $x$ -direction. The curvilinear integral term was computed using a Fourier series expansion. The total error is influenced by both terms, but results show a satisfactory accuracy.

#### 5.4 Concluding remarks

The concept of finite part integration appears to be effective for evaluation of singular integrals arising in the differentiation method based on Green's second identity. Computational experiments confirm that the application of finite part integration yields satisfactory accuracy in both normal derivative computation on harmonic functions and the singular surface integrals involved in second derivative computation of the Poisson equation solution. Using this approach the order of quadrature is significantly reduced.

All known formulation for evaluation of near-singular integrals have high error sensitivity. Since in most practical problems only approximate solution is known, it is not possible to achieve the same accuracy of derivatives as for interior points.

## CHAPTER 6

### Gradient recovery by local smoothing of finite element solutions

The best traditional methods for differentiation on finite element meshes rely on the phenomenon of *superconvergence*. The *local smoothing* proposed by Hinton and Campbell (1974) is a widely accepted method for accurate derivative computation, and it is referred to here as *the conventional local smoothing*. It amounts in essence to bilinear extrapolation of gradients sampled at  $2 \times 2$  Gauss-Legendre integration points. An analogous procedure may be applied to three-dimensional brick elements.

Gradient recovery as discussed in this Chapter is a generalization of a particularly attractive local smoothing method proposed by Zhu and Zienkiewicz (1990) for one-dimensional problems. They showed that the method has  $O(p+1)$  convergence in one-dimensional problems, where  $p$  is the order of finite element approximation. These techniques deal with one element at a time and appear to lend themselves well to parallel computation, although this point has as yet been insufficiently explored.

#### 6.1 The fundamental equations

The discussion in this chapter is restricted to the scalar Helmholtz equation, though it can clearly be extended to some other differential equations as well. Suppose an approximate solution  $\bar{\phi}$  has been found to a boundary value problem whose differential equation is

$$\operatorname{div}(\epsilon \operatorname{grad} \bar{\phi}) + \kappa^2 \bar{\phi} = -g \quad \text{in } \Omega \quad (6.1)$$

with appropriate boundary conditions on  $\partial\Omega$ . This is a slightly generalized form of the scalar Helmholtz equation, where  $\epsilon = \epsilon(x, y, z)$  and  $\kappa^2 = \kappa^2(x, y, z)$  are permitted to vary in space. The field, defined in the usual fashion as

$$\mathbf{E} = -\text{grad } \bar{\phi} \quad (6.2)$$

consequently satisfies

$$\text{div}(\epsilon \mathbf{E}) - \kappa^2 \bar{\phi} = g. \quad (6.3)$$

In practical computation the approximation  $\phi$  is known, not the exact potential  $\bar{\phi}$ . The study presented in this Chapter concentrates on the gradient of their difference,  $\nabla(\bar{\phi} - \phi)$ , which represents the error in the computed field.

## 6.2 Taylor series analysis of error

The approach of MacKinnon and Carey (1989) will be followed in derivation of an error analysis using the Taylor series. The three-dimensional case is presented, since it is the most general.

In finite element analysis the problem domain is first discretized and a set of approximating functions  $\alpha_i(\xi_1, \xi_2, \xi_3)$ , usually expressed in local coordinates  $\xi_i$ , is selected. The potential is then given the elementwise approximation

$$\phi = \sum_i^N \alpha_i(\xi_1, \xi_2, \xi_3) \phi_i, \quad (6.4)$$

where  $\phi_i$  are nodal values of the potential function (degrees of freedom) on a finite element, and  $N$  is the number of degrees of freedom. The field component  $E_k$ , i.e., the directional derivative in direction  $\xi_k$  of a finite element solution  $\phi$ , may be obtained by direct differentiation as

$$E_k = -\frac{\partial \phi}{\partial \xi_k} = \sum_i^N \frac{\partial \alpha_i(\xi_1, \xi_2, \xi_3)}{\partial \xi_k} \phi_i. \quad (6.5)$$

Mackinnon and Carey (1989) used a Taylor series expansion of the potential  $\phi$  to derive an expression for  $E_k$ . Their formula will now be extended to three dimensions. If  $k = 1$ , and the field is evaluated at point  $(\xi_1, \xi_2, \xi_3)$ , then

$$\begin{aligned} E_1 = & -\sum_i^N \frac{\partial \alpha_i}{\partial \xi_1} \phi_i + \sum_{m=p+1}^{\infty} \frac{1}{m!} \sum_{j=1}^3 \left\{ \sum_i^N \frac{\partial \alpha_i}{\partial \xi_1} (\delta_j^i)^m \right\} \frac{\partial^m \phi}{\partial \xi_j^m} \\ & + \sum_{m=1}^{\infty} \frac{1}{(m-1)!} \sum_{r=1}^{\infty} \frac{1}{(r-1)!} \left\{ \sum_i^N \frac{\partial \alpha_i}{\partial \xi_1} (\delta_1^i)^m (\delta_2^i)^r \right\} \frac{\partial^{m+r} \phi}{\partial \xi_1^m \partial \xi_2^r} \\ & + \sum_{r=1}^{\infty} \frac{1}{(r-1)!} \sum_{l=1}^{\infty} \frac{1}{(l-1)!} \left\{ \sum_i^N \frac{\partial \alpha_i}{\partial \xi_1} (\delta_2^i)^r (\delta_3^i)^l \right\} \frac{\partial^{r+l} \phi}{\partial \xi_2^r \partial \xi_3^l} \\ & + \sum_{m=1}^{\infty} \frac{1}{(m-1)!} \sum_{l=1}^{\infty} \frac{1}{(l-1)!} \left\{ \sum_i^N \frac{\partial \alpha_i}{\partial \xi_1} (\delta_1^i)^m (\delta_3^i)^l \right\} \frac{\partial^{m+l} \phi}{\partial \xi_1^m \partial \xi_3^l} \\ & + \sum_{m=1}^{\infty} \frac{1}{(m-1)!} \sum_{r=1}^{\infty} \frac{1}{(r-1)!} \sum_{l=1}^{\infty} \frac{1}{(l-1)!} \left\{ \sum_i^N \frac{\partial \alpha_i}{\partial \xi_1} (\delta_1^i)^m (\delta_2^i)^r (\delta_3^i)^l \right\} \frac{\partial^{m+r+l} \phi}{\partial \xi_1^m \partial \xi_2^r \partial \xi_3^l}, \quad (6.6) \end{aligned}$$

where

$$\delta_j^i = \xi_j^i - \xi_j. \quad (6.7)$$

For second order elements,  $p = 2$ , (6.6) takes the form

$$\begin{aligned} E_1 = & -\sum_i^N \frac{\partial \alpha_i}{\partial \xi_1} \phi_i + \frac{1}{3!} \sum_{j=1}^3 \left\{ \sum_i^N \frac{\partial \alpha_i}{\partial \xi_1} (\delta_j^i)^3 \right\} \frac{\partial^3 \phi}{\partial \xi_j^3} + \frac{\partial^3 \phi}{\partial \xi_1 \partial \xi_2 \partial \xi_3} \sum_i^N \frac{\partial \alpha_i}{\partial \xi_1} (\delta_1^i) (\delta_2^i) (\delta_3^i) \\ & + \frac{\partial^3 \phi}{\partial \xi_1^2 \partial \xi_2} \sum_i^N \frac{\partial \alpha_i}{\partial \xi_1} (\delta_1^i)^2 (\delta_2^i) + \frac{\partial^3 \phi}{\partial \xi_1 \partial \xi_2^2} \sum_i^N \frac{\partial \alpha_i}{\partial \xi_1} (\delta_1^i) (\delta_2^i)^2 \end{aligned}$$

$$\begin{aligned}
& + \frac{\partial^3 \phi}{\partial \xi_1^2 \partial \xi_3} \sum_i^N \frac{\partial \alpha_i}{\partial \xi_1} (\delta_1^i)^2 (\delta_3^i) + \frac{\partial^3 \phi}{\partial \xi_1 \partial \xi_3^2} \sum_i^N \frac{\partial \alpha_i}{\partial \xi_1} (\delta_1^i) (\delta_3^i)^2 \\
& + \frac{\partial^3 \phi}{\partial \xi_2^2 \partial \xi_3} \sum_i^N \frac{\partial \alpha_i}{\partial \xi_1} (\delta_2^i)^2 (\delta_3^i) + \frac{\partial^3 \phi}{\partial \xi_2 \partial \xi_3^2} \sum_i^N \frac{\partial \alpha_i}{\partial \xi_1} (\delta_2^i) (\delta_3^i)^2 + O(\delta^4), \quad (6.8)
\end{aligned}$$

since coefficients corresponding to second-order terms are zero, as well as almost all of third order. Equating all coefficients to zero, a system of simultaneous equations results, whose solution yields the positions of points where the derivative values are exact, provided a third-order polynomial approximation is used. The results are the same for both serendipity-type and Cartesian product elements. For the derivative in the  $\xi_1$  direction, they are planes  $\xi_1 = \pm 1/\sqrt{3}$ . In the other two directions there are two other, corresponding, sets of planes.

### 6.3 Derivation for the two-dimensional problem

For the two-dimensional case, a four-parameter least-squares fit can be constructed by taking Legendre polynomials in the  $\xi$  and  $\eta$  directions:

$$E_\xi^* = E_\xi + \alpha_1 P_p(\xi) + \alpha_2 P_p(\eta) \quad (6.9)$$

$$E_\eta^* = E_\eta + \alpha_3 P_p(\xi) + \alpha_4 P_p(\eta). \quad (6.10)$$

Here  $\xi, \eta \in [-1, 1]$  are local coordinates on the parent rectangular element, while  $x$  and  $y$  are global coordinates. The residual whose square must be minimized is now

$$r_e^* = \frac{\partial(\epsilon E_x^*)}{\partial x} + \frac{\partial(\epsilon E_y^*)}{\partial y} - \kappa^2 \phi - g. \quad (6.11)$$

Squaring and substituting, lengthy expressions result. These can be made more readily comprehensible by defining the *uncorrected* residual  $r_e$  as

$$r_c = \frac{\partial(\epsilon E_x)}{\partial x} + \frac{\partial(\epsilon E_y)}{\partial y} - \kappa^2 \phi - g. \quad (6.12)$$

In terms of the local coordinates,

$$\begin{aligned} r_c = & \frac{\partial(\epsilon E_\xi)}{\partial \xi} \left\{ \left( \frac{\partial \xi}{\partial x} \right)^2 + \left( \frac{\partial \xi}{\partial y} \right)^2 \right\} + \frac{\partial(\epsilon E_\eta)}{\partial \eta} \left\{ \left( \frac{\partial \eta}{\partial x} \right)^2 + \left( \frac{\partial \eta}{\partial y} \right)^2 \right\} \\ & + \left\{ \frac{\partial(\epsilon E_\eta)}{\partial \xi} + \frac{\partial(\epsilon E_\xi)}{\partial \eta} \right\} \left\{ \frac{\partial \xi}{\partial x} \frac{\partial \eta}{\partial x} + \frac{\partial \xi}{\partial y} \frac{\partial \eta}{\partial y} \right\} - \kappa^2 \phi - g \end{aligned} \quad (6.13)$$

and similarly for  $r_c^*$ . For brevity in the development, define the combined derivative terms

$$\begin{aligned} D_{\xi\xi} &= \left( \frac{\partial \xi}{\partial x} \right)^2 + \left( \frac{\partial \xi}{\partial y} \right)^2 \\ D_{\eta\eta} &= \left( \frac{\partial \eta}{\partial x} \right)^2 + \left( \frac{\partial \eta}{\partial y} \right)^2 \\ D_{\xi\eta} &= \frac{\partial \xi}{\partial x} \frac{\partial \eta}{\partial x} + \frac{\partial \xi}{\partial y} \frac{\partial \eta}{\partial y}. \end{aligned} \quad (6.14)$$

On substitution of (6.14), the residuals assume the relatively short forms

$$r_c^* = D_{\xi\xi} \frac{\partial(\epsilon E_\xi^*)}{\partial \xi} + D_{\eta\eta} \frac{\partial(\epsilon E_\eta^*)}{\partial \eta} + D_{\xi\eta} \left\{ \frac{\partial(\epsilon E_\eta^*)}{\partial \xi} + \frac{\partial(\epsilon E_\xi^*)}{\partial \eta} \right\} - \kappa^2 \phi - g, \quad (6.15)$$

$$r_c = D_{\xi\xi} \frac{\partial(\epsilon E_\xi)}{\partial \xi} + D_{\eta\eta} \frac{\partial(\epsilon E_\eta)}{\partial \eta} + D_{\xi\eta} \left\{ \frac{\partial(\epsilon E_\eta)}{\partial \xi} + \frac{\partial(\epsilon E_\xi)}{\partial \eta} \right\} - \kappa^2 \phi - g. \quad (6.16)$$

The smoothed residual may now be written in terms of the unsmoothed one as

$$\begin{aligned} r_c^* = & r_c + \alpha_1 \left\{ D_{\xi\xi} \frac{\partial}{\partial \xi} (\epsilon P_p(\xi)) + D_{\xi\eta} P_p(\xi) \frac{\partial \epsilon}{\partial \eta} \right\} \\ & + \alpha_2 \left\{ D_{\xi\eta} \frac{\partial}{\partial \eta} (\epsilon P_p(\eta)) + D_{\xi\xi} P_p(\eta) \frac{\partial \epsilon}{\partial \xi} \right\} \\ & + \alpha_3 \left\{ D_{\xi\eta} \frac{\partial}{\partial \xi} (\epsilon P_p(\xi)) + D_{\eta\eta} P_p(\xi) \frac{\partial \epsilon}{\partial \eta} \right\} \end{aligned} \quad (6.17)$$

$$+ \alpha_4 \left\{ D_{\eta\eta} \frac{\partial}{\partial \eta} (\epsilon P_p(\eta)) + D_{\xi\eta} P_p(\eta) \frac{\partial \epsilon}{\partial \xi} \right\}.$$

Collecting terms,

$$r_c^* = r_c + \sum_{i=1}^4 \alpha_i K_i \quad (6.18)$$

where

$$K_1 = P_p(\xi) \left( D_{\xi\xi} \frac{\partial \epsilon}{\partial \xi} + D_{\xi\eta} \frac{\partial \epsilon}{\partial \eta} \right) + D_{\xi\xi} \epsilon P'_p(\xi) = P_p(\xi) \chi_1 + D_{\xi\xi} \epsilon P'_p(\xi) \quad (6.19)$$

$$K_2 = P_p(\eta) \left( D_{\xi\xi} \frac{\partial \epsilon}{\partial \xi} + D_{\xi\eta} \frac{\partial \epsilon}{\partial \eta} \right) + D_{\xi\eta} \epsilon P'_p(\eta) = P_p(\eta) \chi_1 + D_{\xi\eta} \epsilon P'_p(\eta) \quad (6.20)$$

$$K_3 = P_p(\xi) \left( D_{\eta\eta} \frac{\partial \epsilon}{\partial \eta} + D_{\xi\eta} \frac{\partial \epsilon}{\partial \eta} \right) + D_{\xi\eta} \epsilon P'_p(\xi) = P_p(\xi) \chi_2 + D_{\xi\eta} \epsilon P'_p(\xi) \quad (6.21)$$

$$K_4 = P_p(\eta) \left( D_{\eta\eta} \frac{\partial \epsilon}{\partial \eta} + D_{\xi\eta} \frac{\partial \epsilon}{\partial \xi} \right) + D_{\eta\eta} \epsilon P'_p(\eta) = P_p(\eta) \chi_2 + D_{\eta\eta} \epsilon P'_p(\eta) \quad (6.22)$$

In the important special case where the material property  $\epsilon$  is uniform in each element, the functions  $K_i$  simplify to

$$K_1 = D_{\xi\xi} \epsilon P'_p(\xi) \quad (6.23)$$

$$K_2 = D_{\xi\eta} \epsilon P'_p(\eta) \quad (6.24)$$

$$K_3 = D_{\xi\eta} \epsilon P'_p(\xi) \quad (6.25)$$

$$K_4 = D_{\eta\eta} \epsilon P'_p(\eta). \quad (6.26)$$

To find values for the set of four parameters  $\{\alpha_i | i = 1, \dots, 4\}$ , the squared residual is now minimized,

$$\frac{\partial}{\partial \alpha_i} \int_{S_c} (r_c^*)^2 dx dy = 0, \quad \forall i. \quad (6.27)$$

This requirement leads to four simultaneous equations,

$$\sum_j \int_{-1}^{+1} \int_{-1}^{+1} K_i K_j \det(\mathbf{J}) d\xi d\eta \alpha_j = - \int_{-1}^{+1} \int_{-1}^{+1} r_e K_i \det(\mathbf{J}) d\xi d\eta \quad (6.28)$$

for  $i = 1, 2, 3, 4$ . Here  $\mathbf{J}$  represents the Jacobian of the coordinate transformation (which may be of the isoparametric type) that maps the square parent element into a quadrilateral;  $\det(\mathbf{J})$  is the determinant of  $\mathbf{J}$ . These four simultaneous equations are readily solved numerically for any given transformation.

In the very restricted, but very important, case of transformation onto a rectangle, the final system of four equations may be written as

$$\begin{bmatrix} s_1 & s_2 & s_1 & s_2 \\ s_2 & s_1 & s_2 & s_1 \\ s_1 & s_2 & s_1 & s_2 \\ s_2 & s_1 & s_2 & s_1 \end{bmatrix} \begin{bmatrix} D_{\xi\xi} \alpha_1 \\ D_{\xi\eta} \alpha_2 \\ D_{\xi\eta} \alpha_3 \\ D_{\eta\eta} \alpha_4 \end{bmatrix} = -\frac{1}{\epsilon} \begin{bmatrix} \int_{-1}^{+1} \int_{-1}^{+1} r_e P'_p(\xi) d\xi d\eta \\ \int_{-1}^{+1} \int_{-1}^{+1} r_e P'_p(\eta) d\xi d\eta \\ \int_{-1}^{+1} \int_{-1}^{+1} r_e P'_p(\xi) d\xi d\eta \\ \int_{-1}^{+1} \int_{-1}^{+1} r_e P'_p(\eta) d\xi d\eta \end{bmatrix} \quad (6.29)$$

where

$$s_1 = \int_{-1}^{+1} \int_{-1}^{+1} (P'_p(\xi))^2 d\xi d\eta = 2 \int_{-1}^{+1} (P'_p(\xi))^2 d\xi \quad (6.30)$$

$$s_2 = \int_{-1}^{+1} \int_{-1}^{+1} P'_p(\xi) P'_p(\eta) d\xi d\eta = \left\{ \int_{-1}^{+1} P'_p(\xi) d\xi \right\}^2 \quad (6.31)$$

are constants for any given  $p$ . The solution of this system of four equations can be found analytically as

$$D_{\xi\xi}\alpha_1 = D_{\xi\eta}\alpha_3 = -\frac{1}{\epsilon(s_1^2 - s_2^2)} \left\{ s_1 \int_{-1}^{+1} \int_{-1}^{+1} r_\epsilon P'_p(\xi) d\xi d\eta - s_2 \int_{-1}^{+1} \int_{-1}^{+1} r_\epsilon P'_p(\eta) d\xi d\eta \right\} \quad (6.32)$$

$$D_{\xi\eta}\alpha_2 = D_{\eta\eta}\alpha_4 = -\frac{1}{\epsilon(s_1^2 - s_2^2)} \left\{ s_1 \int_{-1}^{+1} \int_{-1}^{+1} r_\epsilon P'_p(\eta) d\xi d\eta - s_2 \int_{-1}^{+1} \int_{-1}^{+1} r_\epsilon P'_p(\xi) d\xi d\eta \right\} \quad (6.33)$$

In Table 6.1 values of  $s_1$  and  $s_2$  for  $p \leq 6$  are shown.

Table 6.1.

$p$	1	2	3	4	5	6
$s_1$	4	12	24	40	60	84
$s_2$	4	0	4	0	4	0

Note that for  $p = 1$  coefficients are equal,  $s_1 = s_2$ , so

$$D_{\xi\xi}\alpha_1 = D_{\xi\eta}\alpha_3 = D_{\xi\eta}\alpha_2 = D_{\eta\eta}\alpha_4 = -\frac{1}{8} \int_{-1}^{+1} \int_{-1}^{+1} r_\epsilon d\xi d\eta \quad (6.34)$$

For  $p = 2$ , the coefficients are

$$D_{\xi\xi}\alpha_1 = D_{\xi\eta}\alpha_3 = \frac{1}{12} \int_{-1}^{+1} \int_{-1}^{+1} r_\epsilon P'_p(\xi) d\xi d\eta \quad (6.35)$$

$$D_{\xi\eta}\alpha_2 = D_{\eta\eta}\alpha_4 = \frac{1}{12} \int_{-1}^{+1} \int_{-1}^{+1} r_\epsilon P'_p(\eta) d\xi d\eta \quad (6.36)$$

This procedure is entirely local to an element and therefore does not lead to unique values at nodes located on element interfaces. In practice, the difference

is rarely large, indeed it can serve as an indicator of the quality of differentiation. If desired, the conventional procedure of averaging nodal fields can be applied.

## 6.4 Generalization of the local smoothing of gradients to three dimensions

### 6.4.1 Hinton-Campbell conventional local smoothing

The commonly used local smoothing method of gradients is one proposed by Hinton and Campbell (1975) (also Zienkiewicz and Taylor (1989)). In the standard 20-noded quadratic brick element, the local smoothing is a trilinear extrapolation from the  $2 \times 2 \times 2$  Gaussian point values. It can be shown that the smoothed corner nodal field values may be obtained using superconvergent point values  $E_I \dots E_{VIII}$  from the expression

$$\begin{bmatrix} \bar{E}_1 \\ \bar{E}_2 \\ \bar{E}_3 \\ \bar{E}_4 \\ \bar{E}_5 \\ \bar{E}_6 \\ \bar{E}_7 \\ \bar{E}_8 \end{bmatrix} = \begin{bmatrix} a & b & c & b & b & c & d & c \\ b & a & b & c & c & b & c & d \\ c & b & a & b & d & c & b & c \\ b & c & b & a & c & d & c & b \\ b & c & d & c & a & b & c & b \\ c & b & c & d & b & a & b & c \\ d & c & b & c & c & b & a & b \\ c & d & c & b & b & c & b & a \end{bmatrix} \begin{bmatrix} E_I \\ E_{II} \\ E_{III} \\ E_{IV} \\ E_V \\ E_{VI} \\ E_{VII} \\ E_{VIII} \end{bmatrix} \quad (6.37)$$

where  $a, b, c, d$  are numeric coefficients given by

$$a = \frac{5 + 3\sqrt{3}}{4}, \quad b = -\frac{1 + \sqrt{3}}{4},$$

$$c = -\frac{1-\sqrt{3}}{4}, \quad d = \frac{5-3\sqrt{3}}{4}. \quad (6.38)$$

Generally, for the  $p$ th order function  $E(\xi)$  in the interval  $-1 \leq \xi \leq 1$ , values sampled at the  $p$  Gaussian points uniquely define a function  $\tilde{E}(\xi)$  of order  $p-1$ . This function represents a least squares fit to  $E(\xi)$ . Now, the field at any point can be computed as

$$\tilde{E} = \sum_{i=1}^8 \alpha_i(\xi_1, \xi_2, \xi_3) \tilde{E}_i. \quad (6.39)$$

Since the fields at nodal points computed using local smoothing are not unique, nodal averages may be calculated. It should be noted that the field value at the center of an element is equal to the arithmetic mean of its values at the superconvergent points, and therefore has exceptional accuracy.

#### 6.4.2 Derivation of extended Zhu-Zienkiewicz method for 3-D problems

Analogously to two-dimensional problems, a nine-parameter least-squares fit will be used here. For  $p$ th order elements, the least-squares fit can be constructed by taking the  $p$ th order Legendre polynomials in the  $\xi_1$ ,  $\xi_2$  and  $\xi_3$  directions,

$$E_i^* = E_i + \sum_{j=1}^3 \alpha_{ij} P_p(\xi_j), \quad i = 1, 2, 3 \quad (6.40)$$

Here  $\xi_1, \xi_2, \xi_3 \in [-1, 1]$  are local coordinates on the parent isoparametric brick element,  $x$ ,  $y$  and  $z$  are global coordinates. The residual whose square must be minimized is now

$$r_c^* = \frac{\partial(\epsilon E_x^*)}{\partial x} + \frac{\partial(\epsilon E_y^*)}{\partial y} + \frac{\partial(\epsilon E_z^*)}{\partial z} - \kappa^2 \phi - g, \quad (6.41)$$

and the corresponding uncorrected residual is

$$r_c = \frac{\partial(\epsilon E_x)}{\partial x} + \frac{\partial(\epsilon E_y)}{\partial y} + \frac{\partial(\epsilon E_z)}{\partial z} - \kappa^2 \phi - g. \quad (6.42)$$

Here  $E_x$ ,  $E_y$  and  $E_z$  are the field components,

$$E_x = -\frac{\partial \phi}{\partial x} = -\sum_{i=1}^3 \frac{\partial \phi}{\partial \xi_i} \frac{\partial \xi_i}{\partial x} = \sum_{i=1}^3 E_i \frac{\partial \xi_i}{\partial x}, \quad (6.43)$$

$$E_y = -\frac{\partial \phi}{\partial y} = -\sum_{i=1}^3 \frac{\partial \phi}{\partial \xi_i} \frac{\partial \xi_i}{\partial y} = \sum_{i=1}^3 E_i \frac{\partial \xi_i}{\partial y}, \quad (6.44)$$

$$E_z = -\frac{\partial \phi}{\partial z} = -\sum_{i=1}^3 \frac{\partial \phi}{\partial \xi_i} \frac{\partial \xi_i}{\partial z} = \sum_{i=1}^3 E_i \frac{\partial \xi_i}{\partial z}. \quad (6.45)$$

In terms of the local coordinates,

$$r_c^* = \sum_{i=1}^3 \sum_{j=1}^3 \frac{\partial(\epsilon E_j^*)}{\partial \xi_i} \left\{ \frac{\partial \xi_i}{\partial x} \frac{\partial \xi_j}{\partial x} + \frac{\partial \xi_i}{\partial y} \frac{\partial \xi_j}{\partial y} + \frac{\partial \xi_i}{\partial z} \frac{\partial \xi_j}{\partial z} \right\} - \kappa^2 \phi - g \quad (6.46)$$

and a similar expression obtains for  $r_c$ . For brevity in the development, the combined derivative terms are defined:

$$D_{ij} = \frac{\partial \xi_i}{\partial x} \frac{\partial \xi_j}{\partial x} + \frac{\partial \xi_i}{\partial y} \frac{\partial \xi_j}{\partial y} + \frac{\partial \xi_i}{\partial z} \frac{\partial \xi_j}{\partial z}. \quad (6.47)$$

After substitution of (6.47), the residuals assume the following forms:

$$r_c^* = \sum_{i=1}^3 \sum_{j=1}^3 D_{ij} \frac{\partial(\epsilon E_j^*)}{\partial \xi_i} - \kappa^2 \phi - g, \quad (6.48)$$

$$r_c = \sum_{i=1}^3 \sum_{j=1}^3 D_{ij} \frac{\partial(\epsilon E_j)}{\partial \xi_i} - \kappa^2 \phi - g. \quad (6.49)$$

The smoothed residual may now be written in terms of the unsmoothed one as

$$r_c^* = r_c + \sum_{i=1}^3 \sum_{j=1}^3 D_{ij} \frac{\partial}{\partial \xi_i} \left\{ \epsilon \sum_{k=1}^3 \alpha_{jk} P_p(\xi_k) \right\} \quad (6.50)$$

$$= r_c + \sum_{i=1}^3 \sum_{j=1}^3 D_{ij} \frac{\partial \epsilon}{\partial \xi_i} \left\{ \sum_{k=1}^3 \alpha_{jk} P_p(\xi_k) \right\} + \epsilon \sum_{i=1}^3 \sum_{j=1}^3 D_{ij} \alpha_{ji} P'_p(\xi_i) \quad (6.51)$$

or equivalently as

$$r_c^* = r_c + \sum_{k=1}^3 P_p(\xi_k) \sum_{j=1}^3 \alpha_{jk} \sum_{i=1}^3 D_{ij} \frac{\partial \epsilon}{\partial \xi_i} + \epsilon \sum_{i=1}^3 P'_p(\xi_i) \sum_{j=1}^3 D_{ij} \alpha_{ji} \quad (6.52)$$

$$r_c^* = r_c + \sum_{j=1}^3 \sum_{k=1}^3 \alpha_{jk} \left\{ P_p(\xi_k) \sum_{i=1}^3 D_{ij} \frac{\partial \epsilon}{\partial \xi_i} + \epsilon D_{kj} P'_p(\xi_k) \right\} \quad (6.53)$$

This expression can be written in the alternative form

$$r_c^* = r_c + \sum_{i=1}^9 \gamma_i K_i \quad (6.54)$$

where

$$\gamma_{3(j-1)+k} = \alpha_{jk} \quad k = 1, 2, 3 \quad (6.55)$$

$$K_{3(j-1)+k} = P_p(\xi_k) \sum_{i=1}^3 D_{ij} \frac{\partial \epsilon}{\partial \xi_i} + \epsilon D_{kj} P'_p(\xi_k) \quad k = 1, 2, 3 \quad (6.56)$$

If the material property  $\epsilon$  is uniform in each element, the functions  $K_i$  become

$$K_{3(j-1)+k} = \epsilon D_{kj} P'_p(\xi_k) \quad (6.57)$$

In order to find values for the set of nine parameters  $\gamma_i$ , the squared residual is minimized,

$$\frac{\partial}{\partial \gamma_i} \int_V (r_c^*)^2 dx dy dz = 0, \quad \forall i. \quad (6.58)$$

For  $i = 1$ , this requirement takes the detailed form

$$\sum_{j=1}^9 \gamma_j \int_{-1}^{+1} \int_{-1}^{+1} \int_{-1}^{+1} K_1 K_j \det(\mathbf{J}) d\xi_1 d\xi_2 d\xi_3$$

$$= - \int_{-1}^{+1} \int_{-1}^{+1} \int_{-1}^{+1} r_e K_1 \det(\mathbf{J}) d\xi_1 d\xi_2 d\xi_3, \quad (6.59)$$

where  $\mathbf{J}$  represents the Jacobian of the coordinate transformation (possibly, but not necessarily, isoparametric) that maps the square parent element into a quadrilateral, and  $\det(\mathbf{J})$  is the determinant of  $\mathbf{J}$ . After performing minimization with respect to all nine  $\gamma_i$ , the final result is a system of nine simultaneous equations:

$$\sum_j m_{ij} \gamma_j = h_i. \quad (6.60)$$

Here

$$m_{ij} = \int_{-1}^{+1} \int_{-1}^{+1} \int_{-1}^{+1} K_i K_j \det(\mathbf{J}) d\xi_1 d\xi_2 d\xi_3, \quad (6.61)$$

and

$$h_i = \int_{-1}^{+1} \int_{-1}^{+1} \int_{-1}^{+1} r_e K_i \det(\mathbf{J}) d\xi_1 d\xi_2 d\xi_3. \quad (6.62)$$

### 6.4.3 Brick elements and homogeneous linear materials

In the highly restricted, but very important, case of transformation onto a brick, the final system of nine equations may be reduced to

$$\begin{bmatrix} s_1 & s_2 & s_2 \\ s_2 & s_1 & s_2 \\ s_2 & s_2 & s_1 \end{bmatrix} \begin{bmatrix} \beta_1 \\ \beta_2 \\ \beta_3 \end{bmatrix} = -\frac{1}{3\epsilon} \begin{bmatrix} h_1 \\ h_2 \\ h_3 \end{bmatrix} \quad (6.63)$$

where

$$\beta_1 = D_{11}\alpha_{11} = D_{12}\alpha_{21} = D_{13}\alpha_{31} \quad (6.64)$$

$$\beta_2 = D_{12}\alpha_{12} = D_{22}\alpha_{22} = D_{23}\alpha_{32} \quad (6.65)$$

$$\beta_3 = D_{13}\alpha_{13} = D_{23}\alpha_{23} = D_{33}\alpha_{33} \quad (6.66)$$

$$s_1 = \int_{-1}^{+1} \int_{-1}^{+1} \int_{-1}^{+1} (P'_p(\xi_1))^2 d\xi_1 d\xi_2 d\xi_3 = 4 \int_{-1}^{+1} (P'_p(\xi))^2 d\xi \quad (6.67)$$

$$s_2 = \int_{-1}^{+1} \int_{-1}^{+1} \int_{-1}^{+1} P'_p(\xi_1) P'_p(\xi_2) d\xi_1 d\xi_2 d\xi_3 = 2 \left\{ \int_{-1}^{+1} P'_p(\xi) d\xi \right\}^2 \quad (6.68)$$

$$h_1 = \int_{-1}^{+1} \int_{-1}^{+1} \int_{-1}^{+1} r_e P'_p(\xi_1) d\xi_1 d\xi_2 d\xi_3 \quad (6.69)$$

$$h_2 = \int_{-1}^{+1} \int_{-1}^{+1} \int_{-1}^{+1} r_e P'_p(\xi_2) d\xi_1 d\xi_2 d\xi_3 \quad (6.70)$$

$$h_3 = \int_{-1}^{+1} \int_{-1}^{+1} \int_{-1}^{+1} r_e P'_p(\xi_3) d\xi_1 d\xi_2 d\xi_3 \quad (6.71)$$

The solution is given by

$$\beta_1 = -\frac{(s_1 + s_2)h_1 - s_2(h_2 + h_3)}{3\epsilon(s_1 - s_2)(s_1 + 2s_2)} \quad (6.72)$$

$$\beta_2 = -\frac{(s_1 + s_2)h_2 - s_2(h_1 + h_3)}{3\epsilon(s_1 - s_2)(s_1 + 2s_2)} \quad (6.73)$$

$$\beta_3 = -\frac{(s_1 + s_2)h_3 - s_2(h_1 + h_2)}{3\epsilon(s_1 - s_2)(s_1 + 2s_2)} \quad (6.74)$$

In the case of second order elements,  $s_1 = 24$  and  $s_2 = 0$ , so

$$\beta_i = -\frac{1}{72\epsilon} \int_{-1}^{+1} \int_{-1}^{+1} \int_{-1}^{+1} r_e P_2'(\xi_i) d\xi_1 d\xi_2 d\xi_3 \quad (6.75)$$

For  $p = 3$ ,  $s_1 = 46$  and  $s_2 = 8$ , the coefficients are

$$\beta_1 = -\frac{1}{570\epsilon} \int_{-1}^{+1} \int_{-1}^{+1} \int_{-1}^{+1} r_e \{50 P_3'(\xi_1) - S(P_3'(\xi_2) + P_3'(\xi_3))\} d\xi_1 d\xi_2 d\xi_3 \quad (6.76)$$

$$\beta_2 = -\frac{1}{570\epsilon} \int_{-1}^{+1} \int_{-1}^{+1} \int_{-1}^{+1} r_e \{50 P_3'(\xi_2) - S(P_3'(\xi_1) + P_3'(\xi_3))\} d\xi_1 d\xi_2 d\xi_3 \quad (6.77)$$

$$\beta_3 = -\frac{1}{570\epsilon} \int_{-1}^{+1} \int_{-1}^{+1} \int_{-1}^{+1} r_e \{50 P_3'(\xi_3) - S(P_3'(\xi_1) + P_3'(\xi_2))\} d\xi_1 d\xi_2 d\xi_3 \quad (6.78)$$

This procedure is entirely local to a single element. Consequently, it does not lead to unique values at nodes located on element interfaces. If unique values are desired, the conventional procedure of averaging nodal fields can be applied. A significant advantage of this process, on the other hand, is that only local data need be accessed, so this scheme is particularly attractive for parallel computation on machines with distributed memory.

## CHAPTER 7

### Application to finite element method

Tests were performed to verify that the methods developed in this thesis can be reliably applied to finite element solutions. The examples cover the two-dimensional case, with the application of all elementary regions, comparative analysis of differentiation methods in two dimensions, application of extended Zhu-Zienkiewicz gradient recovery method, differentiation of Helmholtz equation solutions, and application to axisymmetric problems. An application of the method to anisotropic magnetic material modeling was published by Silvester and Omeragić and is presented in Appendix 7.

All tests were performed using single precision arithmetic, i.e., with 32-bit word length using the IEEE floating point notation. Few (if any) of the results obtained are of sufficient precision, or sufficiently sensitive to roundoff error, for word-length to be a significant factor.

#### 7.1 Application to two-dimensional cases

To verify that the differentiation method described is applicable to finite element solutions, Poisson's equation was solved in a square region. The source function was taken to be constant within each element, its value given by

$$g(x, y) = -\frac{1}{A_k} \int 12xy \, d\Omega \quad (x, y) \in \Omega_k \quad (1)$$

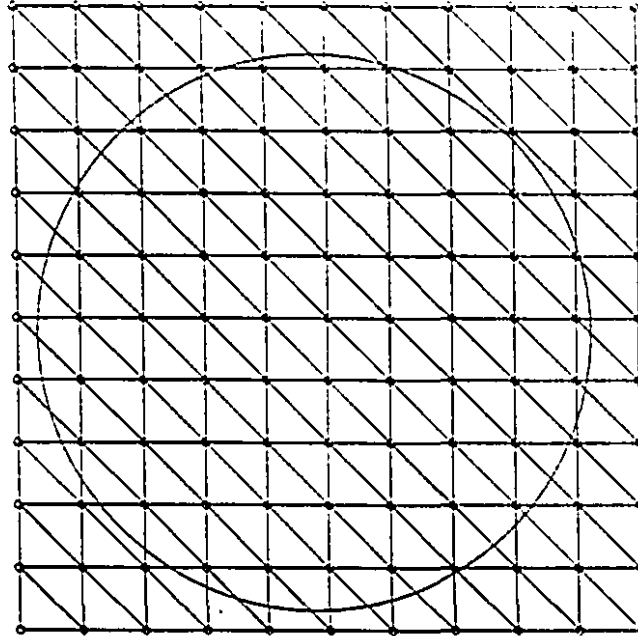


*Figure 7.1.* Circular integration contour embedded in first-order finite element mesh. Potentials on the contour are obtained by using the finite element interpolation functions.

where  $A_k$  is the area of element  $\Omega_k$ ; it approximates to a distribution of  $12xy$  over each triangle. This source function corresponds to a potential function

$$f_1(x, y) = x^3y + xy^3. \quad (7.2)$$

Solution was carried out with first-order triangular elements, with the square  $0 \leq x \leq 2$ ,  $0 \leq y \leq 2$  uniformly subdivided, as indicated in Figure 7.1. Various derivatives of the resulting solution were then computed, the circular contour for integration having a radius of 0.9 and being centered at (1,1). The behavior of computed derivatives extracted from the 200 triangular element mesh is shown in Figure 7.2. Results are presented for derivatives  $\partial f_1/\partial x$ ,  $\partial f_1/\partial y$  and  $\partial^2 f_1/\partial x^2$ ,

when radial position inside the circle is changed, but with the coordinate constant at  $\theta_p = 20^\circ$ . Results appear in Figure 7.3, for a range of mesh sizes, expressed as the number of element edges along the edge of the square. It is worth noting that the potential value is improved by nearly an order of magnitude, and that the error in derivative values is smaller than the error in the potential.

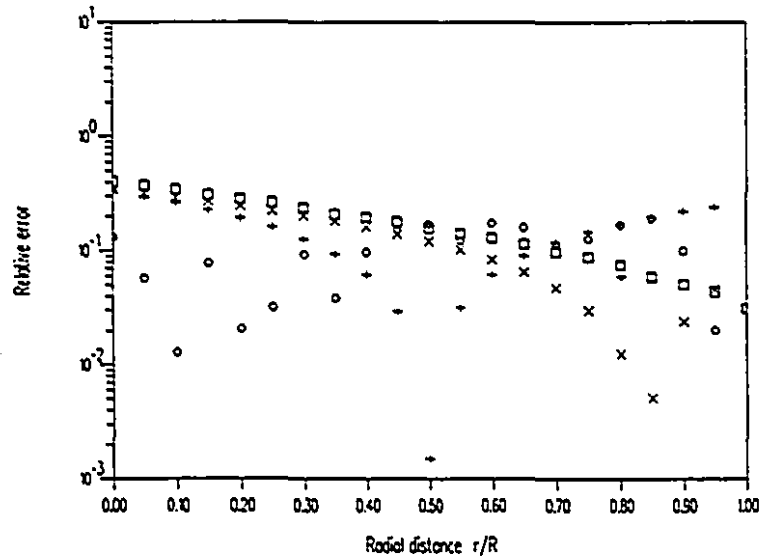


Figure 7.2. Relative error in FEM potential  $f_1$  (□), derivative  $\partial f_1/\partial x$  (+),  $\partial f_1/\partial y$  (×) and  $\partial^2 f_1/\partial x^2$  (○).

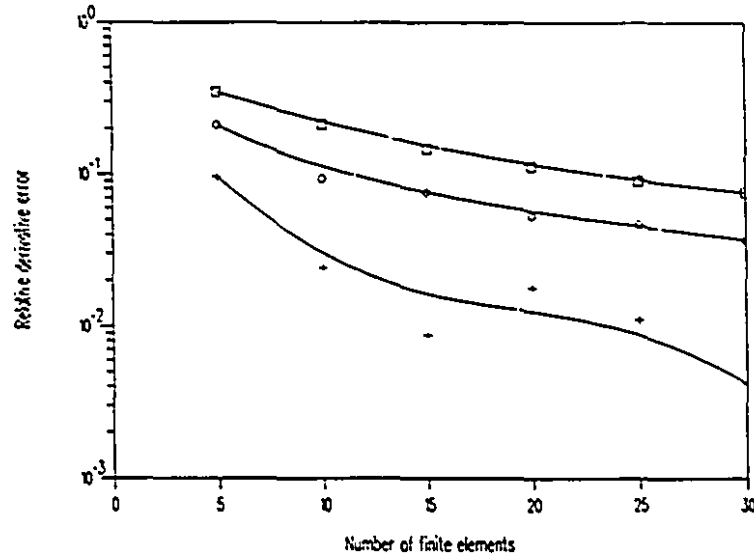


Figure 7.3. Relative error in potential  $f_1$  ( $\square$ ), derivative  $\partial f_1/\partial y$  (+) and  $\partial^2 f_1/\partial x \partial y$  (o) with finite elements. Error decreases with number of elements along the square.

The accuracy of computed derivatives in a rectangular region is shown in Figures 7.4-7.6. Results are obtained for the square  $0 \leq x, y \leq 1$ , along the line  $y = 0.6$ . The accuracy of finite element solution and derivatives obtained using direct differentiation are shown in Figure 7.4. The first derivative results have reduced accuracy, compared to results obtained using a circle, but still, accuracy is better than that of original finite element derivatives obtained using direct differentiation. Figure 7.5 shows the results for a harmonic function, while Figure 7.6 displays the results for a Poisson equation solution.

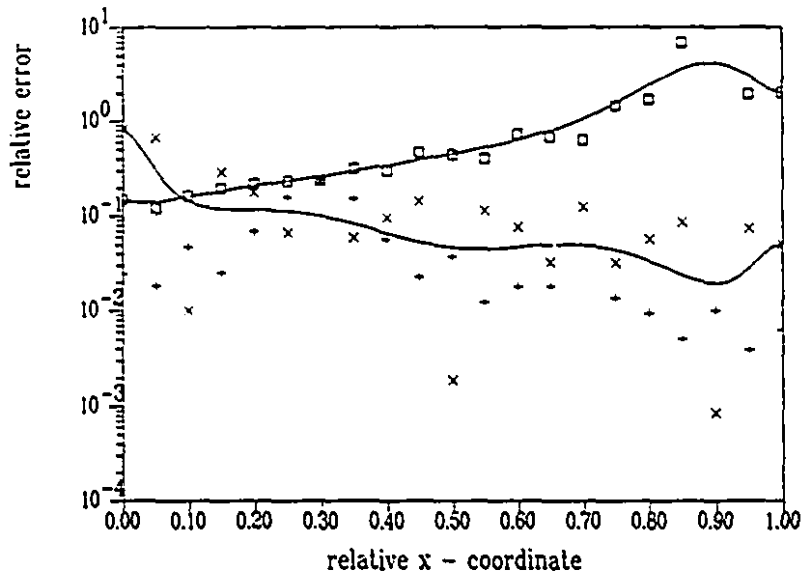
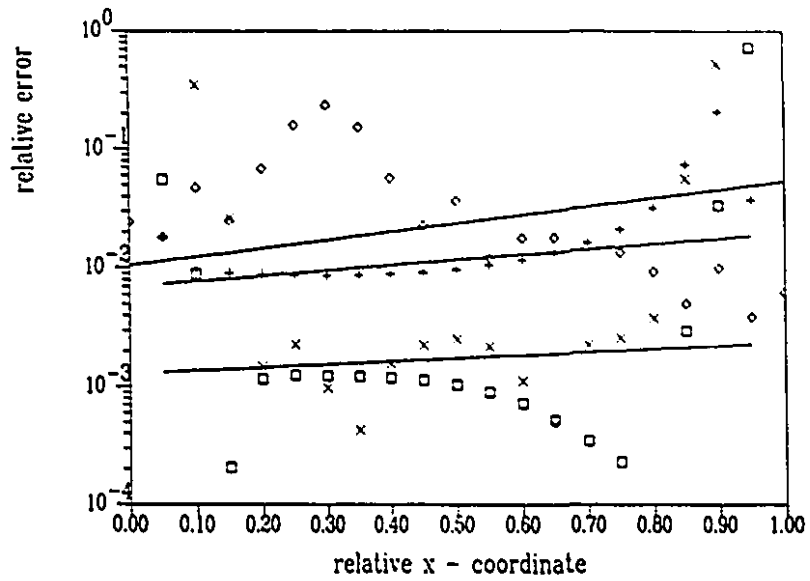
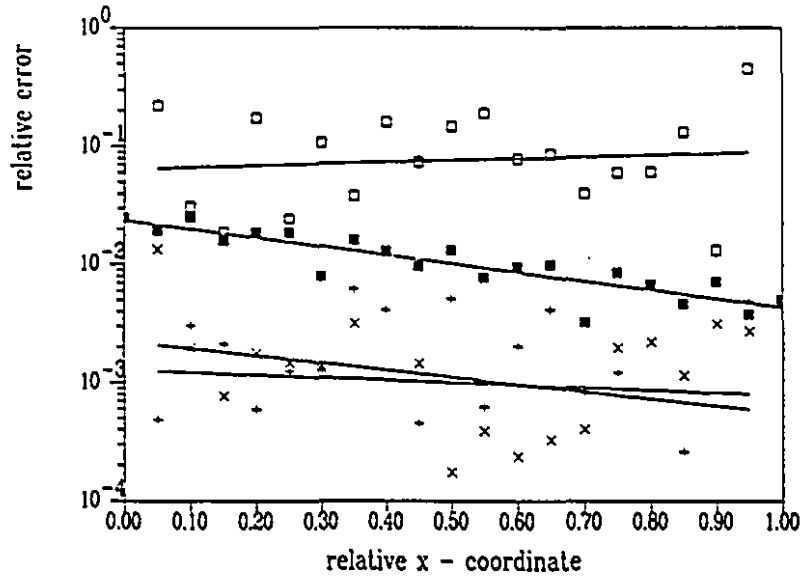


Figure 7.4. Relative error in finite element solution:  $f_3(x,y)$  potential (+),  $\partial f_3(x,y)/\partial x$  (x) and  $\partial f_3(x,y)/\partial y$  (□)



**Figure 7.5.** Relative error in derivatives of harmonic function obtained using the new method, for  $\partial f_3 / \partial x$  (+),  $\partial^2 f_3 / \partial y^2$  (x) and  $\partial^3 f_3 / \partial x^2 \partial y$  (□)



**Figure 7.6.** Relative error in derivatives using the function  $f_1(x,y)$  – the finite element solution (■),  $\partial f_1/\partial x$  (+),  $\partial f_1/\partial y$  (×) and  $\partial f_1/\partial x^2$  (□)

Derivatives obtained using the two circular sectors are presented in Figures 7.7 and 7.8. The sectors are centered at (1,1). The first has the angle  $\theta = 30^\circ$  and the second is a semi-circle ( $\theta = 180^\circ$ ). In both cases the radial position was varied, while the angular coordinate of the observation point was  $\theta_p = 10^\circ$ . The accuracy of results is low for  $r_p/R \leq 0.3$ , while outside that region computed derivatives have the same accuracy as the finite element calculated potentials.

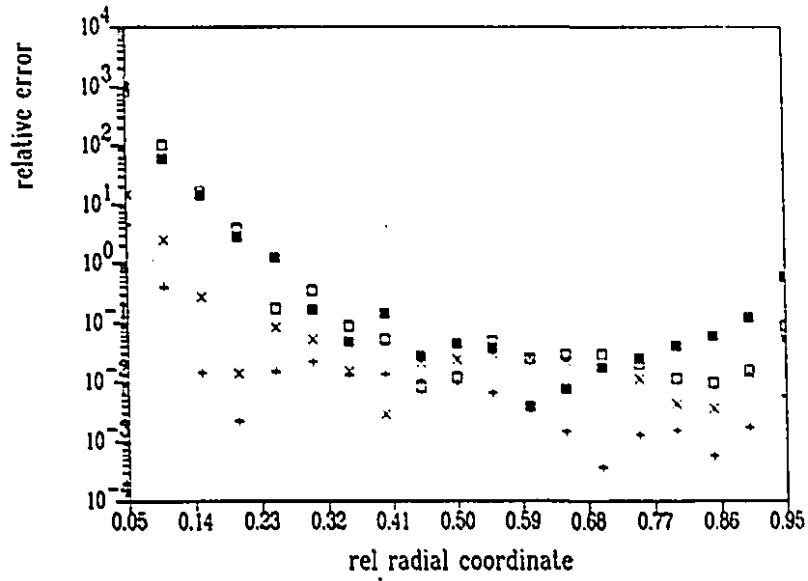


Figure 7.7. Relative error in derivatives with the new method ( $\theta = 30^\circ$  sector), for  $\partial f_3 / \partial x$  (+),  $\partial f_3 / \partial y$  (x),  $\partial^2 f_3 / \partial x^2$  (□) and  $\partial^2 f_3 / \partial x \partial y$  (■)

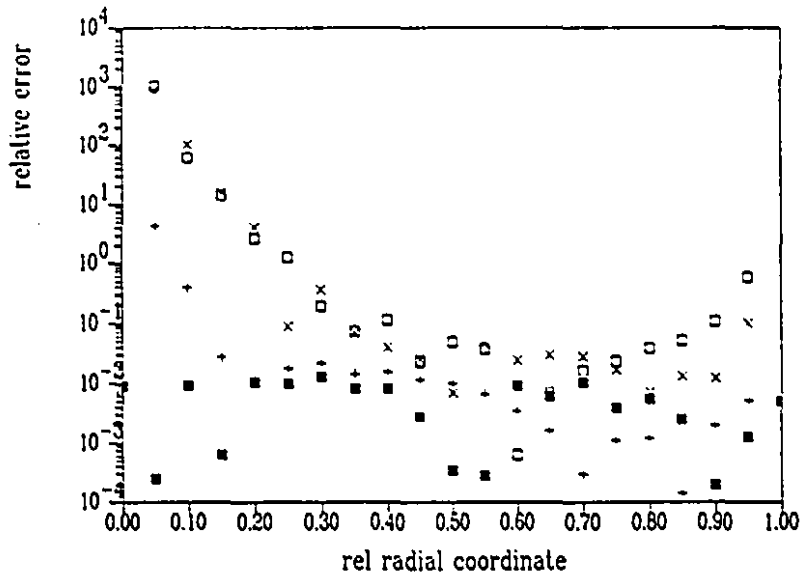


Figure 7.8. Relative error in derivatives with the new method ( $\theta = 180^\circ$  sector), for  $\partial f_3/\partial x$  (+) ,  $\partial f_3/\partial y$  (x) and  $\partial^2 f_3/\partial x^2$  (□) - FEM solution (■)

## 7.2 Comparative study of differentiation methods

This section reports the results of an experimental study in which the various available methods were employed to calculate derivatives of several approximate harmonic functions on different classes of mesh. The first series of tests employed quadrilateral elements of second order, and two test functions: a cubic harmonic polynomial and a logarithmic function. A second test series used the same functions, but on triangular meshes up to fourth order. In the third sequence of tests, the field in a deep parallel-sided electric machine slot was analyzed. In each test, the function was first approximated by computing a finite element

solution to the Dirichlet problem, with known function values prescribed on the boundary of the region. The computed derivative values are therefore the approximate derivatives of a finite element approximation, not merely approximate derivatives of an exactly known function. Each test series involved a variety of meshes and applied all the differentiation techniques reasonably applicable to each mesh type. The results shown in the following may be taken as representative.

In the first test series using quadrilateral meshes, both local smoothing methods were compared with the Poisson integral method and with direct differentiation. Global smoothing was not treated since other workers have found its performance no better than that of local smoothing (Hinton and Campbell (1974), Zienkiewicz and Taylor (1989)). The cubic harmonic polynomial  $h_p(x, y)$  was selected as typical of smooth, bounded solutions that finite element methods ordinarily approximate very well,

$$h_p(x, y) = x^3y - xy^3. \quad (7.3)$$

The second function  $h_t(x, y)$  is also harmonic, but being a singular transcendental function, places greater demands on all differentiation schemes:

$$h_t(x, y) = \log((1+x)^2 + (1+y)^2) \quad (7.4)$$

The polynomial  $h_p$  can be expressed exactly on third and higher order finite elements, but not on elements of second order. The transcendental function  $h_t$  cannot be represented exactly on any conventional finite element mesh.

The second series of tests, on triangular elements up to fourth order, used the same harmonic functions as for the quadrilateral case, thus providing direct comparison. For triangular elements there is no generally accepted superconvergent local smoothing method analogous to that of Hinton and Campbell (1974) for quadrilaterals. However, any local smoothing method would require derivative values from such superconvergent points in order to

extrapolate smoothed results. Consequently, global smoothing was used instead of local. For the same reason, results obtained by the Poisson integral method were compared instead of values at superconvergent points. Since the Poisson integral method is capable of finding higher as well as first derivatives, values of several higher order derivatives obtained by direct differentiation of the finite element solution were compared with results obtained by the Poisson integral method.

In the third test, the field in a deep parallel-sided electric machine slot was analyzed. Here the result is analytically known but not exactly computable by any finite element method. This problem includes a singular field point, where no numerical method can be expected to yield a result of high accuracy; however, results at points not far from the singularity can be compared usefully. An irregular simplicial mesh was used, in order to compare the effectiveness of 'averaging' based on the Poisson integral, and local weighted averages.

### 7.2.1<sup>\*</sup> Second-order quadrilateral elements

Tests on quadrilateral elements used both functions  $h_p$  and  $h_t$ . The region modeled was the square  $0 \leq x, y \leq 2$ . Derivatives were computed along a line of length 0.9, beginning at the point (1,1), i.e., at the center of the square. For the Poisson integral method, the circular contour of integration was centered on (1,1) with a radius of 0.9. The element matrices were computed by numerical integration in the manner usual for second-order isoparametric quadrilaterals. Five-point Gaussian quadratures were used, and their adequacy was tested by comparing with quadratures of higher degree. For the meshes used, the error caused by five-point quadrature appeared to be substantially smaller than differentiation error, and may therefore be considered negligible.

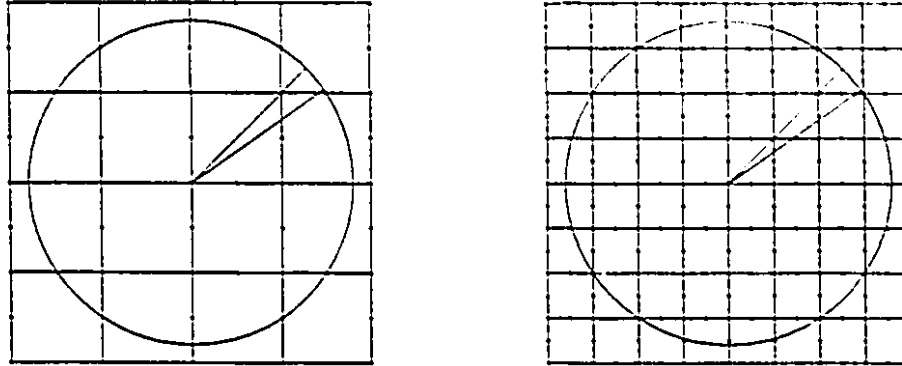


*Figure 7.9.* Finite element meshes, Poisson integral method circle, and lines along which derivatives were computed

Two of the meshes for which analyses were carried out appear in Figure 7.9. The same figure also shows lines along which derivatives were computed, as well as the circular contour of integration used in the Poisson integral method. Derivative values computed for the polynomial  $h_p$  are shown in Figures 7.10 and 7.11, along a line at  $45^\circ$  to the axes. This is the direction with best accuracy for the smoothing methods, and also for direct differentiation, because the line crosses two superconvergence points in each element, as well as its centroid which is a point of high precision for local smoothing methods. Indeed the special nature of these points is clearly evident in the graphs, with error falling drastically at and near each point of superconvergence. By way of contrast, Figure 7.12 shows computed results along a line at  $35^\circ$  to the axes, for the function  $h_p$  using an  $8 \times 8$  element mesh. This line traverses no points of exceptional accuracy, as is clearly visible from the much smoother behavior of the error curves, and the quite naturally higher error.

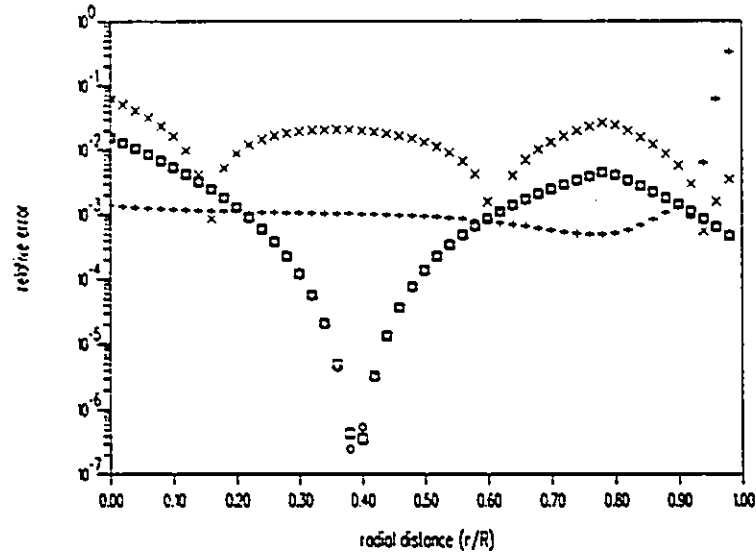


Figure 7.10. Derivative in  $x$  direction; function  $h_p$ ,  $-4 \times 4$  mesh, direction  $45^\circ$ ; (+) Poisson integral, (x) direct method, ( $\square$ ) Zhu-Zienkiewicz and (o) local smoothing method

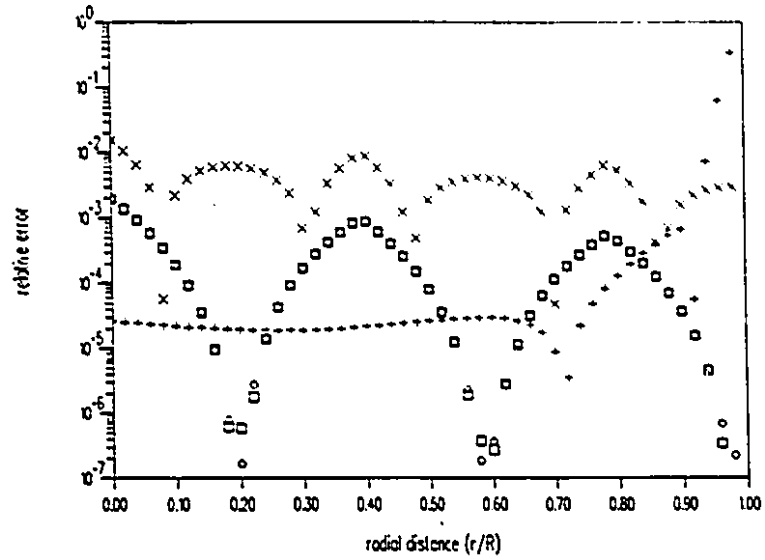


Figure 7.11. Derivative in  $x$  direction; function  $h_p$  -  $8 \times 8$  mesh, direction  $45^\circ$ ; (+) Poisson integral, (x) direct method, (□) Zhu-Zienkiewicz and (o) local smoothing method

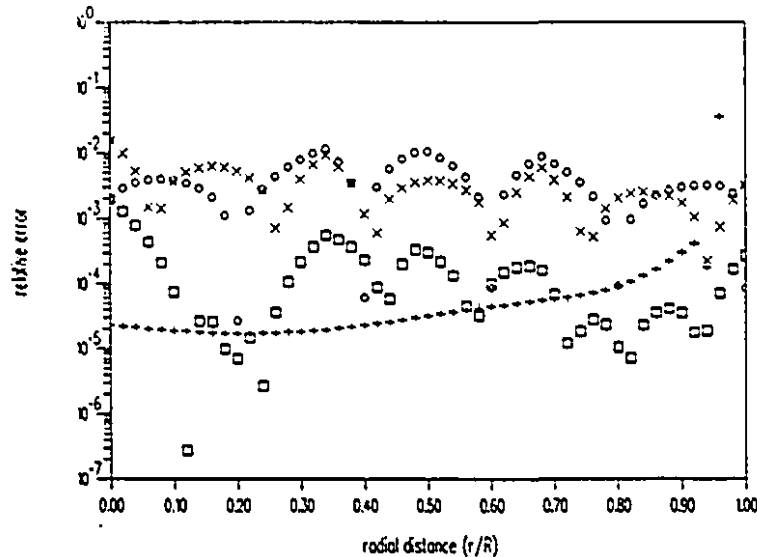
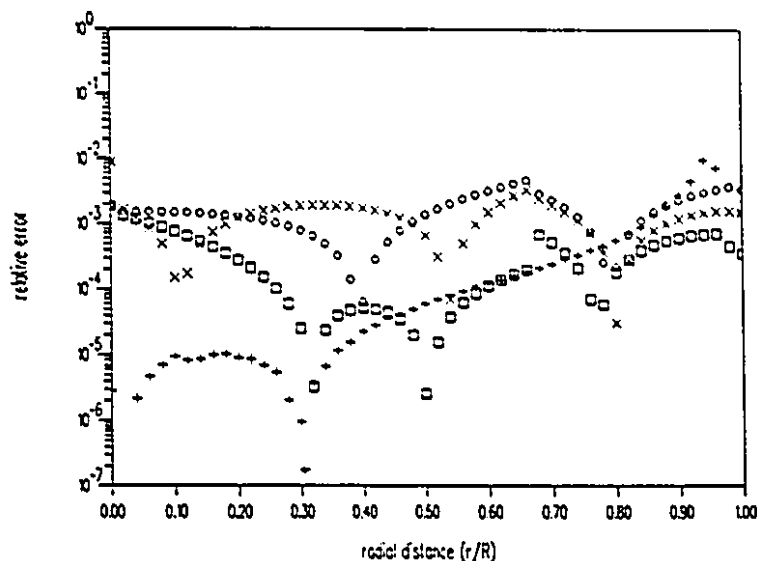


Figure 7.12. Derivative in  $x$  direction; function  $h_p$ ,  $8 \times 8$  mesh, direction  $35^\circ$ ; (+) Poisson integral, (x) direct method, ( $\square$ ) Zhu-Zienkiewicz and (o) local smoothing method

These results may perhaps be summarized by saying that the derivatives obtained with the extended Zhu-Zienkiewicz method are better than the classical local smoothing results, but either way the accuracy is strongly position-dependent. For the polynomial function  $h_p$ , the two local smoothing methods are of almost equal accuracy, and significantly better than direct differentiation of the element functions. This is to be expected, however, for the derivatives of a cubic polynomial are quadratic functions so that error should be exactly zero (aside from any roundoff and quadrature errors) at the points of superconvergence. The results of Figure 7.13, obtained on a  $4 \times 4$  mesh for the transcendental function  $h_t$ , along a line at  $35^\circ$  to the axes, are less kind to the local smoothing techniques. In fact these methods give no visible improvement

over direct differentiation results followed by classical local smoothing. On the other hand, the extended Zhu-Zienkiewicz method provides up to two additional correct significant figures in this more demanding test.



**Figure 7.13.** Derivative in  $x$  direction; function  $h_2$  on  $4 \times 4$  mesh, direction  $35^\circ$ ; (+) Poisson integral, (x) direct method, (□) Zhu-Zienkiewicz and (o) local smoothing method

The results shown in Figures 7.12 and 7.13 confirm the stability, reliability and high accuracy of the Poisson integral method. The superconvergence-based methods are seen to yield very good results near the points of exceptional accuracy, but elsewhere their accuracy is much worse. Nevertheless, the derivatives obtained are often much better than those resulting from direct differentiation, and rarely worse. The Poisson integral method provides a predictably high accuracy, with error rising near the integration contour but low at all interior points. Except near the points of

superconvergence, this method yields the highest accuracy and the highest predictability, but at the highest computing cost. In all methods, accuracy improves substantially with mesh refinement, as it should.

### 7.2.2 Triangular elements

Triangular finite element meshes up to fourth order were used in the second series of tests. Again the two harmonic functions  $h_p$  and  $h_t$  were modeled by solving Laplace's equation with the correct function values along the boundary nodes of a square region similar to that of Figure 7.9. Some typical derivative values at Gaussian (superconvergent) points closest to the center of the region are shown in Tables 7.1 and 7.2. Superconvergent points for tangential derivatives along triangle edges of various orders are shown in Figure 7.14. The mesh density was changed for the various orders of finite element so as to keep the total number of mesh points roughly constant. These results confirm that superconvergence is obtained at the Gaussian points for the tangential field component, but not for the normal derivative, which is calculated with much poorer accuracy. As would be expected, superconvergence provides less improvement for the transcendental function  $h_t$  than for the harmonic polynomial  $h_p$ . For the transcendental function  $h_t$ , the Poisson integral method provides even better accuracy than superconvergence provides for the tangential derivative at Gaussian points.

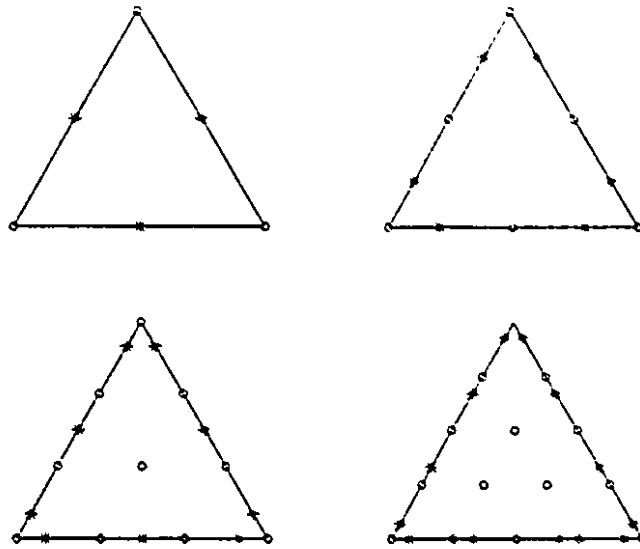


*Figure 7.14.* Position of superconvergent points (\*) for tangential derivative on triangles of various orders

Table 7.1

Percentage error in derivatives at superconvergent points  
on triangular elements, of polynomial  $h_p = x^3y - xy^3$

(a)  $\partial h_p / \partial x$

Number of ele- ments	Method	Order of element $p$			
		1	2	3	4
2	Poisson intg	14.	1.1	0.037	0.0009
	Direct diff	4.3	0.0001	0.0000	0.0000
4	Poisson intg	4.5	0.083	0.0003	0.0008
	Direct diff	1.7	0.0000	0.0000	0.0004
8	Poisson intg	1.3	0.0090	0.0009	0.0003
	Direct diff	0.56	0.0003	0.0002	0.0052
16	Poisson intg	0.35	0.0001	0.0004	0.0003
	Direct diff	0.16	0.0004	0.0064	0.0051

(b)  $\partial h_p / \partial y$

Number of ele- ments	Method	Order of element $p$			
		1	2	3	4
2	Poisson intg	21.	1.9	0.0002	0.0003
	Direct diff	633.	57.	4.5	0.0006
4	Poisson intg	7.1	0.067	0.0004	0.0003
	Direct diff	141.	15.	0.56	0.0003
8	Poisson intg	1.6	0.009	0.0003	0.0008
	Direct diff	52.	4.0	0.069	0.0048
16	Poisson intg	0.39	0.001	0.0010	0.0009
	Direct diff	22.	1.0	0.0009	0.0048

Table 7.2

Percentage error in derivatives at superconvergent points on triangular elements, of function  $h_i = \log[(1+x)^2 + (1+y)^2]$

(a)  $\partial h_i / \partial x$

Number of elements	Method	Order of element $p$			
		1	2	3	4
2	Poisson intg	0.128	0.43	0.011	0.0046
	Direct diff	2.10	0.52	0.19	0.0074
4	Poisson intg	0.189	0.013	0.0006	0.0006
	Direct diff	0.54	0.068	0.024	0.0024
8	Poisson intg	0.0679	0.0001	0.0004	0.0003
	Direct diff	0.14	0.0094	0.0034	0.0031
16	Poisson intg	0.027	0.0002	0.0001	0.0003
	Direct diff	0.032	0.0037	0.0043	0.0001

(b)  $\partial h_i / \partial y$

Number of elements	Method	Order of element $p$			
		1	2	3	4
2	Poisson intg	0.64	0.31	0.0067	0.0048
	Direct diff	32.	0.13	0.98	0.068
4	Poisson intg	0.15	0.011	0.0015	0.0011
	Direct diff	15.	0.46	0.14	0.0054
8	Poisson intg	0.061	0.0003	0.0010	0.0009
	Direct diff	7.0	0.19	0.012	0.015
16	Poisson intg	0.024	0.0009	0.0021	0.0009
	Direct diff	3.3	0.056	0.021	0.016

Comparative results are given in Figures 7.15 and 7.16 for regular meshes of 32 and 128 second order triangular elements (square subdivisions of  $4 \times 4$  and  $8 \times 8$  elements), the derivatives having been computed by global smoothing, direct differentiation, and the Poisson integral method. The test function was  $h_p$ , and results were computed along a line through the center of the square and at  $20^\circ$  to the  $x$  axis. The results obtained for with the transcendental function  $h_t$  were quite similar. They clearly demonstrate the superior accuracy of the Poisson integral method, and show that the global smoothing method does not have high accuracy despite its relatively high computational cost.

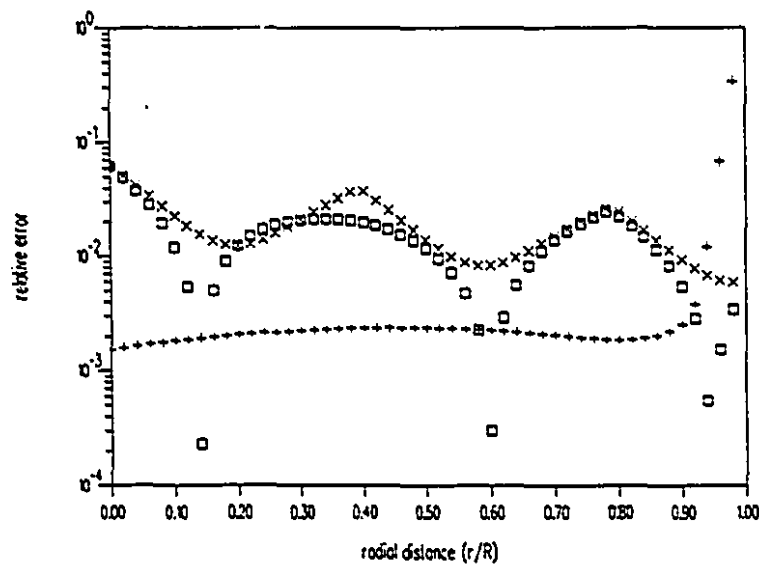
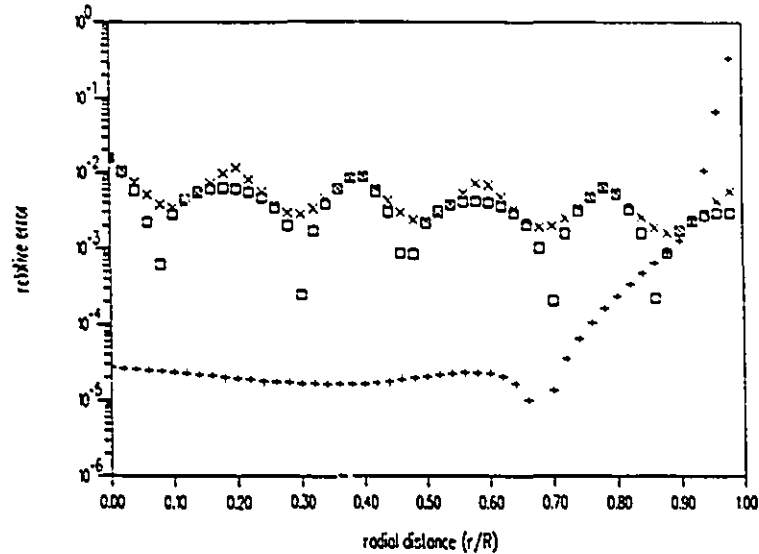


Figure 7.15. Derivative in  $x$  direction for function  $h_p$  using  $4 \times 4$  mesh of second order elements, direction  $20^\circ$ ; (+) Poisson integral, (x) direct differentiation, (□) global smoothing results



**Figure 7.16.** Derivative in  $x$  direction for function  $h_p$  using  $8 \times 8$  mesh of second order elements, direction  $20^\circ$ ; (+) Poisson integral, (x) direct differentiation, ( $\square$ ) global smoothing results

For derivatives higher than the first, the Poisson integral method is clearly superior. Table 7.4 presents the error in computed derivatives, up to third order, for the polynomial function  $h_p$ , evaluated at the point  $r = 0.3$ ,  $\theta = 20^\circ$ , relative to the center point (1,1). Elements up to fourth order were used, and the total number of degrees of freedom was similar in all cases. From the results presented for quadrilateral meshes in Table 2, where even at superconvergent points the Poisson integral method gave the most accurate first derivatives, one would again expect this method to perform well. This expectation is borne out by the results presented in Table 7.4, where the stability and high accuracy of the Poisson integral method are evident. Further, its accuracy is neither dependent on the element order, nor on the position of the point of interest, nor even on the order of derivative.

Table 7.3

Percentage error in higher derivatives  $\phi_{[ij]}$ , of  $\phi = h_p = x^3y - xy^3$ ,

$$\phi_{[ij]} = \partial^{i+j}\phi/\partial x^i\partial y^j$$

Derivative	Method	Order of element $p$		
		2	3	4
$\phi_{[00]}$	Poisson intg	0.0006	0.0027	0.0026
	Direct diff.	0.023	0.0050	0.0014
$\phi_{[10]}$	Poisson intg	0.0023	0.0007	0.0007
	Direct diff.	0.11	0.0059	0.0010
$\phi_{[01]}$	Poisson intg	0.0044	0.0012	0.0013
	Direct diff.	0.24	0.015	0.0011
$\phi_{[20]}$	Poisson intg	0.0021	0.0008	0.0010
	Direct diff.	3.2	0.37	0.0005
$\phi_{[11]}$	Poisson intg	0.013	0.0090	0.0088
	Direct diff.	5.8	0.53	0.0021
$\phi_{[02]}$	Poisson intg	0.0021	0.0009	0.0010
	Direct diff.	2.2	0.043	0.0002
$\phi_{[30]}$	Poisson intg	0.0001	0.0041	0.0046
	Direct diff.		9.29	0.0097
$\phi_{[21]}$	Poisson intg	0.016	0.0079	0.0077
	Direct diff.		4.0	0.027
$\phi_{[12]}$	Poisson intg	0.0001	0.0041	0.0046
	Direct diff.		1.8	0.010
$\phi_{[03]}$	Poisson intg	0.016	0.0079	0.0077
	Direct diff.		2.5	0.034

### 7.2.3 Non-uniform triangular mesh

The third series of tests employed a nonuniform first-order triangular mesh, applied to the fields in an infinitely deep electric machine slot. While this problem embodies most of the characteristics that arise in many problems of applied electromagnetics (e.g., it includes a field singularity), it is still analytically solvable even though very complicated. A typical mesh used to solve this problem appears in Figure 7.17.

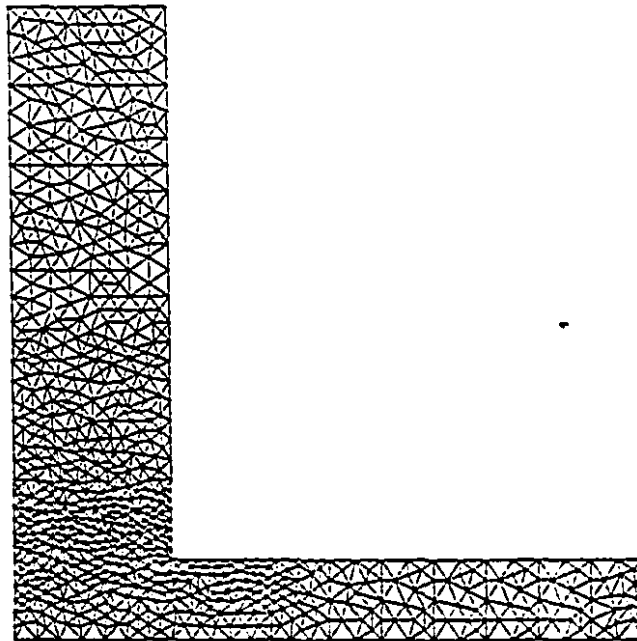


*Figure 7.17.* Finite element mesh used for infinite slot example

Since the practical result most often required in such a problem is the air-gap flux density, Figure 7.18 shows values of the vertical derivative of potential  $A$ , i.e.,  $\partial A/\partial y$ , evaluated at the level  $y = 0.7 \times \text{gap-width}$ . This derivative was

computed in two ways. First, direct differentiation was used, followed by averaging at nodes, and second, by means of the Poisson integral method. Nodal averages were weighted by element area in the first process. The Poisson integral technique was applied to a sequence of circular contours so chosen that the derivative was always evaluated at the center of the circle. From Figure 7.18 it is evident that the weighted averaging process yields useful accuracy and gives results of acceptable smoothness. The Poisson integral approach gives better accuracy and smoother results, but it is more expensive in computer time.

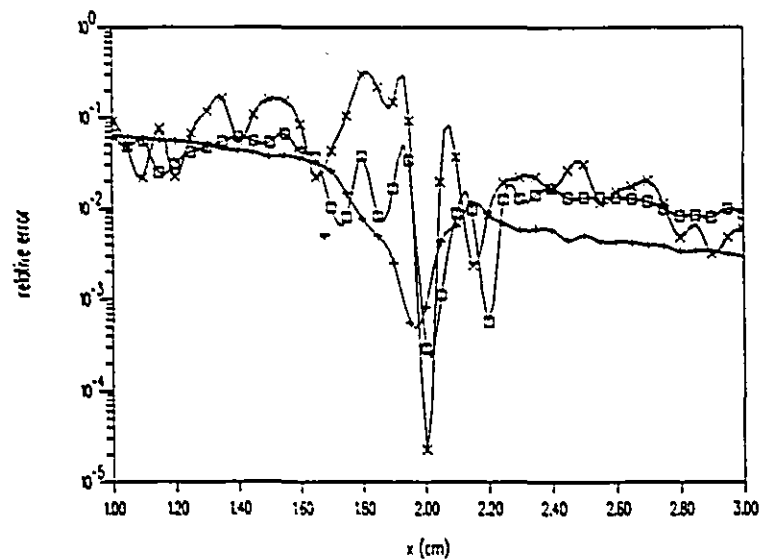


**Figure 7.18.** Derivative in  $y$  direction for infinite depth slot; (+) Poisson integral, ( $\times$ ) direct differentiation method, ( $\square$ ) weighted averages

### 7.3 Tests of procedures dealing with singular integrals

The procedures derived for evaluation of singular integrals are applied to results of the finite element analysis. Tests presented in this section correspond to finite part integration, covering the case of curvilinear singular integrals in the normal derivative computation and singular surface integrals arising in second order derivative calculation.

#### 7.3.1 The normal derivative computation using the Poisson integral method

Tests were done using the harmonic function

$$f_3(x, y) = x^3y - xy^3. \quad (7.5)$$

Figure 7.19 compares results obtained using the Poisson integral method employing 50-point finite part integration with derivatives obtained using direct differentiation method and standard Poisson integral method, without special treatment of singularity using 180 quadrature nodes. It shows the accuracy of the normal derivative computed along the perimeter of a circle of radius  $R = 0.8$ , centered at point  $(1.0, 0.9)$ . Potential results are obtained using a uniform triangular mesh of  $20 \times 20$  linear elements over the region  $0 \leq x, y \leq 2$ . Derivatives computed using Paget's method of evaluating the Poisson integral are of the same order of accuracy as the original finite element solution, with at most one significant digit lost. Compared to results obtained by ignoring the singularity, Paget's approach gives consistently better results, with up to 50 times smaller error. As it is expected, direct differentiation yielded poor accuracy of the normal gradient.

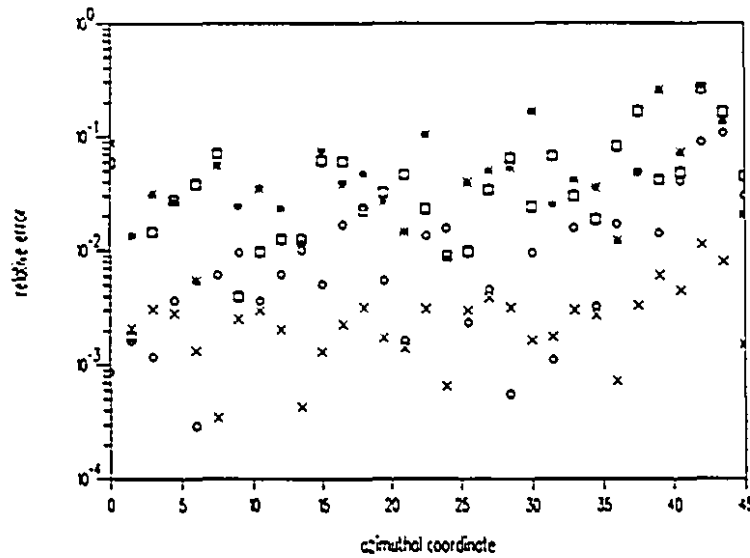


**Figure 7.19.** Accuracy of normal derivative computed along the perimeter of the circle of radius  $R = 0.8$ , centered at point  $(1.0, 0.9)$ . Function  $f_1(x, y)$  used. Poisson integral method with Paget's finite part integration ( $\circ$ ), FEM potentials ( $\times$ ) and direct differentiation ( $\square$ ) and standard Poisson integral (ignoring singularity) ( $*$ ).

### 7.3.2 Second order derivative of the Poisson equation solution

To examine the efficiency of Paget's formulae for finite part integration when applied to approximate results, simulations were done with values of functions

$$f_1(x, y) = x^3 y + x y^3, \quad (7.6)$$

$$f_2(x, y) = (x^2 + y^2)(1 - x^2 - y^2), \quad (7.7)$$

obtained after solving the boundary value problem using the finite element method. The function  $f_2(x, y)$  was chosen in such a way as to eliminate the error in boundary integral computation. Since a circle of radius  $R = 1$  was used as a base region, this function vanishes on its edge. Consequently all derivatives are computed using the domain integral only. Function  $f_1(x, y)$  represents the general case when both integrals must be computed.

Results of analysis are shown in Figure 7.20. They are obtained using a uniform mesh of 200 linear triangles on the region  $0 \leq x, y \leq 2$ . A circle of radius  $R = 0.7$  is centered at  $(1.2, 1.1)$ . The radial position is changed, while the angle is fixed at  $\theta_P = 20^\circ$ . The main source of error in surface integral computation is approximation of the source function by its average value over each element. In order to estimate the influence this approximation of the source function a second test was performed, this time using the exact value of the source function, which is usually known in practical problems. Computed derivatives have the same or even better accuracy than finite element results. Note that it is not possible to compute second derivative from first order finite element approximations by direct differentiation.

The results of analyzing the case when the point  $P$  is on the edge of the circle are given in Figure 7.21. They are obtained using a mesh of 200 second order finite elements to model the function  $f_2(x, y)$  in the domain  $-1 \leq x, y \leq 1$ . Results were extracted from a circle of radius  $R = 1$  centered on  $(0, 0)$ . Again, the source of error is piecewise approximation of the source function. In this case the curvilinear integral is ignored, so the error in results is due to surface integral computation only.

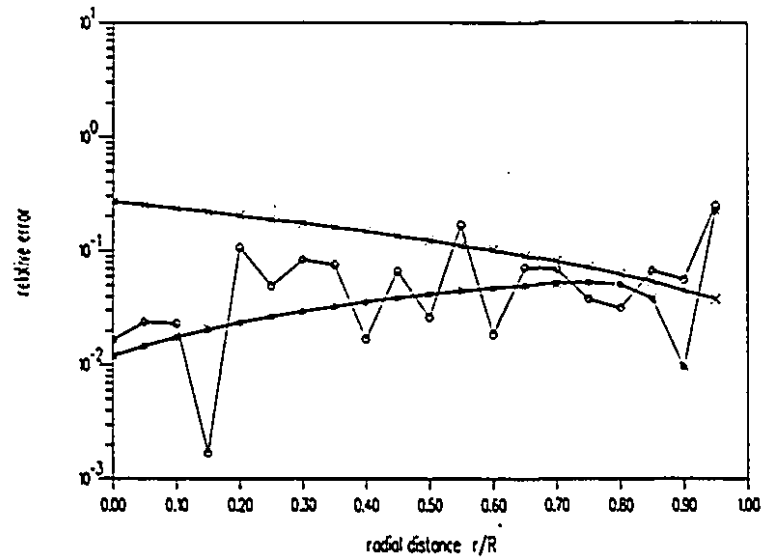


Figure 7.20. Computed derivatives  $\partial^2 f_2 / \partial x \partial y$  when the radial position is changed, while angle is fixed at  $\theta_P = 20^\circ$ . Function  $f_2(x, y)$  is approximated using 200 quadratic triangles. FEM potentials ( $\times$ ), Poisson integral method with Paget's finite path integration ( $\circ$ ), and results using the exact values of the source function ( $*$ ).

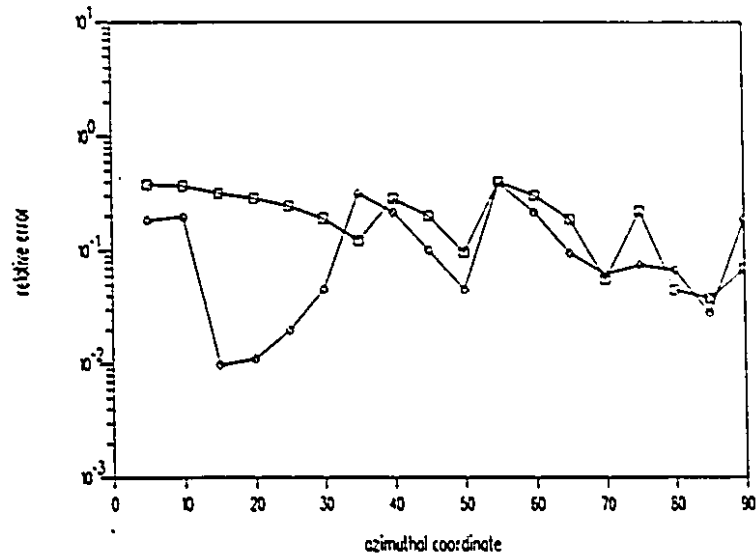
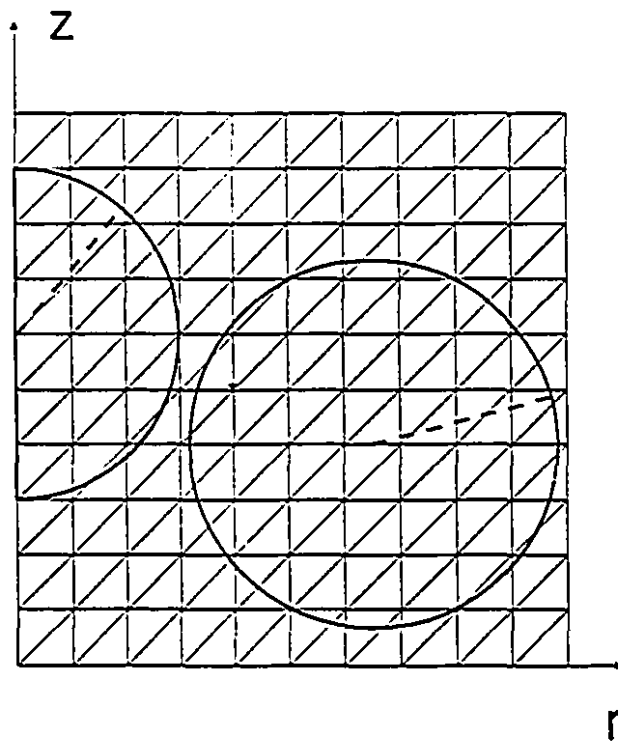


Figure 7.21. Computed derivatives  $\partial^2 f_2 / \partial x^2$  for point  $P$  on the edge, angular position changed. Results extracted from the circle of radius  $R = 1.0$  centered at  $(0., 0.)$ . Function  $f_2(x, y)$  is approximated using 200 triangles. Poisson integral method with Paget's finite part integration (o), and finite element differentiation (□).

## 7.4 Application to axisymmetric problems

The method of differentiating approximations to the harmonic functions in axisymmetric coordinate system is treated in Chapter 3, and its verification in Chapter 4. Tests with results obtained using the finite element solver are presented in this section.



*Figure 7.22.* Contours of a torus and a sphere embedded in first-order finite element mesh, used in differentiation of potentials obtained by using the finite element interpolation functions.

An analytically known function

$$f(r, z) = \frac{1}{\sqrt{(1+r)^2 + (1+z)^2}} \quad (S)$$

was approximated by means of a finite element solution, with function value prescribed on the boundary of the region. Linear triangular elements were used. In all cases the test region was the cylinder  $0 \leq r, z \leq 2$ . In the results presented here, the mesh density in the region of interest was varied, and results are shown for the new method based on differentiation of the fundamental solution of boundary value problem; they are compared with results from direct differentiation. Figure 7.22 shows the finite element mesh and a torus and a sphere embedded in the mesh as used in computation of derivatives. Also shown in Figure 7.22 are lines along which the partial derivative in the  $z$ -direction and the derivative  $\partial^2 f / \partial r^2$  were computed. In the torus the line makes an angle  $\theta = 20^\circ$  with the  $r$ -axis, and for the sphere  $\psi = 40^\circ$  with the  $z$ -axis.

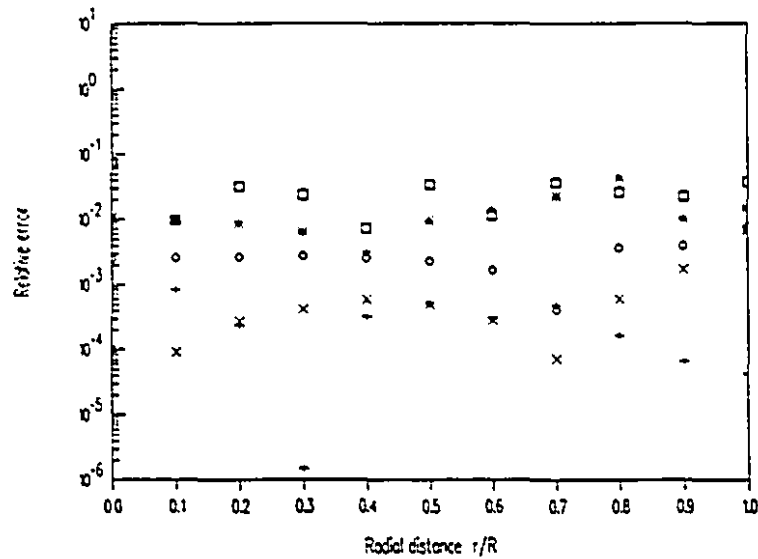


**Figure 7.23.** Relative error in results extracted from the torus, using the 50 finite element solution: error in  $\partial\phi/\partial r$  ( $\times$ ),  $\partial\phi/\partial z$  ( $\circ$ ) and  $\partial^2\phi/\partial z^2$  ( $*$ ) using the new method, error in  $\partial\phi/\partial r$  obtained using direct differentiation ( $\square$ ); original finite element solution ( $+$ ).

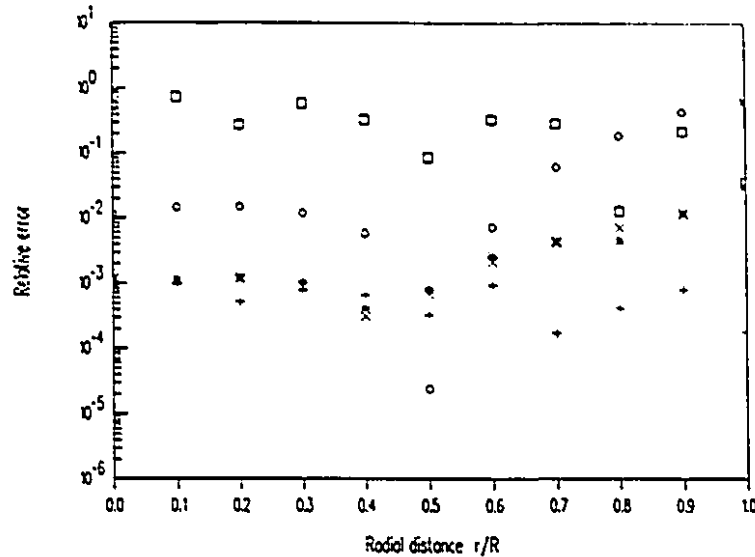
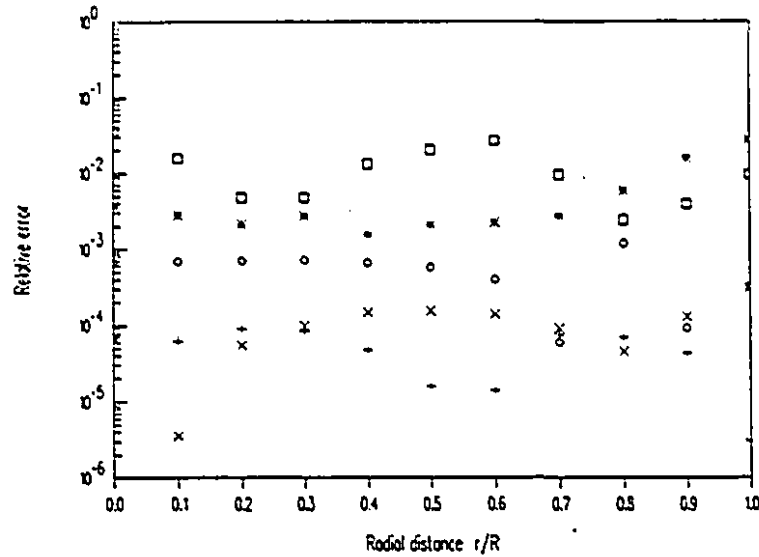


Figure 7.24. Relative error in results extracted from the sphere, using the 50 finite element solution: error in  $\partial\phi/\partial r$  ( $\times$ ),  $\partial\phi/\partial z$  ( $o$ ) and  $\partial^2\phi/\partial z^2$  ( $*$ ) using the new method, error in  $\partial\phi/\partial r$  obtained using direct differentiation ( $\square$ ); original finite element solution ( $+$ ).

Figures 7.23 and 7.24 present the error in computed derivatives using a uniform mesh of 50 finite elements. First order derivative results are significantly improved compared to the direct differentiation technique. First order derivatives extracted from the sphere have the same accuracy as the original finite element results, and not more than one significant digit is lost in the second derivative. Derivatives extracted from the torus have poorer accuracy, but they are still much better than the direct differentiation results. Figures 7.25 and 7.26 give the results with 200 finite elements, i.e. with doubled discretization in both directions. The results have the same behavior as in the previous cases.



**Figure 7.25.** Relative error in results extracted from the torus, using the 200 finite element solution: error in  $\partial\phi/\partial r$  (x),  $\partial\phi/\partial z$  (o) and  $\partial^2\phi/\partial z^2$  (\*) using the new method, error in  $\partial\phi/\partial r$  obtained using direct differentiation ( $\square$ ); original finite element solution (+).

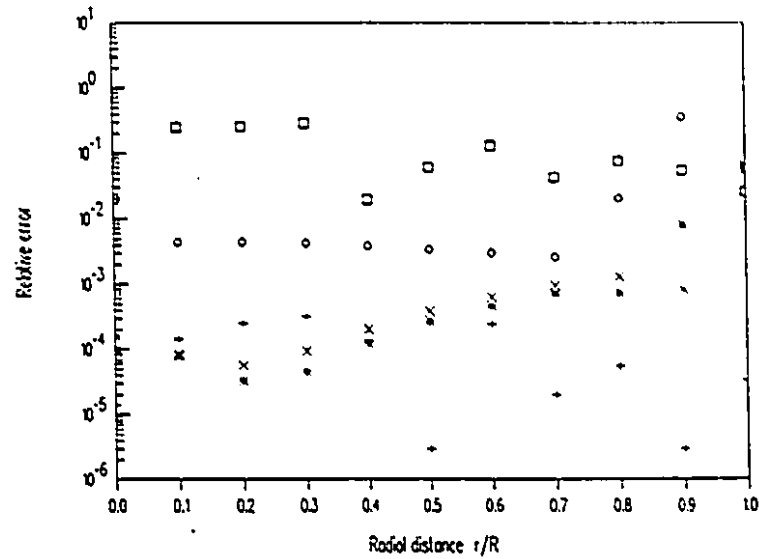


Figure 7.26. Relative error in results extracted from the sphere, using the 200 finite element solution: error in  $\partial\phi/\partial r$  (x),  $\partial^2\phi/\partial z^2$  (\*) and  $\partial^3\phi/\partial r\partial z^2$  (o) using the new method, error in  $\partial\phi/\partial r$  obtained using direct differentiation (□); original finite element solution (+).

### 7.5 Three dimensional local smoothing results

Extensive computational tests have now been performed to compare the performance of the generalized Zhu-Zienkiewicz method with conventional local smoothing and with direct differentiation of the finite element solution. Two test cases were used, in which an analytically known function was approximated by means of a finite element solution, with function value prescribed on the boundary of the region. Tests were carried out using the functions

$$f_1(x, y, z) = xyz + x^3 + y^3 - 3z^2(x + y) \quad (9)$$

and

$$f_2(r, z) = \frac{1}{\sqrt{(1+x)^2 + (1+y)^2 + (1+z)^2}} \quad (10)$$

Both functions are harmonic. As in the two-dimensional case, similar accuracy may be expected for functions satisfying the Poisson and Helmholtz equations. The first function  $f_1$  is a cubic polynomial, so the generalized Zhu-Zienkiewicz method should produce first derivatives exact at the Gaussian points.

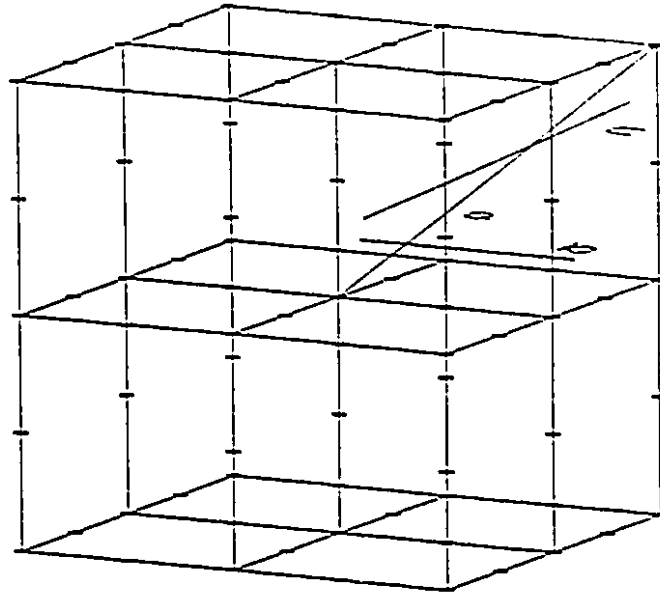


**Figure 7.27.** Finite element discretization with lines along which derivatives were computed

Second order numerically integrated brick elements were used in the tests, and reduced integration was employed (Zlámal (1978), Zienkiewicz and Taylor (1989)). In all cases the test region was the cube  $0 \leq x, y, z \leq 2$ , as shown in Figure 7.27. In this figure, directions along which derivatives were computed are also shown. The segments are:

<i>segment</i>	<i>starting point</i>	<i>end point</i>
<i>a</i>	(1,1,1)	(2,2,2)
<i>b</i>	(1,1.211482,1.211482)	(2,1.211482,1.211482)
<i>c</i>	(1.,1.25,1.3)	(2.,1.75,1.8)

The directions are chosen in such a way as to cover three typical cases. Segment  $a$  is the main diagonal of an element. It contains two superconvergent points and the element center, which has exceptional accuracy in the 2-D case (the derivative there is the arithmetic mean of superconvergent values), so it is the best direction for conventional Hinton-Campbell local smoothing. Segment  $b$  contains two superconvergent points. An arbitrary direction is chosen for segment  $c$ , to illustrate the practical situation where no superconvergent points occur along the desired direction. In all tests the results given refer to the partial derivative in the  $x$  direction, i.e.  $\partial\phi/\partial x$ . In the test cases this coincides with one of the local axes. Various mesh densities were used in the problem region, and results are shown for all three differentiation methods.

The first set of results, shown in Figures 7.28-7.30, corresponds to the function  $f_1(x,y,z)$ . It bears out the expectations about behavior of recovered derivatives that might reasonably be based on the theoretical arguments presented above. Figure 7.28 shows that along the main diagonal both local smoothing methods reach the maximal accuracy possible for the single-precision calculations used in tests. From Figure 7.29 it is clear that there is no improvement of accuracy when classical local smoothing is used. The results presented in Figure 7.30 show that in the Hinton-Campbell type of local smoothing, the correction of derivatives may actually go in the wrong direction. From all results shown, it is clear that a superior accuracy (exact approximation) is obtainable by computing gradients using the generalized Zhu-Zienkiewicz method.

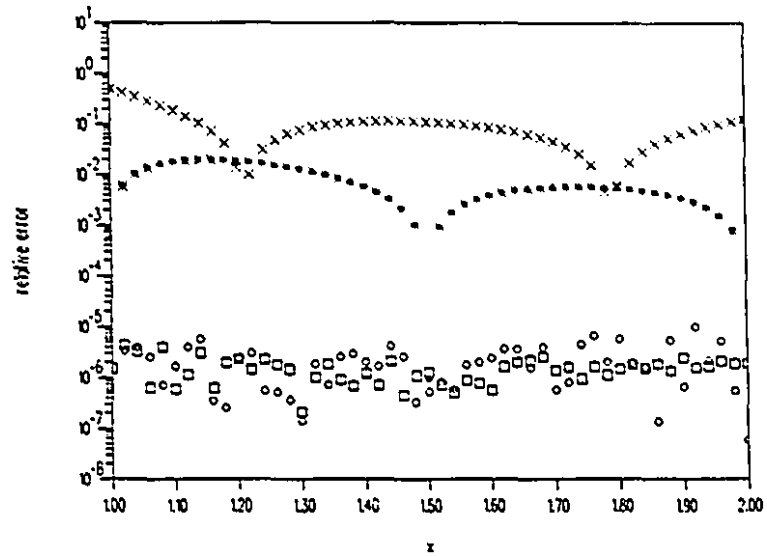


Figure 7.28. Derivative in  $x$  direction along the line  $a$ ; function  $1 - 2 \times 2 \times 2$ ; (\*) potential, (x) direct differentiation, (o) Zhu-Zienkiewicz and (□) local smoothing method

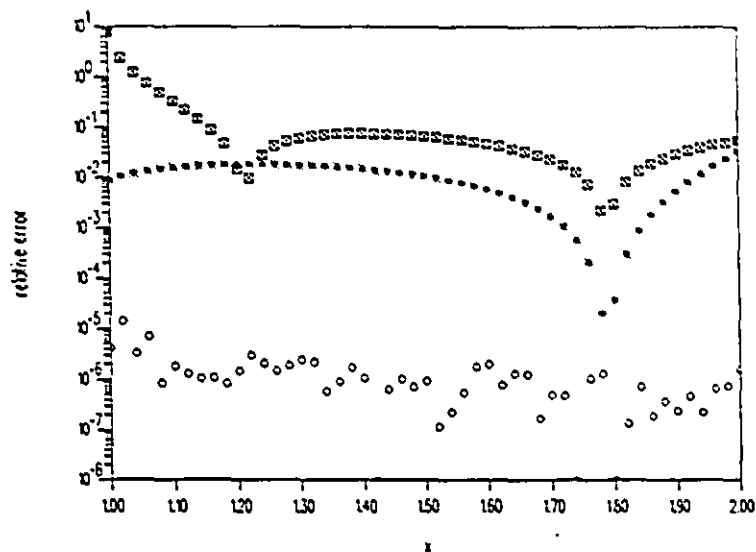


Figure 7.29. Derivative in  $x$  direction along the line  $b$ ; function  $1 - 2 \times 2 \times 2$ ; (\*) potential, (x) direct differentiation, (o) Zhu-Zienkiewicz and (□) local smoothing method

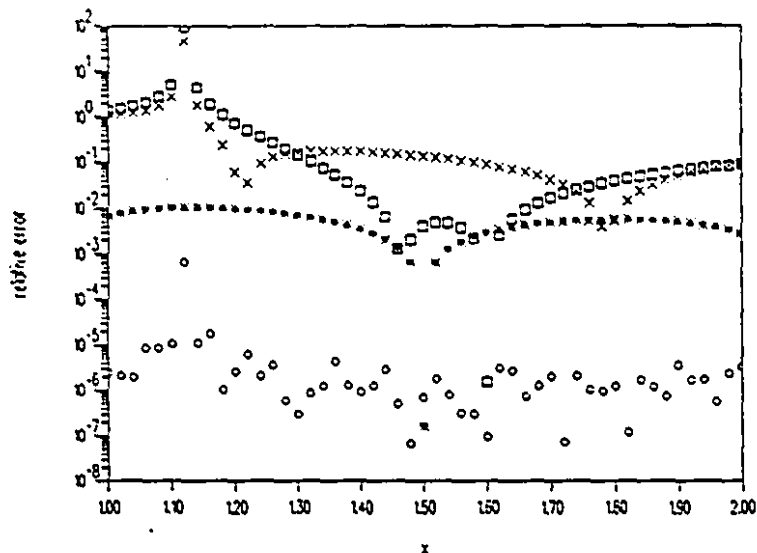
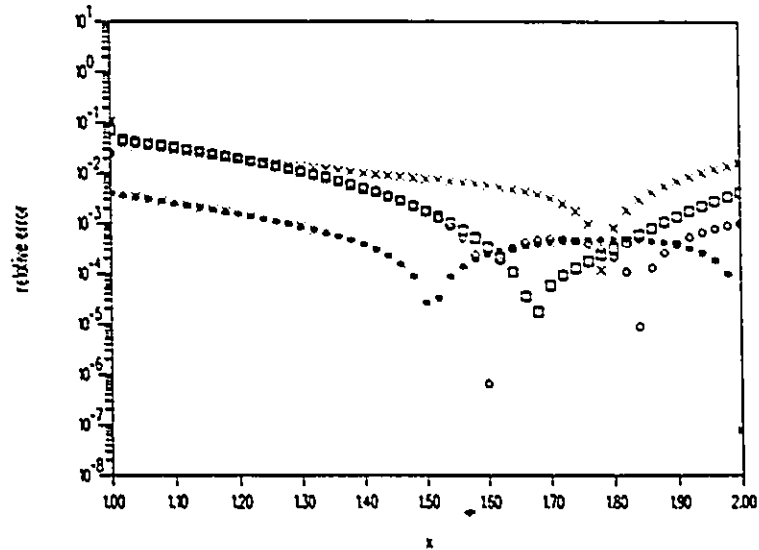


Figure 7.30. Derivative in  $x$  direction along the line  $c$ ; function 1  $-2 \times 2 \times 2$  mesh; (\*) potential, (x) direct differentiation, (o) Zhu-Zienkiewicz and ( $\square$ ) local smoothing method

The second set of results is obtained using the function  $f_2(x, y, z)$ , which is harmonic but not polynomial. Since this function is not a third-order polynomial, the results are not necessarily optimal at the same (Gauss-Legendre) points. The consequence is that local smoothing constructed using both methods is not quite so good as in the first (polynomial) case. The results are seen to be better than obtainable by direct differentiation and conventional local smoothing, but the improvement is not consistent. Figures 7.31–7.33 show results of analysis for segments  $a$ ,  $b$ ,  $c$  respectively, using the  $2 \times 2 \times 2$  finite element mesh. Results for the  $4 \times 4 \times 4$  mesh, on an arbitrary segment  $c$ , are given in Figure 7.34. In this case, potential results are more accurate than in the previous one; the generalized Zhu-Zienkiewicz method shows better performance than local smoothing. Of

course, better derivatives result from mesh refinement, an expectation fully borne out by Figures 7.33 and 7.34.



**Figure 7.31.** Derivative in  $x$  direction along the line  $\alpha$ : function 2 on  $2 \times 2 \times 2$  mesh. (\*) potential, (x) direct differentiation, (o) Zhu-Zienkiewicz and ( $\square$ ) local smoothing method.

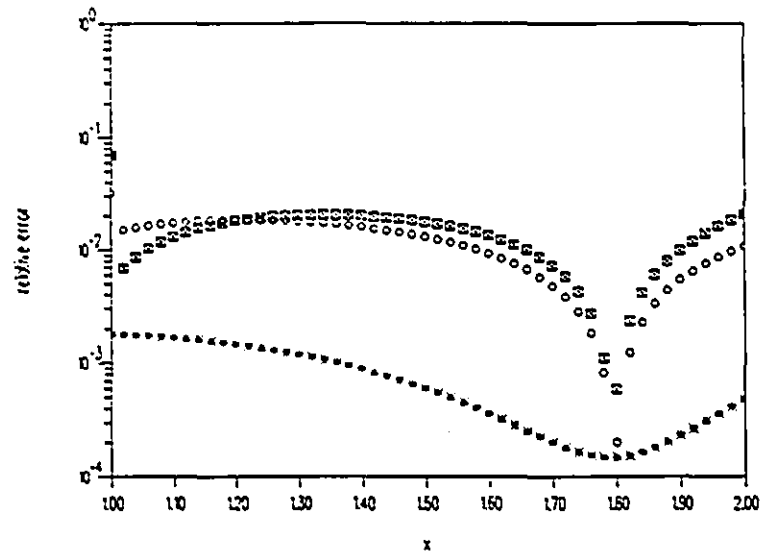


Figure 7.32. Derivative in  $x$  direction along the line  $b$ : function 2 on  $2 \times 2 \times 2$  mesh. (\*) potential, (x) direct differentiation, (o) Zhu-Zienkiewicz and (□) local smoothing method.

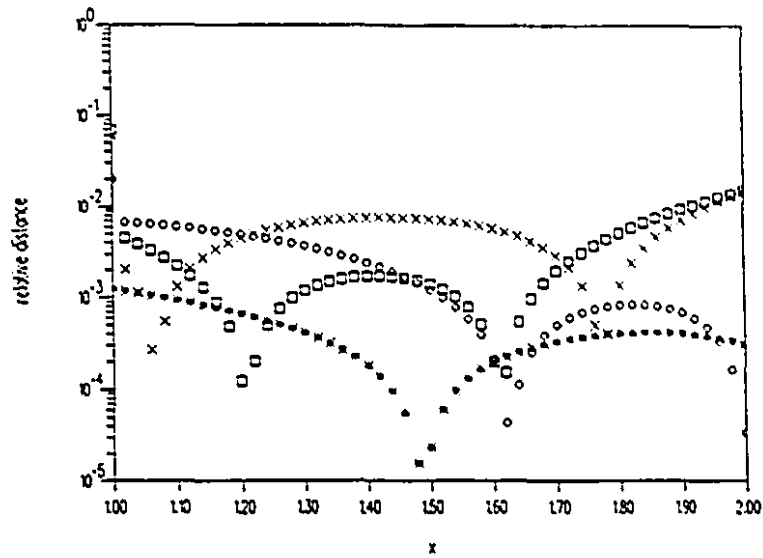
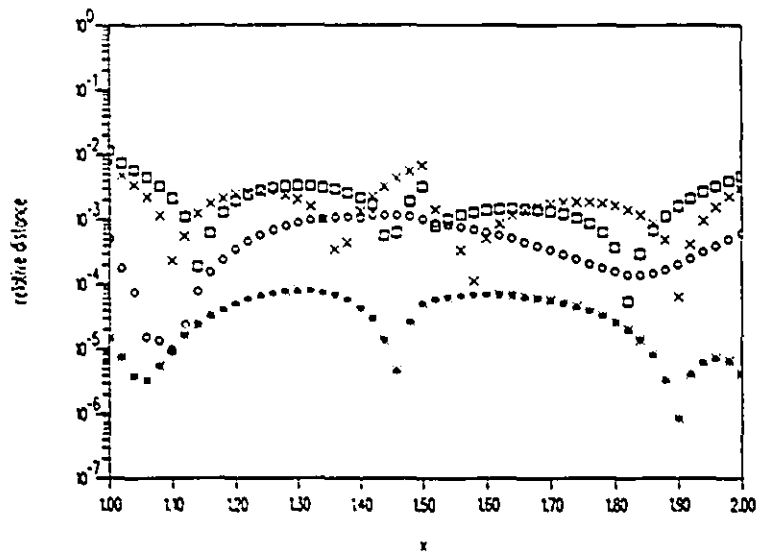


Figure 7.33. Derivative in  $x$  direction along the line  $c$ : function 2 on  $2 \times 2 \times 2$  mesh. (\*) potential, (x) direct differentiation, (o) Zhu-Zienkiewicz and (□) local smoothing method.



**Figure 7.34.** Derivative in  $x$  direction along the line  $c$ : function 2 on  $4 \times 4 \times 4$  mesh. (\*) potential, (x) direct differentiation, (o) Zhu-Zienkiewicz and (□) local smoothing method.

## 7.6 Differentiation of the Helmholtz equation solution

Both methods described in section 2.2.3 were tested using a well-known analytic solution: the  $TM_{11}$  and  $TM_{31}$  modes of a rectangular waveguide. In the following, the term *method L* denotes the technique of using the Green's function for the Laplacian operator, while *method H* is the method using the Green's function for the Helmholtz operator.

Again, as in Chapter 4 the differentiation kernels of the Helmholtz operator were evaluated using 20 terms of the summation in the tests reported here.

A square waveguide was analyzed, i.e., the Helmholtz equation was solved in a square region of side length  $\pi/2$ . Uniform meshes of triangular elements were used to subdivide the region. For the  $TM_{11}$  mode results shown here, a mesh of 200 first-order elements was used, while the results reported for the  $TM_{31}$  mode relate to a mesh of 32 third-order finite elements. Various derivatives of the resulting solutions were computed. In Figure 7.35 a circular integration contour embedded in the first-order finite element mesh is shown. The center of the circle is at the point (0.75, 0.75); the radius of the circle is 0.7.

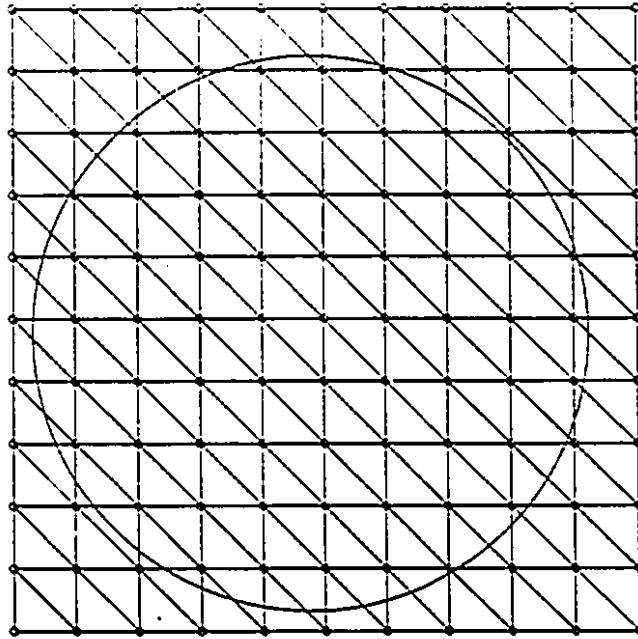


**Figure 7.35.** First order finite element mesh with a circle used in accurate derivative computation.

Vertical derivatives (i.e.,  $\partial\phi/\partial y$ ) computed for the  $TM_{1,1}$  mode using the mesh described are shown in Figure 7.36. Both methods have approximately the same accuracy for  $r/R < 0.75$ . No loss of precision results from differentiation; as can be seen from Figure 7.36, the derivatives actually have better accuracy than the finite element solution itself. Figure 7.37 presents the results of the corresponding computation using *method H*. Near the middle of the circle of integration,  $r/R < 0.5$ , the second derivatives have about the same accuracy as the approximate solution function. For third derivatives, the high-precision region is smaller, about  $r/R < 0.2$ . It should be noted that a first-order finite element solution does not even possess a second or higher derivative, yet the differentiation methods correctly recover derivative information even in this case.

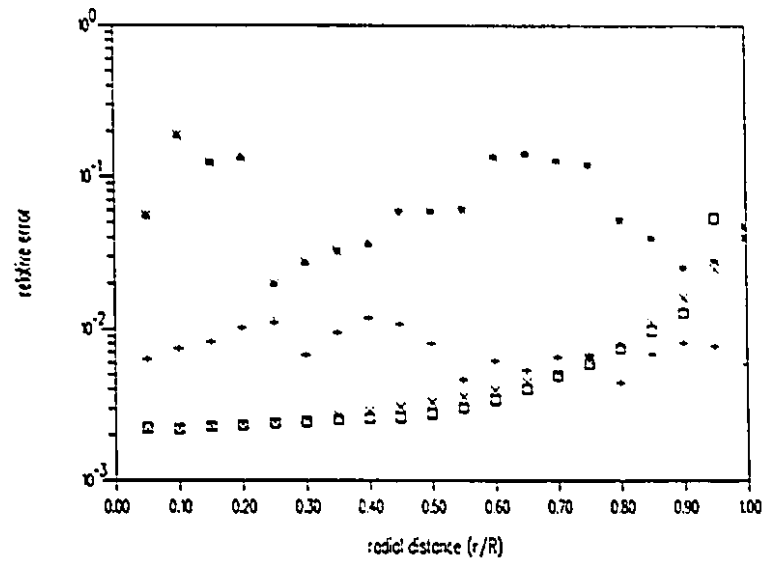


**Figure 7.36.** Relative derivative error of  $TM_{11}$  mode from finite element solution: original finite element solution (+); in  $\partial\phi/\partial y$  using method L ( $\square$ ), method H ( $\times$ ), direct differentiation (\*).

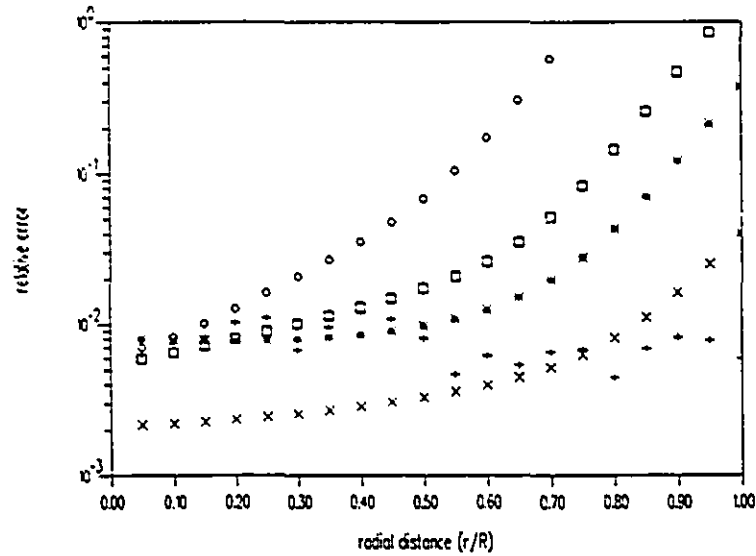


**Figure 7.37.** Relative error in  $TM_{11}$  mode, using Helmholtz operator kernels: original finite element solution (+);  $\partial\phi/\partial y$  ( $\times$ ),  $\partial^2\phi/\partial x\partial y$  ( $\square$ ),  $\partial^2\phi/\partial x^2$  ( $*$ ),  $\partial^3\phi/\partial x\partial y^2$  ( $o$ ).

Results for the  $TM_{31}$  mode appear in Figures 7.38 and 7.39. Again, the results obtained by the two methods have similar accuracy characteristics for the first and second derivatives: the error in derivative values is of the same order as the error in the finite element solution. For the cubic elements used to obtain Figures 7.38 and 7.39, a third method can be used: direct differentiation of the finite element functions themselves. Compared to this direct differentiation, the high-accuracy methods yield at least one, often two, additional correct significant digits in the first derivative  $\partial\phi/\partial y$ , and up to three more significant digits for the second derivative  $\partial^2\phi/\partial x^2$ . The second derivative values obtained by direct differentiation are barely useful. While third derivatives can in principle be

computed, they are so inaccurate as to be useless for any practical purpose.

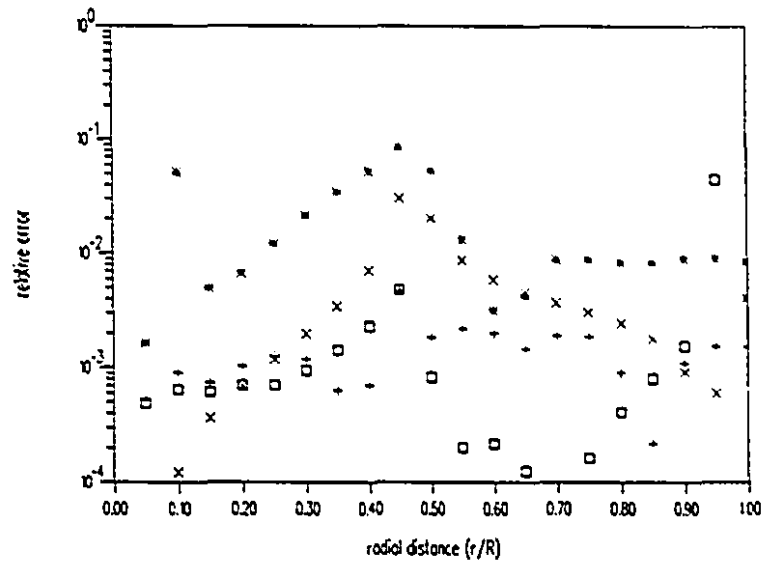


*Figure 7.38.* Relative error of  $TM_{31}$  mode, using third order mesh: original finite element solution (+); in  $\partial\phi/\partial y$  using method L ( $\square$ ), method H ( $\times$ ), finite element differentiation (\*).

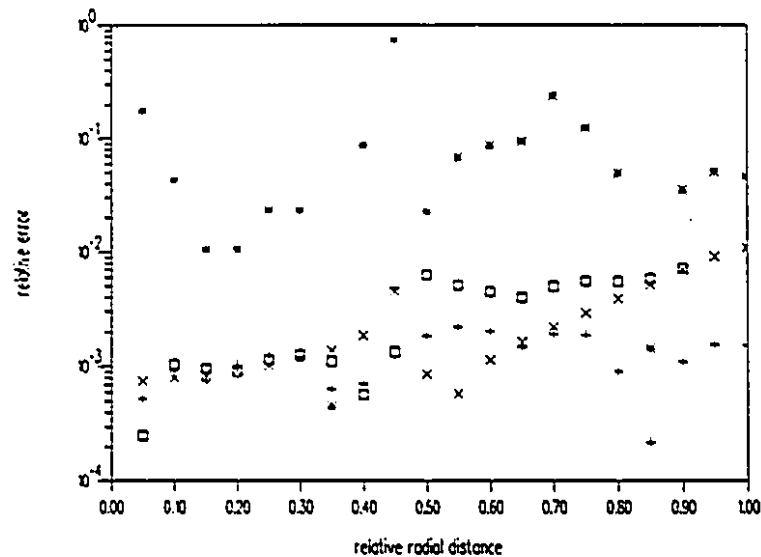


Figure 7.39. Relative error of  $TM_{31}$  mode, using third order mesh: original finite element solution (+); in  $\partial^2\phi/\partial x^2$  using method L (□), method H (×), finite element differentiation (\*).

### 7.7 Concluding remarks

All the methods studied are useful in some circumstances for computing first derivatives; higher derivatives are accurately produced only by the modified Poisson integral technique. In general, the high-accuracy methods are also computationally costly. However the converse is not true.

The proposed methods based on Green's second identity appear to be stable, reliable and highly accurate. Their accuracy is substantially independent of position; it degrades near boundaries but accuracy can in any case be traded

for computing time. This is the only method capable of finding high-order derivatives. Its disadvantage is relatively high computing cost.

The extended Zhu-Zienkiewicz method provides better accuracy and reliability than conventional local smoothing of finite element solutions. Its accuracy is still position-dependent, but less so than the conventional local smoothing method.

Two methods are applied to computing derivatives from finite element solutions of the Helmholtz equation, both based on Green's second identity. One uses the Green's functions for the Laplacian operator, essentially viewing solutions of the Helmholtz equation as equivalent to solutions of the Poisson equation; the other employs Green's functions appropriate to the Helmholtz operator. The second approach is particularly attractive for differentiating solutions of the homogeneous Helmholtz equation. It is capable of computing derivatives of any order, instead of only up to the second order using the Poisson equation approach, and it is computationally more economic than the first technique. It uses integral kernels based on Bessel function series, and the use of optimized polynomials or Padé approximations may further improve the computational economy of this method without affecting its accuracy.

## CHAPTER 8

### Conclusions

The objective of this work has been to develop efficient and reliable methods for high-precision derivative computation from finite element solutions. A formulation based on Green's second identity, using a fundamental solution, meets this goal. The Green's functions and generalized Poisson kernel function derivatives required for this method were derived in this thesis for the Laplacian operator on the circle, sector of circle, rectangle and sector of ring. Corresponding functions were also derived for the Helmholtz operator using a circle as the base domain. The method was evaluated and validated using several test problems with analytical solutions, with results containing random error and with real finite element solutions. A sequence of tests was carried out to cover typical and special cases.

To treat special cases involving singularities, such as the normal derivative on the edge, the finite part integration concept was used. Novel quadrature techniques based on finite part integration were derived.

Two and three-dimensional generalizations of the Zhu-Zienkiewicz method of gradient recovery are also new in this thesis. They are applied to numerically integrated quadrilateral and brick elements. These methods are compared to the conventional local smoothing method, and are included in comparative analysis of the various differentiation methods.

#### 8.1 Characteristics of the generalized Poisson integral method

This method relies on fundamental solutions of boundary value problems for several cases and elementary regions. The work in this thesis has been restricted

to scalar problems described by the Laplace, Poisson and Helmholtz equations. Computational experiments confirm its superior accuracy compared to other methods. In fact this is the only method capable of finding high-order derivatives with high accuracy.

The proposed method has a *negative error amplification*. It is not sensitive to data error nor to random observational error. The sequence of tests performed using results with uniformly distributed random error shows that the accuracy of computed derivatives is usually higher than the data accuracy.

Two very important advantages of the new method are its stability and reliability. Results of computation are not position dependent as they are using other methods. Results are best at interior points of the base region. Accuracy is reduced near boundaries, but in predictable manner.

Two methods of computing derivatives from finite element solutions of the Helmholtz equation in two dimensions are presented and compared. One uses the Green's function for the Laplacian operator, essentially viewing solutions of the Helmholtz equation as equivalent to solutions of the Poisson equation; the other employs Green's functions appropriate to the Helmholtz operator. The second approach is particularly attractive for differentiating solutions of the homogeneous Helmholtz equation. It is capable of computing derivatives of any order, instead of only up to second order using the Poisson equation approach.

The model for axisymmetric problems described by Laplace's equation using a torus and a sphere as base regions is shown to be computationally efficient, but less effective than for the two-dimensional problems. The main difficulty is evaluation of Green's function.

The principal disadvantage of the method is its relatively high computational cost.

## 8.2 Characteristics of the generalized Zhu-Zienkiewicz method

This method appears, on both theoretical and experimental grounds, to provide better accuracy and reliability than conventional local smoothing of finite element solutions. In common with the local smoothing method, its accuracy is position-dependent.

Because this method constructs a smoothed approximation from the Gaussian integration points, its accuracy is essentially dependent on the accuracy of potential values at these points. The advantages of this method include high accuracy, locality of data, and simplicity in application. Computing costs are relatively low, since all arithmetic operations are strictly local to a finite element.

## 8.3 Results of comparative analysis

The new method and the new generalization of the Zhu-Zienkiewicz method, are compared with four other differentiation methods commonly used in postprocessing of finite element results. The results of the comparative analysis and tests described in thesis are summarized in Table 8.1. All the methods are useful in some circumstances for computing first derivatives. Where first derivative values of moderate accuracy are required, the conventional weighted average method appears to produce acceptable results. The superconvergent smoothing methods, based on extrapolation or interpolation from the results at points of exceptional accuracy, produce better results than direct differentiation, but their accuracy is strongly position dependent and restricted to first derivatives.

Table 8.1.

*Summary of characteristics: Five approximate differentiation methods*

Method	Costs	Position dependence	Accuracy
<i>direct differentiation</i>	<i>low</i>	<i>yes</i>	<i>low</i>
<i>weighted averages</i>	<i>low</i>	<i>yes</i>	<i>good</i>
<i>local smoothing</i>	<i>moderate</i>	<i>yes</i>	<i>good</i>
<i>extended Zhu-Zienkiewicz</i>	<i>moderate</i>	<i>yes</i>	<i>very good</i>
<i>global smoothing</i>	<i>high</i>	<i>yes</i>	<i>good</i>
<i>Poisson integral</i>	<i>high</i>	<i>no</i>	<i>excellent</i>

#### 8.4 Further work

The generalized Poisson integral method proposed here has great potential for further development. The following directions are suggested:

- 1) Extension to three dimensional problems.
- 2) Application to vector problems.
- 3) Optimization of existing algorithms. Eventual use of Padé approximations may further improve the computational economy of integral kernels based on Bessel function series.
- 4) Analyze the possibility of computing third order derivatives from Poisson equation solutions.
- 5) Parallelisation of the method.

## APPENDIX 1

### Poisson kernels and surface integral kernels for a circular region

Let the point  $P$  be located at  $(x_P, y_P) = (r_P, \theta_P)$ , within a circle of radius  $R$ . Similarly, let  $Q$  be at  $(x_Q, y_Q)$  or  $(r_Q, \theta_Q)$ . Then the image  $I$  of source point  $Q$  have coordinates  $(x_I, y_I)$  or  $(R^2/r_Q, \theta_Q)$ . Distances from the observation point  $P$  to the source  $Q$  and its image  $I$ , and their derivatives are

$$s_Q^2 = r_P^2 + r_Q^2 - 2r_P r_Q \cos(\theta_P - \theta_Q) \quad (\text{A1.1})$$

$$s_I^2 = r_P^2 + \frac{R^4}{r_Q^2} - 2r_P \frac{R^2}{r_Q} \cos(\theta_P - \theta_Q) \quad (\text{A1.2})$$

$$S_{Qx} = \frac{\partial s_Q}{\partial x_P} = \frac{x_P - x_Q}{s_Q} = -\cos(\alpha_Q + \theta_P) \quad (\text{A1.3})$$

$$S_{Qy} = \frac{\partial s_Q}{\partial y_P} = \frac{y_P - y_Q}{s_Q} = -\sin(\alpha_Q + \theta_P) \quad (\text{A1.4})$$

$$S_{Ix} = \frac{\partial s_I}{\partial x_P} = \frac{x_P - x_I}{s_I} = \frac{x_P - \frac{R^2}{r_Q} x_Q}{s_I} = -\cos(\alpha_I + \theta_P) \quad (\text{A1.5})$$

$$S_{Iy} = \frac{\partial s_I}{\partial y_P} = \frac{y_P - y_I}{s_I} = \frac{y_P - \frac{R^2}{r_Q} y_Q}{s_I} = -\sin(\alpha_I + \theta_P) \quad (\text{A1.6})$$

The first ten Poisson kernel functions are:

$$K_{00}(P; Q) = -\frac{1}{2\pi r_Q} \frac{r_Q^2 - r_P^2}{s_Q^2} = -\frac{1}{\pi r_Q} \frac{c^2}{s_Q^2} \quad (\text{A1.7})$$

$$K_{10} = \frac{s_Q x_P - S_{Qx}(r_P^2 - r_Q^2)}{\pi r_Q s_Q^3} = -\frac{1}{\pi r_Q} \left\{ \frac{c^2}{s_Q^3} \cos(\alpha_Q + \theta_P) - \frac{r_P}{s_Q^2} \cos \theta_P \right\} \quad (\text{A1.8})$$

$$K_{01} = \frac{s_Q y_P - S_{Qy}(r_P^2 - r_Q^2)}{\pi r_Q s_Q^3} = -\frac{1}{\pi r_Q} \left\{ \frac{c^2}{s_Q^3} \sin(\alpha_Q + \theta_P) - \frac{r_P}{s_Q^2} \sin \theta_P \right\} \quad (\text{A1.9})$$

$$\begin{aligned} K_{20} &= -\frac{(1 - 4S_{Qx}^2)(r_P^2 - r_Q^2) - s_Q^2 + 4S_{Qx} s_Q x_P}{\pi r_Q s_Q^4} \\ &= -\frac{2}{\pi r_Q} \left\{ \frac{c^2}{s_Q^4} \cos(2\alpha_Q + 2\theta_P) - \frac{r_P}{s_Q^3} \cos(\alpha_Q + 2\theta_P) \right\} \end{aligned} \quad (\text{A1.10})$$

$$\begin{aligned} K_{11} &= \frac{4S_{Qx} S_{Qy}(r_P^2 - r_Q^2) - 2s_Q(S_{Qx} y_P + S_{Qy} x_P)}{\pi r_Q s_Q^4} \\ &= -\frac{2}{\pi r_Q} \left\{ \frac{c^2}{s_Q^4} \sin(2\alpha_Q + 2\theta_P) - \frac{r_P}{s_Q^3} \sin(\alpha_Q + 2\theta_P) \right\} \end{aligned} \quad (\text{A1.11})$$

$$\begin{aligned} K_{02} &= -\frac{(1 - 4S_{Qy}^2)(r_P^2 - r_Q^2) - s_Q^2 + 4S_{Qx} s_Q y_P}{\pi r_Q s_Q^4} \\ &= \frac{2}{\pi r_Q} \left\{ \frac{c^2}{s_Q^4} \cos(2\alpha_Q + 2\theta_P) - \frac{r_P}{s_Q^3} \cos(\alpha_Q + 2\theta_P) \right\} \end{aligned} \quad (\text{A1.12})$$

$$\begin{aligned} K_{30} &= -\frac{24S_{Qx}^3(r_P^2 - r_Q^2) + 6S_{Qx}(2r_Q^2 - 2r_P^2 + s_{Qx}^2) + 6s_Q x_P - 24S_{Qx}^2 s_Q x_P}{\pi r_Q s_Q^5} \\ &= -\frac{6}{\pi r_Q} \left\{ \frac{c^2}{s_Q^5} \cos(3\alpha_Q + 3\theta_P) - \frac{r_P}{s_Q^4} \cos(2\alpha_Q + 3\theta_P) \right\} \end{aligned} \quad (\text{A1.13})$$

$$\begin{aligned} K_{21} &= -\frac{24S_{Qx}^2 S_{Qy}(r_P^2 - r_Q^2) + 2S_{Qy}(2r_Q^2 - 2r_P^2 + s_{Qx}^2)}{\pi r_Q s_Q^5} \\ &\quad + \frac{8S_{Qx}^2 s_Q y_P + 16S_{Qx} S_{Qy} s_Q x_P - 2s_Q y_P}{\pi r_Q s_Q^5} \\ &= -\frac{6}{\pi r_Q} \left\{ \frac{c^2}{s_Q^5} \sin(3\alpha_Q + 3\theta_P) - \frac{r_P}{s_Q^4} \sin(2\alpha_Q + 3\theta_P) \right\} \end{aligned} \quad (\text{A1.14})$$

$$\begin{aligned}
K_{12} &= -\frac{24 S_{Qx} S_{Qy}^2 (r_P^2 - r_Q^2) + 2 S_{Qx} (2r_Q^2 - 2r_P^2 + s_{Qx}^2)}{\pi r_Q s_Q^5} \\
&\quad + \frac{8 S_{Qy}^2 s_{Qx} x_P + 16 S_{Qx} S_{Qy} s_{Qy} y_P - 2 s_{Qx} x_P}{\pi r_Q s_Q^5} \\
&= \frac{6}{\pi r_Q} \left\{ \frac{c^2}{s_Q^2} \cos(3\alpha_Q + 3\theta_P) - \frac{r_P}{s_Q^4} \cos(2\alpha_Q + 3\theta_P) \right\} \quad (A1.15)
\end{aligned}$$

$$\begin{aligned}
K_{30} &= -\frac{24 S_{Qy}^3 (r_P^2 - r_Q^2) + 6 S_{Qy} (2r_Q^2 - 2r_P^2 + s_{Qx}^2) + 6 s_{Qy} y_P - 24 S_{Qy}^2 s_{Qy} y_P}{\pi r_Q s_Q^5} \\
&= \frac{6}{\pi r_Q} \left\{ \frac{c^2}{s_Q^2} \sin(3\alpha_Q + 3\theta_P) - \frac{r_P}{s_Q^4} \sin(2\alpha_Q + 3\theta_P) \right\} \quad (A1.16)
\end{aligned}$$

The following general formulae are valid:

$$\begin{aligned}
K_{m,0}(P; Q) &= \\
&= -\frac{m!}{\pi R s_Q^{m+1}} \left\{ \frac{R^2 - r_P^2}{s} \cos(m\alpha_Q + m\theta_P) - r_P \cos((m-1)\alpha_Q + m\theta_P) \right\} \quad (A1.17)
\end{aligned}$$

$$\begin{aligned}
K_{m-1,1}(P; Q) &= \\
&= -\frac{m!}{\pi R s_Q^{m+1}} \left\{ \frac{R^2 - r_P^2}{s_Q} \sin(m\alpha_Q + m\theta_P) - r_P \sin((m-1)\alpha_Q + m\theta_P) \right\} \quad (A1.18)
\end{aligned}$$

and

$$\begin{aligned}
K_{m-2k,2k}(P; Q) &= (-1)^k K_{m,0}(P; Q) && \text{for } 2k \leq m, \\
K_{m-2k-1,2k+1}(P; Q) &= (-1)^k K_{m-1,1}(P; Q) && \text{for } 2k < m.
\end{aligned} \quad (A1.19)$$

The surface integral kernels for producing the first five derivatives of a potential function are as follows:

$$J_{00}(P; Q) = -\frac{1}{2\pi} \log \frac{R s_Q}{r_Q s_I} \quad (\text{A1.20})$$

$$J_{10}(P; Q) = \frac{1}{2\pi} \left( \frac{\cos(\alpha_Q + \theta_P)}{s_Q} - \frac{\cos(\alpha_I + \theta_P)}{s_I} \right) \quad (\text{A1.21})$$

$$J_{01}(P; Q) = \frac{1}{2\pi} \left( \frac{\sin(\alpha_Q + \theta_P)}{s_Q} - \frac{\sin(\alpha_I + \theta_P)}{s_I} \right) \quad (\text{A1.22})$$

$$J_{20}(P; Q) = \frac{1}{2\pi} \left( \frac{\cos(2\alpha_Q + 2\theta_P)}{s_Q^2} - \frac{\cos(2\alpha_I + 2\theta_P)}{s_I^2} \right) - \frac{1}{2} \delta(P - Q) \quad (\text{A1.23})$$

$$J_{11}(P; Q) = \frac{1}{2\pi} \left( \frac{\sin(2\alpha_Q + 2\theta_P)}{s_Q^2} - \frac{\sin(2\alpha_I + 2\theta_P)}{s_I^2} \right) \quad (\text{A1.24})$$

$$J_{02}(P; Q) = \frac{1}{2\pi} \left( \frac{\cos(2\alpha_I + 2\theta_P)}{s_I^2} - \frac{\cos(2\alpha_Q + 2\theta_P)}{s_Q^2} \right) - \frac{1}{2} \delta(P - Q) \quad (\text{A1.25})$$

To generate above kernels, a simple routine MATHEMATICA may be used:

```

K00[x_,y_] := -.5/(Pi R) c1[x,y]/sq[x,y]^2
J00[x_,y_] := .5/Pi (Log[rq/R] + Log[si[x,y]/sq[x,y]])

Derivative[1,0][c1][x_,y_] := -2 y
Derivative[0,1][c1][x_,y_] := -2 x

Derivative[1,0][sq][x_,y_] := Squ[x,y]
Derivative[0,1][sq][x_,y_] := Squy[x,y]
Derivative[1,0][Squ][x_,y_] := Squy[x,y]^2/sq[x,y]
Derivative[0,1][Squ][x_,y_] := - Squ[x,y] Squy[x,y]/sq[x,y]
Derivative[1,0][Squy][x_,y_] := - Squ[x,y] Squy[x,y]/sq[x,y]
Derivative[0,1][Squy][x_,y_] := Squ[x,y]^2/sq[x,y]

Derivative[1,0][si][x_,y_] := Six[x,y]
Derivative[0,1][si][x_,y_] := Siy[x,y]
Derivative[1,0][Six][x_,y_] := Siy[x,y]^2/si[x,y]
Derivative[0,1][Six][x_,y_] := - Six[x,y] Siy[x,y]/si[x,y]
Derivative[1,0][Siy][x_,y_] := - Six[x,y] Siy[x,y]/si[x,y]
Derivative[0,1][Siy][x_,y_] := Six[x,y]^2/si[x,y]

K[x_,y_,m_,n_] := D[K00[x,y], {x,m}, {y,n}]
J[x_,y_,m_,n_] := D[J00[x,y], {x,m}, {y,n}]

```

Then, a kernel  $K_{32}$  can be founded by entering

```
K[x,y,3,2]
```

Second order kernels if observation point is on the edge of a circle

For point  $P(r_P, \theta_P)$  on the edge of a circle of radius  $R$ , first and second order Green's kernels are given by the following formulas. The source point is  $Q(r_Q, \theta_Q)$ . Expressions for  $s_Q$  and  $\alpha$  are given in section 3.1.2.1.

$$J_{10}(P; Q) = \frac{\cos \theta_P}{2\pi R s_Q} (s_Q + 2R \cos \alpha_Q) \quad (\text{A1.26})$$

$$J_{01}(P; Q) = \frac{\sin \theta_P}{2\pi R s_Q} (s_Q + 2R \cos \alpha_Q) \quad (\text{A1.27})$$

$$J_{20}(P; Q) = \frac{(s_Q + 2R \cos \alpha_Q)(s_Q \cos 2\theta_P + 2R \sin 2\theta_P \sin \alpha_Q)}{2\pi R^2 s_Q} - \cos^2 \theta_P \delta(P - Q) \quad (\text{A1.28})$$

$$J_{11}(P; Q) = \frac{(s_Q + 2R \cos \alpha_Q)(s_Q \sin 2\theta_P - 2R \cos 2\theta_P \sin \alpha_Q)}{2\pi R^2 s_Q} - \frac{\sin 2\theta_P}{2} \delta(P - Q) \quad (\text{A1.29})$$

$$J_{02}(P; Q) = -\frac{(s_Q + 2R \cos \alpha_Q)(s_Q \cos 2\theta_P + 2R \sin 2\theta_P \sin \alpha_Q)}{2\pi R^2 s_Q} - \sin^2 \theta_P \delta(P - Q) \quad (\text{A1.30})$$

## APPENDIX 2

Extended Poisson kernels and surface integral kernels for a rectangular region

Let  $P$  placed at  $(x_P, y_P)$  be an observation point within a rectangle of sides  $a$  and  $b$ . Similarly, let  $Q$  be at  $(x_Q, y_Q)$ . Then the system of images is shown in Chapter 3 (section 3.1.2.2). The Green's function for a rectangle has the following form:

$$G(P; Q) = \sum_{m=1}^{\infty} \sum_{n=1}^{\infty} G_{mn}(P; Q), \quad (\text{A2.1})$$

where

$$G_{mn}(P; Q) = \frac{1}{2\pi} \text{Log} \frac{s_{2mn} s_{4mn}}{s_{1mn} s_{3mn}} \quad (\text{A2.2})$$

For brevity, introduce the symbols:

$$x_{Qm} = x_Q + 2ma \quad (\text{A2.3})$$

$$y_{Qn} = y_Q + 2nb \quad (\text{A2.4})$$

$$s_{1mn}^2 = (x_{Qm} - x_P)^2 + (y_{Qn} - y_P)^2 \quad (\text{A2.5})$$

$$s_{2mn}^2 = (x_{Qm} + x_P)^2 + (y_{Qn} - y_P)^2 \quad (\text{A2.6})$$

$$s_{3mn}^2 = (x_{Qm} + x_P)^2 + (y_{Qn} + y_P)^2 \quad (\text{A2.7})$$

$$s_{4mn}^2 = (x_{Qm} - x_P)^2 + (y_{Qn} + y_P)^2 \quad (\text{A2.8})$$

The  $m, n$ th terms in Poisson kernel function which corresponds to sides  $x = 0$  and  $x = a$  (with ' - ' sign on front of all expressions) are

$$K_{x00mn} = \frac{1}{2\pi} \left\{ (x_{Qm} + x_P) \left( \frac{1}{s_{2mn}^2} - \frac{1}{s_{3mn}^2} \right) + (x_{Qm} - x_P) \left( \frac{1}{s_{4mn}^2} - \frac{1}{s_{1mn}^2} \right) \right\} \quad (\text{A2.9})$$

$$K_{x10mn} = \frac{2}{\pi} y_P y_{Qn} \left\{ \frac{1}{s_{2mn}^2 s_{3mn}^2} \left( 1 - 2(x_{Qm} + x_P)^2 \left( \frac{1}{s_{2mn}^2} + \frac{1}{s_{3mn}^2} \right) \right) \right. \\ \left. + \frac{1}{s_{1mn}^2 s_{4mn}^2} \left( 1 - 2(x_{Qm} - x_P)^2 \left( \frac{1}{s_{1mn}^2} + \frac{1}{s_{4mn}^2} \right) \right) \right\} \quad (\text{A2.10})$$

$$K_{x01mn} = \frac{2}{\pi} y_{Qn} \left\{ \frac{(x_{Qm} + x_P)}{s_{2mn}^2 s_{3mn}^2} \left( 2y_P \left( \frac{y_{Qn} - y_P}{s_{2mn}^2} - \frac{y_{Qn} + y_P}{s_{3mn}^2} \right) + 1 \right) \right. \\ \left. + \frac{(x_{Qm} - x_P)}{s_{1mn}^2 s_{4mn}^2} \left( 2y_P \left( \frac{y_{Qn} + y_P}{s_{4mn}^2} - \frac{y_{Qn} - y_P}{s_{1mn}^2} \right) - 1 \right) \right\} \quad (\text{A2.11})$$

$$K_{x20mn} = \frac{4}{\pi} y_P y_{Qn} \quad (\text{A2.12}) \\ \left\{ \frac{x_{Qm} + x_P}{s_{2mn}^2 s_{3mn}^2} \left( 4(x_{Qm} + x_P)^2 \left( \frac{1}{s_{2mn}^4} + \frac{1}{s_{2mn}^2 s_{3mn}^2} + \frac{1}{s_{3mn}^4} \right) - 3 \left( \frac{1}{s_{2mn}^2} + \frac{1}{s_{3mn}^2} \right) \right) \right. \\ \left. - \frac{x_{Qm} - x_P}{s_{1mn}^2 s_{4mn}^2} \left( 4(x_{Qm} - x_P)^2 \left( \frac{1}{s_{1mn}^4} + \frac{1}{s_{4mn}^2 s_{1mn}^2} + \frac{1}{s_{4mn}^4} \right) - 3 \left( \frac{1}{s_{1mn}^2} + \frac{1}{s_{4mn}^2} \right) \right) \right\}$$

$$K_{x11mn} = \frac{2}{\pi} y_{Qn} \quad (\text{A2.13}) \\ \left\{ \frac{1}{s_{2mn}^2 s_{3mn}^2} \left( (x_{Qm} + x_P)^2 \left( s y_P \left( \frac{y_{Qn} + y_P}{s_{3mn}^4} + \frac{y_P}{s_{2mn}^2 s_{3mn}^2} - \frac{y_{Qn} - y_P}{s_{2mn}^4} \right) \right) \right. \right. \\ \left. + 1 - \frac{2}{s_{2mn}^2} - \frac{2}{s_{3mn}^2} \right) - 2y_P \left( \frac{y_{Qn} + y_P}{s_{3mn}^2} - \frac{y_{Qn} - y_P}{s_{2mn}^2} \right) \\ \left. + \frac{1}{s_{1mn}^2 s_{4mn}^2} \left( (x_{Qm} - x_P)^2 \left( s y_P \left( \frac{y_{Qn} + y_P}{s_{4mn}^4} + \frac{y_P}{s_{1mn}^2 s_{4mn}^2} - \frac{y_{Qn} - y_P}{s_{1mn}^4} \right) \right) \right. \right. \\ \left. + 1 - \frac{2}{s_{1mn}^2} - \frac{2}{s_{4mn}^2} \right) - 2y_P \left( \frac{y_{Qn} + y_P}{s_{4mn}^2} - \frac{y_{Qn} - y_P}{s_{1mn}^2} \right) \left. \right\}$$

$$K_{x_0 2mn} = \frac{4}{\pi} y_{Qn} \quad (\text{A2.14})$$

$$\left\{ \frac{x_{Qm} + x_P}{s_{2mn}^2 s_{3mn}^2} \left( 4 y_P \left( \frac{(y_{Qn} + y_P)^2}{s_{3mn}^4} + \frac{(y_{Qn} - y_P)^2}{s_{2mn}^4} - \frac{(y_{Qn} - y_P)(y_{Qn} + y_P)}{s_{2mn}^2 s_{3mn}^2} \right) \right. \right. \\ \left. \left. - \frac{1}{s_{2mn}^2} - \frac{1}{s_{3mn}^2} \right) - 2 \left( \frac{y_{Qn} + y_P}{s_{3mn}^2} - \frac{y_{Qn} - y_P}{s_{2mn}^2} \right) \right\} \\ \left. - \frac{x_{Qm} - x_P}{s_{1mn}^2 s_{4mn}^2} \left( 4 y_P \left( \frac{(y_{Qn} + y_P)^2}{s_{4mn}^4} + \frac{(y_{Qn} - y_P)^2}{s_{1mn}^4} - \frac{(y_{Qn} - y_P)(y_{Qn} + y_P)}{s_{1mn}^2 s_{4mn}^2} \right) \right. \right. \\ \left. \left. - \frac{1}{s_{1mn}^2} - \frac{1}{s_{4mn}^2} \right) - 2 \left( \frac{y_{Qn} + y_P}{s_{4mn}^2} - \frac{y_{Qn} - y_P}{s_{1mn}^2} \right) \right\}$$

The  $m, n$ th term in Poisson kernel function corresponding to sides  $y = 0$  and  $y = b$  (with '-' sign on front of all expressions) are

$$K_{y_0 0mn} = \frac{1}{2\pi} \left\{ (y_{Qn} + y_P) \left( \frac{1}{s_{4mn}^2} - \frac{1}{s_{3mn}^2} \right) + (y_{Qn} - y_P) \left( \frac{1}{s_{2mn}^2} - \frac{1}{s_{1mn}^2} \right) \right\} \quad (\text{A2.15})$$

$$K_{y_0 10mn} = \frac{2}{\pi} x_{Qm} \left\{ \frac{(y_{Qn} + y_P)}{s_{3mn}^2 s_{4mn}^2} \left( 2 x_P \left( \frac{x_{Qm} - x_P}{s_{4mn}^2} - \frac{x_{Qm} + x_P}{s_{3mn}^2} \right) + 1 \right) \right. \\ \left. + \frac{(y_{Qn} - y_P)}{s_{1mn}^2 s_{2mn}^2} \left( 2 x_P \left( \frac{x_{Qm} + x_P}{s_{2mn}^2} - \frac{x_{Qm} - x_P}{s_{1mn}^2} \right) - 1 \right) \right\} \quad (\text{A2.16})$$

$$K_{y_0 1mn} = \frac{2}{\pi} x_P x_{Qm} \left\{ \frac{1}{s_{4mn}^2 s_{3mn}^2} \left( 1 - 2(y_{Qn} + y_P)^2 \left( \frac{1}{s_{4mn}^2} + \frac{1}{s_{3mn}^2} \right) \right) \right. \\ \left. + \frac{1}{s_{1mn}^2 s_{2mn}^2} \left( 1 - 2(y_{Qn} - y_P)^2 \left( \frac{1}{s_{1mn}^2} + \frac{1}{s_{4mn}^2} \right) \right) \right\} \quad (\text{A2.17})$$

$$K_{y20mn} = \frac{1}{\pi} x_{Qm} \quad (\text{A2.18})$$

$$\begin{aligned} & \left\{ \frac{y_{Qn} + y_P}{s_{3mn}^2 s_{4mn}^2} \left( 4 x_P \left( \frac{(x_{Qm} + x_P)^2}{s_{3mn}^4} + \frac{(x_{Qm} - y_P)^2}{s_{4mn}^4} - \frac{(x_{Qm} - x_P)(x_{Qm} + x_P)}{s_{3mn}^2 s_{4mn}^2} \right) \right. \right. \\ & \quad \left. \left. - \frac{1}{s_{3mn}^2} - \frac{1}{s_{4mn}^2} \right) - 2 \left( \frac{x_{Qm} + x_P}{s_{3mn}^2} - \frac{x_{Qm} - x_P}{s_{4mn}^2} \right) \right\} \\ & - \frac{y_{Qn} - y_P}{s_{1mn}^2 s_{2mn}^2} \left( 4 x_P \left( \frac{(x_{Qm} + x_P)^2}{s_{1mn}^4} + \frac{(x_{Qm} - x_P)^2}{s_{2mn}^4} - \frac{(x_{Qm} - x_P)(x_{Qm} + x_P)}{s_{1mn}^2 s_{2mn}^2} \right) \right. \\ & \quad \left. \left. - \frac{1}{s_{1mn}^2} - \frac{1}{s_{2mn}^2} \right) - 2 \left( \frac{x_{Qm} + x_P}{s_{2mn}^2} - \frac{x_{Qm} - x_P}{s_{1mn}^2} \right) \right\} \end{aligned}$$

$$K_{y11} = \frac{2}{\pi} x_{Qm} \quad (\text{A2.19})$$

$$\begin{aligned} & \left\{ \frac{1}{s_{3mn}^2 s_{4mn}^2} \left( (y_{Qn} + y_P)^2 \left( s_{xP} \left( \frac{x_{Qm} + x_P}{s_{3mn}^4} + \frac{x_P}{s_{3mn}^2 s_{4mn}^2} - \frac{x_{Qm} - x_P}{s_{4mn}^4} \right) \right. \right. \right. \\ & \quad \left. \left. + 1 - \frac{2}{s_{3mn}^2} - \frac{2}{s_{4mn}^2} \right) - 2 x_P \left( \frac{x_{Qm} + x_P}{s_{3mn}^2} - \frac{x_{Qm} - x_P}{s_{4mn}^2} \right) \right\} \\ & + \frac{1}{s_{1mn}^2 s_{2mn}^2} \left( (y_{Qn} - y_P)^2 \left( s_{xP} \left( \frac{x_{Qm} + x_P}{s_{2mn}^4} + \frac{x_P}{s_{1mn}^2 s_{2mn}^2} - \frac{x_{Qm} - x_P}{s_{1mn}^4} \right) \right. \right. \\ & \quad \left. \left. + 1 - \frac{2}{s_{1mn}^2} - \frac{2}{s_{2mn}^2} \right) - 2 x_P \left( \frac{x_{Qm} + x_P}{s_{2mn}^2} - \frac{x_{Qm} - x_P}{s_{1mn}^2} \right) \right\} \end{aligned}$$

$$K_{y02mn} = \frac{4}{\pi} x_P x_{Qm} \quad (\text{A2.20})$$

$$\begin{aligned} & \left\{ \frac{y_{Qn} + y_P}{s_{4mn}^2 s_{3mn}^2} \left( 4 (y_{Qn} + y_P)^2 \left( \frac{1}{s_{4mn}^4} + \frac{1}{s_{4mn}^2 s_{3mn}^2} + \frac{1}{s_{3mn}^4} \right) - 3 \left( \frac{1}{s_{4mn}^2} + \frac{1}{s_{3mn}^2} \right) \right) \right. \\ & \quad \left. - \frac{y_{Qn} - y_P}{s_{1mn}^2 s_{2mn}^2} \left( 4 (y_{Qn} - y_P)^2 \left( \frac{1}{s_{1mn}^4} + \frac{1}{s_{1mn}^2 s_{2mn}^2} + \frac{1}{s_{2mn}^4} \right) - 3 \left( \frac{1}{s_{1mn}^2} + \frac{1}{s_{2mn}^2} \right) \right) \right\} \end{aligned}$$

The  $m, n$ th term in surface integral kernels:

$$J_{00mn} = \frac{1}{2\pi} \log \frac{s_{2mn} s_{4mn}}{s_{1mn} s_{3mn}} \quad (\text{A2.21})$$

$$J_{10mn} = \frac{1}{2\pi} \left\{ (x_{Qm} - x_P) \left( \frac{1}{s_{1mn}^2} - \frac{1}{s_{4mn}^2} \right) + (x_{Qm} + x_P) \left( \frac{1}{s_{2mn}^2} - \frac{1}{s_{3mn}^2} \right) \right\} \quad (\text{A2.22})$$

$$J_{01mn} = \frac{1}{2\pi} \left\{ (y_{Qn} - y_P) \left( \frac{1}{s_{1mn}^2} - \frac{1}{s_{2mn}^2} \right) + (y_{Qn} + y_P) \left( \frac{1}{s_{4mn}^2} - \frac{1}{s_{3mn}^2} \right) \right\} \quad (\text{A2.23})$$

$$J_{20mn} = \frac{1}{2\pi} \left\{ \frac{(x_{Qm} - x_P)^2 - (y_{Qn} - y_P)^2}{s_{1mn}^2} - \frac{(x_{Qm} + x_P)^2 - (y_{Qn} - y_P)^2}{s_{2mn}^2} \right. \\ \left. + \frac{(x_{Qm} + x_P)^2 - (y_{Qn} + y_P)^2}{s_{3mn}^2} - \frac{(x_{Qm} - x_P)^2 - (y_{Qn} + y_P)^2}{s_{4mn}^2} \right\} - \frac{1}{2} \delta(P - Q) \quad (\text{A2.24})$$

$$J_{11mn} = \frac{1}{\pi} \left\{ \frac{(x_{Qm} - x_P)(y_{Qn} - y_P)}{s_{1mn}^2} + \frac{(x_{Qm} + x_P)(y_{Qn} - y_P)^2}{s_{2mn}^2} \right. \\ \left. + \frac{(x_{Qm} + x_P)(y_{Qn} + y_P)}{s_{3mn}^2} + \frac{(x_{Qm} - x_P)(y_{Qn} + y_P)}{s_{4mn}^2} \right\} \quad (\text{A2.25})$$

$$J_{02mn} = \frac{1}{2\pi} \left\{ -\frac{(x_{Qm} - x_P)^2 - (y_{Qn} - y_P)^2}{s_{1mn}^2} + \frac{(x_{Qm} + x_P)^2 - (y_{Qn} - y_P)^2}{s_{2mn}^2} \right. \\ \left. - \frac{(x_{Qm} + x_P)^2 - (y_{Qn} + y_P)^2}{s_{3mn}^2} + \frac{(x_{Qm} - x_P)^2 - (y_{Qn} + y_P)^2}{s_{4mn}^2} \right\} - \frac{1}{2} \delta(P - Q) \quad (\text{A2.26})$$

### APPENDIX 3

#### Extended Poisson kernels for a sector of circle of angle $\pi/m$

The Green's function for a sector of circle of angle  $\pi/m$  are given in section 3.1.2.3. Let  $P$  placed at  $(x_P, y_P)$  or  $(r_P, \theta_P)$  is the observation point, within a sector of circle of radius  $R$ . Similarly, let the source point  $Q$  be at  $(x_Q, y_Q)$  or  $(r_Q, \theta_Q)$ , then the system of images is presented in Figure 3.3. The Green's function for a sector of circle has the following form:

$$G(P;Q) = \frac{1}{2\pi} \sum_{i=1}^m \left( \log \frac{r_Q s_{Ii}}{R s_{Qi}} - \log \frac{r_Q s_{Ii'}}{R s_{Qi'}} \right) \quad (\text{A3.1})$$

$$= \frac{1}{2\pi} \sum_{i=1}^m \log \frac{s_{Qi'} s_{Ii}}{s_{Ii'} s_{Qi}} = \sum_{i=1}^m G_i(P;Q) \quad (\text{A3.2})$$

where distances  $s$  are given by

$$s_{Qi}^2 = r_P^2 + r_Q^2 - 2r_P r_Q \cos(\theta_P - \theta_Q - (i-1)\frac{2\pi}{m}) \quad (\text{A3.3})$$

$$s_{Ii}^2 = r_P^2 + \frac{R^4}{r_Q^2} - 2r_P r_Q \cos(\theta_P - \theta_Q - (i-1)\frac{2\pi}{m}) \quad (\text{A3.4})$$

$$s_{Qi'}^2 = r_P^2 + r_Q^2 - 2r_P r_Q \cos(\theta_P + \theta_Q - (i-1)\frac{2\pi}{m}) \quad (\text{A3.5})$$

$$s_{Ii'}^2 = r_P^2 + \frac{R^4}{r_Q^2} - 2r_P r_Q \cos(\theta_P + \theta_Q - (i-1)\frac{2\pi}{m}) \quad (\text{A3.6})$$

For brevity, symbols are defined

$$S_{Qix} = \frac{x_P - x_{Qi}}{s_{Qi}} \quad S_{Qiy} = \frac{y_P - y_{Qi}}{s_{Qi}} \quad (\text{A3.7})$$

$$S_{Iix} = \frac{x_P - \frac{R^2}{r_Q} x_{Qi}}{s_{Ii}} \quad S_{Iiy} = \frac{y_P - \frac{R^2}{r_Q} y_{Qi}}{s_{Ii}} \quad (\text{A3.8})$$

The  $i$ th term of Poisson kernels corresponding to sides ( $\theta_Q = 0$  and  $\theta_Q = \frac{\pi}{m}$ ) of the sector are

$$K_{\theta 00i} = \frac{1}{r_Q \pi} (y_P x_{Qi} - x_P y_{Qi}) \left( \frac{1}{s_{Qi}^2} - \frac{R^2}{r_Q^2} \frac{1}{s_{Ii}^2} \right) \quad (\text{A3.9})$$

$$K_{\theta 10i} = \frac{2}{r_Q \pi} (y_P x_{Qi} - x_P y_{Qi}) \left( \frac{R^2 S_{Iix}}{r_Q^2 s_{Ii}^3} - \frac{S_{Qix}}{s_{Qi}^3} \right) - y_{Qi} \left( \frac{1}{s_{Qi}^2} - \frac{R^2}{r_Q^2} \frac{1}{s_{Ii}^2} \right) \quad (\text{A3.10})$$

$$K_{\theta 01i} = \frac{2}{r_Q \pi} (y_P x_{Qi} - x_P y_{Qi}) \left( \frac{R^2 S_{Iiy}}{r_Q^2 s_{Ii}^3} - \frac{S_{Qiy}}{s_{Qi}^3} \right) + y_{Qi} \left( \frac{1}{s_{Qi}^2} - \frac{R^2}{r_Q^2} \frac{1}{s_{Ii}^2} \right) \quad (\text{A3.11})$$

$$K_{\theta 20i} = \frac{2}{r_Q \pi} (y_P x_{Qi} - x_P y_{Qi}) \left( \frac{3 S_{Qix}^2 - S_{Qiy}^2}{s_{Qi}^4} - \frac{R^2 3 S_{Iix}^2 - S_{Iiy}^2}{r_Q^2 s_{Ii}^4} \right) + 4 y_{Qi} \left( \frac{S_{Qix}}{s_{Qi}^3} - \frac{R^2 S_{Iix}}{r_Q^2 s_{Ii}^3} \right) \quad (\text{A3.12})$$

$$K_{\theta 11i} = \frac{2}{r_Q \pi} (y_P x_{Qi} - x_P y_{Qi}) \left( \frac{S_{Qix} S_{Qiy}}{s_{Qi}^4} - \frac{R^2 S_{Iix} S_{Iiy}}{r_Q^2 s_{Ii}^4} \right) + 2 y_{Qi} \left( \frac{S_{Qiy}}{s_{Qi}^3} - \frac{R^2 S_{Iiy}}{r_Q^2 s_{Ii}^3} \right) \quad (\text{A3.13})$$

$$K_{\theta 02i} = \frac{2}{r_Q \pi} (y_P x_{Qi} - x_P y_{Qi}) \left( \frac{3 S_{Qiy}^2 - S_{Qix}^2}{s_{Qi}^4} - \frac{R^2 3 S_{Iiy}^2 - S_{Iix}^2}{r_Q^2 s_{Ii}^4} \right) - 4 x_{Qi} \left( \frac{S_{Qiy}}{s_{Qi}^3} - \frac{R^2 S_{Iiy}}{r_Q^2 s_{Ii}^3} \right) \quad (\text{A3.14})$$

$$K_{\theta 30i} = \frac{24}{r_Q \pi} (y_P x_{Qi} - x_P y_{Qi}) \left( \frac{R^2 S_{Iix} (S_{Iix}^2 - S_{Iiy}^2)}{r_Q^2 s_{Ii}^4} - \frac{S_{Qix} (S_{Qix}^2 - S_{Qiy}^2)}{s_{Qi}^4} \right) + 6 y_{Qi} \left( \frac{3 S_{Qix}^2 - S_{Qiy}^2}{s_{Qi}^4} - \frac{R^2 3 S_{Iix}^2 - S_{Iiy}^2}{r_Q^2 s_{Ii}^4} \right) \quad (\text{A3.15})$$

$$\begin{aligned}
K_{\theta_{21i}} &= \frac{S}{r_Q^\pi} (y_P x_{Qi} - x_P y_{Qi}) \left( \frac{R^2 S_{Iiy} (5 S_{Iix}^2 - S_{Iiy}^2)}{r_Q^2 s_{Ii}^4} - \frac{S_{Qiy} (5 S_{Qix}^2 - S_{Qiy}^2)}{s_{Qi}^4} \right) \\
&+ \frac{16 y_{Qi}}{r_Q^\pi} \left( \frac{S_{Qix} S_{Qiy}}{s_{Qi}^4} - \frac{R^2 S_{Iix} S_{Iiy}}{r_Q^2 s_{Ii}^4} \right) \\
&+ \frac{2 y_{Qi}}{r_Q^\pi} \left( \frac{3 S_{Qix}^2 - S_{Qiy}^2}{s_{Qi}^4} - \frac{R^2 3 S_{Iix}^2 - S_{Iiy}^2}{r_Q^2 s_{Ii}^4} \right)
\end{aligned} \tag{A3.16}$$

$$\begin{aligned}
K_{\theta_{12i}} &= -\frac{S}{r_Q^\pi} (y_P x_{Qi} - x_P y_{Qi}) \left( \frac{R^2 S_{Iiy} (5 S_{Iix}^2 - S_{Iiy}^2)}{r_Q^2 s_{Ii}^4} - \frac{S_{Qiy} (5 S_{Qix}^2 - S_{Qiy}^2)}{s_{Qi}^4} \right) \\
&+ \frac{16 y_{Qi}}{r_Q^\pi} \left( \frac{S_{Qix} S_{Qiy}}{s_{Qi}^4} - \frac{R^2 S_{Iix} S_{Iiy}}{r_Q^2 s_{Ii}^4} \right) \\
&+ \frac{2 y_{Qi}}{r_Q^\pi} \left( \frac{3 S_{Qiy}^2 - S_{Qix}^2}{s_{Qi}^4} - \frac{R^2 3 S_{Iiy}^2 - S_{Iix}^2}{r_Q^2 s_{Ii}^4} \right)
\end{aligned} \tag{A3.17}$$

$$\begin{aligned}
K_{\theta_{03i}} &= \frac{24}{r_Q^\pi} (y_P x_{Qi} - x_P y_{Qi}) \left( \frac{R^2 S_{Iiy} (S_{Iiy}^2 - S_{Iix}^2)}{r_Q^2 s_{Ii}^4} - \frac{S_{Qiy} (S_{Qiy}^2 - S_{Qix}^2)}{s_{Qi}^4} \right) \\
&+ \frac{6 x_{Qi}}{r_Q^\pi} \left( \frac{3 S_{Qiy}^2 - S_{Qix}^2}{s_{Qi}^4} - \frac{R^2 3 S_{Iiy}^2 - S_{Iix}^2}{r_Q^2 s_{Ii}^4} \right)
\end{aligned} \tag{A3.18}$$

Note that kernels for side  $\theta_Q = \pi/m$  have the '-' sign in front of above expressions.

Poisson kernels corresponding to arc  $r_Q = R$  ( $0 \leq \theta_Q \leq \frac{\pi}{m}$ ) may be obtained from Poisson kernels for a circular disc, presented in Appendix 1. It is easy to prove that the  $ij$ th order kernel will be

$$K_{r_{ij}}(r_P, \theta_P; r_Q, \theta_Q) = \tag{A3.19}$$

$$\sum_{n=1}^m \left\{ K_{ij}(r_P, \theta_P; r_Q, \theta_Q + (n-1)\frac{2\pi}{m}) - K_{ij}(r_P, \theta_P; r_Q, -\theta_Q + (n-1)\frac{2\pi}{m}) \right\}.$$

Using the same reasoning, the surface integral kernels are obtainable from kernels for a circular disc, also presented in Appendix 1. The formula for  $ij$ th derivative kernel is

$$J_{ij}^{\text{sect}}(r_P, \theta_P; r_Q, \theta_Q) = \tag{A3.20}$$

$$\sum_{n=1}^m \left\{ J_{ij}(r_P, \theta_P; r_Q, \theta_Q + (n-1)\frac{2\pi}{m}) - J_{ij}(r_P, \theta_P; r_Q, -\theta_Q + (n-1)\frac{2\pi}{m}) \right\}.$$

Also, like in the cases of circle and rectangle, the term  $-\frac{1}{2}\delta(P;Q)$  should be included in expressions for  $J_{20}$  and  $J_{02}$ .

## APPENDIX 4

Extended Poisson kernels and surface integral kernels  
for a sector of ring of angle  $\pi/m$

Let the point  $P$  be located at  $(x_P, y_P) = (r_P, \theta_P)$ , within a sector of ring of inner and outer radii  $a$  and  $b$ , respectively and angle  $\pi/m$ . Similarly, let  $Q_1$  be at  $(x_Q, y_Q)$  or  $(r_Q, \theta_Q)$ . Let the image  $Q_1'$  of source point  $Q$  have coordinates  $(x_Q, -y_Q)$  or  $(r_Q, -\theta_Q)$ . There are  $(m-1)$  pairs of images  $Q_i$  and  $Q_i'$ ,  $i = 2 \dots m$ . For brevity, introduce

$$\mathcal{A}_n = \frac{r_Q^{2n} - a^{2n} r_P^n}{b^{2n} - a^{2n} r_Q^n} + \frac{b^{2n} - r_Q^{2n}}{b^{2n} - a^{2n} r_P^n} \frac{a^{2n}}{r_Q^n} \quad (\text{A4.1})$$

$$\mathcal{C} = \frac{\partial \mathcal{A}_n}{\partial r_P} = \frac{n}{r_P} \left\{ \frac{r_Q^{2n} - a^{2n} r_P^n}{b^{2n} - a^{2n} r_Q^n} - \frac{b^{2n} - r_Q^{2n}}{b^{2n} - a^{2n} r_P^n} \frac{a^{2n}}{r_Q^n} \right\} \quad (\text{A4.2})$$

$$\mathfrak{B} = \frac{1}{n} \frac{\partial \mathcal{A}_n}{\partial r_Q} = \frac{1}{r_Q} \left\{ \frac{r_P^{2n} - a^{2n} r_Q^n}{b^{2n} - a^{2n} r_P^n} - \frac{b^{2n} - r_P^{2n}}{b^{2n} - a^{2n} r_Q^n} \frac{a^{2n}}{r_P^n} \right\} \quad (\text{A4.3})$$

$$\mathfrak{D} = \frac{\partial \mathfrak{B}_n}{\partial r_P} = \frac{n}{r_P r_Q} \left\{ \frac{r_P^{2n} + a^{2n} r_Q^n}{b^{2n} - a^{2n} r_P^n} + \frac{b^{2n} + r_P^{2n}}{b^{2n} - a^{2n} r_Q^n} \frac{a^{2n}}{r_Q^n} \right\}. \quad (\text{A4.4})$$

Then, second derivatives of  $\mathcal{A}_n$  and  $\mathfrak{B}_n$  are given by

$$\frac{\partial^2 \mathcal{A}_n}{\partial r_P^2} = \frac{n^2}{r_P^2} \mathcal{A}_n - \frac{1}{r_P} \mathcal{C}_n \quad (\text{A4.5})$$

$$\frac{\partial^2 \mathfrak{B}_n}{\partial r_P^2} = \frac{n^2}{r_P^2} \mathfrak{B}_n - \frac{1}{r_P} \mathfrak{D}_n. \quad (\text{A4.6})$$

The Green's function will take the form

$$G(P;Q) = \frac{1}{2\pi} \sum_{i=1}^m \left( \log \frac{s_{Q_i'}}{s_{Q_i}} - 2 \sum_{n=1}^{\infty} \mathcal{A}_n \frac{\sin n(\theta_P - \omega_i) \sin n\theta_Q}{n} \right) \quad (\text{A4.7})$$

$$= \sum_{i=1}^m G_i(P;Q) \quad (\text{A4.8})$$

where

$$\omega_i = (i-1) \frac{2\pi}{m} \quad (\text{A4.9})$$

$$s_{Q_i}^2 = r_P^2 + r_Q^2 - 2r_P r_Q \cos(\theta_P - \theta_Q - \omega_i) \quad (\text{A4.10})$$

$$s_{Q_i'}^2 = r_P^2 + r_Q^2 - 2r_P r_Q \cos(\theta_P + \theta_Q + \omega_i) \quad (\text{A4.11})$$

Then, the Poisson kernels corresponding to sides  $\theta_Q = 0$  and  $\theta_Q = \frac{\pi}{m}$  are:

$$K_{\theta_{00i}} = \frac{\partial G_i}{\partial \theta_Q} = \frac{r_P r_Q}{2\pi} \left\{ \frac{\sin(\theta_P - \theta_Q - \omega_i)}{s_{Q_i}^2} + \frac{\sin(\theta_P + \theta_Q - \omega_i)}{s_{Q_i'}^2} \right\} - \frac{1}{\pi} \sum_{n=1}^{\infty} \mathcal{A}_n \sin n(\theta_P - \omega_i) \cos n\theta_Q. \quad (\text{A4.12})$$

$$K_{\theta_{10i}} = \frac{y_{Q_i}}{2\pi r_Q s_{Q_i}^2} + \frac{r_P \sin(\theta_P - \theta_Q - \omega_i)(x_P - x_{Q_i})}{\pi s_{Q_i}^4} + \frac{y_{Q_i'}}{2\pi r_Q s_{Q_i'}^2} + \frac{r_P \sin(\theta_P + \theta_Q - \omega_i)(x_P - x_{Q_i'})}{\pi s_{Q_i'}^4} - \frac{\sin \theta_P}{\pi r_P r_Q} \sum_{n=1}^{\infty} n \mathcal{A}_n \cos n(\theta_P - \omega_i) \cos n\theta_Q + \frac{\cos \theta_P}{\pi r_Q} \sum_{n=1}^{\infty} \mathcal{C}_n \sin n(\theta_P - \omega_i) \cos n\theta_Q. \quad (\text{A4.13})$$

$$K_{\theta_{01i}} = -\frac{x_{Q_i}}{2\pi r_Q s_{Q_i}^2} + \frac{r_P \sin(\theta_P - \theta_Q - \omega_i)(y_P - y_{Q_i})}{\pi s_{Q_i}^4} \quad (\text{A4.14})$$

$$-\frac{x_{Q_i'}}{2\pi r_Q s_{Q_i'}^2} + \frac{r_P \sin(\theta_P + \theta_Q - \omega_i)(y_P - y_{Q_i'})}{\pi s_{Q_i'}^4}$$

$$+ \frac{\cos\theta_P}{\pi r_P r_Q} \sum_{n=1}^{\infty} n \mathcal{A}_n \cos n(\theta_P - \omega_i) \cos n\theta_Q$$

$$+ \frac{\sin\theta_P}{\pi r_Q} \sum_{n=1}^{\infty} \mathcal{C}_n \sin n(\theta_P - \omega_i) \cos n\theta_Q.$$

$$K_{\theta_{20i}} = \frac{r_P r_Q \sin(\theta_P - \theta_Q - \omega_i) - 2y_{Q_i}(x_P - x_{Q_i})}{\pi r_Q s_{Q_i}^4} \quad (\text{A4.15})$$

$$- \frac{4r_P \sin(\theta_P - \theta_Q - \omega_i)(x_P - x_{Q_i})^2}{\pi s_{Q_i}^6}$$

$$+ \frac{r_P r_Q \sin(\theta_P + \theta_Q - \omega_i) - 2y_{Q_i'}(x_P - x_{Q_i'})}{\pi r_Q s_{Q_i'}^4}$$

$$- \frac{4r_P \sin(\theta_P + \theta_Q - \omega_i)(x_P - x_{Q_i'})^2}{\pi s_{Q_i'}^6}$$

$$+ \frac{\sin 2\theta_P}{\pi r_P r_Q} \sum_{n=1}^{\infty} n \left( \frac{1}{r_P} \mathcal{A}_n - \mathcal{C}_n \right) \cos n(\theta_P - \omega_i) \cos n\theta_Q$$

$$+ \frac{\cos 2\theta_P}{\pi r_P r_Q} \sum_{n=1}^{\infty} \left( \frac{n^2}{r_P} \mathcal{A}_n - \mathcal{C}_n \right) \sin n(\theta_P - \omega_i) \cos n\theta_Q$$

$$K_{\theta_{11i}} = \frac{x_{Q_i}(x_P - x_{Q_i}) - y_{Q_i}(y_P - y_{Q_i})}{\pi r_Q s_{Q_i}^4} \quad (\text{A4.16})$$

$$\begin{aligned}
& - \frac{4r_P \sin(\theta_P - \theta_Q - \omega_i)(x_P - x_{Q_i})(y_P - y_{Q_i})}{\pi s_{Q_i}^6} \\
& + \frac{x_{Q_i'}(x_P - x_{Q_i'}) - y_{Q_i'}(y_P - y_{Q_i'})}{\pi r_Q s_{Q_i'}^4} \\
& - \frac{4r_P \sin(\theta_P + \theta_Q - \omega_i)(x_P - x_{Q_i'})(y_P - y_{Q_i'})}{\pi s_{Q_i'}^6} \\
& - \frac{\cos 2\theta_P}{\pi r_P r_Q} \sum_{n=1}^{\infty} n \left( \frac{1}{r_P} \mathcal{A}_n - \mathcal{C}_n \right) \cos n(\theta_P - \omega_i) \cos n\theta_Q \\
& + \frac{\sin 2\theta_P}{\pi r_P r_Q} \sum_{n=1}^{\infty} \left( \frac{n^2}{r_P} \mathcal{A}_n - \mathcal{C}_n \right) \sin n(\theta_P - \omega_i) \cos n\theta_Q \\
K_{\theta_{02i}} = & \frac{r_P r_Q \sin(\theta_P - \theta_Q - \omega_i) - 2x_{Q_i}(y_P - y_{Q_i})}{\pi r_Q s_{Q_i}^4} \tag{A4.17} \\
& - \frac{4r_P \sin(\theta_P - \theta_Q - \omega_i)(y_P - y_{Q_i})^2}{\pi s_{Q_i}^6} \\
& + \frac{r_P r_Q \sin(\theta_P + \theta_Q - \omega_i) - 2x_{Q_i'}(y_P - y_{Q_i'})}{\pi r_Q s_{Q_i'}^4} \\
& - \frac{4r_P \sin(\theta_P + \theta_Q - \omega_i)(y_P - y_{Q_i'})^2}{\pi s_{Q_i'}^6} \\
& - \frac{\sin 2\theta_P}{\pi r_P r_Q} \sum_{n=1}^{\infty} n \left( \frac{1}{r_P} \mathcal{A}_n - \mathcal{C}_n \right) \cos n(\theta_P - \omega_i) \cos n\theta_Q \\
& - \frac{\cos 2\theta_P}{\pi r_P r_Q} \sum_{n=1}^{\infty} \left( \frac{n^2}{r_P} \mathcal{A}_n - \mathcal{C}_n \right) \sin n(\theta_P - \omega_i) \cos n\theta_Q
\end{aligned}$$

For the arcs the Poisson kernel functions become

$$\begin{aligned}
 K_{r_{0i}} &= \frac{\partial G_i}{\partial r_Q} \\
 &= \frac{r_Q - r_P \cos(\theta_P - \theta_Q - \omega_i)}{2\pi s_{Q_i}^2} - \frac{r_Q - r_P \cos(\theta_P + \theta_Q - \omega_i)}{2\pi s_{Q_i'}^2} \\
 &\quad - \frac{1}{\pi} \sum_{n=1}^{\infty} \mathfrak{B}_n \sin n(\theta_P - \omega_i) \sin n\theta_Q.
 \end{aligned} \tag{A4.18}$$

$$\begin{aligned}
 K_{r_{10i}} &= \frac{x_{Q_i}}{2\pi r_Q s_{Q_i}^2} - \frac{[r_P \cos(\theta_P - \theta_Q - \omega_i) - r_Q](x_P - x_{Q_i})}{\pi s_{Q_i}^4} \\
 &\quad - \frac{x_{Q_i'}}{2\pi r_Q s_{Q_i'}^2} + \frac{[r_P \cos(\theta_P + \theta_Q - \omega_i) - r_Q](x_P - x_{Q_i'})}{\pi s_{Q_i'}^4} \\
 &\quad + \frac{\sin \theta_P}{\pi r_P r_Q} \sum_{n=1}^{\infty} n \mathfrak{B}_n \cos n(\theta_P - \omega_i) \sin n\theta_Q \\
 &\quad - \frac{\cos \theta_P}{\pi r_Q} \sum_{n=1}^{\infty} \mathfrak{D}_n \sin n(\theta_P - \omega_i) \sin n\theta_Q.
 \end{aligned} \tag{A4.19}$$

$$\begin{aligned}
 K_{r_{01i}} &= \frac{y_{Q_i}}{2\pi r_Q s_{Q_i}^2} - \frac{[r_P \cos(\theta_P - \theta_Q - \omega_i) - r_Q](y_P - y_{Q_i})}{\pi s_{Q_i}^4} \\
 &\quad - \frac{y_{Q_i'}}{2\pi r_Q s_{Q_i'}^2} + \frac{[r_P \cos(\theta_P + \theta_Q - \omega_i) - r_Q](y_P - y_{Q_i'})}{\pi s_{Q_i'}^4} \\
 &\quad - \frac{\cos \theta_P}{\pi r_P r_Q} \sum_{n=1}^{\infty} n \mathfrak{B}_n \cos n(\theta_P - \omega_i) \sin n\theta_Q
 \end{aligned} \tag{A4.20}$$

$$\begin{aligned}
& -\frac{\sin\theta_P}{\pi r_Q} \sum_{n=1}^{\infty} \mathfrak{D}_n \sin n(\theta_P - \omega_i) \sin n\theta_Q \\
K_{r20i} = & -\frac{r_P r_Q \cos(\theta_P - \theta_Q - \omega_i) - r_Q^2 + 2x_{Qi}(x_P - x_{Qi})}{\pi r_Q s_{Qi}^4} \quad (\text{A4.21}) \\
& + \frac{4[r_P \cos(\theta_P - \theta_Q - \omega_i) - r_Q](x_P - x_{Qi})^2}{\pi s_{Qi}^6} \\
& + \frac{r_P r_Q \cos(\theta_P + \theta_Q - \omega_i) - r_Q^2 + 2x_{Qi'}(x_P - x_{Qi'})}{\pi r_Q s_{Qi'}^4} \\
& - \frac{4[r_P \cos(\theta_P + \theta_Q - \omega_i) - r_Q](x_P - x_{Qi'})^2}{\pi s_{Qi'}^6} \\
& - \frac{\sin 2\theta_P}{\pi r_P r_Q} \sum_{n=1}^{\infty} n \left( \frac{1}{r_P} \mathfrak{B}_n - \mathfrak{D}_n \right) \cos n(\theta_P - \omega_i) \sin n\theta_Q \\
& - \frac{\cos 2\theta_P}{\pi r_P r_Q} \sum_{n=1}^{\infty} n \left( \frac{n^2}{r_P} \mathfrak{B}_n - \mathfrak{D}_n \right) \sin n(\theta_P - \omega_i) \sin n\theta_Q
\end{aligned}$$

$$\begin{aligned}
K_{r11i} = & -\frac{y_{Qi}(x_P - x_{Qi}) + x_{Qi}(y_P - y_{Qi})}{\pi r_Q s_{Qi}^4} \quad (\text{A4.22}) \\
& + \frac{4[r_P \cos(\theta_P - \theta_Q - \omega_i) - r_Q](x_P - x_{Qi})(y_P - y_{Qi})}{\pi s_{Qi}^6} \\
& + \frac{y_{Qi'}(x_P - x_{Qi'}) + x_{Qi'}(y_P - y_{Qi'})}{\pi r_Q s_{Qi'}^4} \\
& - \frac{4[r_P \cos(\theta_P + \theta_Q - \omega_i) - r_Q](x_P - x_{Qi'})(y_P - y_{Qi'})}{\pi s_{Qi'}^6} \\
& + \frac{\cos 2\theta_P}{\pi r_P r_Q} \sum_{n=1}^{\infty} n \left( \frac{1}{r_P} \mathfrak{B}_n - \mathfrak{D}_n \right) \cos n(\theta_P - \omega_i) \sin n\theta_Q
\end{aligned}$$

$$\begin{aligned}
& -\frac{\sin 2\theta_P}{\pi r_P r_Q} \sum_{n=1}^{\infty} \left( \frac{n^2}{r_P} \mathfrak{B}_n - \mathfrak{D}_n \right) \sin n(\theta_P - \omega_i) \sin n\theta_Q \\
K_{r_0 z_i} = & -\frac{r_P r_Q \cos(\theta_P - \theta_Q - \omega_i) - r_Q^2 + 2y_{Q_i}(y_P - y_{Q_i})}{\pi r_Q s_{Q_i}^4} \tag{A4.23} \\
& + \frac{4[r_P \cos(\theta_P - \theta_Q - \omega_i) - r_Q](y_P - y_{Q_i})^2}{\pi s_{Q_i}^6} \\
& + \frac{r_P r_Q \cos(\theta_P + \theta_Q - \omega_i) - r_Q^2 + 2y_{Q_i'}(y_P - y_{Q_i'})}{\pi r_Q s_{Q_i'}^4} \\
& - \frac{4[r_P \cos(\theta_P + \theta_Q - \omega_i) - r_Q](y_P - y_{Q_i'})^2}{\pi s_{Q_i'}^6} \\
& + \frac{\sin 2\theta_P}{\pi r_P r_Q} \sum_{n=1}^{\infty} n \left( \frac{1}{r_P} \mathfrak{B}_n - \mathfrak{D}_n \right) \cos n(\theta_P - \omega_i) \sin n\theta_Q \\
& + \frac{\cos 2\theta_P}{\pi r_P r_Q} \sum_{n=1}^{\infty} \left( \frac{n^2}{r_P} \mathfrak{B}_n - \mathfrak{D}_n \right) \sin n(\theta_P - \omega_i) \sin n\theta_Q
\end{aligned}$$

The surface integral kernels are given by:

$$J_{00i} = \frac{1}{2\pi} \log \frac{s_{Q_i'}}{s_{Q_i}} - \frac{1}{\pi} \sum_{n=1}^{\infty} \mathcal{A}_n \frac{\sin n(\theta_P - \omega_i) \sin n\theta_Q}{n} \quad (\text{A4.24})$$

$$\begin{aligned} J_{10i} &= \frac{x_P - x_{Q_i'}}{2\pi s_{Q_i'}^2} - \frac{x_P - x_{Q_i}}{2\pi s_{Q_i}^2} \quad (\text{A4.25}) \\ &+ \frac{\sin\theta_P}{\pi r_P} \sum_{n=1}^{\infty} \mathcal{A}_n \cos n(\theta_P - \omega_i) \sin n\theta_Q \\ &- \frac{\cos\theta_P}{\pi} \sum_{n=1}^{\infty} \frac{1}{n} \mathcal{C}_n \sin n(\theta_P - \omega_i) \sin n\theta_Q. \end{aligned}$$

$$\begin{aligned} J_{01i} &= \frac{y_P - y_{Q_i'}}{2\pi s_{Q_i'}^2} - \frac{y_P - y_{Q_i}}{2\pi s_{Q_i}^2} \quad (\text{A4.26}) \\ &- \frac{\cos\theta_P}{\pi r_P} \sum_{n=1}^{\infty} \mathcal{A}_n \cos n(\theta_P - \omega_i) \sin n\theta_Q \\ &- \frac{\sin\theta_P}{\pi} \sum_{n=1}^{\infty} \frac{1}{n} \mathcal{C}_n \sin n(\theta_P - \omega_i) \sin n\theta_Q. \end{aligned}$$

$$\begin{aligned} J_{20i} &= \frac{(x_P - x_{Q_i})^2 - (y_P - y_{Q_i})^2}{2\pi s_{Q_i}^4} - \frac{(x_P - x_{Q_i'})^2 - (y_P - y_{Q_i'})^2}{2\pi s_{Q_i'}^4} \quad (\text{A4.27}) \\ &- \frac{\sin 2\theta_P}{\pi r_P} \sum_{n=1}^{\infty} \left( \frac{1}{r_P} \mathcal{A}_n - \mathcal{C}_n \right) \cos n(\theta_P - \omega_i) \sin n\theta_Q \\ &- \frac{\cos 2\theta_P}{\pi r_P} \sum_{n=1}^{\infty} \left( \frac{n}{r_P} \mathcal{A}_n - \frac{1}{n} \mathcal{C}_n \right) \sin n(\theta_P - \omega_i) \sin n\theta_Q - \frac{1}{2} \delta(P; Q) \end{aligned}$$

$$J_{11i} = \frac{(x_P - x_{Q_i})(y_P - y_{Q_i})}{\pi s_{Q_i}^4} - \frac{(x_P - x_{Q_i'})(y_P - y_{Q_i'})}{\pi s_{Q_i'}^4} \quad (\text{A4.28})$$

$$+ \frac{\cos 2\theta_P}{\pi r_P} \sum_{n=1}^{\infty} \left( \frac{1}{r_P} \mathcal{A}_n - \mathcal{C}_n \right) \cos n(\theta_P - \omega_i) \sin n\theta_Q$$

$$- \frac{\sin 2\theta_P}{\pi r_P} \sum_{n=1}^{\infty} \left( \frac{n}{r_P} \mathcal{A}_n - \frac{1}{n} \mathcal{C}_n \right) \sin n(\theta_P - \omega_i) \sin n\theta_Q$$

$$J_{02i} = \frac{(x_P - x_{Q_i'})^2 - (y_P - y_{Q_i'})^2}{2\pi s_{Q_i'}^4} - \frac{(x_P - x_{Q_i})^2 - (y_P - y_{Q_i})^2}{2\pi s_{Q_i}^4} \quad (\text{A4.29})$$

$$+ \frac{\sin 2\theta_P}{\pi r_P} \sum_{n=1}^{\infty} \left( \frac{1}{r_P} \mathcal{A}_n - \mathcal{C}_n \right) \cos n(\theta_P - \omega_i) \sin n\theta_Q$$

$$+ \frac{\cos 2\theta_P}{\pi r_P} \sum_{n=1}^{\infty} \left( \frac{n}{r_P} \mathcal{A}_n - \frac{1}{n} \mathcal{C}_n \right) \sin n(\theta_P - \omega_i) \sin n\theta_Q - \frac{1}{2} \delta(P; Q)$$

## APPENDIX 5

### Extended Poisson kernels for the Helmholtz operator on a circular region

The Poisson kernels required for derivative evaluation are lengthy; their algebraic derivation is both tedious and error-prone. Kernel functions were therefore determined by means of a symbolic algebra package, and the results are recorded here for future reference. Let the point  $P$  be located at  $(x_P, y_P) = (r_P, \theta_P)$  within a circle of radius  $R$ . Similarly, let  $Q$  be at  $(R, \theta_Q)$ . Then the boundary integral kernels for producing the derivatives up to third order are as follows. Introduce, for brevity,

$$f_{i,j}^{(m+n)} = \frac{(\kappa r_P)^j}{r_P^{m+n}} J_{i+j}(\kappa r_P). \quad (5.1)$$

(Note that  $i$  and  $j$  are summation indices, not imaginary units.) With this abbreviation,

$$K_H(P; Q) = \sum_{i=0}^{\infty} a_i f_{i,0} \cos[i\theta_P - i\theta_Q] \quad (A5.2)$$

$$\begin{aligned} K_{H10}(P; Q) = \sum_{i=0}^{\infty} a_i \{ & -f_{i,1} \cos\theta_P \cos[i\theta_P - i\theta_Q] \\ & + i f_{i,0} \cos[(i-1)\theta_P - i\theta_Q] \} \end{aligned} \quad (A5.3)$$

$$\begin{aligned} K_{H01}(P; Q) = \sum_{i=0}^{\infty} a_i \{ & -f_{i,1} \sin\theta_P \cos[i\theta_P - i\theta_Q] \\ & - i f_{i,0} \cos[(i-1)\theta_P - i\theta_Q] \} \end{aligned} \quad (A5.4)$$

$$K_{H20}(P;Q) = \sum_{i=0}^{\infty} a_i \left\{ (f_{i,2} \cos^2 \theta_P - (i+1) f_{i,1}) \cos[i\theta_P - i\theta_Q] \right. \\ \left. + i(-f_{i,1} + (i-1) f_{i,0}) \cos[(i-2)\theta_P - i\theta_Q] \right\} \quad (A5.5)$$

$$K_{H11}(P;Q) = \sum_{i=0}^{\infty} a_i \left\{ f_{i,2} \cos \theta_P \sin \theta_P \cos[i\theta_P - i\theta_Q] \right. \\ \left. + i(f_{i,1} - (i-1) f_{i,0}) \sin[(i-2)\theta_P - i\theta_Q] \right\} \quad (A5.6)$$

$$K_{H02}(P;Q) = \sum_{i=0}^{\infty} a_i \left\{ (f_{i,2} \sin^2 \theta_P - (i+1) f_{i,1}) \cos[i\theta_P - i\theta_Q] \right. \\ \left. + i(f_{i,1} - (i-1) f_{i,0}) \cos[(i-2)\theta_P - i\theta_Q] \right\} \quad (A5.7)$$

$$K_{H30}(P;Q) = \sum_{i=0}^{\infty} a_i \left\{ (-f_{i,3} \cos^2 \theta_P + (i+3) f_{i,2}) \cos \theta_P \cos[i\theta_P - i\theta_Q] \right. \\ \left. + i(f_{i,2} \cos^2 \theta_P - (i+2) f_{i,1}) \cos[(i-1)\theta_P - i\theta_Q] \right. \\ \left. + i(f_{i,2} - (i-1) f_{i,1}) \cos \theta_P \cos[(i-2)\theta_P - i\theta_Q] \right. \\ \left. + i(i-1)(-f_{i,1} + (i-2) f_{i,0}) \cos[(i-3)\theta_P - i\theta_Q] \right\} \quad (A5.8)$$

$$K_{H21}(P;Q) = \sum_{i=0}^{\infty} a_i \left\{ (-f_{i,3} \cos^2 \theta_P + (i+1) f_{i,2}) \sin \theta_P \cos[i\theta_P - i\theta_Q] \right. \\ \left. + i(-f_{i,2} \cos^2 \theta_P + i f_{i,1}) \sin[(i-1)\theta_P - i\theta_Q] \right. \\ \left. + i(f_{i,2} - (i-1) f_{i,1}) \sin \theta_P \cos[(i-2)\theta_P - i\theta_Q] \right. \\ \left. + i(i-1)(f_{i,1} - (i-2) f_{i,0}) \sin[(i-3)\theta_P - i\theta_Q] \right\} \quad (A5.9)$$

$$\begin{aligned}
K_{H12}(P; Q) = \sum_{i=0}^{\infty} a_i \left\{ & \left( -f_{i,3} \sin^2 \theta_P + (i+1) f_{i,2} \right) \cos \theta_P \cos [i \theta_P - i \theta_Q] \right. \\
& + i \left( f_{i,2} \sin^2 \theta_P - i f_{i,1} \right) \cos [(i-1) \theta_P - i \theta_Q] \\
& + i \left( -f_{i,2} + (i-1) f_{i,1} \right) \cos \theta_P \cos [(i-2) \theta_P - i \theta_Q] \\
& \left. + i(i-1) \left( f_{i,1} - (i-2) f_{i,0} \right) \cos [(i-3) \theta_P - i \theta_Q] \right\} \quad (A5.10)
\end{aligned}$$

$$\begin{aligned}
K_{H03}(P; Q) = \sum_{i=0}^{\infty} a_i \left\{ & \left( -f_{i,3} \sin^2 \theta_P + (i+3) f_{i,2} \right) \sin \theta_P \cos [i \theta_P - i \theta_Q] \right. \\
& + i \left( -f_{i,2} \sin^2 \theta_P + (i+2) f_{i,1} \right) \sin [(i-1) \theta_P - i \theta_Q] \\
& + i \left( -f_{i,2} + (i-1) f_{i,1} \right) \sin \theta_P \cos [(i-2) \theta_P - i \theta_Q] \\
& \left. + i(i-1) \left( -f_{i,1} + (i-2) f_{i,0} \right) \sin [(i-3) \theta_P - i \theta_Q] \right\} \quad (A5.11)
\end{aligned}$$

The coefficients  $a_i$  are given by

$$a_i = \frac{k}{2\epsilon_i} \left\{ Y_{i+1}(kR) - \frac{Y_i(kR)}{J_i(kR)} J_{i+1}(kR) \right\}. \quad (A5.12)$$

## APPENDIX 6

Formulae for differentiation of harmonic function in axisymmetric coordinates

### *Differentiation formulae for a torus*

The base formula for potential inside the torus given by

$$\phi(\alpha, \beta) = \chi(\alpha, \beta) \sum_{n=0}^{\infty} \left\{ a_n \cos(n\beta) + b_n \sin(n\beta) \right\} Q_{n-1/2}(\cosh\alpha), \quad (\text{A6.1})$$

may be rewritten as follows:

$$\phi(\alpha, \beta) = \chi(\alpha, \beta) \sum_{n=0}^{\infty} \mathcal{A}_n(\beta) Q_{n-1/2}(\cosh\alpha). \quad (\text{A6.2})$$

Functions  $\chi(\alpha, \beta)$  and  $Q_{n-1/2}$  are defined in Chapter 3 (section 3.2.2.1), as well as coefficients  $a_n$  and  $b_n$  and toroidal coordinates.

If function  $\mathfrak{B}(\beta)$  is defined by

$$\mathfrak{B}_n(\beta) = \frac{1}{n} \frac{d\mathcal{A}_n(\beta)}{d\beta} = -a_n \sin(n\beta) + b_n \cos(n\beta), \quad (\text{A6.3})$$

then derivatives with respect to toroidal coordinates are

$$\begin{aligned} \frac{\partial \phi(\alpha, \beta)}{\partial \alpha} = & \frac{\chi(\alpha, \beta)}{\sinh \alpha} \sum_{n=0}^{\infty} \left( n + \frac{1}{2} \right) \mathcal{A}_n(\beta) Q_{n+1/2}(\cosh \alpha) \\ & - \frac{\chi(\alpha, \beta)}{\sinh \alpha} \left\{ \cosh \alpha \sum_{n=0}^{\infty} n \mathcal{A}_n(\beta) Q_{n-1/2}(\cosh \alpha) \right. \\ & \left. - \frac{\cosh \alpha \cos \beta - 1}{2(\cosh \alpha - \cos \beta)} \sum_{n=0}^{\infty} \mathcal{A}_n(\beta) Q_{n-1/2}(\cosh \alpha) \right\} \end{aligned} \quad (\text{A6.4})$$

$$\begin{aligned} \frac{\partial \phi(\alpha, \beta)}{\partial \beta} &= \chi(\alpha, \beta) \sum_{n=0}^{\infty} n \mathfrak{B}_n(\beta) Q_{n-1/2}(\cosh \alpha) \\ &\quad - \frac{\chi(\alpha, \beta) \sin \beta}{2(\cosh \alpha - \cos \beta)} \sum_{n=0}^{\infty} \mathcal{A}_n(\beta) Q_{n-1/2}(\cosh \alpha) \end{aligned} \quad (\text{A6.5})$$

$$\begin{aligned} \frac{\partial^2 \phi(\alpha, \beta)}{\partial \alpha^2} &= \frac{\chi(\alpha, \beta)}{\sinh^2 \alpha} \sum_{n=0}^{\infty} \left(n + \frac{1}{2}\right) \left(n + \frac{3}{2}\right) \mathcal{A}_n(\beta) Q_{n+3/2}(\cosh \alpha) \\ &\quad - \chi(\alpha, \beta) \left\{ 2 \frac{\cosh \alpha}{\sinh^2 \alpha} \sum_{n=0}^{\infty} \left(n + \frac{1}{2}\right) \left(n + \frac{3}{2}\right) \mathcal{A}_n(\beta) Q_{n+1/2}(\cosh \alpha) \right. \\ &\quad \quad \left. - \frac{1}{\cosh \alpha - \cos \beta} \sum_{n=0}^{\infty} \left(n + \frac{1}{2}\right) \mathcal{A}_n(\beta) Q_{n+1/2}(\cosh \alpha) \right\} \\ &\quad + \chi(\alpha, \beta) \left\{ \frac{\cosh^2 \alpha}{\sinh^2 \alpha} \sum_{n=0}^{\infty} n^2 \mathcal{A}_n(\beta) Q_{n-1/2}(\cosh \alpha) \right. \\ &\quad \quad + \left( 2 \frac{\cosh^2 \alpha}{\sinh^2 \alpha} - \frac{2 \cosh \alpha - \cos \beta}{\cosh \alpha - \cos \beta} \right) \sum_{n=0}^{\infty} n \mathcal{A}_n(\beta) Q_{n-1/2}(\cosh \alpha) \\ &\quad \quad \left. + \left( \frac{3 \cosh^2 \alpha}{4 \sinh^2 \alpha} - \frac{1}{2} - \frac{\sinh^2 \alpha}{4(\cosh \alpha - \cos \beta)^2} \right) \sum_{n=0}^{\infty} \mathcal{A}_n(\beta) Q_{n-1/2}(\cosh \alpha) \right\} \end{aligned} \quad (\text{A6.6})$$

$$\begin{aligned} \frac{\partial^2 \phi(\alpha, \beta)}{\partial \alpha \partial \beta} &= \frac{\chi(\alpha, \beta)}{\sinh \alpha} \sum_{n=0}^{\infty} n \left(n + \frac{1}{2}\right) \mathfrak{B}_n(\beta) Q_{n+1/2}(\cosh \alpha) \\ &\quad + \chi(\alpha, \beta) \left\{ \frac{\cosh \alpha}{\sinh \alpha} \sum_{n=0}^{\infty} n \left(n + \frac{1}{2}\right) \mathfrak{B}_n(\beta) Q_{n-1/2}(\cosh \alpha) \right. \\ &\quad \quad \left. - \frac{\sinh \alpha}{2(\cosh \alpha - \cos \beta)} \sum_{n=0}^{\infty} n \mathfrak{B}_n(\beta) Q_{n-1/2}(\cosh \alpha) \right\} \end{aligned} \quad (\text{A6.7})$$

$$\begin{aligned}
& + \frac{\chi(\alpha, \beta) \sin \beta}{2 \sinh \alpha (\cosh \alpha - \cos \beta)} \sum_{n=0}^{\infty} \left(n + \frac{1}{2}\right) \mathcal{A}_n(\beta) Q_{n+1/2}(\cosh \alpha) \\
& + \frac{\chi(\alpha, \beta)}{2 \sinh \alpha} \left\{ - \frac{\cosh \alpha \sin \beta}{(\cosh \alpha - \cos \beta)} \sum_{n=0}^{\infty} n \mathcal{A}_n(\beta) Q_{n-1/2}(\cosh \alpha) \right. \\
& \quad \left. + \frac{\cosh \alpha \cos \beta - 1}{2(\cosh \alpha - \cos \beta)^2} \sum_{n=0}^{\infty} \mathcal{A}_n(\beta) Q_{n-1/2}(\cosh \alpha) \right\} \\
\frac{\partial^2 \phi(\alpha, \beta)}{\partial \beta^2} & = \frac{\chi(\alpha, \beta) \sin \beta}{\cosh \alpha - \cos \beta} \sum_{n=0}^{\infty} \mathfrak{B}_n(\beta) Q_{n-1/2}(\cosh \alpha) \\
& - \chi(\alpha, \beta) \sum_{n=0}^{\infty} n^2 \mathcal{A}_n(\beta) Q_{n-1/2}(\cosh \alpha) \tag{A6.S} \\
& - \frac{1}{4} \left( 1 - \frac{\sinh^2 \alpha}{(\cosh \alpha - \cos \beta)^2} \right) \sum_{n=0}^{\infty} \mathcal{A}_n(\beta) Q_{n-1/2}(\cosh \alpha).
\end{aligned}$$

Using expressions from 3.2.2.1

$$\begin{aligned}
\frac{\partial \beta}{\partial r} & = - \frac{\sinh \alpha \sin \beta}{c} & \frac{\partial \beta}{\partial z} & = \frac{\cosh \alpha \cos \beta - 1}{c} \\
\frac{\partial \alpha}{\partial r} & = - \frac{\cosh \alpha \cos \beta - 1}{c} & \frac{\partial \alpha}{\partial z} & = - \frac{\sinh \alpha \sin \beta}{c} \\
\frac{\partial \chi(\alpha, \beta)}{\partial r} & = - \frac{\sinh \alpha \cos \beta}{2c} \chi(\alpha, \beta) & \frac{\partial \chi(\alpha, \beta)}{\partial z} & = - \frac{\cosh \alpha \sin \beta}{2c} \chi(\alpha, \beta).
\end{aligned}$$

derivatives with respect to  $r$  and  $z$  may be found as

$$\begin{aligned}
\frac{\partial \phi(\alpha, \beta)}{\partial r} &= \frac{\partial \phi(\alpha, \beta)}{\partial \alpha} \frac{\partial \alpha}{\partial r} + \frac{\partial \phi(\alpha, \beta)}{\partial \beta} \frac{\partial \beta}{\partial r} \\
&= -\frac{\sinh \alpha \cos \beta}{2c} \phi(\alpha, \beta) + \frac{\chi(\alpha, \beta)}{c} \times \\
&\quad \left\{ -\sinh \alpha \sin \beta \sum_{n=0}^{\infty} n \left\{ -a_n \sin(n\beta) + b_n \cos(n\beta) \right\} Q_{n-1/2}(\cosh \alpha) + \right. \\
&\quad \frac{1 - \cosh \alpha \cos \beta}{\sinh \alpha} \sum_{n=0}^{\infty} \left( n + \frac{1}{2} \right) \left\{ a_n \cos(n\beta) + b_n \sin(n\beta) \right\} Q_{n+1/2}(\cosh \alpha) + \\
&\quad \left. \frac{1 - \cosh \alpha \cos \beta}{\sinh \alpha} \cosh \alpha \sum_{n=0}^{\infty} \left( n + \frac{1}{2} \right) \left\{ a_n \cos(n\beta) + b_n \sin(n\beta) \right\} Q_{n-1/2}(\cosh \alpha) \right\},
\end{aligned} \tag{A6.9}$$

$$\begin{aligned}
\frac{\partial \phi(\alpha, \beta)}{\partial z} &= \frac{\partial \phi(\alpha, \beta)}{\partial \alpha} \frac{\partial \alpha}{\partial z} + \frac{\partial \phi(\alpha, \beta)}{\partial \beta} \frac{\partial \beta}{\partial z} \\
&= -\frac{\cosh \alpha \sin \beta}{2c} \phi(\alpha, \beta) + \frac{\chi(\alpha, \beta)}{c} \times \\
&\quad \left\{ (-1 + \cosh \alpha \cos \beta) \sum_{n=0}^{\infty} n \left\{ -a_n \sin(n\beta) + b_n \cos(n\beta) \right\} Q_{n-1/2}(\cosh \alpha) \right. \\
&\quad - \sin \beta \sum_{n=0}^{\infty} \left( n + \frac{1}{2} \right) \left\{ a_n \cos(n\beta) + b_n \sin(n\beta) \right\} Q_{n+1/2}(\cosh \alpha) + \\
&\quad \left. \cosh \alpha \sin \beta \sum_{n=0}^{\infty} \left( n + \frac{1}{2} \right) \left\{ a_n \cos(n\beta) + b_n \sin(n\beta) \right\} Q_{n-1/2}(\cosh \alpha) \right\}.
\end{aligned} \tag{A6.10}$$

The second order derivatives may be found as

$$\begin{aligned}
\frac{\partial^2 \phi(\alpha, \beta)}{\partial r^2} &= \frac{\partial^2 \phi(\alpha, \beta)}{\partial \alpha^2} \left( \frac{\partial \alpha}{\partial r} \right)^2 + \frac{\partial \phi(\alpha, \beta)}{\partial \alpha} \frac{\partial^2 \alpha}{\partial r^2} + 2 \frac{\partial^2 \phi(\alpha, \beta)}{\partial \alpha \partial \beta} \frac{\partial \alpha}{\partial r} \frac{\partial \beta}{\partial r} \\
&\quad + \frac{\partial^2 \phi(\alpha, \beta)}{\partial \beta^2} \left( \frac{\partial \beta}{\partial r} \right)^2 + \frac{\partial \phi(\alpha, \beta)}{\partial \beta} \frac{\partial^2 \beta}{\partial r^2}
\end{aligned} \tag{A6.11}$$

$$\begin{aligned} \frac{\partial^2 \phi(\alpha, \beta)}{\partial r \partial z} &= \frac{\partial^2 \phi(\alpha, \beta)}{\partial \alpha^2} \frac{\partial \alpha}{\partial r} \frac{\partial \alpha}{\partial z} + \frac{\partial \phi(\alpha, \beta)}{\partial \alpha} \frac{\partial^2 \alpha}{\partial r \partial z} + \frac{\partial^2 \phi(\alpha, \beta)}{\partial \alpha \partial \beta} \frac{\partial \alpha}{\partial r} \frac{\partial \beta}{\partial z} \\ &+ \frac{\partial^2 \phi(\alpha, \beta)}{\partial \beta^2} \frac{\partial \beta}{\partial r} \frac{\partial \beta}{\partial z} + \frac{\partial \phi(\alpha, \beta)}{\partial \beta} \frac{\partial^2 \beta}{\partial r \partial z} + \frac{\partial^2 \phi(\alpha, \beta)}{\partial \alpha \partial \beta} \frac{\partial \alpha}{\partial z} \frac{\partial \beta}{\partial r} \end{aligned} \quad (\text{A6.12})$$

$$\begin{aligned} \frac{\partial^2 \phi(\alpha, \beta)}{\partial z^2} &= \frac{\partial^2 \phi(\alpha, \beta)}{\partial \alpha^2} \left( \frac{\partial \alpha}{\partial z} \right)^2 + \frac{\partial \phi(\alpha, \beta)}{\partial \alpha} \frac{\partial^2 \alpha}{\partial z^2} + 2 \frac{\partial^2 \phi(\alpha, \beta)}{\partial \alpha \partial \beta} \frac{\partial \alpha}{\partial z} \frac{\partial \beta}{\partial z} \\ &+ \frac{\partial^2 \phi(\alpha, \beta)}{\partial \beta^2} \left( \frac{\partial \beta}{\partial z} \right)^2 + \frac{\partial \phi(\alpha, \beta)}{\partial \beta} \frac{\partial^2 \beta}{\partial z^2}. \end{aligned} \quad (\text{A6.13})$$

**Differentiation formula for a sphere with the center on z axis**

The general  $m, n$ th derivative of a harmonic function at point  $(\rho, z)$  is

$$\begin{aligned} \frac{\partial^{m+n} \phi}{\partial \rho^m \partial z^n} &= \frac{1}{R^{m+n} \sin^m \theta} \sum_{j=0}^{\infty} \frac{(j+m+n)!}{j!} f_{j+m+n} \left( \frac{\rho}{R} \right)^j \times \\ &\quad \left\{ \sum_{k=0}^m (-1)^k \binom{m}{k} \cos^k \theta P_{j+m-k}(\cos \theta) \right\}. \end{aligned} \quad (\text{A6.14})$$

Coefficients  $f_i$  are given in Chapter 3 (section 3.2.2.2).

## APPENDIX 7

### Application to modeling of anisotropic soft magnetic materials

The paper 'Differentiation algorithms for soft magnetic material models' by P.P. Silvester and D. Omeragić was presented at 1993. International Magnetism Conference (INTERMAG '93), which was held April 13 – 16, 1993. in Stockholm, Sweden. It will be published in IEEE Transaction on Magnetism, Vol. 31.

# Differentiation algorithms for soft magnetic material models

Peter P. Silvester and Dževat Omeragić  
 Department of Electrical Engineering, McGill University  
 3480 University Street, Montreal, Canada H3A 2A7

**Abstract** — Anisotropic soft materials are fully described by mapping the stored energy or coenergy density over the space of flux density or magnetic field components. This method requires accurate numerical differentiation and reliable data. Two algorithms are described; one is fast and suitable for starting Newton iterations, the other is more costly but yields accurate second derivatives. Current laboratory techniques are sufficiently accurate but measurements must be spread over the coordinate space so that numerous points lie in the multidimensional knee region of the material.

## INTRODUCTION

Of the various methods available for numerical modeling of soft magnetic material properties, the most economic for data storage was described by Silvester and Gupta [1]. They showed that the stored energy density  $w$  and coenergy density  $w'$  are given by

$$w' = \int_0^{\mathbf{H}} \mathbf{B}(\mathbf{H}) \cdot d\mathbf{H}; \quad w = \int_0^{\mathbf{B}} \mathbf{H}(\mathbf{B}) \cdot d\mathbf{B}. \quad (1)$$

Consequently, the field  $\mathbf{H}$  can be recovered from stored values of energy density, a scalar, by differentiation in a space defined by the flux density components:

$$\mathbf{H} = \nabla_{\mathbf{B}} w = \mathbf{i}_x \frac{\partial w}{\partial B_x} + \mathbf{i}_y \frac{\partial w}{\partial B_y} + \mathbf{i}_z \frac{\partial w}{\partial B_z}. \quad (2)$$

An analogous expression is readily obtained for  $\mathbf{B}$  as the gradient of coenergy density,  $\mathbf{B} = \nabla_{\mathbf{H}} w'$ . It thus suffices to store either  $w(\mathbf{B})$  or  $w'(\mathbf{H})$ , and to form gradients with respect to the components of  $\mathbf{B}$  or  $\mathbf{H}$  as needed. This requires an accurate method of differentiating numerically stored data. The present paper gives two algorithms and shows briefly what levels of accuracy are required in order to recover fields reliably, as guidance to experimentalists as well as analysts.

## DIFFERENTIATION BY POISSON KERNELS

The energy-based material model requires a differentiation algorithm of good quality. Because the usual form of Newton iteration requires second as well

as first derivatives, the best available method (indeed the only one to yield sufficiently accurate second derivatives) is the Poisson integral technique of Silvester and Omeragić [2]. To employ this method, the energy density  $w$  is differentiated twice:

$$\frac{\partial^2 w}{\partial B_x^2} + \frac{\partial^2 w}{\partial B_y^2} = \tau(\mathbf{B}). \quad (3)$$

A similar development applies to coenergy density  $w'$ . The source term  $\tau(\mathbf{B}) = \text{tr}(\nu_{\text{in}}^{-1})$ , the trace of the incremental reluctivity tensor of the material, is obtained from the experimentally known values of  $w$ . The differentiation methods for solutions of the Poisson equation are then directly applicable to  $w(\mathbf{B})$  of (3). Applying Green's second identity to the solution yields

$$w_P = - \int_{\Omega} G(P;Q) \tau(\mathbf{B}(Q)) d\Omega_Q - \oint_{\partial\Omega} w_Q \nabla_Q G(P;Q) \cdot d\mathbf{S}_Q \quad (4)$$

where  $G(P;Q)$  is the Green's function for some region  $\Omega$  that embeds the point  $P$ . To find derivatives of  $w$ , equation (4) is differentiated. In this process, the differentiation operator is applied to the Green's function  $G(P;Q)$  and its gradient  $\nabla_Q G(P;Q)$ , functions analytically known for some simple regions  $\Omega$ . Thus

$$\frac{\partial^{m+n} w_P}{\partial B_x^m \partial B_y^n} = \int_{\Omega} J_{mn}(P;Q) \tau(\mathbf{B}(Q)) d\Omega_Q - \oint_{\partial\Omega} w_Q K_{mn}(P;Q) \cdot d\mathbf{S}_Q. \quad (5)$$

The kernel functions  $J_{mn}$  have been tabulated [2] and

$$K_{mn}(P;Q) = \frac{\partial^{m+n}}{\partial B_x^m \partial B_y^n} \nabla_Q G(P;Q). \quad (6)$$

In effect, numerical differentiation is here replaced by analytic differentiation and numerical integration. This process is so stable that the source term  $\tau(\mathbf{B}(Q))$  may be computed by a simple finite-difference algorithm from the stored energy density. Numerical evaluation of the singular surface integral in (5) is computationally fairly costly. However, the precision of this method is largely independent of the order of derivative.

In early development of this differentiation technique, a circle was used as the integration region  $\Omega$ .

However, for magnetic material models the rectangle is preferred, for it allows direct use of data tabulated on a rectangular grid. The Green's function for a rectangle is readily obtained by the method of images:

$$G(P;Q) = \frac{1}{2\pi} \sum_{m=1}^{\infty} \sum_{n=1}^{\infty} \log \frac{s_{2mn} s_{4mn}}{s_{1mn} s_{3mn}}, \quad (7)$$

where  $s_{kmn}$  ( $k=1,2,3,4$ ) are distances from the observation point  $P$  to images of the source point  $Q$  in cell  $(m,n)$  of the rectangular grid.

#### DIFFERENTIATION BY LOCAL SMOOTHING

A second, computationally cheaper, method for finding derivatives is a local smoothing technique based on that of Zhu and Zienkiewicz [3]. Let the  $B_x$ - $B_y$  plane be subdivided into rectangular cells. A four-parameter least-squares fit can be constructed on every cell of the space, by taking approximate derivatives (e.g., by a differencing technique) and improving them by adding Legendre polynomials  $P_p(B)$  in both directions:

$$H_x^* = \left( \frac{\partial w}{\partial B_x} \right) + \alpha_1 P_p(B_x) + \alpha_2 P_p(B_y) \quad (8)$$

and similarly for  $H_y^*$ . Here  $p$  is the order of approximation,  $H_x^*$  the improved derivative value. To find values for the set of four parameters  $\{\alpha_i | i = 1, \dots, 4\}$ , the squared residual is minimized,

$$\frac{\partial}{\partial \alpha_i} \int_{S_e} \left( \frac{\partial(H_x^*)}{\partial B_x} + \frac{\partial(H_y^*)}{\partial B_y} - \tau(B) \right)^2 dB_x dB_y = 0. \quad (9)$$

This method can only produce first derivatives with reasonable accuracy. It is fast, but it only provides subquadratic convergence of Newton iterations. It may be attractive at the start of a Newton process where the convergence rate is anyway poor [4]. Since its fixed point is independent of second derivatives, Newton iteration still converges to the right solution, even if slowly.

#### ERROR SENSITIVITY

Numerical differentiation is usually considered an error-sensitive process, in which data error is magnified. A major concern is therefore the accuracy to which energy density maps must be measured and stored. To explore this question, error was deliberately introduced into the energy map of a hypothetical magnetic material, one whose properties are generally similar to a real electrical sheet steel but have an exact, analytically known, form. This material is characterized by

$$w = \rho_1 \exp(B_x^2 + \sigma_1 B_y^2) + \rho_2 (B_x^2 + \sigma_2 B_y^2) + \rho_3 \quad (10)$$

An equal-energy contour map for such a material

appears in Fig. 1, for the parameter values used in much of the subsequent error study:  $\rho_1 = 1.000$ ,  $\sigma_1 = 3.000$ ,  $\rho_2 = 10.000$ ,  $\sigma_2 = 2.000$ ,  $\rho_3 = -1.000$ . Its surface is roughly parabolic near the origin, as might be expected. The knee region of its  $B$ - $H$  characteristic corresponds to a rapid change in slope of the energy surface near the upper and right edges of the map.

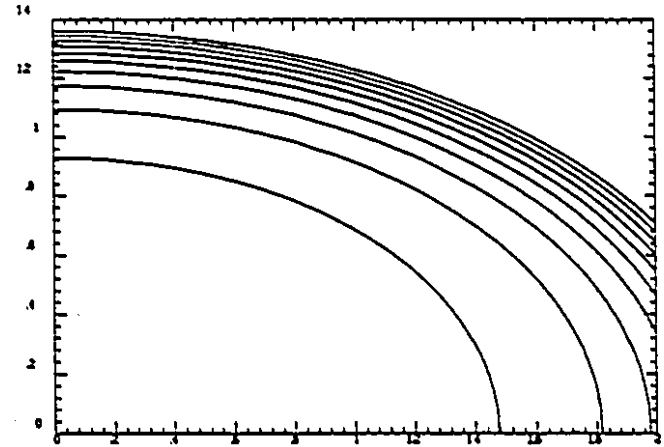


Fig. 1. Equal-energy contours used in error-propagation studies, plotted in  $B_x$ - $B_y$  plane.

Assuming that the measurement procedure contributes negligible systematic error, the data used in computing fields can be taken to consist of the energy density given by (10) plus some random error. Computational experiments were therefore carried out, in which randomly distributed error (white noise) of known amplitude was added to the energy density of (10), and the error in field was correlated with the error in the stored energy density  $w$ .

The performance of the Poisson kernel differentiation method is graphically depicted in Fig. 2. What is plotted here is the error amplification, i.e., the ratio of peak error in the derivative to peak error in the energy density data. As may be seen, the error in derivative values is actually lower than the data error; that is to say, the Poisson kernel differentiation method attenuates data error rather than enhancing it. Plots are shown for two cases:  $\partial w / \partial B_y$  (lower trend line and points marked +) and  $\partial^2 w / \partial B_x^2$  (upper curve and  $\square$ ). Both derivatives are more accurate than the data, by about a full significant figure. The apparent downward trend of derivative error with increasing data error is probably not of significance, given the scatter of data points in Fig. 2.

Error behavior of the local smoothing method has been investigated in detail and the results will be reported elsewhere. It is significantly better than divided dif-

ference interpolation, but still yields much larger error than the Poisson kernel technique.

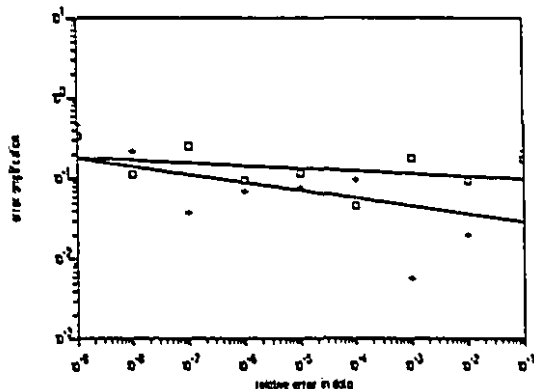


Fig. 2. Error amplification by the Poisson kernel differentiation process.

#### DATA REQUIREMENTS

Energy density plots for magnetic materials are rare; experimental data are usually presented as sets of scalar  $B$ - $H$  curves in various directions. These do not always correlate well with each other, and sometimes hide those features of the  $w$ - $B$  map that the analyst finds most valuable. High experimental accuracy alone does not yield usable energy maps; experiments need to be guided by the computational model that will eventually use the results. To illustrate, Fig. 3 shows the measured energy density distribution of a typical transformer steel. Although the experiment was conducted with great care and excellent equipment, the resulting plot is unsatisfactory for the models discussed here. The unexpected cusps and rough patches in it appear to result from a sparsity of data points in critical areas.

The measurements for Fig. 3 were taken as a family of curves in five well-spaced radial directions. This material exhibits anisotropy ranging from about 3:1 to more than 10:1, so that radial lines in the  $B_x$ - $B_y$  plane intersect iso-energy contours at small angles. Interpolation in the directions of steepest descent is therefore unreliable. Unfortunately, it is just there that high accuracy is needed! The authors believe that a similar number of data points (a total of about 200) would be adequate if they were (1) distributed along contour and gradient lines, i.e., roughly following the shape of the energy map, (2) concentrated in areas of rapid change of gradient. The latter correspond to the knee region (region of rapid change of curvature) of a scalar  $B$ - $H$  curve. At issue here is not the experimenters' skill or care. On the contrary, present measurement techniques

seem adequate to the task, and typical quantities of data appear sufficient; it is rather that in the absence of a clear computational model, the experimentalist cannot know in what regions data should be concentrated. All comments made here are intended to help in this respect.

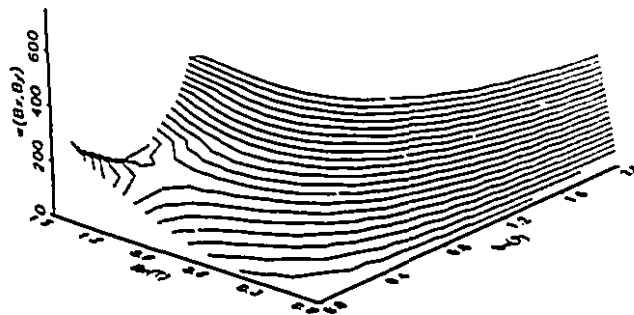


Fig. 3. Energy surface for anisotropic sheet, roughened by poor placement of data points.

#### CONCLUSIONS

The stored energy density representation of magnetic material properties, when coupled with differentiation methods based on Poisson kernels, yields numerically stable interpolation of multidimensional  $B$ - $H$  characteristics without undue requirements on accuracy of the underlying numerical data.

#### ACKNOWLEDGMENT

The authors are grateful to Professor T. Nakata of Okayama University for his kind help in providing experimental data and to Professor J.P. Webb of McGill University for his able and generous assistance with the paper presentation.

#### REFERENCES

- [1] P.P. Silvester and R.P. Gupta, 'Effective computational models for anisotropic soft  $B$ - $H$  curves,' *IEEE Transactions on Magnetics*, vol. 27, pp. 3804-3807, 1991.
- [2] P.P. Silvester and D. Omeragić, 'Differentiation of finite element solutions of the Poisson equation', *IEEE Transactions on Magnetics*, vol. 29, pp. 1993-1996, 1993.
- [3] P.P. Silvester and D. Omeragić, 'A two-dimensional Zhu-Zienkiewicz method for gradient recovery from finite element solutions', *COMPEL*, (in press), 1993.
- [4] P.P. Silvester and R.L. Ferrari, *Finite elements for electrical engineers*. 2nd edition. Cambridge: Cambridge University Press, 1990.

## APPENDIX 8

Published work based in part or whole on this thesis

- Silvester, P.P., and Omeragić, D. (1993), 'A comparative experimental study of differentiation on finite elements', *International Journal of Applied Electromagnetics in Materials* (in press), 1993.
- Silvester, P.P. and Omeragić, D. (1993), 'Differentiation of finite element solutions of the Poisson equation', *IEEE Transactions on Magnetics*, vol. MAG-29, pp. 1993-1996, 1993.
- P.P. Silvester and D. Omeragić, 'Differentiation algorithms for soft magnetic material models', *IEEE Transactions on Magnetics*, vol. 31, (in press), 1993.
- D. Omeragić and P.P. Silvester, 'Differentiation of approximate solutions of the Helmholtz equation', *International Journal of Applied Electromagnetics in Materials*, (in press), 1993.
- P.P. Silvester and D. Omeragić, 'A two-dimensional Zhu-Zienkiewicz method for gradient recovery from finite element solutions', *COMPEL*, (in press), 1993.
- D. Omeragić, and P.P. Silvester: 'Three-dimensional gradient recovery by local smoothing of finite element solutions', *COMPEL*, (submitted), 1993.

## REFERENCES

- Abramowitz, M. and Stegun, I.A. (1965), *Handbook of mathematical functions with formulas, graphs, and mathematical tables*, Washington: National Bureau of Standards, 1965.
- Ainsworth, M. and Craig, A. (1992), 'A posteriori error estimators in the finite element method', *Numerische Mathematik*, vol. 60, pp. 429-463, 1992.
- Aliabadi, M.H. and Hall, W.S. (1989), 'The regularizing transformation integration method for boundary element kernels. Comparison with series expansion and weighted Gaussian integration methods', *Engineering Analysis with Boundary Elements*, Vol. 6, No. 2, pp. 66-71, 1989.
- Andreev, A.B. and Lazarov, R.D. (1988), 'Superconvergence of the gradient for quadratic triangular elements', *Numer. Meth. Partial Differential Equations*, vol. 4, pp. 15-32, 1988.
- Atkin, R.H. (1962), *Theoretical electromagnetism*, New York: John Wiley & Sons Inc., 1962.
- Babister, W. (1967), *Transcendental functions satisfying nonhomogenous linear differential equations*, New York: Macmillan, 1967.
- Babuška, I., Izadpanah, K and Szabó, B. (1984a), 'The post-processing technique in the finite element method: Theory and experience' in *Unification of finite element methods*, ed. H. Kardestuncer, Amsterdam: Elsevier Science Publishers, 1984.
- Babuška, I. and Miller, A. (1984b), 'The post-processing approach in the finite element method. Part 1: Calculation of displacements, stresses and other higher derivatives of the displacements.' *International Journal for*

- Numerical Methods in Engineering*, vol. 20, pp. 1085-1109, 1984.
- Babuška, I. and Miller, A. (1984c), 'The post-processing approach in the finite element method. Part 2: The calculation of stress intensity factors', *International Journal for Numerical Methods in Engineering*, vol. 20, pp. 1111-1129, 1984.
- Babuška, I. and Miller, A. (1984d), 'The post-processing approach in the finite element method. Part 3: A posteriori error estimates and adaptive mesh selection', *International Journal for Numerical Methods in Engineering*, vol. 20, pp. 2311-2324, 1984.
- Babuška, I. and Rheinboldt, W.C. (1978), 'A posteriori error estimates for the finite element method', *International Journal for Numerical Methods in Engineering*, vol. 12, pp. 1597-1615, 1978.
- Babuška, I. and Rheinboldt, W.C. (1979), 'Adaptive approaches and reliability estimations in finite element analysis', *Computer Methods in Applied Mechanics and Engineering*, vol. 17/18, pp. 519-540, 1979.
- Babuška, I., Planck, L. and Rodriguez, R. (1992), 'Basic problems of a posteriori error estimation', *Computer Methods in Applied Mechanics and Engineering*, vol. 101, pp. 97-112, 1992.
- Babuška, I. and Rodriguez, R. (1993), 'The problem of the selection of an a posteriori error indicator based on smoothening techniques', *International Journal for Numerical Methods in Engineering*, vol. 36, pp. 539-567, 1993.
- Beahman, P.L., Shephard, M.S. and Flaherty, J.E. (1992), 'A posteriori error estimation for triangular and tetrahedral quadratic elements using interior residuals', *International Journal for Numerical Methods in Engineering*, vol. 34, pp. 979-996, 1992.
- Barlow, J. (1976), 'Optimal stress locations in finite element models', *International Journal for Numerical Methods in Engineering*, vol. 10, pp. 243-251, 1976.

- Bôcher, (1906). 'Theory of Fourier series'. *Annals of Mathematics*, ser. 2, vol. 7, pp. 81-152, 1906.
- Bramble, J.H. and Schatz, A.H. (1977). 'Higher order local accuracy by averaging in the finite element method', *Mathematics of Computation*, vol. 31, pp. 94-111, 1977.
- Brebia, C.A., Telles, J.C.F. and Wrobel, L.C. (1984), *Boundary element techniques: theory and applications in engineering*. New York: Springer-Verlag, 1984.
- Bui, Q.V. (1977), *Permanent-magnet models in finite element analysis*. Montreal: McGill University, 1977. (M. Eng. thesis)
- Budak, B.M, Samarskii, A.A. and Tikhonov, A.N. (1964), *A collection of problems on mathematical physics*. [A.R.M. Robson, transl.] Oxford: Pergamon Press Ltd., 1964.
- Carey, G.F., Chow, S.S. and Seager, M.K. (1985), 'Approximate boundary-flux calculations', *Computer Methods in Applied Mechanics and Engineering*, vol. 50, pp. 107-120, 1985.
- Char, B.W., Geddes, K.O., Gonnet, G.H, Leong, B.L., Monagan, M.B. and Watt, S.M. (1991), *MAPLE V Language Reference Manual*. New York: Springer - Verlag, 1991.
- Chari, M.V.K. and Silvester, P.P. (1980), *Finite elements in electrical and magnetic field problems*. New York: John Wiley & Sons Inc., 1980.
- Ciarlet, P.G. and Lions, J.L. (1990), *Handbook of numerical analysis*. New York: Elsevier Science Pub., 1990.
- Courant, R. and Hilbert, D. (1953), *Methods of mathematical physics*. Vols. 1.&2. New York: Interscience, 1953.
- Crotty Sisson, J.M. (1990), 'Accurate interior point computation in the boundary integral equation method', *Computer Methods in Applied Mechanics and Engineering*, vol. 79, pp. 281-307, 1990.

- Davis, P.J. and Rabinowitz, P. (1984), *Methods of numerical integration*, Orlando: Academic Press, 1984.
- Durand, R., Muschiatti, M.A. and Rodriguez, R. (1991), 'On the asymptotic exactness of error estimators for linear triangular finite elements', *Numerische Mathematik*, vol. 59, pp. 107-127, 1991.
- Feuillibois, F. (1990), 'Precise calculation of numerical derivatives using Lagrange and Hermite interpolation', *Computers Math. Applic.*, vol. 19, No. 5, pp. 1-11, 1990.
- Gallagher, R.S. and J.P. Nagtegaal, J.P. (1989), 'An efficient 3-D visualization technique for finite element models and other coarse volumes', *Computer Graphics*, vol. 23, pp. 185-194, 1989.
- Gibbs, W.J. (1958), *Conformal transformations in electrical engineering*. London: Chapman & Hall, 1958.
- Goodsell, G. and Whiteman, H.R. (1989), 'A unified treatment of superconvergence recovered gradient functions for piecewise linear finite element approximations', vol. 27, pp. 469-481, 1989.
- Gray, L.J. and Chang, S.J. (1992), 'Hypersingular integral formulation of elastic wave scattering', *Engineering Analysis with Boundary Elements*, vol. 10, pp. 337-343, 1992.
- Gray, L.J. and Soucie, C.S. (1993), 'A Hermite interpolation algorithm for hypersingular boundary integrals', *International Journal for Numerical Methods in Engineering*, vol. 36, pp. 2357-2367, 1993.
- Hawken, D.M., Townsend, P. and Webster, M.F. (1991), 'A comparison of gradient recovery methods in finite-element calculations', *Communications in Applied Numerical Methods*, vol. 7, pp. 195-204, 1991.
- Hall, W.S. (1988), 'Integration methods for singular boundary element integrands', *Boundary Element Method - Mathematical & Computational Aspects*, vol. 10, pp. 219-326, 1988.

- Hinton, E. and Campbell, J.S. (1974), 'Local and global smoothing of discontinuous finite element functions using a least squares method', *International Journal for Numerical Methods in Engineering*, vol. 8, pp. 461-480, 1974.
- Hoole, S.R.H. (1989), *Computer-aided analysis and design of electromagnetic devices*. New York: Elsevier, 1989.
- Hunter, D.B. (1972), 'Some Gauss-type formulae for the evaluation of Cauchy principal values of integrals', *Numerische Mathematik*, vol. 19, pp. 419-424, 1972.
- Infolytica Corporation, (1992), *MagNet 5 User Guide*. Montreal: Infolytica Corporation, 1992.
- Ioakimidis, N.I. (1985), 'On the uniform convergence of Gaussian quadrature rules for Cauchy principal value integrals and their derivatives', *Mathematics of Computation*, vol. 44, pp. 191-198, 1985.
- Ioakimidis, N.I. and Pitta, M.S. (1988), 'Remarks on the Gaussian quadrature rule for finite-part integrals with a second order singularity', *Computer Methods in Applied Mechanics and Engineering*, vol. 69, pp. 325-343, 1988.
- Jahnke, E. and Emde, F. (1945), *Tables of functions with formulae and curves*. 4th ed., New York: Dover Publications, 1945.
- Kantorovich, L.V. (1964), *Approximate methods of higher analysis* [C.D. Benster, transl.], New York: Wiley, 1964.
- Kaya, A.C. and Erdogan, F. (1987), 'On the solution of integral equations with strongly singular kernels', *Quarterly of Applied Mathematics*, vol. 45, pp. 105-122, 1987.
- Kellogg, O.D. (1967), *Foundations of potential theory*. Berlin: Springer-Verlag, 1967.
- Kellogg, O.D. (1931), 'On the derivative of harmonic functions on the boundary'

- Annals of Mathematics*, ser. 2. vol. 32, pp. 486-510, 1931.
- Kelly, D.W. (1984) 'The self-equilibration of residuals and complementary *a posteriori* error estimates in the finite element method', *International Journal for Numerical Methods in Engineering*, vol. 20, pp. 1491-1506, 1984.
- Kotiuga, P.R. and Silvester, P.P. (1985), 'Calculations of fields and force densities from finite element approximations of potentials'. *Jour. Appl. Phys.*, vol. 57, pt. 2B, p. 3856, 1985.
- Křížek, M. and Neittaanmäki, P. (1984), 'Superconvergence phenomenon in the finite element method arising from averaging gradients', *Numerische Mathematik*, vol. 45, pp. 105-116, 1984.
- Křížek M. and Neittaanmäki, P. (1987), 'On superconvergence techniques', *Acta Applicandae Mathematicae*, vol. 9, pp. 175-198, 1987.
- Krylov, V.I. (1962), *Approximate calculation of integrals*. [A. Stroud, transl.] New York: Macmillan, 1962.
- Kutt, H.R. (1975), 'The numerical evaluation of principal value integrals by finite-part integration', *Numerische Mathematik*, vol. 24, pp. 205-210, 1975.
- Ladopoulos, E.G. (1990), 'Gauss quadrature rules for finite part integrals', *International Journal for Numerical Methods in Engineering*, vol. 30, pp. 13-26, 1990.
- Lebedev, N.N. (1965), *Special functions and their applications*. [R.A. Silverman, transl.], Englewood Cliffs: Prentice-Hall, 1965.
- Levine, N. (1985), 'Superconvergent recovery of the gradient from piecewise linear finite-element approximations', *IMA Journal on Numerical Analysis*, vol. 5, pp. 407-427, 1985.
- Lin Qun and Zhu, Q. (1984), 'Asymptotic expansion for the derivative of finite elements', *J. Comput. Math.*, vol. 2, pp. 361-363, 1984.

- Lin Qun and Xu Jinchao (1985). 'Linear finite elements with high accuracy', *J. Comput. Math.*, vol. 3, pp. 115-133, 1985.
- Louis, A. (1979) 'Acceleration of convergence for finite element solution of the Poisson equation', *Numerische Mathematik*, vol. 33, pp. 43-53, 1979.
- Lowther, D.A. and Silvester P.P. (1986), *Computer-aided design in magnetics*. New York: Springer-Verlag, 1986.
- Lutz, E. (1992), 'Exact Gaussian quadrature methods for near-singular integrals in the boundary element method', *Engineering Analysis with Boundary Elements*, vol. 9, pp. 233-245, 1992.
- Ly, B.L. (1990), 'Numerical differentiation using the Gaussian quadrature', *Journal of Engineering Mechanics*, vol. 116, pp. 2568-2572, 1990.
- MacKinnon, R.J., and Carey, G.F. (1989), 'Superconvergent derivatives: a Taylor series analysis', *International Journal for Numerical Methods in Engineering*, vol. 28, pp. 489-509, 1989.
- Mathews, J. and Walker, R.L. (1965), *Mathematical methods of physics*. New York: W.A. Benjamin, Inc., 1965.
- Mikhlin, S.G. and Smolitskiy, K.L. (1967), *Approximate methods for solution of differential and integral equations*. [R.E. Kalaba transl.] New York: American Elsevier Publishing Company, 1967.
- Mikhlin, S.G. (1964). *Variational methods in mathematical physics*. [T. Boddington, transl.] Oxford: Pergamon Press, 1964.
- Mikhlin, S.G. (1965), *Multidimensional singular integrals and integral equations*. [W.J.A. Whyte, I.N. Sneddon, transl.] Oxford: Pergamon Press, 1965.
- Mikhlin, S.G. (1967), *Linear equations of mathematical physics*. [H. Hochstadt, transl.] Toronto: Holt, Rinehart and Winston, 1967.
- Mikhlin, S.G. (1970), *Mathematical physics, an advanced course*. Amsterdam: North-Holland Publishing Company, 1970.
- Miranda, C. (1970), *Equations of mathematical physics*. New York: Springer-

- Verlag, 1970.
- Moan, T. (1974), 'Experiences with orthogonal polynomials and "best" numerical integration formulas on a triangle; with particular reference to finite element approximations'. *ZAMM*, vol. 54, pp. 501-508, 1974.
- Morse, P.M. and Feshbach, H. (1953), *Methods of theoretical physics*, Vols. 1&2, New York: McGraw-Hill, 1953.
- Muskhelishvili, N.I. (1958), *Singular integral equations: boundary problems of function theory and their applications to mathematical physics*. [J.R.M. Radok, transl.], Groningen: Wolters-Noordhoff, 1958.
- National Bureau of Standards (1952), *Construction and application of conformal maps*. Proceeding of a Symposium held in June 22-25, 1949, at the Institute for Numerical Analysis of the National Bureau of Standards at the University of California, Los Angeles. Washington: U.S. Govt. Print. Off., 1952.
- Ninham, B.W. (1966), 'Generalized functions and divergent integrals', *Numerische Mathematik*, vol. 8, pp. 444-457, 1966.
- Niu, Q. and Shephard, M.S. (1993), 'Superconvergent extraction techniques for finite element analysis', *International Journal for Numerical Methods in Engineering*, vol. 36, pp. 811-836, 1993.
- Ohtsubo, H. and Kitamura, M. (1990), 'Element by element *a posteriori* error estimation and improvement of stress solutions for two-dimensional elastic problems', *International Journal for Numerical Methods in Engineering*, vol. 29, pp. 223-244, 1990.
- Ohtsubo, H. and Kitamura, M. (1992a), 'Element by element *a posteriori* error estimation of the finite element analysis for three-dimensional elastic problems', *International Journal for Numerical Methods in Engineering*, vol. 33, pp. 1755-1769, 1992.
- Ohtsubo, H. and Kitamura, M. (1992b), 'Numerical investigation of element-wise *a posteriori* error estimation in two and three dimensional elastic

- problems', *International Journal for Numerical Methods in Engineering*, vol. 34, pp. 969-977, 1992.
- Paget, D.F. (1981 a), 'The numerical evaluation of Hadamard finite-part integrals', *Numerische Mathematik*, vol. 36, pp. 447-453, 1981.
- Paget, D.F. (1981 b) 'A quadrature rule for finite-part integrals', *BIT*, Vol. 21, pp. 212-220, 1981.
- Sabonnadière, J.C. and Coulomb, J.L. (1987), *Finite element methods in CAD: electrical and magnetic fields*, New York: Springer-Verlag, 1987.
- Silvester, P.P. (1972), 'Tetrahedral polynomial finite elements for the Helmholtz equation', *International Journal for Numerical Methods in Engineering*, vol. 4, pp. 405-413, 1972.
- Silvester, P.P. (1978), 'Construction of triangular finite element universal matrices', *International Journal for Numerical Methods in Engineering*, vol. 12, pp. 237-244, 1978.
- Silvester, P.P. (1989), 'Weighted Gaussian quadratures for singular and near-singular integrands', *International Journal of Numerical Modeling*, Vol. 2, pp. 131-142, 1989.
- Silvester, P.P. (1991 a), 'Differentiation of finite element approximations to harmonic functions', *IEEE Transactions on Magnetics*, vol. 27, pp. 3774-3779, 1991.
- Silvester, P.P. (1991 b), 'Extended Poisson kernels for differentiation of harmonic functions', *Electrosoft*, vol. 2, pp. 284-300, 1991.
- Silvester, P.P. (1992), 'Computer algebra in finite element software construction', *International Journal of Applied Electromagnetic in Materials*, vol. 3, pp. 169-177, 1992.
- Silvester, P.P. and Ferrari, R.L. (1990), *Finite elements for electrical engineers*, 2nd edition, Cambridge: Cambridge University Press, 1990.
- Sladek, V. and Sladek, J. (1992), 'Non-singular boundary integral interpretation

- of potential field gradients'. *International Journal for Numerical Methods in Engineering*, vol. 33, pp. 1181-1196, 1992.
- Sneddon, I.N. (1957), *Elements of partial differential equations*. New York: McGraw-Hill, 1957.
- Sohn, J.L. and Heinrich, J.C. (1990), 'A Poisson equation formulation for pressure calculations in penalty finite element models for viscous incompressible flows', *International Journal for Numerical Methods in Engineering*, vol. 30, pp. 349-361, 1990.
- Spanier, J. and Oldham, K.B. (1987), *An atlas of functions*, Washington: Hemisphere Publishing Corporation, 1987.
- Spiegel, M.R. (1981), *Schaum's outline of theory and problems of complex variables: with an introduction to conformal mapping and its application*, New York: McGraw-Hill, 1981.
- Stakgold, I. (1979), *Green's functions and boundary value problems*. New York: John Wiley & Sons Inc., 1979.
- Strang, G. and Fix, G. (1973), *An analysis of the finite element method*. Englewood Cliffs, NJ: Prentice-Hall, 1973.
- Stroud, A.H. (1971), *Approximate calculation of multiple integrals*. Englewood Cliffs, NJ: Prentice-Hall, 1971.
- Szabó, B. and Babuška, I. (1991), *Finite element analysis*, New York: John Wiley & Sons Inc., 1991.
- Tarnhuvud, T. and Reichert, K. (1988), 'Accuracy problems of force and torque calculation in FE systems', *IEEE Transactions on Magnetics*, vol. MAG-24, pp. 443-446, 1988.
- Tikhonov, A.N. and Samarskii, A.A. (1963), *Equations of mathematical physics*. [A.R.M. Robson and P.Basu, transl.] Oxford: Pergamon Press Ltd., 1963.
- Trefethen, L.N. (1980), 'Numerical computation of the Schwartz-Christoffel transformation', *SIAM Journal for Scientific and Statistical*

- Computation*, vol. 1, no. 1, pp. S2-102, 1980.
- Tricomi, F.G. (1957), *Integral equations*, New York: Interscience, 1957.
- Tsamasphyros, G. and Dimou, D. (1990), 'Gauss quadrature rules for finite part integrals', *International Journal for Numerical Methods in Engineering*, vol. 30, pp. 13-26, 1990.
- Tyn Myint U. (1973), *Partial differential equations of mathematical physics*. New York: American Elsevier Pub. Co., 1973.
- Van Bladel, J. (1985), *Electromagnetic fields*. Washington: Hemisphere Pub. Co., 1985.
- Vladimirov, V. (1971), *Equations of mathematical physics*. [A. Littlewood, transl.] New York: M. Dekker Co., 1971.
- Weber, E. (1950), *Electromagnetic fields - theory and applications* Vol.1, New York: John Wiley & Sons Inc., 1950.
- Wolfram, S. (1988), *Mathematica: A system for doing mathematics by computer*, New York: Addison-Wesley, 1988.
- Wong, S. and Cendes, Z. (1986), 'A  $C^1$  quadratic interpolant for magnetic field computation', *IEEE Transactions on Magnetics*, vol. MAG-22, pp. 1034-1036, 1986.
- Zhu, J.Z. and Zienkiewicz, O.C. (1990), 'Superconvergence recovery technique and a posteriori error estimators', *International Journal for Numerical Methods in Engineering*, vol. 30, pp. 1321-1339, 1990.
- Zienkiewicz, O.C. and Taylor, R.L. (1989), *The finite element method*. 4th ed. London: McGraw-Hill, 1989.
- Zienkiewicz, O.C., Vilotte, J.P., Toyoshima, S. and Nakazawa, S. (1985), 'Iterative method for constrained and mixed approximation, an inexpensive improvement of F.E.M. performance', *Computer Methods in Applied Mechanics and Engineering*, vol. 51, pp. 3-29, 1985.
- Zienkiewicz, O.C. and Zhu, J.Z. (1992a), 'The superconvergent patch recovery

- and *a posteriori* error estimates. Part 1: The recovery technique', *International Journal for Numerical Methods in Engineering*, vol. 33, pp. 1331-1364, 1992.
- Zienkiewicz, O.C. and Zhu, J.Z. (1992b), 'The superconvergent patch recovery and *a posteriori* error estimates. Part 2: Error estimates and adaptivity', *International Journal for Numerical Methods in Engineering*, vol. 33, pp. 1365-1382, 1992.
- Zlámal, M. (1978), 'Superconvergence and reduced integration in the finite element method', *Mathematics of Computation*, vol. 32, pp. 663-685, 1978.